

Aus dem Fachbereich der Molekularen Biophysik
Theoretische Medizin und Biowissenschaften der Medizinischen Fakultät
der Universität des Saarlandes, Homburg/Saar

Investigating Calcium Dependent Regulation of IL-1 α Release: Unravelling the Significant Role of Purinergic Signaling with Implications in Chronic Kidney Disease.

DISSERTATION

Zur Erlangung des akademischen Grades
eines Doktor der Naturwissenschaften
der Medizinischen Fakultät
der Universität des Saarlandes
2025

vorgelegt von

Maryam Amini

Geb. am 23.04.1992 in Teheran

To my loved ones,

To my dad, whose warm presence I deeply miss.

To my mom, who has been the foundation of my life.

To my precious sister and brothers, whose boundless love and steadfast support have been the guiding light of my journey.

To my beloved partner, who walked by my side through every step and every moment.

Table of Contents

Summary	10
Zusammenfassung	12
Abbreviations	14
Introduction	17
1 Chronic kidney disease	17
2 Inflammation in CKD	17
2.1 Recognition of the stimulus by the cell surface pattern receptors	18
2.1.1 Toll Like Receptors.....	19
2.2 Activation of the inflammatory pathways	19
2.3 Secretion of cytokines and/chemokines	20
3 IL-1 cytokine family	20
3.1 IL-1 α and IL-1 β production, cleavage, and release	21
3.2 IL-1 and CKD disease	23
4 Monocytes origin and subpopulations	23
4.1 Monocyte subtypes characteristics and functions	24
5 Ca ²⁺ signaling in monocytes.	25
5.1 Store operated Ca ²⁺ entry (SOCE).....	26
5.2 TRP channels.....	27
5.3 Purinergic receptors.....	29
5.3.1 Purinergic receptors as modulators of cytokine release	32
5.3.2 Purinergic receptors in CKD.....	33
Material	34
1 Antibodies.....	34
2 Agonists sand antagonists.....	35
3 Chemicals and reagents.....	36
4 Buffers and medium.....	39

5	Primers	41
6	Equipments	42
7	Resources	44
	Methods	45
1	Cell Isolation and culture	45
1.1	PBMC Isolation	45
1.2	Monocyte Isolation	45
1.3	Treating and harvesting monocytes	46
1.4	Cell line cultures	48
2	Transfection and Nucleofection	48
3	ELISA experiments	49
4	Protein detection using SDS gels	49
4.1	TCA sample preparation	49
4.2	Cell lysate preparation	49
4.3	SDS-PAGE	50
4.4	Western Blotting	50
5	Flow cytometry experiments	51
5.1	Immunophenotyping	51
6	Cloning	54
6.1	Polymerase Chain Reaction (PCR)	54
6.2	DNA analysis and purification by gel electrophoresis	55
6.3	Ligation	55
6.4	Competent cell preparation and transformation	56
6.5	Colony PCR	57
6.6	Plasmid preparation	57
6.7	DNA sequencing	58

7	Quantitative real-time PCR.....	58
7.1	RNA isolation using kit.	58
7.2	RNA isolation using guanidinium thiocyanate-phenol-chloroform extraction method.	59
7.3	RNA gels.....	60
7.1	Reverse transcription.....	60
7.2	Real time PCR.....	61
8	Single cell Ca ²⁺ imaging	62
9	Live cell fluorescent imaging.....	63
10	Statistical analysis.....	63
	Results	65
1	ROS-induced Ca ²⁺ signals are not altered in CKD monocytes	65
2	Store operated Calcium entry and expression levels of STIM and ORAI genes are comparable in monocytes derived from CKD patients or healthy subjects.	66
3	Concentrations of ATP and Ca ²⁺ in extracellular buffer affect ATP induced Ca ²⁺ signals.	67
4	CKD patients' monocytes showed increased ATP induced Ca ²⁺ responses.	70
5	LPS treatment reduces ATP induced Ca ²⁺ signals.	72
6	Both intracellular Ca ²⁺ release and Ca ²⁺ influx are essential for ATP induced IL-1 α release.....	73
7	ATP mediated activation of P2X7 is crucial for IL-1 α release.....	77
8	Signaling through P2X7 and P2X4 is altered in CKD derived monocytes.....	83
9	ATP stimulation affects surface expression of monocytes markers, which can be restored by P2X7 inhibition	87
10	Purinergic signaling regulates IL-1 α biogenesis by activating kinases	96
11	IL-1 α localization in overexpression systems.....	101
12	RNA sequencing showed altered CKD monocytes gene expression.....	104
13	MMPs have multiple effects on IL-1 α biogenesis	114
	Discussion	120
1	Calcium is essential for IL-1 α secretion.	120

2	Signaling through P2X7 modulates monocyte subpopulations.	123
3	Altered P2X7 Ca^{2+} signaling in CKD patients leads to altered IL-1 α surface expression.	125
4	PKC β 2 is modulating the expression and release of IL-1 α	126
5	IL-1 α release and surface expression is regulated by MMPs.....	127
6	IL-1 α localization differs in mature and immature monocytes.....	128
	References	130
	Declaration of Academic Integrity	147
	Acknowledgments	148

Figure 1 IL-1 α and IL-1 β release pathway.	23
Figure 2 Store operated Ca ²⁺ entry.	27
Figure 3 TRPM2 signaling pathway in immune cells.	29
Figure 4 ATP activation concentrations of P2 family.	30
Figure 5 Intracellular signaling pathway induced upon P2Y2 activation.....	32
Figure 6 PBMCs and monocytes gating strategy in FACS measurements.	53
Figure 7 Ca ²⁺ Signals through TRPM2 and expression levels of TRP channels are not altered in CKD monocytes.....	66
Figure 8 SOCE signaling and expression of STIM and ORAI channels is comparable in CKD and healthy monocytes.	67
Figure 9 Ca ²⁺ signals induced by ATP in U937 cells were increased by higher extracellular Ca ²⁺ concentrations but decreased by higher ATP concentration.....	69
Figure 10 Ca ²⁺ responses to 100 μ M and 2 mM ATP are comparable in U937 cell line.	69
Figure 11 Ca ²⁺ signals in response to different ATP concentrations and extracellular Ca ²⁺ concentrations in primary human monocytes.	70
Figure 12 ATP induced Ca ²⁺ signals are significantly altered in the monocytes of CKD patients.	71
Figure 13 LPS treatment reduces the Ca ²⁺ responses activated by ATP.	72
Figure 14 Absence of Ca ²⁺ in extracellular buffer significantly reduces the ATP induced signals.....	73
Figure 15 Store operated Ca ²⁺ entry is not involved in Ca ²⁺ signals in response to ATP.	74
Figure 16 Increase in [Ca ²⁺] _i is essential for IL-1 α and IL-1 β release.	75
Figure 17 Calpain inhibition abolishes IL-1 α release but not IL-1 β	76
Figure 18 Calpain inhibition affects intracellular concentrations of mature IL-1 α	76
Figure 19 P2X7 activation is crucial for IL-1 α release.	77
Figure 20 Effects of P2Y2 agonist and antagonist on [Ca ²⁺] _i in untreated and LPS treated primary monocytes.....	78
Figure 21 Effects of P2X7 agonist and antagonist on [Ca ²⁺] _i in untreated and LPS treated primary monocytes.....	79
Figure 22 Effects of P2X4 agonist and antagonist on [Ca ²⁺] _i in untreated and LPS treated primary monocytes.....	80
Figure 23 P2X4 and P2X7 play an essential role in IL-1 α release.....	81

Figure 24 Inhibition of P2X7 and P2X4 result in reduced IL-1 β release from primary monocytes.	82
Figure 25 Inhibition of P2X4, P2X7 or P2Y2 reduces intracellular mature IL-1 α	83
Figure 26 Effects of P2X7 antagonist on [Ca ²⁺] _i in untreated and LPS treated primary monocytes from healthy or CKD donors.....	85
Figure 27 Effects of P2X7 inhibition on IL-1 α release from LPS treated monocytes are comparable between CKD and healthy individuals.	85
Figure 28 Effects of P2X4 antagonist on [Ca ²⁺] _i in untreated and LPS treated primary monocytes from healthy or CKD donors.....	86
Figure 29 P2X7 has higher impact on ATP responses in CKD monocytes.	87
Figure 30 Immunophenotyping of PBMCs isolated from the whole blood of healthy and CKD donors.	88
Figure 31 ATP application and P2X7 inhibition affect CD16 surface expression on CKD monocytes.	91
Figure 32 Intermediate monocytes population upon LPS treatment is significantly higher in CKD patients.....	92
Figure 33 Representative histograms of IL-1 α surface expression on CKD and healthy monocytes in correlation with CD14 or CD16 markers.	94
Figure 34 Analysis of IL-1 α surface expression on CKD and healthy monocytes in correlation with CD14 or CD16 markers.....	95
Figure 35 PKC β 2 activity is critical for IL-1 α release.	97
Figure 36 Both Pro and mature IL-1 α are reduced upon PKC β 2 inhibition.....	98
Figure 37 Effects of kinase inhibitions on intracellular IL-1 α concentrations.	99
Figure 38 IL-1 α , CD16 and CD14 surface expression in human primary monocytes in presence of inhibitors.....	100
Figure 39 NF κ B modulates the surface expression of IL-1 α and CD16 on monocytes.	101
Figure 40 IL-1 α shows exclusive nuclear localization in HEK cells.	102
Figure 41 Exogenously expressed IL-1 α localization in primary monocytes.	103
Figure 42 IL-1 α has both cytoplasmic and nuclear localization in primary monocytes.....	104
Figure 43 RNA sequencing comparison between healthy and CKD donors.....	105
Figure 44 Expression analysis of some candidate genes measured by RNA sequencing.	114

Figure 45 Inhibition of MMPs after LPS treatment leads to reduced secretion of IL-1 α in response to ATP.	115
Figure 46 MMP9 inhibition before LPS treatment leads to higher IL-1 α and IL-1 β concentrations in medium.	116
Figure 47 MMP9 inhibition before or after LPS treatment leads to a significant increase in mature IL-1 α concentration in the medium.	117
Figure 48 MMPs inhibition does not affect intracellular IL-1 α concentrations.	118
Figure 49 Membrane bound IL-1 α is cleaved by MMPs.....	119

Table 1 P2Ys activators and G proteins coupled to them.....	30
Table 2 Primary antibodies used for western blots.....	34
Table 3 Secondary antibodies used for western blot	34
Table 4 Antibodies used for flow cytometry.	34
Table 5 Agonists and antagonists	35
Table 6 Chemicals and reagents	36
Table 7 Transfection reagents	38
Table 8 commercially available kits.....	38
Table 9 Supplies	39
Table 10 Buffers used for western blots.....	39
Table 11 Cell culture buffers and media	40
Table 12 Buffers used for Flow cytometry.....	41
Table 13 DNA oligos used in qPCR.....	41
Table 14 DNA oligos used in PCR and qPCR.	42
Table 15 Used equipment.....	42
Table 16 AXIO observer system	43
Table 17 Ca ²⁺ Imaging system	43
Table 18 Used concentrations of agonists, antagonists, and inhibitors.	47
Table 19 The general composition of PCR mixture	54
Table 20 The standard program of PCR amplification.....	55
Table 21 Restriction enzyme reaction mixture.....	56
Table 22 Ligase reaction	56
Table 23 Colony PCR mixture	57
Table 24 The standard protocol for colony PCR.....	57
Table 25 DNA mixture for sequencing	58
Table 26 Reverse transcription protocol.....	60
Table 27 Master mix for QuantiTect Primer	61
Table 28 Master mix for Homemade primers	62

Table 29 PCR program used for qPCR.	62
Table 30 Effects of pharmacological modulation of purinergic receptors on $[Ca^{2+}]_i$	80
Table 31 Percentage of CD3+, CD19+ and CD56+ cells in CKD (n=6) and healthy (n=4) PBMC population.	89
Table 32 Analysis of monocytes subpopulations in PBMC directly after isolation from CKD and healthy donors (Data are shown as mean \pm SEM).....	91
Table 33 Percentage of IL-1 α expressing monocytes upon each treatment. (Data are shown as mean \pm SEM).	96
Table 34 Genes significantly up-regulated in CKD (Fold changes are calculated based on Read counts)	105
Table 35 Genes significantly down-regulated in CKD (Fold changes are calculated based on Read counts)	110

Summary

Chronic kidney disease (CKD) is characterized by irreversible changes in kidney function persisting for more than three months. Lethal cardiovascular events in CKD patients account for 7.6% of cardiovascular disease-related deaths. Elevated levels of IL-1 α have been observed in monocytes of CKD patients. In this study, we aimed to investigate the importance of Ca²⁺ signals in IL-1 α biogenesis and release, as well as the channels mediating these signals and their alterations in monocytes from CKD donors. Moreover, IL-1 α localization in monocytes and transcriptional alterations associated with CKD were investigated.

To investigate the importance of Ca²⁺ in IL-1 α release, concentrations of IL-1 α and IL-1 β released in the medium upon chelating Ca²⁺ with EGTA or BAPTA-AM were measured using ELISA, showing a significant reduction in both cytokines when intracellular Ca²⁺ was chelated. Inhibition of calpain, a Ca²⁺-dependent protease known to cleave IL-1 α , showed a significant reduction in IL-1 α in the medium, but had no effect on IL-1 β . Moreover, Ca²⁺ signaling through three main Ca²⁺ pathways, including TRPM2, store-operated calcium entry (SOCE), and the purinergic family, were investigated using live-cell Ca²⁺ imaging. Although no significant alterations were observed in expression levels or Ca²⁺ signals via SOCE or TRPM2 in CKD monocytes, purinergic signaling was significantly increased compared to control cells. Expression analysis using qPCR showed higher expression levels of P2Y11, P2X4, and P2X7 in monocytes from CKD patients. Our results showed that the activation of P2X7 is crucial for IL-1 α release, and inhibition of P2X7 and to a lesser extent P2X4 reduced IL-1 α and IL-1 β release from monocytes. Analysis of monocyte surface markers showed alterations of the fraction of CD16⁺ monocytes following priming and treatment with ATP in CKD monocytes.

The current work also studied the effects of several kinases activated downstream of the P2 family on IL-1 α release and surface expression. Release of IL-1 α but not IL-1 β was significantly inhibited by PKC β 2 inhibition. Moreover, surface expression of IL-1 α and the CD16 marker were increased upon NF κ B inhibition. RNA sequencing results identified 143 up-regulated and 79 downregulated genes in CKD monocytes. Among these, MMP25 and MMP9 were significantly up-regulated. Incubating LPS-primed cells with an MMP pan-inhibitor led to a significant decrease in IL-1 α release while an increased surface expression of IL-1 α was observed only if the inhibitor was included during priming with LPS.

To explore intracellular localization, IL-1 α was overexpressed with a GFP tag at the N-terminus and mCherry at the C-terminus in HEK293 cell line or primary monocytes. We observed nuclear localization of IL-1 α in mature monocytes with a bean-shaped nucleus and cytoplasmic localization in immature monocytes with a round nucleus.

In conclusion, our findings highlight the pivotal role of P2X4, P2X7, PKC β 2, and MMPs in IL-1 α release and surface expression. Additionally, we observed a strong correlation between CD16 and IL-1 α surface expression.

Zusammenfassung

Die chronische Nierenerkrankung (CKD) ist durch irreversible Veränderungen der Nierenfunktion gekennzeichnet, die länger als drei Monate andauern. Tödliche kardiovaskuläre Ereignisse bei CKD-Patienten machen 7.6 % der an Herz-Kreislauf-Erkrankungen bedingten Todesfälle aus. Bei den Monozyten von CKD-Patienten wurden erhöhte IL-1 α Spiegel beobachtet. In dieser Studie wollten wir die Bedeutung von Ca²⁺ Signalen für die Biogenese und Freisetzung von IL-1 α untersuchen, ebenso wie die Kanäle, die diese Signale vermitteln, und deren Veränderungen in Monozyten von CKD Spendern. Darüber hinaus wurden die Lokalisation von IL-1 α in Monozyten und die mit CKD assoziierten transkriptionellen Veränderungen analysiert.

Um die Bedeutung von Ca²⁺ bei der Freisetzung von IL-1 α zu untersuchen, wurden mittels ELISA die Konzentrationen von IL-1 α und IL-1 β gemessen, die nach der Chelatierung von Ca²⁺ mit EGTA oder BAPTA-AM in das Medium freigesetzt wurden. Dabei zeigte sich, dass beide Zytokine signifikant reduziert wurden, wenn das intrazelluläre Ca²⁺ geheliert wurde. Die Hemmung von Calpain, einer Ca²⁺ abhängigen Protease, die dafür bekannt ist, IL-1 α zu spalten, führte zu einer signifikanten Verringerung von IL-1 α im Medium, während IL-1 β unbeeinflusst blieb. Außerdem wurde die Ca²⁺ Signalübertragung über drei Hauptwege: TRPM2, store-operated calcium entry (SOCE) und die purinerge Familie, mittels Live-Cell-Ca²⁺-Imaging untersucht. Obwohl in CKD Monozyten weder signifikante Veränderungen der Expressionsniveaus noch der Ca²⁺ Signale über SOCE oder TRPM2 festgestellt wurden, war die purinerge Signalübertragung im Vergleich zu Kontrollzellen signifikant erhöht. Eine Expressionsanalyse mittels qPCR ergab zudem höhere Expressionsniveaus von P2Y11, P2X4 und P2X7 in den Monozyten von CKD-Patienten. Unsere Ergebnisse zeigten, dass die Aktivierung von P2X7 entscheidend für die Freisetzung von IL-1 α ist und dass die Hemmung von P2X7 – und in geringerem Maße von P2X4, die Freisetzung von IL-1 α und IL-1 β aus den Monozyten reduziert. Die Analyse der Oberflächenmarker der Monozyten ergab Veränderungen im Anteil der CD16⁺ Monozyten nach dem Priming und der Behandlung mit ATP in CKD-Monozyten.

Die vorliegende Arbeit untersuchte zudem die Effekte mehrerer Kinasen, die nachgeschaltet der P2 Familie aktiviert werden, auf die Freisetzung und Oberflächenexpression von IL-1 α . So wurde die Freisetzung von IL-1 α , nicht aber die von IL-1 β , durch die Hemmung von PKC β 2 signifikant reduziert. Darüber hinaus führte die Hemmung von NF κ B zu einer erhöhten Oberflächenexpression von IL-1 α und des CD16-Markers. RNA Sequenzierungsergebnisse

identifizierten 143 hochregulierte und 79 herunterregulierte Gene in CKD Monozyten. Unter diesen waren MMP25 und MMP9 signifikant hochreguliert. Die Inkubation von LPS geprimten Zellen mit einem MMP-Pan-Inhibitor führte zu einer signifikanten Abnahme der IL-1 α Freisetzung, während eine erhöhte Oberflächenexpression von IL-1 α nur beobachtet wurde, wenn der Inhibitor bereits während des Primings mit LPS hinzugefügt wurde.

Um die intrazelluläre Lokalisation zu untersuchen, wurde IL-1 α in der HEK293-Zelllinie oder in primären Monozyten überexprimiert, wobei ein GFP Tag am N-Terminus und mCherry am C-Terminus angefügt wurde. Dabei beobachteten wir in reifen Monozyten mit bohnenförmigem Zellkern eine nukleäre Lokalisation von IL-1 α , während in unreifen Monozyten mit rundem Zellkern eine zytoplasmatische Lokalisation vorherrschte.

Zusammenfassend heben unsere Ergebnisse die zentrale Rolle von P2X4, P2X7, PKC β 2 und MMPs bei der Freisetzung und Oberflächenexpression von IL-1 α hervor. Zudem wurde eine starke Korrelation zwischen der Oberflächenexpression von CD16 und IL-1 α festgestellt.

Abbreviations

Absence in melanoma 2 (AIM2) like receptors

Acetoxymethylester-group (AM)

Activator protein-1 (AP-1)

adenosine diphosphate (ADP)

Adenosine triphosphate (ATP)

Bone marrow derived macrophages (BMDM)

Calcium released activated calcium (CRAC) channels.

Chronic Kidney Disease (CKD)

complementary DNA (cDNA)

C-type lectin receptors (CLRs)

Danger associated molecular patterns (DAMPs)

Dithiothreitol (DTT)

Endoplasmic reticulum (ER)

Enhanced chemiluminescence development (ECL)

Enzyme-linked immunosorbent assay (ELISA)

Extracellular fluid (ECF)

fetal calf serum (FCS)

Fluorescence minus one (FMO)

Focal adhesion related tyrosine kinase (Pyk2)

Forward scatter (FSC)

Fragments Per Kilobase of transcript sequence per Millions base pairs sequenced (FPKM)

Glomerular Filtration Rate (GFR)

Half maximal inhibitory concentration (IC₅₀)

Hank's buffer (HBSS)

Human Fc receptors (FcRs)

Inhibitor (Inh.)

Inositol-trisphosphate (IP3)

Interferon regulatory factor 3 (IRF3)

Interferons (IFNs)

Interleukin-1 (IL-1)

Interleukin-1 receptors (IL-1R)

Interleukin-6 (IL-6)

Kilo base (Kb)

Kilo Dalton (kDa)

Knock out (KO)

Leucin-rich repeats (LRRs)

Median Fluorescent Intensity (MFI)

Microgram (μg)

Microliter (μl)

Minimal Essential Medium (MEM)

Minute (min)

Mitogen activated protein kinase (MAPK)

Myeloid differentiation factor 88 (MyD88)

Natural killer cells (NKs)

NLR family pyrin domain containing 3 (NLRP3)

NOD like receptors (NLRs)

Nuclear factor kappa B (NF κ B)

Paraformaldehyde (PFA)

Pattern recognition receptors (PRRs)

peripheral blood mononuclear cells (PBMC)

Phosphatidylinositol 3-kinase (PI3K)

Phosphatidylinositol 4,5-bisphosphate (PIP2)

polyacrylamide gel electrophoresis (PAGE)

Polymerase Chain Reaction (PCR)

Protein kinase B (Akt)

RIG-like receptors (RLRs)

Room temperature (RT)

Second (Sec)

Shrimp Alkaline Phosphatase (rSAP)

Side scatter parameter (SSC)

Sodium dodecyl sulphate (SDS)

Stimulating factors (CSFs)

Tapsigargin (Tg)

Toll like receptors (TLRs)

Toll/IL-1R Domain (TIR domain)

Transforming growth factors (TGFs)

Trichloroacetic acid (TCA)

Tumor necrosis factor (TNF)

Uridine diphosphate (UDP)

Uridine triphosphate (UTP)

Ultraviolet (UV)

Vascular cell adhesion molecule-1 (VCAM-1)

Introduction

1 Chronic kidney disease

Kidney diseases are classified as either acute or chronic based on their duration and severity. Acute kidney disease (AKI) is characterized by a sudden and often reversible damage to the kidneys which leads to reduced glomerular filtration rate (GFR) (Goyal et al., 2024). AKI can lead to CKD, while recent studies show that a pre-existing CKD is one of the major risk factors for developing AKI (Ishani et al., 2009; James et al., 2015). Chronic kidney disease (CKD) is defined as irreversible damage to kidney function and structure lasting for more than three months. The damage in kidney is estimated by examining GFR, described as the flow rate of filtered fluid through the nephrons per unit of time (Webster et al., 2017). Based on GFR, CKD is classified into five stages. While a normal kidney has a GFR of 90 to 120 ml/min, stage 1 of CKD is defined by a GFR of more than 90, stage 2 by a GFR of 60 to 89, and stage 3 by 30-59 ml/min, respectively. Stage 4 and 5 are considered as end stage kidney disease, with GFR of 15 to 29 for stage 4 and less than 15 ml/min for the fifth stage. End stage renal disease can only be treated by kidney transplantation or be tolerated by compensating for kidney function with dialysis (Levey & Coresh, 2012).

The risk factors most commonly associated with CKD include diabetes, hypertension, glomerulonephritis and obesity (Webster et al., 2017). In a study by the Global burden of disease in 2017, the prevalence of CKD was estimated to be 9.1% of the world population, with 2.1 million CKD related deaths 4.6% of total mortality. Additionally, in 1.4 million cases, CKD led to lethal cardiovascular events thus constituting 7.6% of all cardiovascular disease related deaths (Bikbov et al., 2020). Therefore, CKD associated cardiovascular complications are considered one of the growing causes of mortality worldwide. CKD disease pathogenesis and progression have been associated with a chronic inflammatory status induced by factors such as oxidative stress, increased production of pro-inflammatory cytokines, and altered metabolism of adipose tissue (reviewed by Mihai et al., 2018).

2 Inflammation in CKD

Inflammation is the response of the immune system to pathogens, tissue injuries or toxic compounds. While inflammation is necessary for maintaining the tissue homeostasis and survival after an injury or infection, an excessive inflammation can cause tissue damage (Sherwood & Toliver-Kinsky, 2004). In the case of an infection, innate immune cells such as

monocytes, neutrophils, natural killer cells (NKs) and macrophages are recruited to the site of inflammation. These cells eradicate the threat by either phagocytosis of the infectious pathogens or secretion of cytokines and chemokines, which activate lymphocytes and trigger adaptive immune responses. Activation of inflammatory responses are also crucial for wound healing and tissue repair (reviewed by G. Y. Chen & Nuñez, 2010).

“Sterile inflammation” is the term used when inflammatory responses are activated in the absence of pathogens. Trauma, chemically induced injury, or ischemia injury are some examples that can initiate sterile inflammation (reviewed by G. Y. Chen & Nuñez, 2010). In CKD patients, the sterile inflammation is a result of the accumulation of substances or inflammatory cytokines, which are not cleared as in normal conditions due to the decline in glomerular filtration rate (reviewed by Yan & Shao, 2023).

The inflammatory responses differ based on the triggering stimuli, but they have common mechanisms:

1. Recognition of the stimulus by cell surface pattern receptors
2. Activation of the inflammatory pathways
3. Secretion of cytokines and/or chemokines (notably tumor necrosis factor (TNF))
4. Recruitment of inflammatory cells (reviewed by L. Chen et al., 2017)

2.1 Recognition of the stimulus by the cell surface pattern receptors

Recognition of microbial structures, known as pathogen associated molecular patterns (PAMPs), and subsequent activation of proinflammatory responses are mediated by pattern recognition receptors (PRRs). Besides PAMPs, some PRRs can identify endogenous patterns known as danger associated molecular patterns (DAMPs) (Medzhitov, 2008). DAMPs are host biomolecules that are released from injured or dying cells. DAMPs induce inflammatory responses in the absence of an infectious agent (reviewed by Roh & Sohn, 2018). The inflammation induced by DAMPs has been reported to be a key event in several human diseases examples (reviewed by Land, 2015).

There are five different classes of PRRs: Toll like receptors (TLRs) and C-type lectin receptors (CLRs) which are transmembrane proteins, and three cytoplasmic proteins, including NOD like receptors (NLRs), RIG-like receptors (RLRs) and absent in melanoma 2 (AIM2) like receptors. Recognition of PAMPs or DAMPs by PRRs activates signaling pathways, including the nuclear factor kappa B (NFκB) and mitogen activates protein kinase (MAPK). With subsequent up-

regulation of pro-inflammatory cytokines, chemokines, mediators of PRR signaling, and type I interferons (IFNs) (Takeuchi & Akira, 2010). Among all PRRs, the TLR family is the most studied and well characterized for its role in pathogen sensing in both extracellular and intracellular space (endosome and lysosomes) (Akira et al., 2006).

2.1.1 Toll Like Receptors

The TLR family consists of 10 members in human and 13 members in mouse, which are highly conserved from worm to mammals (Takeuchi & Akira, 2010). Some TLRs are located on the cell membrane, including TLR1, TLR2, TLR4, TLR5, TLR6, while others, such as TLR3, TLR7, TLR8 and TLR9, are located in intracellular compartments like endosomes, lysosomes or endoplasmic reticulum (ER) (reviewed by El-Zayat et al., 2019). TLRs have a conserved region in the cytoplasmic tail, which is identical to interleukin-1 receptors (IL-1R) and it is known as the Toll/IL-1R (TIR) domain (Takeuchi & Akira, 2010). However, the extracellular region is markedly different. While IL-1Rs have three immunoglobulin like domains, the extracellular region of TLRs is comprised of leucine-rich repeats (LRRs) (Bell et al., 2003). TLRs are expressed in a wide range of cells, including innate and adaptive immune cells and non-immune cells such as fibroblasts, endothelial and epithelial cells. Several studies have reported the contribution of TLR signaling dysregulation in development and progression of several diseases such as cancer, autoimmune diseases, chronic inflammation, and infectious diseases. Among these, TLR2 and TLR4 have been shown to be involved in several inflammatory diseases associated by obesity and type 2 diabetes and hypertension (reviewed by El-Zayat et al., 2019).

2.2 Activation of the inflammatory pathways

As mentioned previously TLRs and IL-1Rs share a conserved intracellular domain, therefore stimulation of TLRs activates the same signaling pathway as IL-1R activation (reviewed by Akira & Takeda, 2004). Upon stimulation, TLRs dimerize and recruit adaptor proteins containing a TIR domain, such as myeloid differentiation factor 88 (MyD88), which leads to activation of downstream signaling pathways (reviewed by Czerkies & Kwiatkowska, 2014). Activation of these cascades leads to nuclear localization of several transcription factors like interferon regulatory factor 3 (IRF3), mitogen activated protein kinases (MAPK), activator protein-1 (AP-1) and NF κ B and therefore to the expression of many genes crucial for inflammatory response (reviewed by L. Chen et al., 2017; El-Zayat et al., 2019).

2.3 Secretion of cytokines and/chemokines

Cytokines are key signaling molecules predominantly secreted by immune cells such as monocytes, macrophages, and lymphocytes. These molecules play crucial roles in either promoting (pro-inflammatory cytokines) or inhibiting (anti-inflammatory cytokines) inflammation. The broad family of inflammatory cytokines includes interleukins (ILs), colony-stimulating factors (CSFs), interferons (IFNs), tumor necrosis factors (TNFs), transforming growth factors (TGFs), and chemokines. These cytokines are primarily responsible for attracting leukocytes to sites of infection or injury, thereby orchestrating the immune system's response to such events (reviewed by Turner et al., 2014). This is achieved through a complex web of interactions that regulate both the immune response to infection or inflammation and the process of inflammation itself. However, an overproduction of inflammatory cytokines can have detrimental effects, including tissue damage, significant hemodynamic alterations, organ failure, and in severe cases, death. Effectively understanding and regulating cytokine pathways could enhance the identification of inflammation caused by specific agents and improve the management of inflammatory diseases (reviewed by L. Chen et al., 2017). The main pro-inflammatory cytokines are interleukin-1 (IL-1), interleukin-6 (IL-6) and TNF α (reviewed by Turner et al., 2014). In this study we aimed to investigate the biogenesis and release of IL-1 α , a member of the IL-1 cytokine family, and its role in CKD disease.

3 IL-1 cytokine family

Cytokine members of IL-1 family are key molecules modulating inflammatory responses in both innate and adaptive immunity (Fields et al., 2019). This family consists of 11 cytokines and 10 receptors, divided into three subfamilies: IL-18, IL-36 and IL-1 subfamilies. Considering that TLR receptors and IL-1 family receptors have a similar cytoplasmic domain, the TIR domain, many inflammatory responses like chemokine and cytokine production, nitric oxide production and increased expression levels of adhesion molecules are initiated by both TLR and IL-1 receptors (reviewed by Dinarello, 2018). The term “IL-1 cytokine” used to refer to the two main cytokines of this family, IL-1 α and IL-1 β (reviewed by Gabay et al., 2010) and the effects of these cytokines are under tight control by inhibitors in the same family, such as IL-1 receptor type II (IL-1RII) and IL-1 receptor antagonist (IL-1Ra) (reviewed by Gabay et al., 2010). While IL-1 β has been extensively studied, IL-1 α biogenesis and its role in inflammation remain poorly understood (reviewed by Di Paolo & Shayakhmetov, 2016a).

Although some similarities have been found between the two IL-1 cytokines, different regulatory mechanisms and functions have been reported. Both cytokines are synthesized as 31 kDa pro-protein, which is then cleaved into a mature form of 17 kDa, but the cleavage process and enzymes are distinct (Lamkanfi & Dixit, 2014). Since binding to the same receptor activates the same biological responses, equal potential for activating the inflammation has been reported for both IL-1 α and IL-1 β (reviewed by Di Paolo & Shayakhmetov, 2016). However, it has been shown that IL-1 α has a higher affinity for IL-1R1 and IL-1 β has a higher affinity for the decoy receptor, IL-1R2, which does not transduce a signal and acts as a "sink for IL-1 β (Dinarello, 1996). It is noteworthy that only mature IL-1 β is biologically active and able to initiate inflammation, while both pro- and mature IL-1 α are able to act as pyrogens and to bind to the IL-1R1 receptor (B. Kim et al., 2013). Unlike IL-1 β , which is a secreted protein, IL-1 α is functional as both a released and membrane bound cytokine (Kurt-Jones et al., 1985). Interestingly, while IL-1 β is expressed upon activation in cells of hematopoietic origin, IL-1 α is expressed in a wide range of cells, even under healthy conditions (Bersudsky et al., 2014). The distinct functions of IL-1 α and its role independent of IL-1 β in inflammation are still poorly understood.

3.1 IL-1 α and IL-1 β production, cleavage, and release

The mechanism leading to the IL-1 β expression and secretion is very well studied. In order to tightly regulate the inflammation activation, two separate signals are necessary for releasing the mature IL-1 β from the cells. The first signal, or the so-called priming signal, is initiated by activation of pattern recognition receptors, like TLR4 or IL-1R1. This triggers the expression of NLR family pyrin domain containing 3 (NLRP3), along with inflammasome components, pro-IL-1 α , pro-IL-1 β and the necessary components for cleavage (reviewed by Swanson et al., 2019). The second signal, which is the activation signal, is triggered by PAMPs or DAMPs, such as pore forming toxins (Mariathasan et al., 2006), microbial DNA and RNA (Kanneganti et al., 2006; Muruve et al., 2008), cholesterol crystals (Rajamäki et al., 2010) or extracellular ATP (Amores-Iniesta et al., 2017). The cellular stress induced by any of these molecules can lead to multiple upstream signals such as, K⁺ or Cl⁻ efflux, Ca²⁺ influx, mitochondrial dysfunction and metabolic changes. These activation signals induce NLRP3 inflammasome complex assembly and caspase-1 activation, which in turn cleaves pro-IL-1 β and produces mature cytokine.

IL-1 α release also requires these two signals, but the cleavage mechanism is different. The cleavage of pro-IL-1 α is known to be mediated by the calcium-dependent neutral protease, calpain-I, which cleaves IL-1 α at Phe118 into two sections, 14 kDa N-terminal piece (NTP) and 17kDa C-terminal piece (CTP) (Kobayashi et al., 1990). Moreover, in the extracellular space, granzyme B can cleave IL-1 α at Asp130 and produce a form of mature IL-1 α , which is more biologically active (Afonina et al., 2011). Pro- IL-1 α contains a nuclear localization signal (NLS), LKKRRL, which remains in the IL-1 α -NTP variant following cleavage by calpain or other proteolytic enzymes, as shown in Figure 1. Both pro-IL-1 α and IL-1 α -NTP have the ability to translocate into the nucleus (Wessendorf et al., 1993). However, it is not yet clear if a uniform mechanism exists that governs the nuclear import of pro-IL-1 α and IL-1 α -NTP across different cell types (reviewed by Di Paolo & Shayakhmetov, 2016a). Release of both cytokines has been shown to be Ca²⁺ dependent (Brough et al., 2003). IL-1 β secretion has been shown to be dependent on Ca²⁺ influx from the extracellular space and a sustained rise in cytosolic calcium (Gudipaty et al., 2003).

The pro-form of IL-1 α can be glycosylated and bound to the membrane or be released from the cells. Its attachment to the cell membrane is mediated by a lectin-like association, which can be specifically dissociated with D-mannose (Brody & Durum, 1989). The role of membrane bound IL-1 α is poorly studied. A recent study by Schunk et. al, suggested that IL-1 α mediates the adhesion of monocytes to the endothelial cells at the site of atherosclerotic plaques (Schunk et al., 2021).

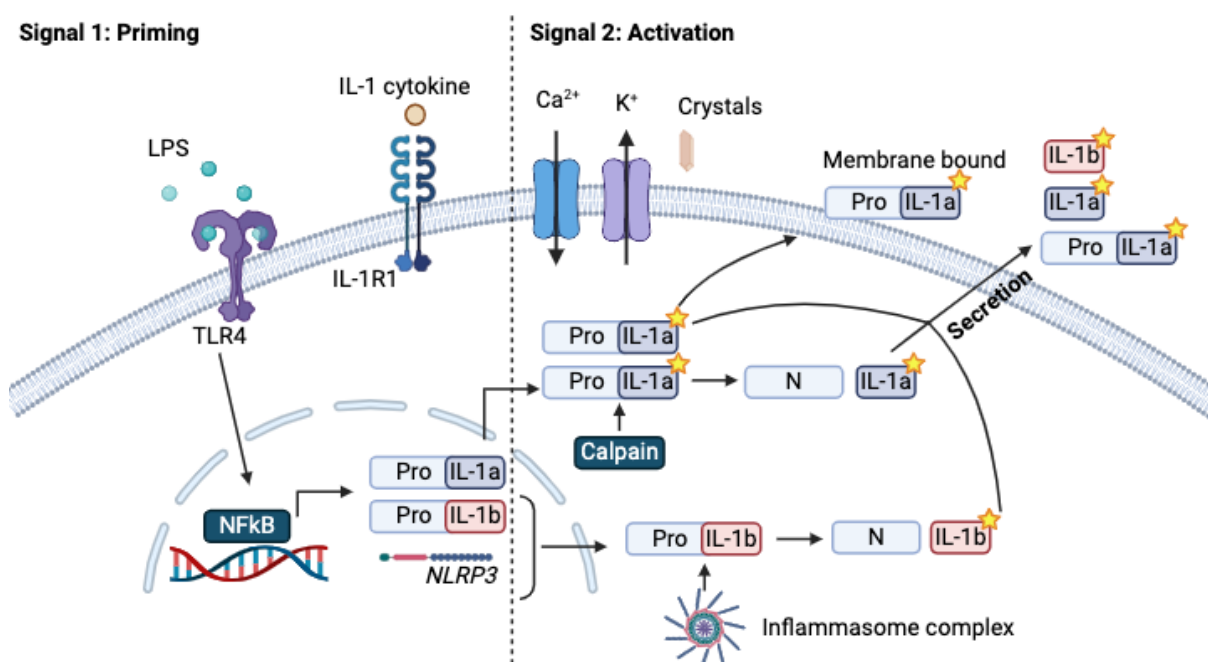


Figure 1 IL-1 α and IL-1 β release pathway.

Schematic view of IL-1 α and IL-1 β release processes from the cells. The release of IL-1 cytokines requires two steps, priming and activation. During priming, a signal through the TLR4 receptor activates the expression levels of cytokines and NLRP3 inflammasome complex. The IL-1 cytokines are expressed as pro forms and are activated and released upon a second stimulus, such as K⁺ efflux, Ca²⁺ influx or cholesterol crystals. IL-1 α is biologically active in both pro- and mature form, therefore, pro IL-1 α can bound to the membrane or be released as is, or calpain 1 can cleave the construct into a 17 kDa mature IL-1 α (C-terminal) and a 14 kDa N terminal. IL-1 β is only active after cleavage. (reviewed by Di Paolo & Shayakhmetov, 2016a; Gabay et al., 2010) (Image created by BioRender).

3.2 IL-1 and CKD disease

The precursor of IL-1 α is naturally found within the epithelial layers spanning the entire gastrointestinal tract, as well as in the lungs, liver, kidneys, endothelial cells, and astrocytes. Upon cell death via necrosis, which can happen during acute renal failure, pro-IL-1 α is released from the cells. Since the precursor form of IL-1 α is active, it triggers sterile inflammation by initiating a cascade of inflammatory responses (C.-J. Chen et al., 2007; Rider et al., 2011).

For the first time in 1983 Henderson et. al. proposed that the complications and mortality in patients with end stage CKD is associated with IL-1 α release from circulating monocytes (Henderson et al., 1983). Additionally, IL-1 gene polymorphisms have been shown to be in association with the risk of CKD and its outcomes (Braosi et al., 2012). Increased levels of IL-1 α along with IL-1RA and IL-6 is observed in plasma of CKD patients (Perlman et al., 2015). Furthermore, Salti et. al. suggested that the key molecule in renal inflammation in diabetic nephropathy is IL-1 α release from renal tubular cells, but not IL-1 β (Salti et al., 2020). Recently, a higher IL-1 α expression has been reported on the surface of CKD patients' monocytes, which correlates with a higher risk of cardiovascular events. Moreover, surface expression of IL-1 α is required for the expression of vascular cell adhesion molecule-1 (VCAM-1) on endothelial cells, therefore mediating the adhesion of monocytes and initiating the formation of atherosclerotic lesions (Schunk et al., 2021). Interestingly, using a vaccine to neutralize IL-1 α in a murine model of atherosclerosis led to reduced inflammation and the progression of atherosclerosis plaque (Tissot et al., 2013). Altogether, these studies emphasize the impact of IL-1 α expression in monocytes on CKD disease outcomes and survival.

4 Monocytes origin and subpopulations

Monocytes are essential cells of the innate immune system, which play a vital role in the body's defense mechanisms. These bone marrow derived cells constitute about 5 to 10% of the total white blood cells (Prinyakupt & Pluempitiwiriawej, 2015) and are key players in maintaining

cellular homeostasis, particularly during infections and inflammatory responses. Monocytes are between 12 to 20 μm in diameter (Espinoza & Emmady, 2023) and their half-life circulating in blood is about one to three days (Chaintreuil et al., 2023). Mature monocytes have bean-shaped nucleus, whereas immature blood monocytes have a circular nucleus (reviewed by Osman et al., 2021). In anti-microbial immunity, monocytes are key players maintaining direct responses, such as cytokine production or phagocytosis. As mentioned, patients suffering from CKD are at higher risk of cardiovascular disease and atherosclerosis is the major cause of cardiovascular complications in CKD patients (reviewed by Poznyak et al., 2022). During inflammation, monocytes migrate into the infected tissue and differentiate into resident macrophages and dendritic cells. These resident macrophages can also have pathophysiological effects in inflammatory diseases, like atherosclerosis. During the first steps of atherosclerosis, monocytes adhere to endothelial cells and migrate to the vascular intima. By internalizing modified lipids, monocytes form so called “foam cells”. The accumulation of these cells leads to pro-inflammatory cytokine production and atherosclerosis plaque formation (reviewed by Cormican & Griffin, 2020).

The development of flow cytometry in the 1970s further advanced monocyte research. Flow cytometry enabled identification of monocytes based on surface protein levels, specifically using the pattern recognition receptor CD14 and the Fc gamma III receptor CD16. Three populations of monocytes were identified: classical monocytes, which express higher CD14 and lower amounts of CD16 (CD14⁺, CD16⁻), non-classical monocytes with low expression of CD14 and higher expression of CD16 (CD14^{dim}, CD16⁺) and the intermediate subtype characterized by expressing both CD16 and CD14 (CD14⁺, CD16⁺). Circulating monocytes in humans are comprised of 85% classical monocytes, the remaining ~15% are intermediate and non-classical subtype (Wong et al., 2011). Monocyte subsets are known to display unique functional properties. A study by Koraishy et. al. suggested an increased risk of mortality in patients with low GFR is associated with monocyte counts greater than 0.56 k/cmm (Koraishy et al., 2018). Additionally, several studies reported an increased in intermediate monocytes population and its correlation with CKD complications and mortality (Heine et al., 2008; H. W. Kim et al., 2011; Lee et al., 2013; Naicker et al., 2018).

4.1 Monocyte subtypes characteristics and functions

Differences in monocytes' functional properties and their association with diseases are mainly due to differences in gene expression. Classical monocytes have been identified to participate

in phagocytosis, tissue repair and coagulation (Wong et al., 2011). They have been shown to have higher expression levels of chemokine receptors like CCR1, CCR2, CCR5, CXCR1 and CXCR2. This highlights classical subtype capability to migrate towards injured or inflamed sites (reviewed by Kapellos et al., 2019). Additionally, classical monocytes secrete the highest levels of IL-6, IL-10, CCL2 granulocyte colony-stimulating factor (G-CSF) compared to the other subtypes. They also produce pro-inflammatory molecules including IL-8, CCL3, and CCL5 (Wong et al., 2011).

Intermediate monocytes have weaker adhesion ability and higher expression of class II molecules compared to classical ones, resulting an enhanced capability of stimulating T-cells (Wong et al., 2011). Zawanda et. al. revealed that, intermediate monocytes are the main reactive oxygen species (ROS) producers (Zawada et al., 2011), while expressing cytokines at intermediate levels compared to non-classical monocytes (Wong et al., 2011). However, TNF- α and IL-1 β in response to LPS stimulation were exclusively produced by CD16 $^{+}$, CD14 $^{+}$ monocytes (Cros et al., 2010). Conversely, another study showed highest expression of these cytokines in the non-classical subtype (Wong et al., 2011).

Non-classical monocytes participate in complement and Fc gamma phagocytosis and surface adhesion (reviewed by Kapellos et al., 2019). Regarding the gene expression levels, non-classical monocytes are reported to have comparable levels to intermediate monocytes. Genes involved in cytoskeleton rearrangements have been shown to have high expressions in non-classical monocytes, which may explain their in vivo patrolling behavior and FcR-mediated phagocytosis (Wong et al., 2011).

5 Ca^{2+} signaling in monocytes.

Calcium ions (Ca^{2+}) represent secondary messengers, which play a pivotal role in a variety of cellular processes such as cell division, activation, proliferation, and apoptosis. The concentration of Ca^{2+} in the extracellular fluid (ECF) is typically ~1-2 mM and ~0.5-1 mM in the endoplasmic reticulum (ER) lumen. In contrast, the cytosolic Ca^{2+} concentration is ~ 100 nM, which is remarkably 10,000 times lower than that of the ECF. There are primarily two main pathways to increase the cytosolic [Ca^{2+}], it can be either released from internal stores like the ER and mitochondria, or as Ca^{2+} influx from the extracellular space. The most important Ca^{2+} pathways involved in monocytes activation and function are mediated by CRAC channels, TRP channels and purinergic receptors, (reviewed by Feske et al., 2015) which will be further introduced in the next section.

5.1 Store operated Ca^{2+} entry (SOCE)

In non-excitable cells, like immune cells, store operated Ca^{2+} entry (SOCE) is the primary mechanism mediating Ca^{2+} entry. Activation of several plasma membrane receptors can lead to Ca^{2+} store-depletion. Classically, this signaling is initiated by phospholipases that convert phosphatidylinositol 4,5-bisphosphate (PIP₂), a component of the cell membrane, into inositol-trisphosphate (IP₃). IP₃ binds IP₃-receptors located on the ER membrane and acting receptor operated calcium channels (reviewed by Berridge, 1993). Upon IP₃ receptor activation, ER Ca^{2+} stores are released. Low Ca^{2+} concentrations in the ER are sensed by detachment of Ca^{2+} from the EF-hand domain of STIM Ca^{2+} sensors. STIM molecules undergo conformational changes and form oligomers to activate calcium released activated calcium (CRAC) channels. The opening of CRAC channels allows Ca^{2+} entry of , leading to the activation of calcium-dependent signaling pathways and refilling the ER (reviewed by Clemens & Lowell, 2019; Kodakandla et al., 2023).

The involvement of CRAC channels in cytokine release from monocytes has not been extensively studied. One research conducted on human monocytes found that CRAC channels play a significant role in the production of ROS and the elimination of bacteria. The study revealed that while ORAI1 is mainly responsible for the CRAC current in the resting state, ORAI3 is essential in protecting the CRAC channel from oxidative damage during ROS generation *invitro* (Bogeski et al., 2010). Experiments showed that in mice with staphylococcal infections and also in human monocytes treated with bacterial peptides, the ORAI3/ORAI1 ratio was increased (Saul et al., 2016). This suggests that the coping mechanism might amplify Ca^{2+} signaling in monocytes during inflammatory responses.

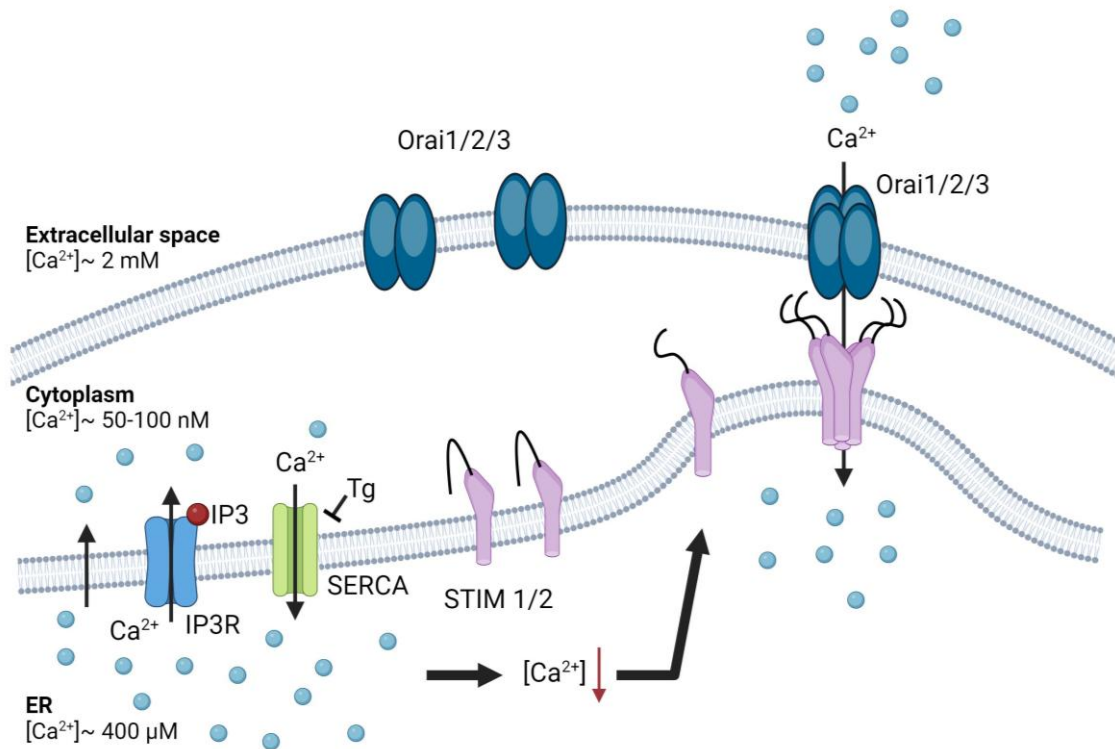


Figure 2 Store operated Ca^{2+} entry.

Under normal conditions, Ca^{2+} is transported into the ER via the SERCA pump and is released either through passive transport or by IP3 receptors (IP3R) upon the binding of IP3. When the SERCA pump is inhibited, as with Thapsigargin (Tg), or when ER Ca^{2+} levels drop, STIM proteins sense this depletion. This prompts their oligomerization and migration toward the plasma membrane, where they bind to ORAI channels, initiating Ca^{2+} influx (reviewed by Kodakandla et al., 2023) (Image created by Biorender).

5.2 TRP channels

The transient receptor potential channels (TRP channels) are a family of ubiquitously expressed non-specific cation channels. These channels consist of an intracellular N- and C- terminal and six transmembrane domains (S1-S6), with a pore forming loop located between S5 and S6. Thirty TRP channel members in mammals are categorized according to their function and amino acid sequence homology into six subfamilies: TRP ankyrin (TRPA; TRPA1), TRP canonical (TRPC; TRPC1-7), TRP melastatin (TRPM; TRPM1-8), TRP mucolipin (TRPML; TRPML1-3), TRP polycystin (TRPP; TRPP2, TRPP3, TRPP5), and TRP vanilloid (TRPV; TRPV1-6) (Santoni et al., 2015). Most TRP channels are non-selective Ca^{2+} channels with a permeability ratio of $\text{PCa}^{2+}/\text{PNa} < 10$, whereas TRPV5 and TRPV6 are highly Ca^{2+} selective ($\text{PCa}^{2+}/\text{PNa} > 100$) and TRPM4 and TRPM5 are Ca^{2+} impermeable. The TRP family of channels commonly acts as cellular sensors by responding to environmental changes such as

radiation/oxidation, chemicals, pressure, temperature, pH and osmolarity (reviewed by Kaneko & Szallasi, 2014).

The TRPA subfamily has only one member TRPA1, which is known for its role in chronic visceral inflammation and pain. Activation by nociceptive signals and sensitivity to pro-inflammatory mediators sheds light on TRPA1 together with TRPV1 as potential targets in inflammatory pain treatment (reviewed by Lapointe & Altier, 2011). Among TRPCs, TRPC3 and TRPC6 are involved in cardiac hypertrophy (Onohara et al., 2006), vascular inflammation (Weber et al., 2015), progressive kidney failure (Reiser et al., 2005), hypertension (reviewed by P. Wang et al., 2013) and cancer (D. Wang et al., 2014). The six members of TRPV subfamily are chemical and Temperature sensitive channels. TRPV1 plays a role in neurogenic inflammation and pain, specifically in burning pain sensation. A variety of stimuli can activate TRPV1 such as inflammatory mediators, vanilloid and membrane depolarization (White et al., 2011).

Within the TRPM subfamily, TRPM2, M4 and M5 are sensitive to high temperatures, in contrast to TRPM8, which is sensitive to temperatures lower than 20°C. TRPM1 is reported to act as a tumor suppressor (Santoni et al., 2015). H₂O₂-induced Ca²⁺ influx mediated by TRPM2 has been shown to induce chemokine and cytokine production in monocytes (reviewed by Syed Mortadza et al., 2015; Yamamoto et al., 2008). In another study, TRPM2 was identified as a key factor in IL-1 β maturation and secretion, by linking oxidative stress to NLRP3 inflammasome activation (Zhong et al., 2013). During tissue damage and inflammation, reactive oxygen species (ROS), H₂O₂, and NAD⁺ accumulate, and can be utilized by extracellular enzymes like CD38 and CD157 to produce ADPR, cADPR and NAADP. ADPR binds to membrane receptors like P2Ys (introduced below) and increases the [Ca²⁺]_i. Extracellular H₂O₂ is also able to pass through the cell membrane or via aquaporin water channels (AQP) and activate the TRPM2 channel. In monocytes, TRPM2 Ca²⁺ signals in response to H₂O₂, lead to focal adhesion related tyrosine kinase (Pyk2) phosphorylation and ERK activation. Ca²⁺ signals through TRPM2 can also activate the cell death pathways which activates caspase-3 activation (reviewed by Takahashi et al., 2011). Collectively, this data suggests a critical role of TRPM2 in monocyte activation and cytokine production during tissue damage and inflammation.

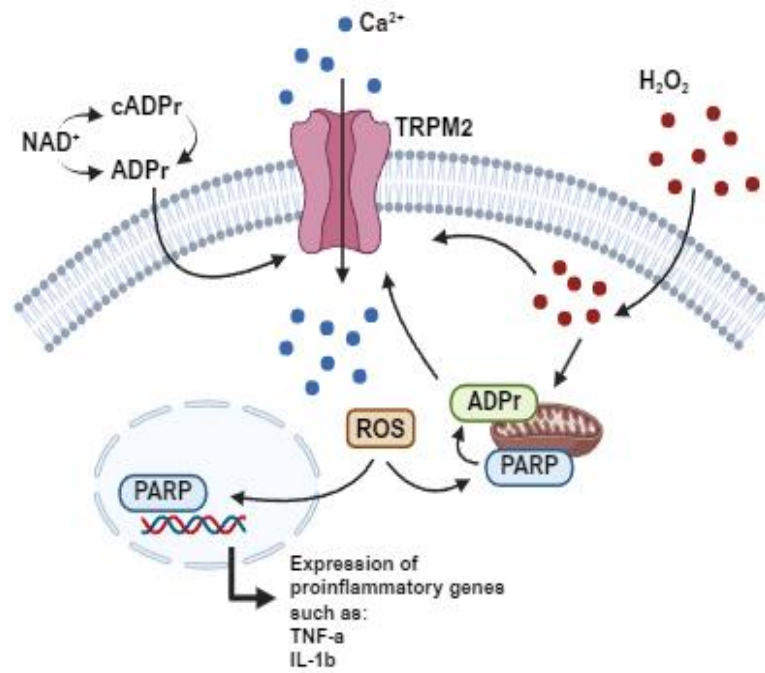


Figure 3 TRPM2 signaling pathway in immune cells.

Ros production in mitochondria is increased during inflammation, which leads to PARP activation in mitochondria or nucleus. PARP increases the production of ADPR, an activator of TRPM2 channel. When TRPM2 is activated, it mediates a Ca^{2+} influx, which results in increased ROS production. This cycle of Ca^{2+} influx and ROS production, along with Ca^{2+} signals, increases the expression of inflammatory cytokines including $\text{IL-1}\beta$ and $\text{TNF}\alpha$ (Reviewed by Zong et al., 2022) (Image created in BioRender).

5.3 Purinergic receptors

Purinergic receptors are a class of membrane-bound receptors, which play an essential role in various physiological and pathophysiological processes (Huang et al., 2021). These receptors are activated by purine nucleotides, particularly adenosine and ATP. They are broadly classified into two families: adenosine receptors P1R, and ATP receptors P2R. The P2 family is further subdivided into P2X and P2Y receptors. P2Xs are ligand-gated ion channels, while P2Ys function as G-protein-coupled receptors (Linden, 1999). Extracellular ATP has been shown to be an important immune modulator over the last 20 years. In the cytoplasm, ATP concentrations are between 1 and 10 mM, while its concentration in the extracellular space ranges between 1 and 10 nM. Therefore, upon cell damage, cell death or stress, intracellular ATP can be released to the extracellular space. In cases of acute tissue stress or damage, this increase in extracellular ATP concentrations is a signal to recruit the innate immune system and is considered as a danger signal (reviewed by Bours et al., 2011).

Expression of P2Y1, P2Y2, P2Y4, P2Y6, P2Y11, P2Y12, P2Y13, P2X1, P2X4 and P2X7 has been reported in human monocytes (L. Wang et al., 2004). ATP activates all P2Xs and P2Ys, except P2Y6 and P2Y14. Among those activated by ATP, the activation concentrations vary, as shown in Figure 4 and Table 1. ATP concentrations of ~ 0.0001 mM activate P2X1, P2X3, P2Y1, P2Y2, P2Y11 and P2Y13, while activation of P2X2, P2X4, P2Y13 and P2Y4 requires higher concentrations of ~ 0.001 mM. P2X7 requires the highest activation concentration, namely ~ 1 mM (Xing et al., 2016). Besides ATP, P2Y1, P2Y12 and P2Y13 can also be activated by ADP, whereas P2Y2 and P2Y4 are activated by Uridine triphosphate (UTP). Uridine diphosphate (UDP) is the only activator known for P2Y6 and P2Y14 is activated by both UDP and UDP-glucose (reviewed by Erb et al., 2006; Harden et al., 2010). Specific activators, $K_{1/2}$ for activation by ATP and the G protein coupled to P2Y receptors are summarized in Table 1.

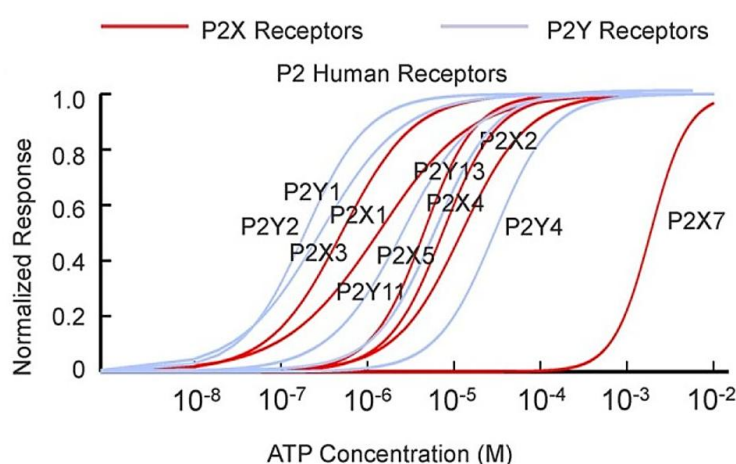


Figure 4 ATP activation concentrations of P2 family.

All P2Xs and P2Ys, except for P2Y6 and P2Y14, are activated by ATP, but with different sensitivities. This image shows the activation range of ATP concentrations for P2Xs (red) or P2Ys (blue). (Source: Xing et al., 2016)

Table 1 P2Ys activators and G proteins coupled to them.

Receptor	Agonist (human)	$K_{1/2}$ to ATP (mM)	G protein	References
P2Y1	ADP	$(3.0 \pm 0.3) \times 10^{-4}$	Gq/11	(Khan et al., 2014; Rajagopal et al., 2011; Simon et al., 1995)
P2Y2	ATP UTP	$(2.0 \pm 0.4) \times 10^{-4}$	Gq/11 GoG12	(Ivanov et al., 2007; Nicholas et al., 1996)
P2Y4	UTP	$(2.9 \pm 0.2) \times 10^{-2}$	Gq/11 Go	(Communi, Motte, et al., 1996)
P2Y6	UDP	Not activated by ATP	Gq/11	(Communi, Parmentier, et al., 1996)

P2Y11	ATP	$(5 \pm 2) \times 10^{-6}$	Gq/11 Gs	(Communi et al., 1997; Morrow et al., 2014)
P2Y12	ADP	$(3.7 \pm 0.7) \times 10^{-3}$	Gi	(reviewed by Entsie et al., 2023)
P2Y13	ADP	$(5 \pm 2) \times 10^{-3}$	Gi/o	(Dsouza & Komarova, 2021; Harden et al., 2010)
P2Y14	UDP UDP-glucose	Not activated by ATP	Gi/o	(Chambers et al., 2000)

Several signaling cascades are activated upon purinergic family activation. The detailed mechanisms of these signaling cascades for most P2Xs are not completely understood. The increased levels of cytoplasmic Ca^{2+} initiate a wide range of intracellular events by activating MAPKs, PKC and calmodulin. Activation of ERK1/2 and P38 upon P2X7 activation has been shown in astrocytes (Panenka et al., 2001). ERK1/2 activation by P2X7 has also been reported in macrophages (Aga et al., 2004), HEK cells (Amstrup & Novak, 2003), T cells (Budagian et al., 2011) and mast cells (Amores-Iniesta et al., 2017), by P2X1 in platelets (Oury et al., 2002) and in PC12 cells by P2X2 (reviewed by Swanson et al., 2019). NF κ B activation has also been reported through P2X7 in macrophages (Aga et al., 2004) and osteoclasts (Korcok et al., 2004).

As mentioned before, P2Ys are G protein coupled receptors (Table 1). The P2Y2 receptor is coupled to the G α q/11, ATP or UTP stimulation of P2Y2 activates PLC β via G α q. This results in the hydrolysis of phosphoinositol (4,5) phosphate to IP3 and DAG. IP3 induces Ca^{2+} release from the ER Ca^{2+} store and DAG activates PKC proteins (Fig. 5). In short, the activation of P2Y2 leads to activation of proto-oncogene tyrosine-protein kinase Src, followed by the activation of the PyK2. PyK2 phosphorylates growth factor receptors, which then activates the serine threonine kinases, such as ERK1/2, JNK, P38 and transcription factors such as NF κ B, c-FOS, and c-JUN. These transcription factors regulate the expression of genes mediating inflammation, apoptosis, and cell differentiation. Additionally, Src is also involved in the activation of phosphatidylinositol 3-kinase (PI3K) and protein kinase B (Akt). Inhibition of MEK1 and JNK has been shown to significantly reduce IL-1 β secretion in peritoneal monocyte-derived macrophages, while inhibition of PI3K leads to an increase in IL-1 β release (Tapia-Abellán et al., 2014). Moreover, P2Y2 activates metalloproteinases (ADAM10 and ADAM17) leading to the cleavage of EGFR ligands (reviewed by Erb et al., 2006).



5.3.1 Purinergic receptors as modulators of cytokine release

32

to release IL-1 β in response to ATP application. Higher expression of P2X7 has been shown to be associated with increased levels of IL-1 β and TNF- α in monocytes of type 2 diabetes mellitus patients (Wu et al., 2015). These results emphasize the role of P2X7 in IL-1 β release. On the other hand, the correlation between IL-1 α release and P2X7 is not well studied. Murine bone marrow derived dendritic cells showed that P2X7 dependent IL-1 β release requires the P2X4 receptor (Sakaki et al., 2013). Similarly, treating the macrophage cell line RAW264.7 with P2X4 shRNA resulted in reduced IL-1 β release from these cells (Kawano et al., 2012). Altogether these findings emphasize the role of P2 family in cytokine release and inflammation.

5.3.2 Purinergic receptors in CKD

Involvement of P2 family in renal diseases and diabetic nephropathy has been widely investigated. Tubulointerstitial inflammation, which is initiated by activation of NLRP3, is promoting the development and progression of Diabetic nephropathy (DN). The role of P2X4 mediated signaling in mediating high glucose induced activation of the NLRP3 inflammasome and IL-1 β secretion, leading to development and progression of diabetic nephropathy has been shown by (K. Chen et al., 2013). Additionally, increased P2X7 expression levels have been reported in acute kidney injury like in the renal tubes of mouse models for ischemic reperfusion injury (Y. Yan et al., 2015) or in rat models of type 1 diabetics (Vonend et al., 2004). It has been shown that inhibition of P2X7 can protect against ischemic acute kidney injury in mice (Y. Yan et al., 2015). These findings suggest the P2 family as therapeutic targets in renal diseases.

According to the findings introduced above, we hypothesize that IL-1 α expression and release from monocytes play a central role as mediators of CKD associated outcomes. To test this hypothesis, this study investigates the biogenesis and regulation of IL-1 α in monocytes derived from CKD patients. Specifically, we examine alterations in calcium signaling pathways and their influence on IL-1 α processing, including cleavage, release, and surface expression. Additionally, we explore the role of key kinases involved in these processes. To provide a broader molecular context, RNA sequencing was employed to compare gene expression profiles between monocytes from healthy donors and CKD patients, offering insights into the transcriptional changes associated with disease progression.

Material

1 Antibodies

Table 2 Primary antibodies used for western blots

Antibodies	Class/Clone	Host/Isotype	Supplier / Cat. No.	Dilution
Anti-Human IL-1 α	Polyclonal	Rabbit	Peprtech / 500-P21A	1:500
Anti-GAPDH	Monoclonal	14C10 Rabbit	Cell Signaling / 2118	1:2000
Anti- β -actin	Monoclonal	AC15 Mouse IgG1	Abcam / ab6276	1:1000
Anti-calnexin	Polyclonal	Rabbit	Enzo / SPA-865	1:1000
Anti-GFP	Monoclonal	Rabbit	Cell Signaling / 2956	1:1000
Anti-mCherry	Monoclonal	Mouse	Biorbyt / orb66657	1:1000

Table 3 Secondary antibodies used for western blot

Antibodies	Host/Isotype	Supplier / Cat. No.	Dilution
Anti-Rabbit IgG HRP linked F(ab') ₂ fragment	Donkey GE	Healthcare Amersham / NA9340	1:10000
Anti-Mouse IgG HRP linked whole Ab	Sheep GE	Healthcare Amersham / NA931	1:5000

Table 4 Antibodies used for flow cytometry.

Antigen	Fluorophore	Supplier	Order No.
CD14	APC	Biolegend	325608
CD14	PE	BD	5571540
CD16	Brilliant Violet™ 421	BD	562874
CD56	APC	BD	555518
CD3	PE-Cy7	BD	557851
CD19	PerCP-Cy5.5	BD	561295
IL-1 α	PE	Biolegend	500106
Human TruStain FcXtm	-	Biolegend	422302

2 Agonists sand antagonists.

Table 5 Agonists and antagonists

Reagent name	Target / Effect	Supplier	Order No
MRS 2365	P2Y1 agonist	Tocris	2157/1
MRS 2500 tetra-ammonium salt	P2Y1 antagonist	Tocris	2159/1
2-ThioUTP tetrasodium salt	P2Y2 agonist	Tocris	3280/1
AR-C 118925XX	P2Y2 antagonist	Tocris	4890/5
NF546	P2Y11 Agonist	Tocris	3892.10
NF340	P2Y11 antagonist	Santa Cruz	SC-361274
5-BDBD	P2X4 antagonist	Tocris	3579/10
Ivermectin	P2X4 agonist	Tocris	1260/100
BzATP triethylammonium salt	P2X7 agonist	Tocris	3312/1
A804598	P2X7 antagonist	Tocris	4473/10
Adenosine 5'-triphosphate disodium salt hydrate (ATP)	Non-selective P2 agonist	Sigma	A7699-1G
ATPγS tetralithium salt	Non hydrolysable analog of ATP	Biotechnne	4080/10
Adenosin-5'-[β,γ-imido] triphosphat Tetralithiumsals Hydrat (AMP-PNP)	Non hydrolysable analog of ATP	Sigma	A2647-5MG
Thapsigargin	SERCA inhibitor	Fisher Scientific	10226822
SB202190	MAPKp38 inhibitor	Merck /sigma	S7067-5MG
SP600125	JNK inhibitor	Merck /sigma	S5567-10MG
Hydrogen peroxide solution	TRPM2 activator	Sigma Aldrich	16911-250ML
Adenosine 5'-diphosphate sodium salt (ADP)	Purinergic receptor activator	Merck	A2754-1G
Ilomastat	MMP PAN inhibitor	MedChemExpress	HY-15768
MMP 9 in 1	MMP 9 inhibitor	MedChemExpress	HY-135232
EGTA	Extracellular Calcium chelator	Sigma Aldrich	E-4378
BAPTA-AM	Intracellular Calcium chelator	Tocris	2787/25
Calpain Inh. III	Calpain inhibitor	Calbiochem	208722-25
Wortmannin	PI3 kinase Inh.	Abcam	ab120148

PD0325901	MEK Inh.	Sigma Aldrich	PZ0162
MK-2206	AKT Inh.	Selleckchem	S1078
Caffeic acid phenethyl ester (CAPE)	NFκB Inh.	R&D	2743
Rapamycin	mTor Inh.	Merck Milipore	553210
FR180204	ERK1/2 Inh.	Biomol	Cay15544-1
Gö 6983	PKC PAN Inh.	Calbiochem	365251
Ro-31-8220	PKC PAN Inh.	Calbiochem	557521
CGP 53353	PKCβ2 Inh.	Biotechnie	373312

3 Chemicals and reagents

Table 6 Chemicals and reagents

Chemical	Supplier	Order No.
Western Blots		
Ammonium persulfate (APS)	Sigma Aldrich	248614-56
Methanol	Carl Roth	4627.5
Complete™ ULTRA Tablets, Mini, EDTA-free, EASYpack Protease Inhibitor Cocktail	Sigma Aldrich	05892791001
Sodium dodecyl sulphate (SDS)	Acros organics	327315000
Precision Plus Protein Dual Color	Bio-Rad	161-032
Tween-20	Sigma Aldrich	P1379
N,N,N',N' Tetramethylethylenediamin (TEMED)	Sigma Aldrich	T9281
Whatman™ Blotting-Papier, Cytiva	Fisher Scientific	10427806
2-Mercaptoethanol	Sigma Aldrich	M3148-250ML
Acrylamid-Bisacrylamid	Sigma Aldrich	A7168
TCA	Sigma Aldrich	522082
Skim Milk Powder 1 kg	Serva	42590.02
Agarose Broad Range	Carl Roth GmbH	T846.3
GTQ-agarose gel	Carl Roth GmbH	6352.4
No-Stain™ Protein Labeling Reagent	Invitrogen	A44449
Cell culture		
Albumin from bovine serum (BSA)	Thermo Fisher Scientific	C3100MP

Fetal calf serum (FCS)	Thermo Fisher Scientific	10270-106
Ultrapure LPS, E. coli 0111:B4	InvivoGen	tlrl-3pelps
Penicillin/Streptomycin	Sigma Aldrich	P4333
Acridine Orange / Propidium Iodide Stain	BioCat	F23001
RNA Isolation		
Ethanol	Sigma Aldrich	32205
Isopropanol	VWR	ACRO327270010
Trizol Reagent	Invitrogen	15596-026
Chloroform 99 %	Sigma Aldrich	C-2432
Bleach	Eau de Javel	
Glycogen	Fisher Scientific	10814-010
RNA dye	peqLAB	PEQL37-5000
RNA ladder	NEB	N0362S
RNA prep, cDNA synthesis and RT-PCR		
SuperScript II Reverse Transcriptase	Life Technologies	18064
RNase out	Invitrogen	10777019
dNTP mix	VWR	733-1363
Cloning		
1 Kb Plus DNA Ladder	Invitrogen	10787-018
Gel Loading Dye, Purple (6X)	NEB	B7024S
PeqGREEN DNA Dye	peqLAB	732-2960
Kanamycin	Sigma Aldrich	K0254-20ML
Ampicillin	Sigma Aldrich	A9393
Q5 High-Fidelity DNA Polymerase	NEB	M0491S
T4 DNA Ligase, 20.000u	NEB	M0202S
DreamTaq Green PCR Master Mix	Fisher Scientific	K1082
Shrimp Alkaline Phosphatase (rSAP)	NEB	M0371L
Calcium Imaging		
Fura-2AM	Invitrogen	F1221
Poly-L-ornithine hydrobromide	Sigma Aldrich	P3655

Thapsigargin (Tg)	Invitrogen	T7458
Dimethylsulfoxid (DMSO)	Sigma Aldrich	D8418-500ML
Flow cytometry		
Paraformaldehyde (PFA)	Polysciences	00380-250

Table 7 Transfection reagents

Reagent	Used for	Supplier	Order No.
Jurkat-FHCRC Cell Avalanche	DNA	EZ Biosystems	EZT-JURK-1
Hilymax	DNA	Interbiotech	FO8031
Helix-IN	DNA	Oz Biosciences	HX10100
DreamFect	DNA	Oz Biosciences	DF40500
Turbofect	DNA	Fisher Scientific	R0532
Metafectine	DNA	Biontex	T040-1.0
K2 Transfection System	DNA, mRNA	Biontex	T060-0.75
jetOPTIMUS	DNA	Polyplus	117-07
jetMESSENGER	mRNA	Polyplus	101000056
Viromer red	DNA, mRNA	Lipocalyx	VR-01LB-00
Viromer mRNA	mRNA	Lipocalyx	VmR-01LB-00
P3 Primary Cell 4D-Nucleofector® X Kit	DNA	Lonza	V4XP-3024
SF Cell Line 4D-Nucleofector™ X Kit	DNA	Lonza	V4XC-2032
SE Cell Line 4D-Nucleofector™ X	DNA	Lonza	V4XC-1032
HiScribe™ T7 ARCA mRNA Kit	mRNA	NEB	E2065S

Table 8 commercially available kits

Kits	Supplier	Order No.
BCA Protein Assay Kit	Fisher Scientific	23225
Clarity Western ECL Solution	Bio-Rad	1705060
HiSpeed Plasmid Maxiprep Kit	Quiagen	12663
QIAquick Gel extraction Kit	Quiagen	28706
QuantiTect SYBR Green PCR Kit	Qiagen	204145

QIAprep Spin Miniprep Kit	Quiagen	27106X4
Monarch® Total RNA Miniprep Kit	NEB	T2010S
Pan Monocyte Isolation Kit	Miltenyi	130-096-537
LS column	Miltenyi	130-042-401
Human IL-1 alpha/IL-1F1 DuoSet ELISA	R&D	DY200
Human IL-1 beta/IL-1F2 DuoSet ELISA	R&D	DY201
DuoSet ELISA Ancillary Reagent Kit 2	R&D	DY008
Zombie Aqua Fixable Viability Kit	Biolegend	423101
Zombie NIR™ Fixable Viability Kit	Biolegend	423105

Table 9 Supplies

Supply	Supplier
Nitrocellulose-Membrane Hybond N	Amersham Pharmacia
Sterile containers for laboratory and cell culture Falcon	BD Biosciences
Sterile disposable pipettes Falcon	Becton Dickinson Labware
Filter Tip FT 20, 200 and 1000	Peqlab and Biozyme
Petri dishes	Sarstedt
Sephadex TM G-50	Amersham Pharmacia
PVDF membrane Immobilon™-P	Millipore
S-Monovette® Lithium Heparin LH	Sarstedt

4 Buffers and medium

Table 10 Buffers used for western blots

Buffers	Composition
RIPA lysis buffer 1x	10 mM Tris pH 7.4 1 % Triton X-100 0.5 % NP40 150 mM NaCl in PBS; pH 7.5
Laemmli buffer 5x	125 mM Tris pH 6.8 0.1% Bromophenol blue 25% β-Mercaptoethanol 2.5% SDS 60% Glycerin

Inflammasome sample buffer 1 x	1 M Tris HCl pH 6.8 10 mg Bromophenol Blue 5 % β -Mercaptoethanol 2 % SDS 25% Glycerol	in H ₂ O dest.
Stacking buffer	0.5 M Tris-HCl 0.4% SDS	in H ₂ O dest; pH 6.8
Separating buffer	1.6 M Tris-HCl 0.4% SDS	in H ₂ O dest; pH 8.8
Electrophoresis running buffer	250 mM Tris 1.92 M glycine 1% SDS	in H ₂ O dest; pH 8.3
Blotting buffer 20% Methanol	250 mM Tris-HCl 1.92 M Glycin 1% SDS 20% Methanol	in H ₂ O dest; pH 8.3
Tris-buffered saline (TBS 10x)	500 mM Tris-HCl 1.5 M NaCl	in H ₂ O dest; pH 7.5
Western blot primary antibody	1% BSA 0.02% NaN ₃	in PBS
Western blot secondary antibody	5% skimmed milk in 1x TBS buffer plus 0.1% Tween	

Table 11 Cell culture buffers and media

Buffers	Composition/ Catalog number
RPMI MEDIUM 1640 (CE)	Fisher Scientific / 11530586
DPBS	Fisher Scientific / 14190094
MEM Medium	Fisher Scientific / 31095-029
Lymphocyte Separation Medium 1077	PromoCell / C-44010
HBSS, Hanks' Balanced Salt solution	H6648-6X500ML / Sigma
Erythrocyte lysis buffer	155 mM NH ₄ Cl 10 mM KHCO ₃ 0.1 mM EDTA (pH 7.3)
0-5 mM Ca ²⁺ buffer	145 mM NaCl 4 mM KCl 10 mM HEPES (pH 7.4) 10 mM Glucose

	2 mM MgCl ₂
	0/0.5/1/2/5 mM CaCl ₂
	310 mosm
	pH 7.4 (adjusted with NaOH)

Table 12 Buffers used for Flow cytometry

Buffers	Composition/ Catalog number
FACS buffer	5 % FCS 0.5 % BSA 0.07 % NaN ₃ In PBS
Sheath Fluid	BD 342003

5 Primers

Table 13 DNA oligos used in qPCR.

Identifier	Primer sequence or order number/ Supplier
Hs_P2RX1_1_SG QuantiTect Primer Assay	QT00009240 / Qiagen
Hs_P2RX4_1_SG QuantiTect Primer Assay	QT00049693 / Qiagen
Hs_P2RX7_1_SG QuantiTect Primer Assay	QT00083643 / Qiagen
Hs_P2RY1_1_SG QuantiTect Primer Assay	QT00199983 / Qiagen
Hs_P2RY2_1_SG QuantiTect Primer Assay	QT00199675 / Qiagen
Hs_P2RY4_1_SG QuantiTect Primer Assay	QT00245623 / Qiagen
Hs_P2RY6_1_SG QuantiTect Primer Assay	QT00005131 / Qiagen
Hs_P2RY11_2_SG QuantiTect Primer Assay	QT01150282 / Qiagen
Hs_P2RY12_3_SG QuantiTect Primer Assay	QT01155175 / Qiagen
Hs_P2RY13_1_SG QuantiTect Primer Assay	QT00246771 / Qiagen
Hs_P2RY14_1_SG QuantiTect Primer Assay	QT01662199 / Qiagen
Hs_POLR2A_1_SG QuantiTect Primer Assay	QT00033264 / Qiagen
Hs_TBP_1_SG QuantiTect Primer Assay	QT00000721 / Qiagen

Table 14 DNA oligos used in PCR and qPCR.

Identifier	Primer sequence or order number/ Supplier
Human pro IL-1 α	<p>Forward with Kozak sequence and EcoRV restriction site (BAN 1618) gtacctGATATCGCCGCCACCATGGCCAAAGTTCCAGACAT</p> <p>Reverse with stop codon and EcoRV restriction site (BAN 1619) gtacctGATATCCTACGCCTGGTTTTCCAGT</p> <p>Reverse without stop codon, with EcoRV restriction site (BAN 1990) taacttGATATCCGCCTGGTTTTCCAGTATC</p> <p>Reverse without stop and with SacI restriction site (BAN 1628) gtacctGAGCTCCGCCTGGTTTTCCAGTATC</p> <p>Forward opens to insert mCherry at L141 (BAN 704) CTCAATCAAAGTATAATTTCGAG</p> <p>Reverse opens to insert mCherry at L141 (BAN 705) GGCGTCATTCAGGATGAATT</p> <p>Forward with Kozak and SmaI restriction site (BAN 2027) gtacctCCCGGGGGCCGCCACCATGGCCAAAGTTCCAGACAT</p>
Pro hIL-1 α opens to insert GFP at N102	<p>Forward (BAN 1624): AATGACTCAGAGGAAGAAATC</p> <p>Reverse (BAN 1623): GGCGATGGCCTCCAGGT</p>
Pro hIL-1 α opens to insert mCherry at E133	<p>Forward (BAN 1626): TTCATCCTGAATGACGCCC</p> <p>Reverse (BAN 1627): TTCGTATTTGATGATCCTCATA</p>
mCherry/GFP	<p>Forward with SacI restriction site (BAN 1629) gtacctGAGCTCATGGTGAGCAAGGGCGAG</p> <p>Reverse with stop codon and with SacI restriction site (BAN 1630) gtacctGAGCTCctaCTTGTACAGCTCGTCCATG</p>

6 Equipments

Table 15 Used equipment

Equipment	Manufacturer
4D-Nucleofector™ X Unit	Lonza
Thermocycler, PeqSTAR	VWR Peqlab
Vortex thriller	Peqlab
Water bath A100	Lauda

NanoDrop One Microvolume UV-Vis spectrophotometer	Thermo Fisher Scientific
Microscope Ax10	Zeiss
Master cycler Personal 5332	Eppendorf
M200 Plate Reader	Tecan
Centrifuge Mikro 220R	Hettich
Centrifuge Mini Spin 5452	Eppendorf
Centrifuge Universal 32 R	Hettich
Centrifuge FACS	Eppendorf
ChemiDoc™ XRS	BioRad
FACSVerse	BD Bioscience
Gel electrophoresis Mini Protean Tetra Cell	BioRad
Heating Block	Bioer
Incubator Heracell 150i	Thermo Fisher Scientific
Incubator Hereaus	Thermo Fisher Scientific
LUNA-FL Dual Fluorescence Cell Counter	Logos Biosystems
Power supply Power Pac HC	BioRad
Sub-cell agarose gel electrophoresis systems	BioRad

Table 16 AXIO observer system

Machine	Manufacturer
Axio Observer A1	Zeiss
Light source: HXP 120V	Leistungselektronik JENA
filter set 21HE	Zeiss
filter set 38HE	Zeiss
filter set 46HE	Zeiss
Prime 95B sCMOS camera	Photometrics

Table 17 Ca²⁺ Imaging system

Machine	Manufacturer
Photochrome IV	Photonics
IMAGO Camera	Photonics
IX70 inverted microscope	Olympus

7 Resources

AmershamPharmacia Biotec (Freiburg, GER)
AppliChem (Darmstadt, GER)
Applied Biosystems (Foster City, USA)
BD Biosciences (Bedford, USA)
Beckman (München, GER)
Becton Dickinson Labware (Franklin Lakes, NJ, USA)
Bio-Rad Laboratories (München, GER)
Biozym (Hessisch Oldendorf, GER)
Cell signaling (Frankfurt, GER)
Eppendorf (Hamburg, GER)
Fuji (Düsseldorf, GER)
Hettich (Tuttlingen, GER)
IKA (Staufen, GER)
Infors-HT (Bottmingen, Switzerland)
Integra Bioscience (Fernwald, GER)
Invitrogen (San Diego, USA)
Merck (Darmstadt, GER)
Millipore (Schwalbach/Ts, D)
New England Biolabs (NEB) (Frankfurt, GER)
Peqlab (Erlangen, GER)
Qiagen (Hilden, GER)
Roche (Basel, CH)
Roth (Karlsruhe, GER)
Sarstedt (Nürnbrecht, GER)
Sigma (Deisenhofen, GER)
Stratagene (Heidelberg, GER)
ThermoScientific (Gert-Jan Bakkenes, GER)
Wescor (Langenfeld, GER)
Whatman (Brentford, UK)
Zeiss (Oberkochen, GER)

Methods

1 Cell Isolation and culture

1.1 PBMC Isolation

Peripheral blood mononuclear cells (PBMC) were isolated from blood samples collected in Heparin tubes. The samples from healthy subjects were donated by Saarland University personnel and CKD samples were collected from CKD patients in Internal medicine, Nephrology and Hypertension, Saarland University, Homburg. Research was approved by the local ethical committee ethic votes. For experiments where comparison with CKD donors was not needed, blood samples were provided by the Institute of Clinical Hemostaseology and Transfusion Medicine, Saarland University, Homburg under ethical approval number 83/15; FOR2289-TP6, Niemeyer/Alansary. In this case, residual blood from preparative hemapheresis kits was delivered in the LRS or Amicus chambers (Knörck et al., 2018).

PBMC isolation from whole blood was performed by Ficoll gradient centrifugation. In this technique, cells are sorted into distinct layers according to their density. The white layer at the interface between the Ficoll and plasma consists of platelets and PBMCs. The whole blood was diluted in 1:2 ratio using Hank's buffer (HBSS) and was overlaid onto 17ml of Lymphocyte Separation Medium 1077, followed by a centrifugation step at 440 rcf for 40 min at 22°C, without brake or acceleration. PBMCs were then transferred to a new falcon containing 2 ml of HBSS buffer and centrifuged at 250 rcf for 15 min. To remove the remaining erythrocytes, the pellet was incubated with 2 ml of erythrocyte lysis buffer for 2 min. After the incubation time, 48 ml of HBSS buffer was added to stop the reaction and the tube was centrifuged at 250 rcf for 10 min. Cells were stained with Acridine Orange / Propidium Iodide and counted using LUNA-FL Dual Fluorescence Cell Counter. PBMCs were used for monocyte isolation and immunophenotyping using flow cytometry techniques.

1.2 Monocyte Isolation

Monocytes were isolated from PBMCs using the Pan Monocyte Isolation Kit, following the manufacturer's instructions. This kit is designed to isolate untouched monocytes from PBMCs by an indirect magnetic labeling system. By depleting magnetically labeled cells, the kit provides a highly pure population of unlabeled monocytes. Following the manufacturer's protocol, PBMCs were resuspended in PBS containing 5% BSA (PBS/BSA) and after incubation with FcR Blocking Reagent and Biotin-Antibody Cocktail, Anti-Biotin Microbeads

were added. In case of using a higher number of cells, the volumes were adjusted accordingly. Finally, cells were loaded into a LS column, which was placed in a magnetic field pre-equilibrated with PBS/BSA in advance. Therefore, by attachment of magnetically labeled cells to the column, the flow through contains only monocytes. Isolated cells were counted using LUNA-FL and centrifuged at 250 g for 10 min. Cells were resuspended in RPMI medium containing 10% fetal calf serum (FCS), without antibiotic, and cultured at a density of 0.8×10^6 cells per 500 μ l per well, in a 24 well plate. Medium was supplemented with FCS to improve viability and efficiency of cultured monocytes and was changed to RPMI without FCS (starvation medium) and antibiotic two hours after the initial culturing. Cells were incubated overnight at 37°C and 5% CO₂.

For single cell Ca²⁺ imaging experiments, after isolation, 100000 monocytes were placed on the center of a pre-coated coverslip with 0.1 mg/ml Poly-L-Ornithine for 30 minutes in a 25 mm dish. After 10 min incubation at room temperature, 1.5 ml/dish of RPMI medium containing FCS was added, and cells were incubated for two hours at 37 °C and 5% CO₂. Then, the medium was changed to the starvation medium.

1.3 Treating and harvesting monocytes

As mentioned before, two signals are required for IL-1 α and IL-1 β release from monocytes. In the current study, cells were primed with 100 ng/ml ultrapure LPS in starvation medium and cytokine production was triggered by application of 2 mM ATP for 30 min, unless otherwise indicated. To avoid monocytes differentiation into macrophages, monocytes were kept in culture for only one overnight, unless otherwise indicated. Supernatants were collected and kept at -80°C for further analysis. Cells were harvested by application of 2 ml cold PBS buffer for 10 minutes.

To investigate the effects of different agonists and antagonists (see the results section) on ATP induced cytokine secretion, cells were treated with the substance of interest for the indicated time either before or during the LPS incubation or before ATP application as indicated in the results section. Due to its negative effect on cell viability, medium containing BAPTA-AM was exchanged before ATP application, otherwise pharmacological reagents were kept during incubation with ATP. The used pharmacological reagents and their final concentrations are listed in Table 18.

Table 18 Used concentrations of agonists, antagonists, and inhibitors.

Activity	Commercial name	Final con.	Incubation time
Purinergic receptor activator	Adenosine 5'-triphosphate disodium salt hydrate	2 mM	30 min
P2Y1 agonist	MRS 2365	100 μ M	30 min
P2Y1 antagonist	MRS 2500 tetra ammonium salt	100 μ M	30 min
P2Y2 agonist	2-ThioUTP tetrasodium salt	100 μ M	30 min
P2Y2 antagonist	AR-C 118925XX	100 μ M	30 min
P2Y11 agonist	NF546	10 μ M	30 min
P2Y11 antagonist	NF340	10 μ M	30 min
P2X4 antagonist	5BDBD	10 μ M	30 min
P2X4 agonist	Ivermectin	3 μ M	30 min
P2X7 agonist	BzATP triethylammonium salt	100 μ M	30 min
P2X7 antagonist	A804598	100 μ M	30 min
Negative Ctrl	DMSO	1%	30 min
Calcium chelator	EGTA	2 mM	30 min
Intracellular Calcium chelator	BAPTA-AM	50 μ M	30 min
Calpain Inh.	Calpain Inh. III	20 μ M	60 min
SERCA pump inhibitor	Thapsigargin	1 μ M	30 min
PI3 kinase Inh.	Wortmannin	100 nM	60 min
MEK Inh.	PD0325901	100 nM	60 min
AKT Inh.	MK-2206	100 nM	60 min
NF κ B Inh.	CAPE	50 μ M	60 min
mTor Inh.	Rapamycin	100 nM	60 min
MAPKp38 Inh.	SB202190	3 μ M	30 min
JNK Inh.	SP600125	20 μ M	30 min
ERK1/2 Inh.	FR180204	60 μ M	30 min
PKC PAN Inh.	Gö 6983	5 μ M 1 μ M	30 min
PKC PAN Inh.	Ro-31-8220	5 μ M	30 min
PKC β 2 Inh.	CGP 53353	100 μ M	30 min

MMP PAN Inh.	Ilomastat.	25 μ M	60 min
MMP9 Inh.	MMP-9-IN-1	100 μ M	60 min

1.4 Cell line cultures

Human monocytic cell lines U937 and THP-1 cells were cultured in RPMI medium, and for HEK293 cells, Minimal Essential Medium (MEM) was used. Cells were cultured at the density of 0.8×10^6 cells/ml and mediums were supplemented with 200 unit/ml penicillin-G-sodium, 100 μ g/ml streptomycin, 4 mM L-glutamine and 10 % FCS.

2 Transfection and Nucleofection

Monocytes and monocytic cell lines are described as difficult to transfect cells (Dong et al., 2020; Moradian et al., 2020). To transfect the fluorescently tagged IL-1 α plasmids into monocytes, different transfection approaches, such as various DNA chemical transfections (listed in Table 7), *invitro* synthesized mRNA chemical transfection and nucleofection were tested. Nucleofection proved to be the most successful method. During the nucleofection process, an electrical pulse permeabilizes the cell membrane facilitating DNA uptake. Nucleofection was performed using a 4D-Nucleofector™ X Unit and commercially available kits. For monocytes, $3-5 \times 10^6$ cells were resuspended in 100 μ l of P3 Primary Cell 4D-Nucleofector® X Kit with 3 μ g plasmid DNA, transferred to a Nucleocuvette™ Vessels and pulsed with the 4D-Nucleofector™ X Unit using monocytes-specific protocol (EA-100). Immediately following the pulse, medium was added to the cuvette and cells were cultured in 24 well plate in density of $1.5-2.5 \times 10^6$ cells per 1500 μ l medium, per well. Experiments were performed 24 hours post transfection. For THP-1 and U937, either the P3 primary cell kit or the SF Cell Line 4D-Nucleofector™ X Kit was used following the same procedure, but applying cell type specific pulsing protocol.

HEK cells were transfected using the jetOPTIMUS® DNA Transfection Reagent. In principle, This reagent forms positively charged complexes with plasmid DNA, which are taken up via endocytosis. For this purpose, 0.5 μ g of plasmid DNA was mixed with 50 μ l jetOPTIMUS® buffer and vortexed briefly. Then, 0.5 μ l of jetOPTIMUS® reagent was added and vortexed again. The mixture was incubated at room temperature (RT) for 10 min and then applied to 0.2×10^6 HEK cells cultured in MEM medium.

3 ELISA experiments

Enzyme-linked immunosorbent assay (ELISA) is a technique used to detect the presence of soluble substances in biological samples, based on highly specific antibody-antigen interactions. We used the so called “Sandwich ELISA” technique, in which a multi-well plate is coated with a capture antibody specific for one or more epitopes of the antigen of interest to immobilize it. After incubating the plate with samples, a secondary antibody conjugated to an enzyme or a tag was added to enable visualization and quantification of the antigen. Commercially available ELISA kits for IL-1 α , IL-1 β and the supplementary kit were used following the manufacturer’s protocol.

All steps were performed at room temperature and between each step, wells were washed 3 times with a 1x dilution of the washing buffer, provided by the kit. To obtain homogenous distribution of antigens or antibodies within the wells, the plate was placed on a plate shaker during incubations. IL-1 concentrations in the samples were calculated using the sigmoidal Four Parameter Logistic (4PL) Curve Calculator in GraphPad Prism software.

4 Protein detection using SDS gels.

4.1 TCA sample preparation

To analyze the IL-1 α release into the medium, Trichloroacetic acid (TCA) was used to precipitate the proteins, and the cytokine content was analyzed by Western blot. For protein precipitation, 200 μ l of medium was mixed with a final concentration of 20% TCA and incubated on ice for 30 min. Samples were then centrifuged for 20 min at 16000 rcf, 4°C. The supernatant was removed, and pellet was washed three times with 500 μ l ice- cold acetone and centrifugation for 5 min at 16000 rcf, 4°C. The pellets were air dried for 20 minutes and then resuspended in 30 μ l Inflammasome sample buffer. Samples were denatured for 5 min at 95 °C, vortexed, cooled down on ice then stored at -20 °C for further experiments.

4.2 Cell lysate preparation

To analyze intracellular protein content, cell pellets were collected and washed twice with PBS. Afterward, cells were resuspended in RIPA lysis buffer, supplemented with protease inhibitors cocktail, and placed in a tube shaker for an overnight at 4°C. The next day, remaining cell debris was removed by centrifugation at 15000 g for 20 min at 4°C and cleared cell lysates were collected. Total protein concentration was determined using BCA assay kit and volume

corresponding to 15 µg of protein was mixed with 5X Laemmli buffer and the samples were denatured at 65 °C for 15 min.

4.3 SDS-PAGE

Sodium dodecyl sulphate–polyacrylamide gel electrophoresis (PAGE) is a technique used for separating proteins in a mixture based on their size. The SDS detergent present in the Laemmli buffer not only denatures the secondary structure of proteins, but also adds a negative charge to the protein. The mixture of denatured and charged molecules were loaded to a polyacrylamide matrix, in a vertical chamber placed in 1X SDS running buffer. Upon application of an electrical field, negatively charged molecules migrate toward the positive pole with a speed inversely proportional to the molecular mass allowing separation.

In this study, samples from either TCA pellets or cell lysates, were loaded on acrylamide gel with 6.5% acrylamide stacking gel and a 12% separating gel. The gels were placed in a Gel electrophoresis Mini Protean Tetra Cell system from Bio-Rad and subjected to 80 V for 20 min, and then increased to 120 V.

4.4 Western Blotting

During the blotting step, proteins separated on the gel are transferred to a membrane, enabling protein identification using monoclonal or polyclonal antibodies. The blotting sandwich was prepared in a blotting cassette in the following order: one pad, two filter papers, gel containing proteins, membrane, two filter papers and another pad. The cassette was then placed in a blotting chamber, filled with blotting buffer and an electrical field was applied. Following the same principle as SDS-PAGE, negatively charged proteins from the gel move toward the positive pole and enter the membrane positioned between the gel and the filter papers.

Since mature IL-1 α is a relatively small protein, we used a PVDF membrane, a synthetic membrane with high protein binding capacity. Before blotting, the membrane was activated in methanol for 1 min. Blotting was performed using the Bio-Rad “Gel electrophoresis Mini Protean Tetra Cell” chamber with 0.35 A current for 75 min in the cold room. To avoid unspecific binding of antibody, blots were blocked for 1 hour with 5% skimmed milk and incubated overnight with the primary antibody of interest.

The day after, blots were washed 3×10 min, with 1x TBS buffer plus 0.1% Tween and incubated with secondary antibody diluted in 5% non-fat dry milk for at least 1 hour. The secondary antibody, which is conjugated to a reporter enzyme, binds to the primary antibody. Addition of

the enzyme substrate facilitates protein detection by producing a chemiluminescence signal. Then, blots were washed two times with 1x TBS buffer plus 0.1% Tween and one time with TBS, followed by incubation for 5 min with 1:1 mixture of Enhanced chemiluminescence development (ECL) buffers. ChemiDoc™ XRS System was used to detect protein signals. Protein levels were quantified by normalizing the signal intensity of the protein of interest to a housekeeping protein, such as calnexin or GAPDH. For quantification of TCA blots, signal intensities were normalized to the total protein content of each lane. To achieve this, blots were stained using “No-Stain™ Protein Labeling Reagent”. The quantification was performed using “Image Lab” software from Bio-Rad. All the Western blot buffers compositions are mentioned in Table 10 in the Material section.

5 Flow cytometry experiments

5.1 Immunophenotyping

PBMCs represent a heterogenous population including monocytes, lymphocytes (T, B, and NK cells), and dendritic cells. Immunophenotyping is a flow cytometry technique, which identifies cell types by labeling specific cell markers with fluorescent coupled antibodies. By vibrating the fluid stream containing cells, the FACS system breaks the fluid into droplets containing single cells. These components are excited by the laser and the resulting fluorescence from the labeled cell is collected using a set of emission filters and signal amplifying detectors, thus allowing cell identification. The volume of a cell is detected by a detector aligned with the light beam, so called Forward Scatter (FSC). In the perpendicular position to the light beam another detector identifies the Side Scatter (SSC), which represents the internal complexity of the cells, such as granularity or nuclear structure. Different fluorescent detectors are recruited to detect the fluorescent signals.

After PBMC and monocyte isolation, 100000 cells were washed twice with FACS buffer by centrifuging for 5 min, at 500 rcf and 4°C. Human Fc receptors (FcRs), which are expressed on cells such as monocytes, were blocked using Human TruStain FcXtm at 1:50 dilution in 25 µl FACS for 10 min at RT to prevent unspecific antibody binding. Dead cells were identified by incubating the samples with 1:500 dilution of the “Zombie Aqua Fixable Viability Kit” in FACS buffer for 15 min at RT. Fluorescently conjugated antibodies against CD14 and CD16 (monocyte markers), CD19 (B-lymphocyte marker), CD56 (marker for Natural Killer cells) and CD3 (T-lymphocyte marker) were added to the cell suspension in 1:50 dilution and incubated for 30 min. After staining/labeling cells were washed three times with 1 ml FACS buffer at 500

ref for 5 min, 4°C. The pellet was then resuspended in 300 µl of FACS buffer and analyzed using the FACSVerse flow cytometer by Becton Dickinson and BD FACSuite™ software.

To analyze IL-1α surface expression following different treatments, cells were fixed to prevent the detachment of surface-bound proteins. For this purpose, after removing the medium, cells were washed briefly with PBS and incubated with 1:500 dilution of Zombie NIR™ Fixable Viability Kit for 10 min, then fixed using PBS containing 4% Paraformaldehyde (PFA) at 4 °C for 20 min, followed by washing with PBS containing 0.1 M Glycine. Glycine inhibits the formation of protein–protein cross-linked complexes by rapidly forming cross-linked adducts with proteins or with itself, resulting in protein–glycine and glycine–glycine bonds instead (Hoffman et al., 2015). Cells were then washed twice with PBS, collected in FACS tube, and stained as described for live cell samples.

The FACSVerse is equipped with three lasers; a blue laser: 488 nm, filters: 530/30, 575/26, 670/14, 695/40, 780/60; a red laser (640 nm), filter: 660/20, 780/60; violet laser: 405 nm, filter: 450/40, 525/50). All incubation steps were performed at room temperature with minimal exposure to light. The percentage of cells expressing the protein of interest on their surface was analyzed using FlowJo software. Buffers used in FACS system are summarized in Table 12. Monocyte subtypes were identified using sequential gating, as shown in Figure 6. First, cells were arranged based on their granularity and size through SSC-area (SSC-A) and FSC area (FSC-A). Droplets and dead cells were excluded by using forward scatter height (FSC-H) vs. FSC-A gating and staining with Zombie Aqua Fixable Viability Kit, respectively. After filtering out T-cells (CD3), B cells (CD19) and NK cells (CD56), monocytes were classified based on CD14 and CD16 expression into classical, intermediate, and non-classical. To adjust the gates appropriately, fluorescence interference between channels was compensated for each set of experiments. Also, negative and positive populations for each antibody were defined using Fluorescence minus one (FMO), where samples contained all antibodies except the antibody of interest.

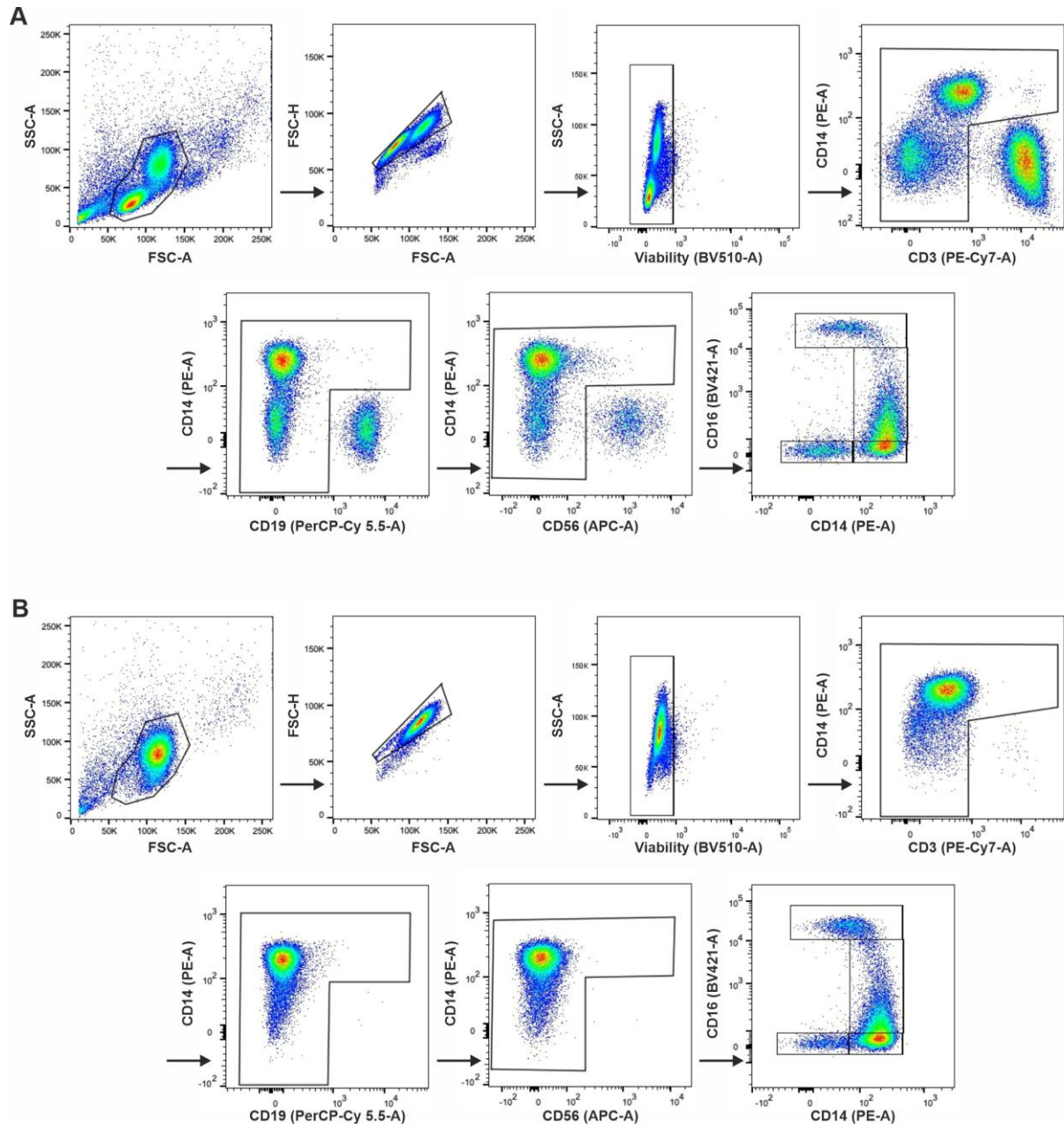


Figure 6 PBMCs and monocytes gating strategy in FACS measurements.

(A) Immunophenotyping and gating strategy of primary human PBMCs directly after isolation and (B) immunophenotyping of kit isolated monocytes obtained from the PBMCs in (A). Monocytes were first defined based on their size and granularity. After excluding doublets and dead cells, cells positive for CD3, CD19 and CD56 were excluded sequentially. Then, monocytes were gated using CD16 and CD14 markers.

6 Cloning

6.1 Polymerase Chain Reaction (PCR)

Polymerase chain reaction (PCR) is a technique for *invitro* amplification of a DNA fragment. The reaction is carried out by subjecting a mixture containing template DNA, Primers, the four deoxyribonucleoside triphosphates (dNTPs) and Taq polymerase to repetitive temperature cycles in a thermocycler. In the first step (Denaturation) double stranded DNA is denatured at 95°C, allowing cleavage of hydrogen bonds between the two DNA strands. During the Annealing phase, designed primers bind to their complementary sequence on the template DNA. The annealing temperature depends on the target DNA sequence and primarily controls the specificity of PCR. The annealing temperature can be estimated using the following equation (Farrell, 2023):

$$T_m \text{ (in } ^\circ\text{C)} = 2 \times \text{count (A, T)} + 4 \times \text{count (G, C)}$$

Finally, during the extension phase, the complementary strand is synthesized at 72 °C by Taq polymerase. At this temperature, Taq polymerase binds to DNA template and catalyzes DNA replication using dNTPs present in the PCR mixture. After each cycle, both the original DNA and the amplified PCR product of the previous cycle/cycles serve as templates for the next cycle.

The PCR reactions in this study were performed using a PeqSTAR thermocycler and the reaction mixture composition and thermal cycling conditions are provided in Table 19 and Table 20.

Table 19 The general composition of PCR mixture

Volume	
x µl	Template DNA (30-50 ng/µl)
2.5 µl	Forward primer (10 pmol/µl)
2.5 µl	Reverse primer (10 pmol/µl)
10 µl	5X High Fidelity Buffer
1µl	dNTPs (10 mM of dATP, dCTP, dGTP, dTTP)
0.5 µl	Phusion DNA polymerase
up to 50 µl	H ₂ O

Table 20 The standard program of PCR amplification

Temperature	Time	Description	Number of cycles
98°C	30 sec	Initial denaturation	1 ×
98 °C	20 sec	Denaturing phase	} 20-40 ×
T _m (56-58°C)	20 sec	Annealing phase	
72°C	20 sec/Kb	Extension phase	
72°C	10 min	Final extension	1 ×
4°C	∞	Storage	

Addition of sequence encoding recognition site of restriction endonuclease was used to enable sub-cloning of the desired DNA into expression vectors or to facilitate the fusion of a sequence encoding fluorescent proteins like GFP or mCherry to the protein of interest. Primers used in this study are listed in Table 14.

6.2 DNA analysis and purification by gel electrophoresis

Agarose gels were used for various applications, such as DNA construct identification, clone screening after colony PCR and extracting specific DNA fragment. In principle, samples are loaded into the wells of a gel stained with DNA dye and subjected to an electric current. The negatively charged DNA molecules migrate through the agarose matrix and will be separated based on their size. An intercalating dye and Ultraviolet (UV) light is used for visualizing the fragments. For this study, a 1.2% agarose gel was prepared by dissolving 0.72 gr agarose in 60 ml TAE buffer and PeqGREEN DNA Dye was used as the intercalating dye. Samples were loaded using NEB gel loading dye and a 1 Kb Plus DNA Ladder from Thermofischer was used as a molecular weight marker.

6.3 Ligation

Transferring a DNA fragment into mammalian cells is facilitated by a small circular DNA, usually bacterial plasmid, called vector. To insert the DNA of interest into a plasmid, both the plasmid and the DNA fragment are cut with the same restriction enzyme. A restriction enzyme is an endonuclease that cleaves the double strand of DNA at sites with specific sequences, producing DNA fragments with a known sequence at each end. The restriction sites are usually palindromic sequences of about 4 to 8 base pair in lengths. The resulting cut end can either have an overhang, referred to as “Sticky end”, or lack an overhang, which is called “Blunt end”. Enzymes used for cloning in this study, such as EcoRV-HF, SacI-HF, SmaI and XhoI, were

purchased from NEB and used according to the manufacturer's protocol in a reaction mixture described in Table 21. To prevent re-ligation, the plasmid ends were dephosphorylated using 2 μ l Shrimp Alkaline Phosphatase (rSAP).

Table 21 Restriction enzyme reaction mixture

Volume	
6 μ g	Plasmid or the whole PCR product
3 μ l	BSA (in case of NEB enzymes with NEB buffers number 1, 2 or 3)
3 μ l	10X NEB buffer
2 μ l	NEB Enzyme
up to 30 μ l	H ₂ O

To ligate the amplified DNA fragment to the plasmid, T4 DNA-Ligase was used in a reaction set as described in Table 22. For re-ligation control, an identical reaction mixture without the insert was prepared and samples were incubated overnight at 16 °C.

Table 22 Ligase reaction

Volume	
2 μ l	PEG 8000
1.5 μ l	Plasmid
5 μ l	Insert
1 μ l	T4 DNA-Ligase
2 μ l	T4 DNA Ligase Buffer (10X)
up to 20 μ l	H ₂ O

6.4 Competent cell preparation and transformation

For the present study, XL1-Blue subcloning grade competent cells (Stratagene) were used. For transformation, the ligation mixture was added to 50 μ l competent cells, and incubated on ice for 10 min. To induce the transformation, cells were subjected to a heat shock at 42 °C for 90 sec, followed by 2 min incubation on ice. Afterwards, 1 ml LB medium was added, and cells were incubated for at least 1 hour at 37 °C on a shaking heat block. These cultures were then centrifuged at 5000 rpm for 5 min and the pellet was resuspended in 100 μ l LB medium. Transformed competent cells were cultured on an agar plate containing the selection antibiotic corresponding to the plasmid and incubated overnight at 37 °C.

6.5 Colony PCR

Colony PCR is a technique used to screen clones growing on an agar plate after transformation, verifying both plasmid transfer and the orientation of the ligated fragment within the plasmid. For this purpose, one primer is designed for the 5' site of the insert and the second for the 3' site of the vector, or vice versa. As a result, a PCR product is obtained only if the insert has been ligated in the correct orientation. A small portion of each clone was placed directly into the PCR mixture described in Table 23 and subjected to the PCR program listed in Table 24. Afterwards, PCR product was screened via an agarose gel and clones with a band at the expected size were cultured in 5 ml LB medium overnight at 37°C with shaking.

Table 23 Colony PCR mixture

Volume	
10 µl	DreamTaq Green PCR Master Mix (2X)
1 µl	Primer 1 (10 pmol/µl)
1 µl	Primer 2 (10 pmol/µl)
8 µl	H ₂ O

Table 24 The standard protocol for colony PCR

Temperature	Time	Description	Number of cycles
98°C	3 min	Thermocycler lid heating	1×
98 °C	20 sec	Denaturing phase	} 20-40×
58°C	20 sec	Annealing phase	
72°C	1 min/kb	Extension phase	
72°C	10 min	Final extension	1×
4°C	∞	Storage	

6.6 Plasmid preparation

The recombinant DNA was extracted from selected clone cultures using Qiaprep Spin Mini Kit from Qiagen. The DNA isolation process is carried out by alkaline lysis of bacterial cells, followed by adsorption of DNA onto silica membrane in the presence of high salt concentrations. This process consists of three main steps, first preparation and clearing of bacterial lysate. During this step, the cell pellet was resuspended in resuspension buffer containing RNases to degrade RNA contaminants. After mixing thoroughly, detergent rich lysis buffer was added to lyse the cells. Then the lysate was neutralized and adjusted to high

salt binding conditions by adding the neutralizing buffer. To remove cell debris and chromosomal DNA, the mixture was centrifuged, and supernatant was retained while the pellet was discarded. The second step is DNA binding to the QIAprep membrane. In principle, the silica membrane used in QIAprep columns enables the selective adsorption of plasmid DNA in a high salt buffer and its elution in low salt buffer. Therefore, the lysate from the previous step was passed through a spin column, where the plasmid DNA bound to the membrane, while the flow-through was discarded. During the last step, which is washing and elution of plasmid DNA, a medium salt buffer is used to wash the column. After removing the residual buffer by centrifugation, the DNA was eluted using the elution buffer. The purity of DNA was assessed by measuring UV absorbance at 260/280 nm using a Nano drop system, while absorbance at 260/230 nm was used to evaluate potential contaminants.

6.7 DNA sequencing

To ensure that the cloning process was successful and that the recombinant DNA contained the correct sequence without mutations, the extracted plasmid DNA was sequenced using the commercially available sequencing services of SeqLab. The DNA samples were sent to the company, diluted in the following buffer composition.

Table 25 DNA mixture for sequencing

Volume	
1.2 µg	Plasmid DNA
3 µl	Primer (10 pmol/µl)
Up to 15 µl	H ₂ O

7 Quantitative real-time PCR

7.1 RNA isolation using kit.

To investigate mRNA expression levels in cells, RNA extraction was performed using Monarch® Total RNA Miniprep Kit, following manufacturer's protocol. In short, cell pellets were resuspended in 1X DNA/RNA Protection Reagent. Proteinase K was added to samples to prevent RNA degradation by rapidly inactivating DNases and RNases. After incubation at 55 °C for 30 min, an equal volume of RNA Lysis Buffer was added. Samples were passed through a gDNA Removal Column, and the flow through containing RNA was mixed with ethanol to precipitate RNA and DNA. The mixture was then transferred to RNA purification Column,

where RNA bound to the column and flow through was discarded. Afterwards, residual salts were removed using RNA Washing Buffer and remaining genomic DNA was eliminated by treating the sample with “DNase I” diluted in 75 µl “DNase I Reaction Buffer”. After 15 min incubation at room temperature, RNA Priming Buffer was added to the column, followed by centrifugation. The column was then washed twice with RNA washing buffer and dried by centrifugation. Maximum RNA elution was achieved by addition of 30 µl Nuclease-free water and incubation for 5 min two times, using the flow through from the first elution step (eluted RNA) for the second elution. After the final centrifugation, the quality and concentration of extracted RNA were assessed by measuring the UV absorbance using NanoDrop™ systems and RNA agarose gel electrophoresis.

7.2 RNA isolation using guanidinium thiocyanate-phenol-chloroform extraction method.

Extracting RNA from cell lines was performed using guanidinium thiocyanate-phenol-chloroform extraction method. Cultured cells were centrifuged and washed two times with PBS to remove the excessive medium. The pellet was resuspended in 800 µl Trizol containing Phenol and Guanidinium thiocyanate and stored at -80 °C. Guanidinium thiocyanate is used to lyse the cells and deactivate RNases and DNases. On the day of the experiment, samples were thawed on ice slowly and centrifuged at 12000 rcf for 10 min at 4°C. Supernatant was transferred to a new tube and incubated for 5 min at room temperature. Afterwards, 200 µl chloroform was added and samples were incubated for 2-3 min and centrifuged at 12000 rcf for 15 min at 4°C. Chloroform induces a phase separation, which isolates RNA from DNA and proteins in the sample. After centrifugation, three phases appear in the tube; proteins are located in the lowest phase, the intermediate phase contains DNA and the aqueous layer on top contains RNA. The RNA containing layer was taken to a new tube and 1 µl glycogen was added. Glycogen significantly increases the nucleic acid recovery by forming a precipitate that traps nucleic acids and forms a visible pellet easing the handling (Razak et al., 2022). Free nucleic acids were removed from precipitated RNA by addition of 500 µl Isopropanol and incubation for 10 min at room temperature. The samples were then centrifuged for 10 min, 4 °C and the supernatant was discarded. RNA pellet was washed with 1 ml of 75% ethanol, diluted in DEPC-treated H₂O and centrifuged again at 12000 rcf for 10 min. Ethanol was removed, the pellet was air dried and then dissolved in 10 µl DEPC-treated water by incubating on ice for at least 1 hour. The quality of RNA was tested as described before.

7.3 RNA gels

RNA integrity was tested using the so called “bleach agarose gel” developed by Aranda et. al. (Aranda et al., 2012). In this protocol RNases, which are present ubiquitously everywhere, are blocked by adding the commercially available bleach in agarose gel composition. An agarose gel was prepared in TAE buffer using standard protocol, and 2 % commercially available bleach was added during the cooling step. The gel was placed in a chamber containing TAE buffer and isolated RNA was loaded to the bleach gel. As described for DNA gels, maintaining an electric field causes negatively charged RNA fragments to move toward the positive pole. Gels were visualized using the UV light in ChemiDoc™ XRS system.

7.1 Reverse transcription

For expression analysis, isolated RNA was used to synthesize complementary DNA (cDNA) using a PCR cycler. During this process, reverse transcriptase enzyme uses RNA as template to produce a DNA strand complementary to the RNA strand. All the steps and reaction mixtures are summarized in Table 26. Dithiothreitol (DTT) is used to disrupt the secondary structure of RNA by breaking disulfide bonds, thereby facilitating initiation of reverse transcription. cDNA samples were then stored at -20 °C until further use for mRNA expression analysis by qPCR.

Table 26 Reverse transcription protocol

Step 1	
0.8 µg	Total RNA
1 µl	oligo-dt primers (0.5 µg/µl)
1 µl	dNTPs mixture
Up to 12 µl	H ₂ O
Annealing at 65°C for 5 min in a Master cycler	
Step 2	
2 µl	Dithiothreitol (DTT) (0.1 M)
4 µl	5x first strand buffer
1 µl	RNase OUT (RNase out Kit)
Heating for 2 min at 42°C	
Step 3	
1 µl	SupeSscript II Reverse Transcriptase
Incubation at 42°C for 50 min	

Step 4

Incubation at 72°C for 15 min

7.2 Real time PCR

The synthesized cDNA is used for Real-time PCR (RT-PCR) or quantitative PCR (q-PCR). This method allows the detection and quantification of gene expression changes using fluorescent chemical approaches. In principle, the concentration of the PCR product correlates with the fluorescence intensity, which is monitored after each cycle. First, a threshold value is set at approximately ten times more than the standard deviation of the baseline fluorescent value. The threshold cycle (Ct) is defined as the cycle at which the fluorescent signal surpasses the adjusted threshold. A gene with high expression levels correlates with an increased concentration of its cDNA template in the sample, resulting in lower Ct values. In this study, we have used QuantiTect SYBR Green PCR Kit from Qiagen. The kit contains a master mix composed of a modified form of Taq DNA polymerase, QuantiTect SYBR Green PCR Buffer, SYBR Green I, and ROX passive reference dye. The DNA polymerase is chemically modified to remain inactive at room temperature, minimizing primer dimer formation during sample preparation. The balanced combination of (NH₄)₂SO₄ and KCl in the QuantiTect SYBR Green PCR Buffer enhances the specificity of PCR and the reference dye stabilizes the baseline for normalizing PCR signals. The SYBR Green I dye fluorescent signal identifies the concentration of PCR product by binding to the minor groove of double stranded DNA. During the PCR reaction, as more double-stranded DNA is generated, SYBR Green fluorescence increases proportionally.

For each reaction, 5 µl of diluted cDNA was added to 20 µl of primer master mix, prepared as mentioned in Table 27 and Table 28, in a 96 well plate. PCR temperatures used for amplification are described in Table 29. Data was analyzed by comparing the Ct value obtained from the gene of interest to a housekeeping gene such as TBP or RNA Pol.

Table 27 Master mix for QuantiTect Primer

Volume	
12.5 µl	Qiagen (2x MM)
2.5 µl	10x Primer Assay
5 µl	H ₂ O

Table 28 Master mix for Homemade primers

Volume	
12.5 µl	Qiagen (2x MM)
0.75 µl	Primer 1
0.75 µl	Primer 2
6 µl	H ₂ O

Table 29 PCR program used for qPCR.

Temperature	Time	Description	Number of cycles
95 °C	15 min	Initial heat activation for HotStar Taq DNA Polymerase	
95 °C	30 sec	Denaturation	} 45 cycles
58 °C	30 sec	Annealing	
72 °C	30 sec	Extension	
Plate Read			
95 °C	30 sec	Denaturation	
65 °C-95 °C, increment 0.5 °C	5 sec	Melt curve	

8 Single cell Ca²⁺ imaging

Changes in intracellular Ca²⁺ concentrations ([Ca²⁺]_i) are key to a wide range of cellular signaling pathways. To investigate alterations in [Ca²⁺]_i, upon application of different stimuli, an intracellular Ca²⁺ sensitive dye, Fura-2AM, was used. Fura-2AM is a ratiometric Ca²⁺ indicator conjugated to an acetoxymethyl ester-group (AM), which provides cell permeability. Within the cytosol, cellular esterases remove the AM group, preventing Fura from diffusing out of the cell. Fura-2 has two excitation wavelengths. In absence of Ca²⁺, it has an excitation peak at 380 nm. However, when Ca²⁺ binds to Fura-2, the excitation peak shifts to 340 nm. Thus, changes in [Ca²⁺]_i can be measured by calculating the ratio of fluorescence excitation at 340 nm to that at 380 nm. The emission peak of Fura-2AM is at 510 nm and it's independent of Ca²⁺ concentrations.

For Ca²⁺ imaging experiments, cells were loaded with 1 µM Fura2-AM in medium for 30 min at 37 °C, shaking. Afterwards, the coverslip was washed twice using 0.5 mM Ca²⁺ ringer buffer and placed in a measuring chamber. The chamber was placed on an Olympus IX70 microscope. During experiments, a perfusion system was used to deliver subsequent buffers. Fura-2 was

excited every 5 sec using a Photocrome IV lamp and images were taken using a Imago camera. Data was analyzed using Axiovision software.

For store operated Ca^{2+} entry measurements, experiments began with cells resting in 0.5 mM Ca^{2+} ringer's buffer for 100 s, followed by a switch to Ca^{2+} free buffer. After 300 s, 1 μM Tg was applied to inhibit the SERCA pump, leading to the depletion of intracellular Ca^{2+} stores. Upon store depletion, STIM and ORAI channels are activated and by re-adding extracellular Ca^{2+} (700 sec later), the increase in $[\text{Ca}^{2+}]_i$ was monitored and analyzed.

For experiments involving ATP or an agonist, cells were allowed to rest in 0.5 mM Ca^{2+} ringer buffer for 150 sec before stimulus application. In the case of investigating the effect of an antagonist, cells were incubated with the antagonist of interest for 30 min at room temperature, after Fura-2AM loading.

9 Live cell fluorescent imaging

Where indicated, transfected primary monocytes or cell lines were used to study IL-1 α biogenesis using live cell fluorescent imaging technique. For this purpose, cells were cultured after transfection with corresponding plasmid in Corning low adherent plates and were treated overnight with 100 ng/ml LPS. Directly before the experiment, approximately 200000 cells were centrifuged for 3 min at 3000 rcf and resuspended in 50 μl of 0.5 mM Ca^{2+} buffer. Cells were then placed on a 25 mm coverslip coated with Poly-L-Ornithine (0.1 mg/ml). The coverslip was incubated at room temperature for 5 min to allow cell adherence, then washed with 1 ml PBS and 800 μl of 2 mM Ca^{2+} buffer was added to the imaging chamber. The chamber was placed on the imaging system. HEK cells were imaged using an Axio observer A1 from Zeiss, equipped with HXP 120V light source, a Prime 95B sCMOS camera and three filter sets: 21 HE, 38 HE and 46 HE. TIRF imaging was performed using AM TIRF MC system, which was equipped with an HCX Plan Apo oil objective 100x, Wide band suppression filter 600/40 and Wide band suppression filter 525/50, all purchased from Leica.

10 Statistical analysis

Data analyses were performed using GraphPad Prism and Microsoft Office Excel software. Data are presented as mean \pm SEM. In case of comparing between two groups, statistical significance was assessed using an unpaired two-tailed Student T-test. When comparing more than two groups, Brown-Forsythe and Welch one-way or two-way analysis of variance (ANOVA) tests were performed, followed by a multiple comparison test. In Ca^{2+} Imaging

experiment, 50-100 cells were measured, and each measurement condition was performed for several donors and for each donor at least 2 replicates were measured. Data were analyzed by averaging the means of individual measurements.

Results

1 ROS-induced Ca^{2+} signals are not altered in CKD monocytes

Changes in cytoplasmic Ca^{2+} concentration are one of the major intracellular messengers in innate immune cells (reviewed by Clemens & Lowell, 2019). Additionally, since IL-1 α cleavage is mediated by the Ca^{2+} dependent protease, calpain I, an increase in intracellular Ca^{2+} is critical for IL-1 α maturation (reviewed by Di Paolo & Shayakhmetov, 2016a). Therefore, we hypothesized that the increased IL-1 α secretion levels in monocytes from CKD patients could correlate with alterations in Ca^{2+} signaling in these cells.

The first candidate channel investigated was TRPM2 channel, which is known to have a crucial role in inflammation mediated by monocytes (Wehrhahn et al., 2010). In monocytes derived from HD or CKD, the TRPM2 channel was activated by the extracellular application of 1 mM H_2O_2 in ringer buffer containing 5 mM Ca^{2+} , and changes in $[\text{Ca}^{2+}]_i$ were observed using live cell Ca^{2+} Imaging. Extracellular H_2O_2 enters the cells by passing through the cell membrane or via aquaporin water channels (AQP), and induces calcium influx by binding to the intracellular activation domain of TRPM2 (reviewed by Syed Mortadza et al., 2015). Changes in $[\text{Ca}^{2+}]_i$ mediated by TRPM2 activation were comparable between CKD and healthy monocytes (Fig 7A, B). In correlation with Ca^{2+} imaging data, TRPM2 mRNA expression was also not significantly altered in CKD patients' monocytes (Fig. 7C).

High blood pressure is an established risk factor for CKD patients and altered expression levels of TRPC1, TRPC3 and TRPC6 have been reported in monocytes isolated from patients with high blood pressure and chronic kidney disease (Liu et al., 2011; Wuensch et al., 2010). Our expression analysis using qPCR showed almost no expression of these channels in human monocytes. Moreover, mRNA expression levels of TRPM7 and TRPV1 were also comparable between the two study groups (Fig. 7C).

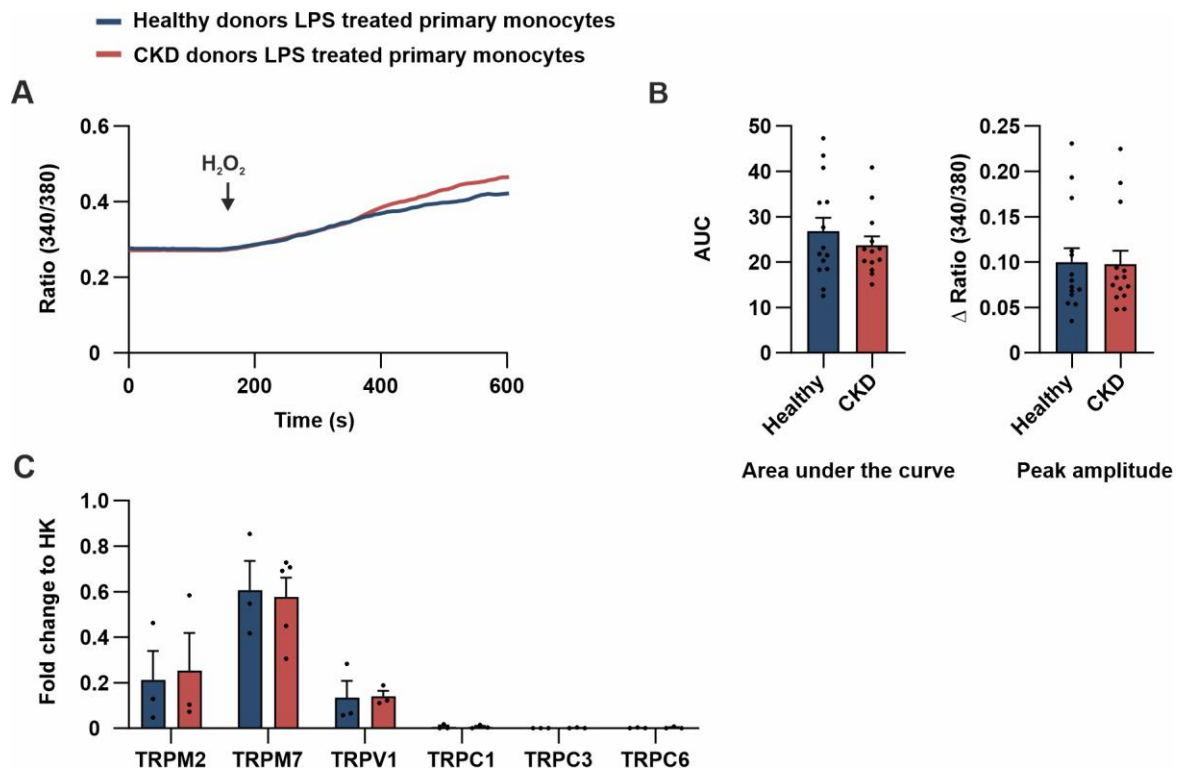


Figure 7 Ca^{2+} Signals through TRPM2 and expression levels of TRP channels are not altered in CKD monocytes.

(A) Average traces of experiments (7 healthy and 7 CKD donors, each with 2-3 replicates, total of 400 cells each) measuring $[Ca^{2+}]_i$ upon TRPM2 activation by the extracellular application of 1 mM H_2O_2 in the presence of 5 mM extracellular Ca^{2+} in monocytes isolated from CKD (red) and healthy (blue) donors. (B) Analysis of the area under the curve and peak amplitude of Ca^{2+} signals. (C) mRNA expression analysis of TRPM2, TRPM7, TRPV1, TRPC1, TRPC3 and TRPC6 (n=5). Data are shown as mean +SEM and significances were tested by unpaired t-test followed by Welch's correction test (* $P < 0.05$, ** $P < 0.01$, *** $P < 0.001$, **** $P < 0.0001$).

2 Store operated Calcium entry and expression levels of *STIM* and *ORAI* genes are comparable in monocytes derived from CKD patients or healthy subjects.

SOCE is a crucial Ca^{2+} signaling pathway in immune cells (reviewed by Clemens & Lowell, 2019). Therefore, we aimed to investigate whether SOCE is altered in monocytes isolated from CKD donors. To address this question, kit isolated monocytes were cultured overnight in serum free medium, without FCS in a non-adherent 24 well plate before measurement. The following day, cells were prepared and measured as described in the Methods section. Briefly, during SOCE measurements, first the extracellular buffer was replaced with Ca^{2+} free buffer. Then, 1 μM Tg was applied to inhibit the SERCA pump, leading to depletion of intracellular Ca^{2+} stores. Upon store depletion, STIM and ORAI channels are activated and the re-addition of extracellular Ca^{2+} triggers a massive increase in $[Ca^{2+}]_i$. Tg induced Ca^{2+} store depletion revealed comparable ER Ca^{2+} stores between CKD and healthy monocytes. Moreover, the

increase in $[Ca^{2+}]_i$ upon re-addition of extracellular Ca^{2+} was not significantly different between the control group and CKD patients (Fig. 8A, B). Consistent with the Ca^{2+} imaging data, mRNA expression analysis of *STIM* and *ORAI* showed similar expression of SOCE-related genes (Fig. 8C).

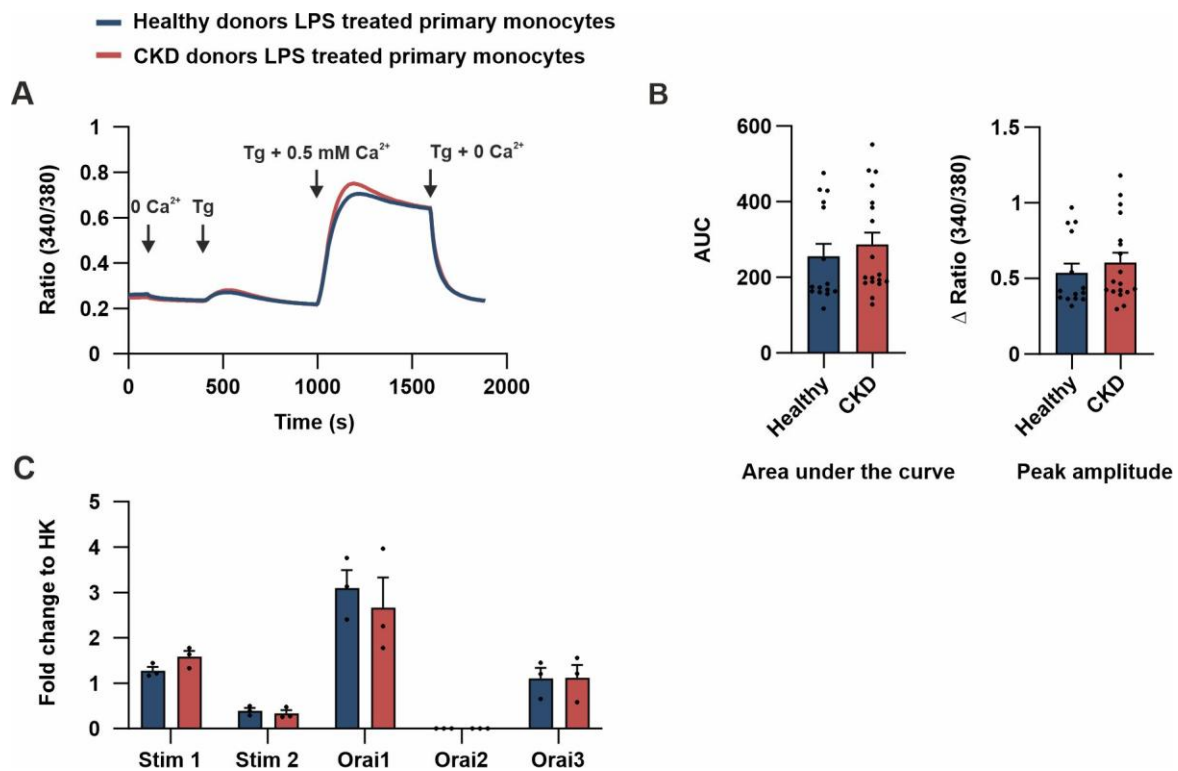


Figure 8 SOCE signaling and expression of STIM and ORAI channels is comparable in CKD and healthy monocytes.

(A) Average traces of measurements (8 healthy and 8 CKD donors each with 2-3 replicates, total of 699 and 720 cells respectively) representing $[Ca^{2+}]_i$ changes in CKD (red) and healthy (blue) monocytes in response to intracellular Ca^{2+} stores depletion by 1 μ M Tg applied in Ca^{2+} free buffer, followed by the replacement of the extracellular buffer with 0.5 mM Ca^{2+} . (B) Analysis of the area under the curve and peak amplitude of Ca^{2+} signals. (C) Expression analysis of *STIM* and *ORAI* in 3 healthy and 3 CKD donors using qPCR. Data are shown as mean +SEM and significances were tested by unpaired t-test followed by Welch's correction test (* $P < 0.05$, ** $P < 0.01$, *** $P < 0.001$, **** $P < 0.0001$).

3 Concentrations of ATP and Ca^{2+} in extracellular buffer affect ATP induced Ca^{2+} signals.

As mentioned before, the secretion process of IL-1 α and IL-1 β requires two signals. First, TLR receptors are activated by a ligand such as LPS, which leads to increased expression of essential inflammasome components and induces transcription of proinflammatory cytokines. The release of cytokines is then triggered by a second signal, such as ATP, which leads to Ca^{2+} influx or K^+ efflux (reviewed by Di Paolo & Shayakhmetov, 2016a). This is one of the main

known pathways for IL-1 α release, thus the next experiments were designed to examine the changes in $[Ca^{2+}]_i$ using this signaling pathway.

First, we examined the impact of different $[ATP]_o$ and $[Ca^{2+}]_o$ on ATP induced Ca^{2+} signals. For this purpose, we compared four different conditions:

1. 2 mM ATP applied in 0.5 mM extracellular Ca^{2+} buffer
2. 2 mM ATP applied in 2 mM extracellular Ca^{2+} buffer
3. 5 mM ATP applied in 0.5 mM extracellular Ca^{2+} buffer
4. 5 mM ATP applied in 2 mM extracellular Ca^{2+} buffer

In LPS treated U937 cells, higher Ca^{2+} concentrations in the extracellular buffer led to stronger Ca^{2+} signals in response to the same ATP concentration (comparing dark and light lines of each color in Fig. 9). By comparing Ca^{2+} signals observed from experiments where different ATP concentrations were applied in the presence of the same extracellular Ca^{2+} concentrations (comparing dark red to dark blue and light red to light blue), we observed that the application of 5 mM ATP induced lower Ca^{2+} signals compared to 2 mM ATP (Fig. 9). In general, the maximal response was observed when 2 mM ATP was applied in the presence of 2 mM extracellular Ca^{2+} . Moreover, in our experiments, the presence of 5 mM ATP for longer than 30 min showed a toxic effect on cells (data not shown).

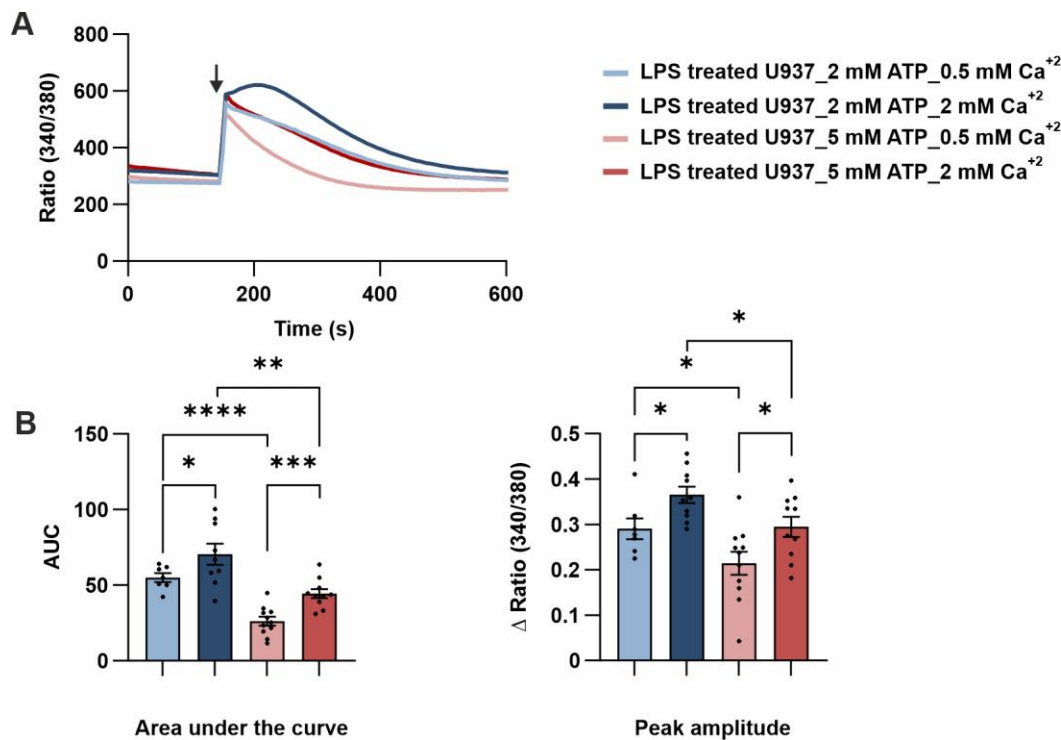


Figure 9 Ca^{2+} signals induced by ATP in U937 cells were increased by higher extracellular Ca^{2+} concentrations but decreased by higher ATP concentration.

(A) Average traces representing changes in $[\text{Ca}^{2+}]_i$ of U937 monocytic cell line and (B) the corresponding analysis of the area under the curve and peak amplitude in response to the application of: 2 mM ATP in the presence of 2 mM extracellular Ca^{2+} (dark blue) or 0.5 mM Ca^{2+} (light blue), and 5 mM ATP in the presence of 2 mM extracellular Ca^{2+} (dark red) or 0.5 mM Ca^{2+} (light red). Data are shown as mean \pm SEM and significances were tested by unpaired t-test followed by Welch's correction test (4 experimental days, each with 2-3 replicates, total of 1020 cells in condition 1, 1377 cells in condition 2, 1442 cells in condition 3 and 1478 cells in condition 4) (* $P < 0.05$, ** $P < 0.01$, *** $P < 0.001$, **** $P < 0.0001$).

To examine whether a 2 mM ATP concentration has toxic effects and therefore impacts our results, we performed experiments comparing Ca^{2+} signals induced by 2 mM and 100 μM ATP. Since the same protocol was planned for measuring IL-1 α release in the medium, which requires both LPS treatment and ATP application, the experiments were conducted in LPS treated cells. Application of 100 μM ATP induced comparable Ca^{2+} responses to 2 mM ATP application (Fig. 10). Thus, all the experiments were conducted using 2 mM ATP in the presence of 2 mM extracellular Ca^{2+} buffer.

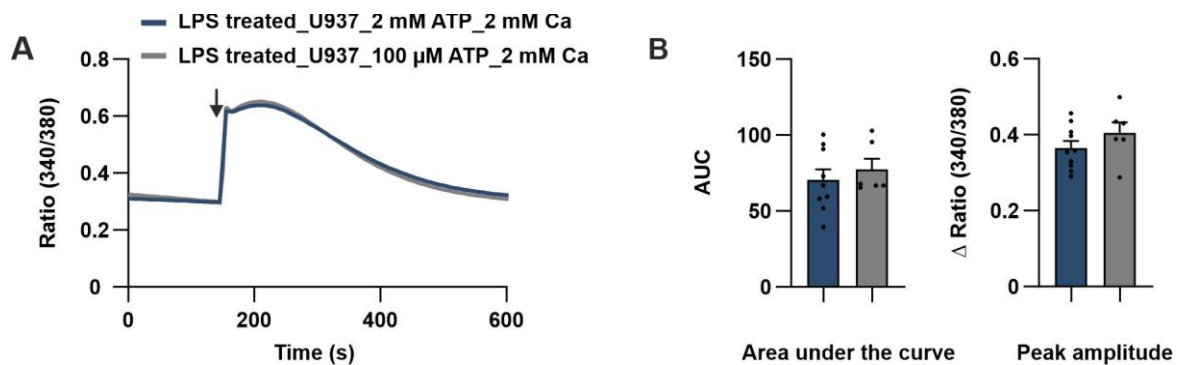


Figure 10 Ca^{2+} responses to 100 μM and 2 mM ATP are comparable in U937 cell line.

(A) Average traces representing $[\text{Ca}^{2+}]_i$ changes in response to application of 2 mM (blue) or 100 μM ATP (gray). (B) Analysis of the area under the curve and peak amplitude of Ca^{2+} signals. Data are shown as mean \pm SEM and significances were tested by unpaired t-test followed by Welch's correction test (3 experimental days each with 2 replicates, total of 800 cells) (* $P < 0.05$, ** $P < 0.01$, *** $P < 0.001$, **** $P < 0.0001$).

The same conditions were applied to primary monocytes and similar tendencies were observed, except for the fact that not all differences were significant due to the final increase in $[\text{Ca}^{2+}]$ when 5 mM ATP was applied. As in U937 cells, the highest signal was observed when 2 mM ATP was applied in the presence of 2 mM Ca^{2+} in extracellular buffer (Fig. 11).

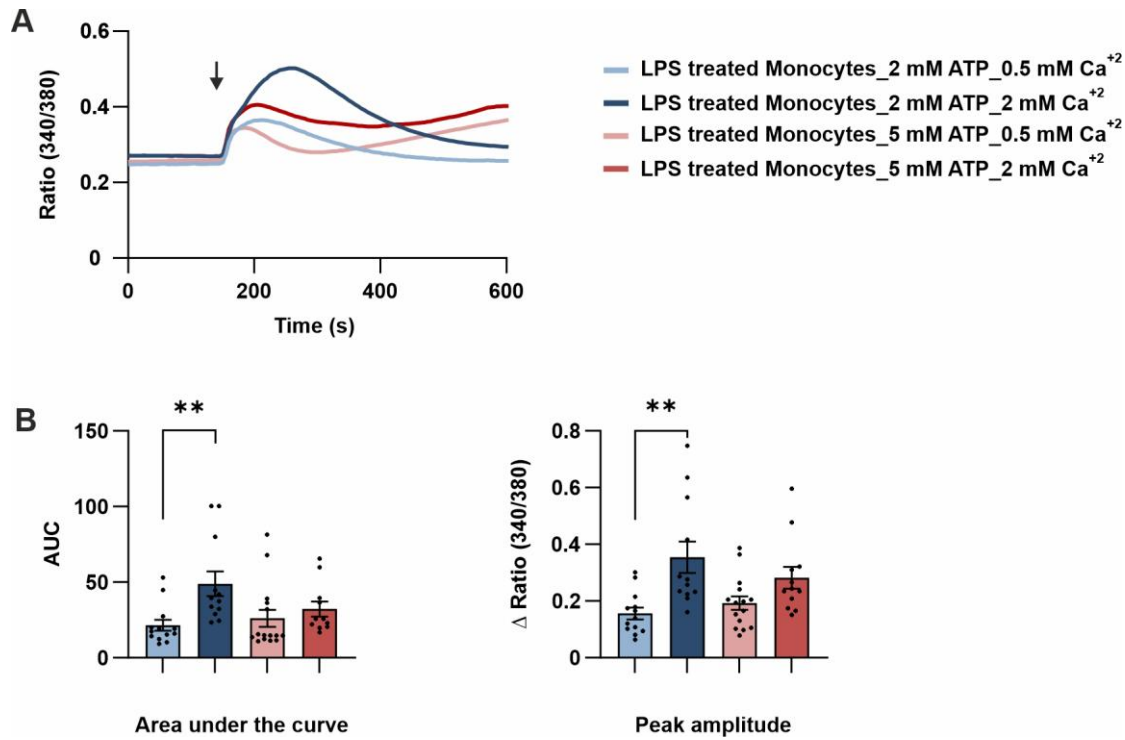


Figure 11 Ca^{2+} signals in response to different ATP concentrations and extracellular Ca^{2+} concentrations in primary human monocytes.

Average traces representing $[\text{Ca}^{2+}]_i$ changes in primary human monocytes and the corresponding analysis of the area under the curve and peak amplitude in response to the application of: 2 mM ATP in the presence of 2 mM extracellular Ca^{2+} (dark blue) or 0.5 mM Ca^{2+} (light blue) and 5 mM ATP in the presence of 2 mM extracellular Ca^{2+} (dark red) or 0.5 mM Ca^{2+} (light red). Data are shown as mean \pm SEM and significances were tested by unpaired t-test followed by Welch's correction test (5 donors each with 2-3 replicates, total of 728 cells in condition 1, 795 cells in condition 2, 1115 cells in condition 3 and 803 cells in condition 4) (* $P < 0.05$, ** $P < 0.01$, *** $P < 0.001$, **** $P < 0.0001$).

4 CKD patients' monocytes showed increased ATP induced Ca^{2+} responses.

Using optimized concentrations of applied ATP and extracellular Ca^{2+} , we aimed in the next section to compare ATP induced Ca^{2+} signals in monocytes obtained from CKD and healthy subjects. For this purpose, isolated monocytes were cultured overnight for recovery and then stimulated with 100 ng/ml LPS for 16-20 hours before measurement. Changes in $[\text{Ca}^{2+}]_i$ were measured in response to the application of 2 mM ATP in the presence of 2 mM extracellular Ca^{2+} . As shown in Figure 12, ATP application activates P2Ys, which induces a transient increase in intracellular Ca^{2+} levels from intracellular Ca^{2+} stores, followed by a second increase during the later phase of the experiment, which is mediated by Ca^{2+} entry via P2Xs activation. CKD monocytes showed a lower response during the first 200 sec after ATP application, while higher $[\text{Ca}^{2+}]_i$ was observed during the later phase (Fig. 12A, B). Changes in $[\text{Ca}^{2+}]_i$ throughout the measurement period showed significantly higher Ca^{2+} concentrations in CKD monocytes.

ATP binds to purinergic receptors, P2Xs and P2Ys (reviewed by Jacob et al., 2013), and therefore the expression levels of P2 family were investigated in both groups using qPCR. Among the investigated P2 members, a significant up-regulation of P2Y11, P2X4 and P2X7 was observed in CKD monocytes (Fig. 12C, D).

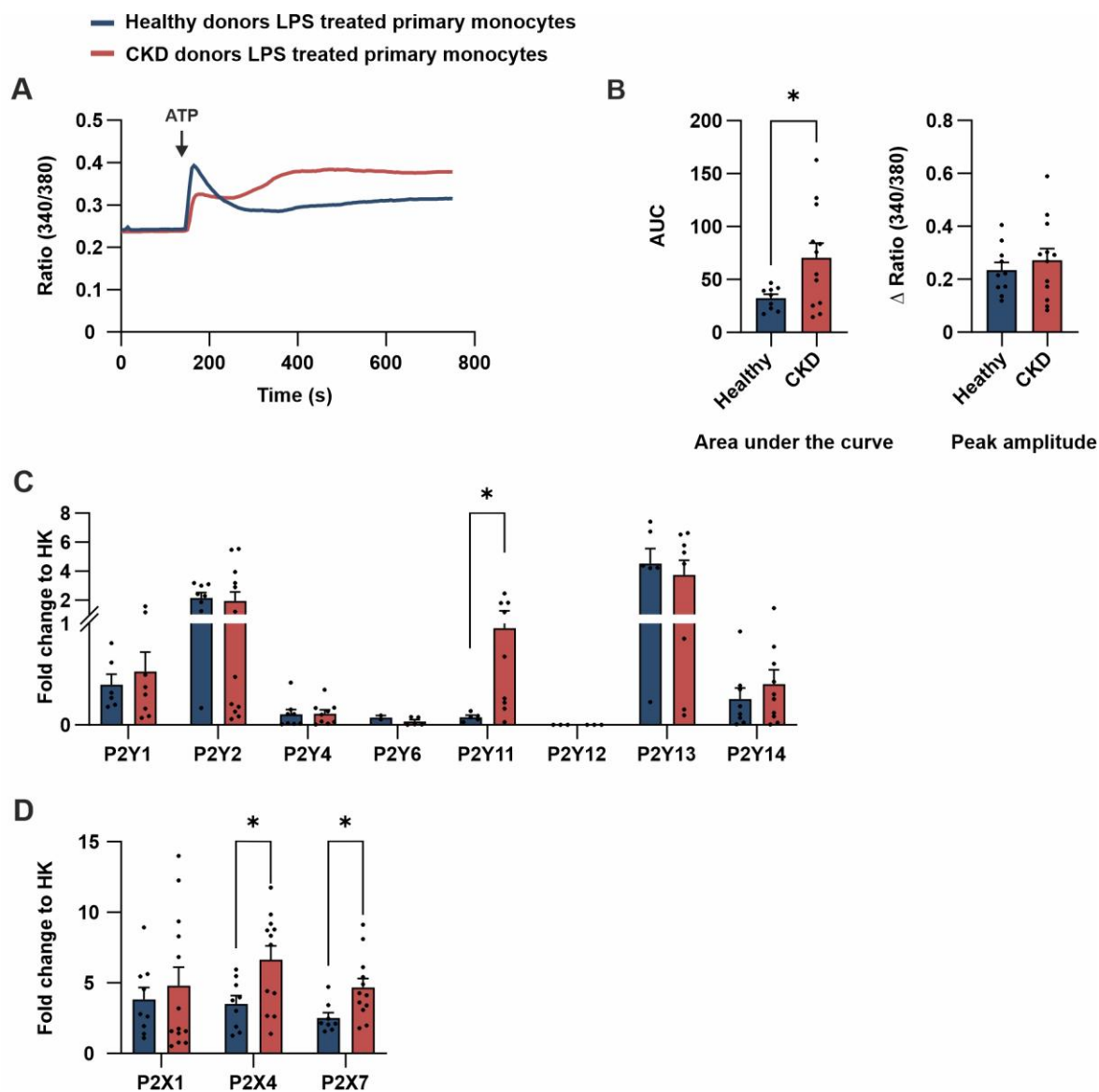


Figure 12 ATP induced Ca²⁺ signals are significantly altered in the monocytes of CKD patients.

(A) Average traces of measurements (5 healthy and 6 CKD donors each with 2-3 replicates, total of 549 and 589 cells respectively) representing [Ca²⁺]_i changes in CKD (red) and healthy (blue) monocytes in response to 2 mM ATP application in the presence of 2 mM extracellular Ca²⁺. (B) Analysis of the area under the curve and peak amplitude of Ca²⁺ signals. (C and D) Expression analysis of purinergic receptors in monocytes isolated from CKD and healthy donors using qPCR. Data are shown as mean +SEM and significances were tested by unpaired t-test followed by Welch's correction test (n=12) (* P<0.05, ** P<0.01, *** P<0.001, **** P<0.0001).

5 LPS treatment reduces ATP induced Ca^{2+} signals.

LPS stimulation, which is the first signal in the IL-1 α and IL-1 β release process, initiates several signaling pathways that result in the expression or up-regulation of many proteins. Therefore, we examined the impact of LPS stimulation on Ca^{2+} signals mediated by P2 receptors. For this purpose, changes in $[\text{Ca}^{2+}]_i$ were measured in either LPS stimulated or unstimulated primary monocytes upon application of 2 mM ATP in the presence of 2 mM Ca^{2+} . Interestingly, untreated cells showed a higher response to extracellular ATP application in both cell lines and primary monocytes (Fig. 13A, B). Analysis of mRNA expression levels revealed a significant increase in P2X4 expression and a decrease in P2Y11 expression after LPS treatment (Fig. 13C).

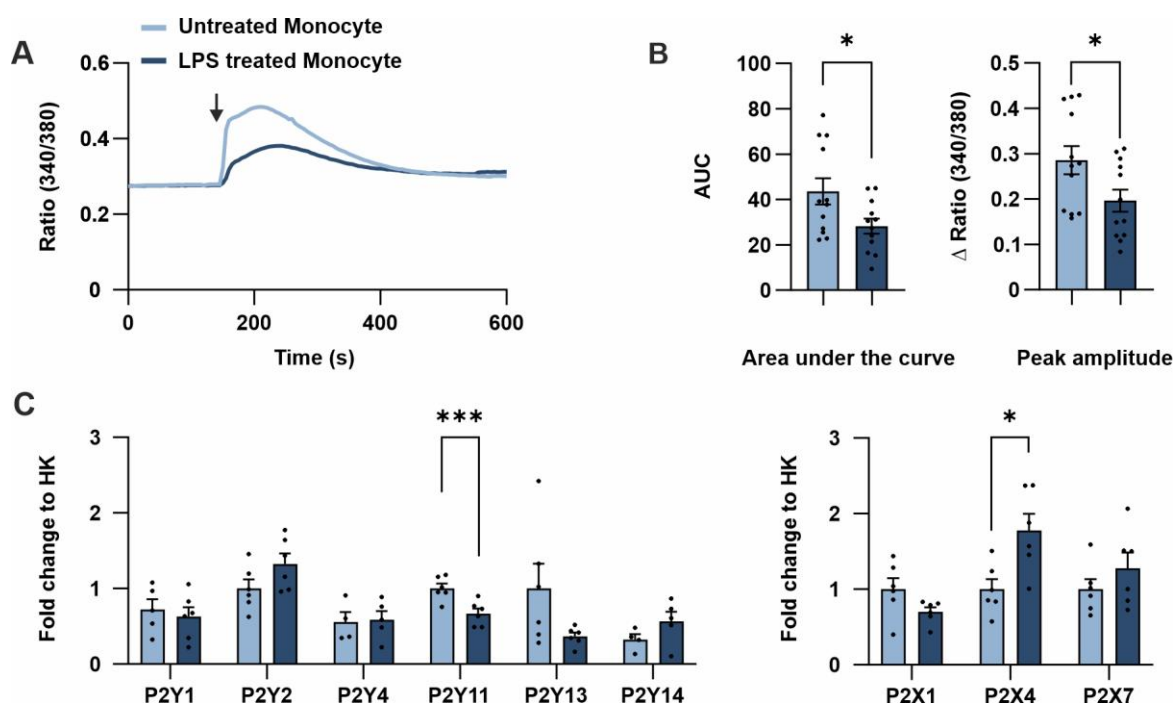


Figure 13 LPS treatment reduces the Ca^{2+} responses activated by ATP.

(A) Average traces of experiments (6 donors each with 2-3 replicates, total of 1566 untreated cells 912 LPS treated cells) representing $[\text{Ca}^{2+}]_i$ changes in primary monocytes upon application of 2 mM ATP in the presence of 2 mM Ca^{2+} in extracellular buffer. Cells were either untreated (light blue) or treated with 100 ng LPS overnight (dark blue). (B) Analysis of the area under the curve and peak amplitude of corresponding traces. (C) Expression analysis of mRNA from P2RY1, P2Y2, P2Y4, P2Y11, P2Y13, P2Y14, P2X1, P2X4 and P2X7 using qPCR. Data are shown as mean +SEM and significances were tested by unpaired t-test followed by Welch's correction test (n=6) (* $P < 0.05$, ** $P < 0.01$, *** $P < 0.001$, **** $P < 0.0001$).

6 Both intracellular Ca^{2+} release and Ca^{2+} influx are essential for ATP induced IL-1 α release

ATP activates a variety of P2Ys and P2Xs, which leads to an increase in $[\text{Ca}^{2+}]_i$ by either Ca^{2+} release from intracellular stores or Ca^{2+} influx from the extracellular space. To identify which source of Ca^{2+} is crucial for IL-1 α biogenesis and release, live cell Ca^{2+} imaging experiments were performed by applying ATP to primary monocytes resting in Ca^{2+} free buffer. In absence of Ca^{2+} in extracellular buffer, the transient increase in $[\text{Ca}^{2+}]_i$ was still observed, but the subsequent increase in Ca^{2+} levels was abolished (Fig. 14A, B). This suggests that the ATP induced Ca^{2+} signals represent the sum of intracellular release and Ca^{2+} influx.

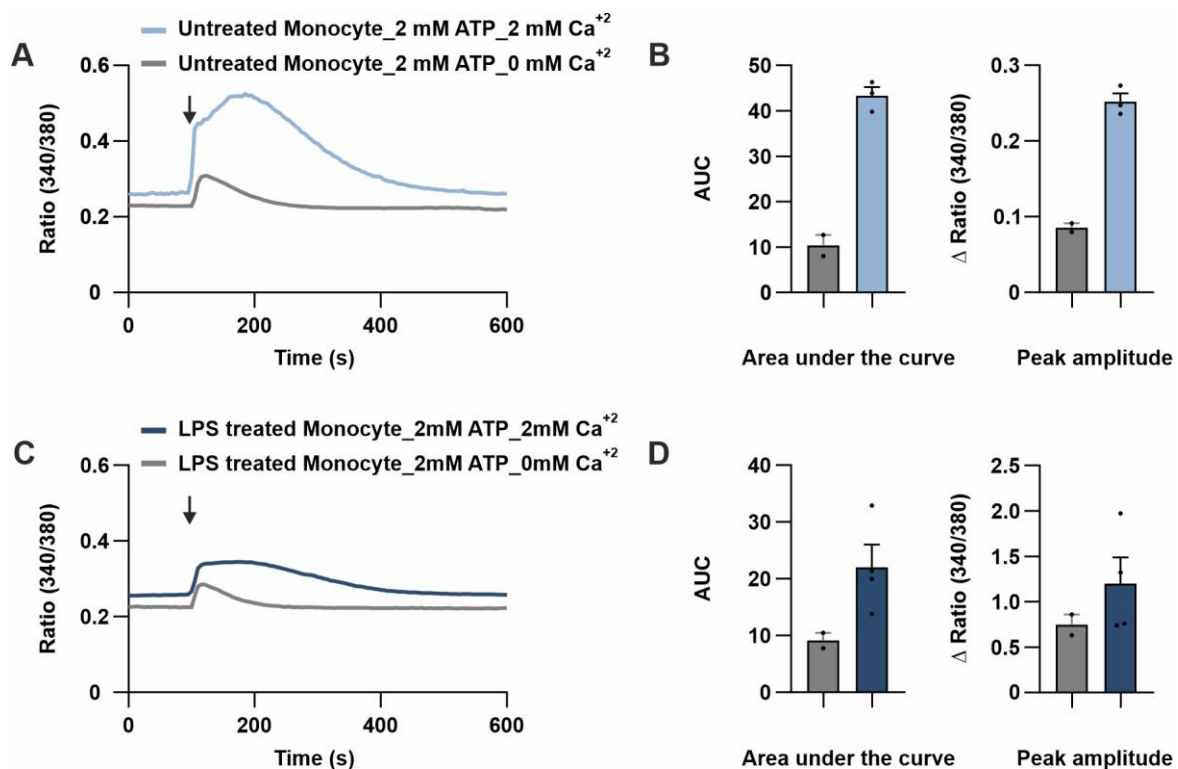


Figure 14 Absence of Ca^{2+} in extracellular buffer significantly reduces the ATP induced signals.

Average traces representing changes in $[\text{Ca}^{2+}]_i$ of untreated (A) or LPS (C) treated primary monocytes upon the application of 2 mM ATP in the presence of either 2 mM Ca^{2+} (blue) or Ca^{2+} free (grey) extracellular buffer. (B and D) Analysis of the area under the curve and peak amplitude of corresponding traces. Data are shown as mean + SEM and due to the low number of replicates, statistical significance was not tested. (2-4 experiments for each condition, including 161 untreated cells in Ca^{2+} free buffer, 100 LPS treated cells in Ca^{2+} free buffer, 606 untreated cells in 2 mM Ca^{2+} buffer, and 120 LPS treated cells in 2 mM Ca^{2+} buffer from 1 donor).

Since store depletion results in the clustering of STIM molecules, leading to the activation of ORAI channels, the experiments in the next section aimed to estimate the contribution of SOCE to the measured ATP-induced Ca^{2+} influx. To this end, the ATP-induced Ca^{2+} influx was measured in LPS primed monocytes treated with 3 μM BTP-2, a commonly used inhibitor of ORAI channels. Compared to DMSO treated control cells, inhibition of ORAI channels showed no significant effect on both LPS stimulated and unstimulated cells (Fig. 15). This data suggests that signaling through purinergic receptors is the main pathway underlying the ATP induced increase in $[\text{Ca}^{2+}]_i$ and that ATP application induces both intracellular Ca^{2+} release and Ca^{2+} influx mediated by P2Ys and P2Xs, respectively.

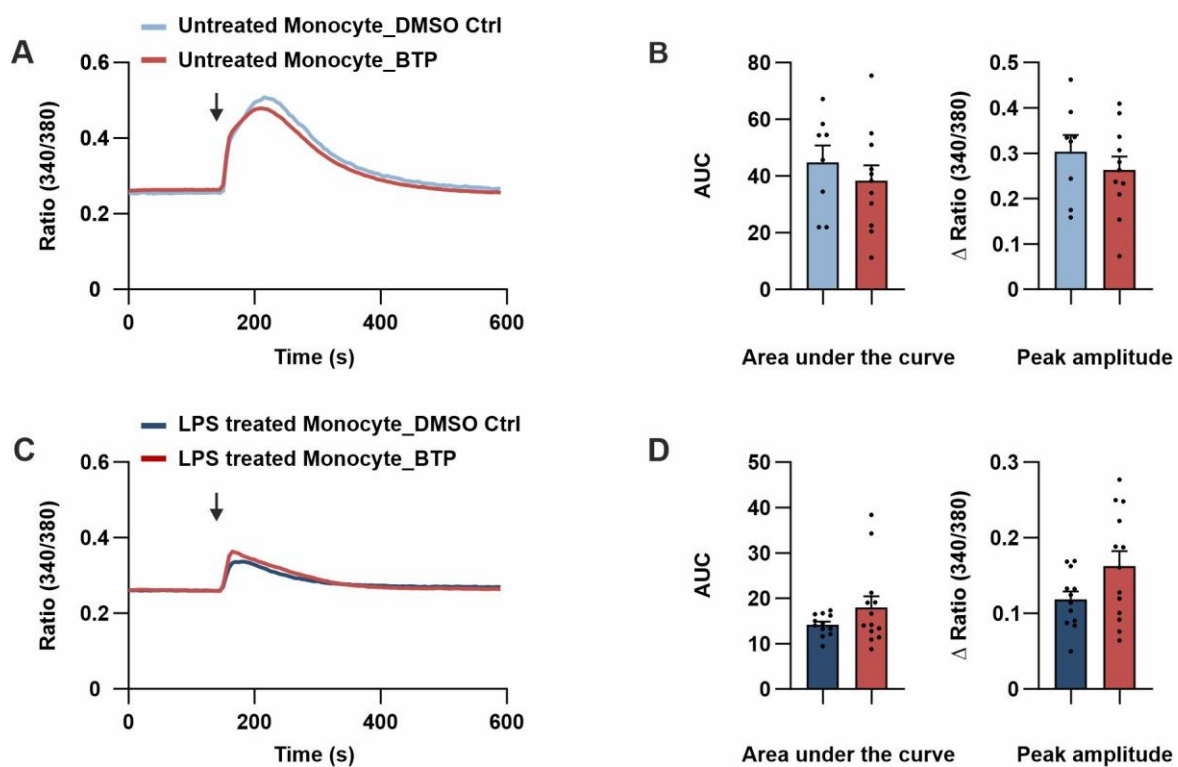


Figure 15 Store operated Ca^{2+} entry is not involved in Ca^{2+} signals in response to ATP.

Average traces representing changes in $[\text{Ca}^{2+}]_i$ in response to the 2 mM ATP application in the presence of 2 mM extracellular Ca^{2+} buffer. Prior to measurements, untreated primary monocytes (A) or LPS treated monocytes (C) were incubated with either 3 μM BTP (red traces) or v/v DMSO (blue traces). (B and D) Analysis of the area under the curve and peak amplitude of the corresponding traces. Data are shown as mean +SEM and significances were tested by unpaired t-test followed by Welch's correction test (5 donors each with 2-3 replicates, total of 881 untreated / 401 LPS treated cells with DMSO application and 1220 untreated / 462 LPS treated cells with BTP application) (* $P < 0.05$, ** $P < 0.01$, *** $P < 0.001$, **** $P < 0.0001$).

To identify the Ca^{2+} source relevant to regulation of IL-1 α release, either EGTA or BAPTA-AM were used to chelate extracellular or intracellular Ca^{2+} , respectively. ELISA measurements

revealed that chelating extracellular Ca^{2+} with EGTA had no effect on IL-1 α release, whereas chelating intracellular Ca^{2+} resulted in a significant reduction in IL-1 α levels detected in the medium (46%) (Fig. 16A). Additionally, chelating intracellular Ca^{2+} with BAPTA-AM, but not extracellular Ca^{2+} with EGTA, resulted in a significant reduction in IL-1 β release by monocytes (Fig. 16B). These results show that increased levels of intracellular $[\text{Ca}^{2+}]_i$ is essential for IL-1 α release.

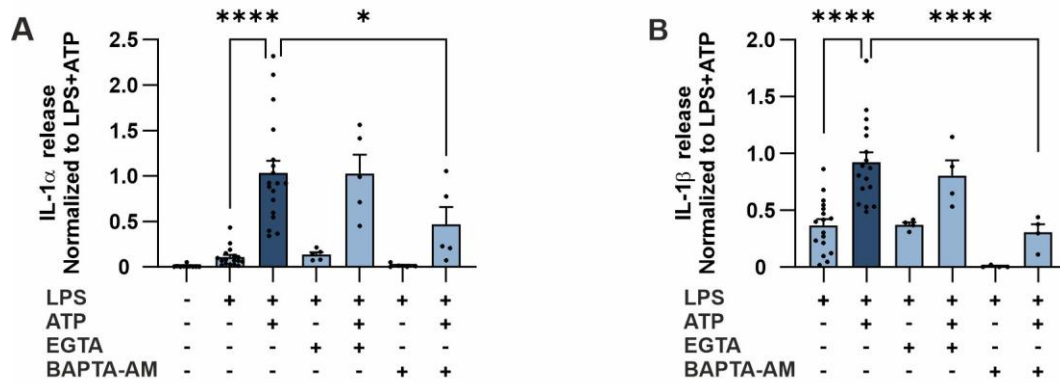


Figure 16 Increase in $[\text{Ca}^{2+}]_i$ is essential for IL-1 α and IL-1 β release.

Bar graphs representing normalized release of IL-1 α (A) and IL-1 β (B) from LPS treated primary monocytes incubated with either 2 mM EGTA or 50 μM BAPTA-AM for 30 minutes, followed by 2 mM ATP application for a further 30 minutes. Cytokine concentrations were measured by ELISA and normalized to the cytokine release in response to ATP of corresponding donor. Data represents average of 5 measurements +SEM and significances were tested by one-way ANOVA followed by Dunnett's test (n=4-17). (* $P < 0.05$, ** $P < 0.01$, *** $P < 0.001$, **** $P < 0.0001$)

To examine the effect of these changes in $[\text{Ca}^{2+}]_i$ upon ATP application on the calcium dependent cleavage of IL-1 α by calpain I, LPS primed primary monocytes were incubated with 20 μM calpain I inhibitor for 1 hour before experiments. Analyzing released IL-1 α concentrations showed a significant reduction in IL-1 α release in response to calpain inhibition (Fig. 17A). As expected, calpain inhibition did not alter IL-1 β secretion (Fig. 17B, C).

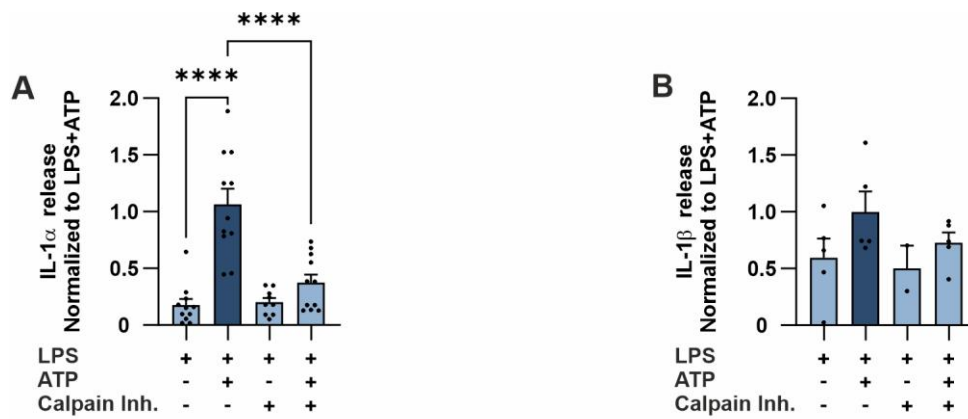


Figure 17 Calpain inhibition abolishes IL-1 α release but not IL-1 β .

Bar graphs representing the normalized release of IL-1 α (A) and IL-1 β (B) from LPS treated primary monocytes incubated with 20 μ M calpain inhibitor III for 30 minutes, followed by 2 mM ATP application for another 30 minutes. Cytokine concentrations were measured by ELISA and normalized to the cytokine release in response to ATP from the corresponding donor. Each column represents mean +SEM and significances were tested by one-way ANOVA followed by Dunnet test. (n=9-11 for IL-1 α and 2-5 for IL-1 β) (* P<0.05, ** P<0.01, *** P<0.001, **** P<0.0001).

Western blot analysis of total cell lysate showed that treating cells with calpain inhibitor did not alter the level of mature IL-1 α retained intracellularly after ATP treatment (Fig. 18). This suggests that calpain may be involved in regulating the release of IL-1 α either by cleaving the pro-form or by contributing directly to the release process of pro-IL1 α .

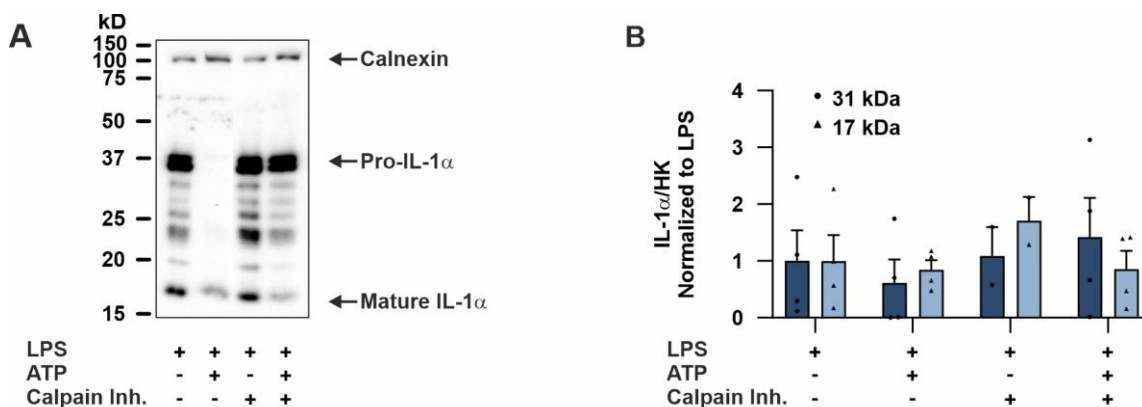


Figure 18 Calpain inhibition affects intracellular concentrations of mature IL-1 α .

Representative Western blot image of cell lysates of LPS treated primary monocytes with or without 20 μ M calpain inhibitor III incubation followed by ATP application (A). (B) Graphs representing intracellular concentrations of pro- (dark blue) and mature (light blue) IL-1 α protein in human primary monocytes from the cells treated as described in A. Protein concentrations were normalized to the housekeeping protein. To compare across treatments, all signal intensities were then normalized to the protein concentration of LPS-treated cells from the corresponding donor. Each column represents the

average of 2-4 measurements +SEM and significances were tested by two-way ANOVA followed by Bonferroni's test (* $P<0.05$, ** $P<0.01$, *** $P<0.001$, **** $P<0.0001$).

7 ATP mediated activation of P2X7 is crucial for IL-1 α release.

Although ATP is known to be an agonist for almost all P2Rs, there are other nucleotides which can activate specific members (Table 1, Fig. 5). Therefore, we measured the IL-1 α concentrations induced by nucleotides other than ATP. Interestingly, only 2 mM ATP induced IL-1 α release from LPS primed monocytes (Fig. 19A).

Different purinergic receptor subtypes are activated by specific ATP concentration (Fig. 4). The contribution of purinergic receptors to IL-1 α release from human monocytes was tested by using different ATP concentrations. For this purpose, IL-1 α release was triggered by using 1 μ M ATP (activation range of P2Y1 and P2Y2), 100 μ M ATP (activation range of P2X4, P2Y4, P2Y11 and P2Y13) and 2 mM ATP (activates P2 members, including P2X7). ATP concentrations below the activation range of P2X7 failed to induce IL-1 α release from LPS treated monocytes (Fig. 19B). These results highlight the critical role of P2X7 activation on IL-1 α secretion.

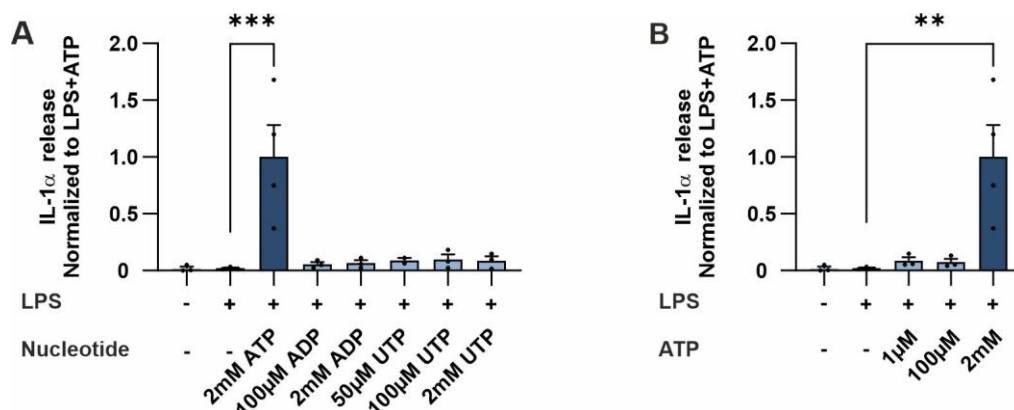


Figure 19 P2X7 activation is crucial for IL-1 α release.

Graphs representing normalized concentrations of IL-1 α released from primary human monocytes into the medium in response to: (A) different nucleotide stimuli at various concentrations and (B) different ATP concentrations to activate P2Rs based on their ATP activation threshold. Protein concentrations were normalized to the response to 2 mM ATP for the corresponding donor. Data are presented as the average of minimum 3 measurements +SEM and significances were tested by one-way ANOVA followed by Dunnett's test. (n=2-3) (* $P<0.05$, ** $P<0.01$, *** $P<0.001$, **** $P<0.0001$).

To further investigate the contribution of different P2R members to IL-1 α release and address whether this contribution is Ca^{2+} dependent, changes in $[\text{Ca}^{2+}]_i$ were measured in response to specific agonists or to ATP in cells pretreated with antagonists of P2Y2, P2X4 and P2X7. In comparison to the ATP induced Ca^{2+} signals, application of 100 μ M P2Y2 agonist could induce

only 36% increase in $[Ca^{2+}]_i$ in LPS treated cells. In contrast, in untreated cells, agonist application induced comparable Ca^{2+} response to ATP application. Furthermore, inhibition of P2Y2 in LPS treated cells led to an increase in $[Ca^{2+}]_i$, while no significant change was observed in untreated cells (Fig. 20). This suggests that signaling through P2Y2 has a greater effect on cells in resting conditions and this effect is altered in primed cells.

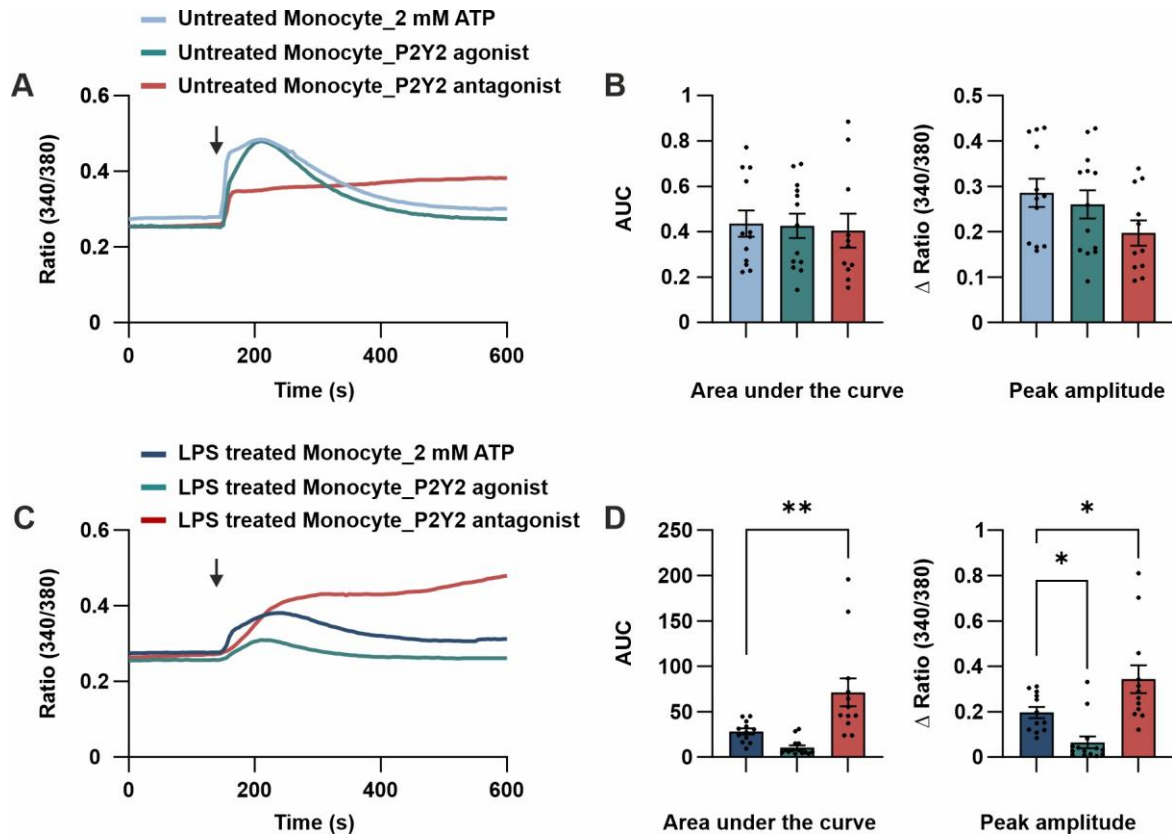


Figure 20 Effects of P2Y2 agonist and antagonist on $[Ca^{2+}]_i$ in untreated and LPS treated primary monocytes.

Average traces representing changes in $[Ca^{2+}]_i$ of primary monocytes upon the application of either 2 mM ATP (blue) or 100 μM P2Y2 agonist (green) on untreated cells (A) or LPS treated cells (C). The effect of the P2Y2 antagonist was also measured by applying 2 mM ATP in the presence of either 100 μM P2Y2 antagonist (red) or the same v/v DMSO. All measurements were performed in an extracellular buffer containing 2 mM Ca^{2+} . (B, D) Analysis of the area under the curve and peak amplitude of corresponding traces of Ca^{2+} signals. Data are shown as mean +SEM and significances were tested by one-way ANOVA followed by Dunnett's test (6 donors, a total of 1566/ 1349/ 1467 untreated and 912/ 1147/ 626 LPS treated cells were subjected to ATP/ P2Y2 agonist/ P2Y2 antagonist application) (* $P < 0.05$, ** $P < 0.01$, *** $P < 0.001$, **** $P < 0.0001$).

Next, Ca^{2+} influx induced by BzATP, a P2X7 agonist, was measured. Application of 100 μM BzATP induced 43% of ATP induced Ca^{2+} signals in LPS treated and 36% in untreated monocytes, which was significantly lower than ATP induced signals. Inhibition of P2X7

resulted in 26% reduction in ATP mediated Ca^{2+} signals in LPS treated cells and 36% in untreated cells, although these changes were not significant (Fig. 21).

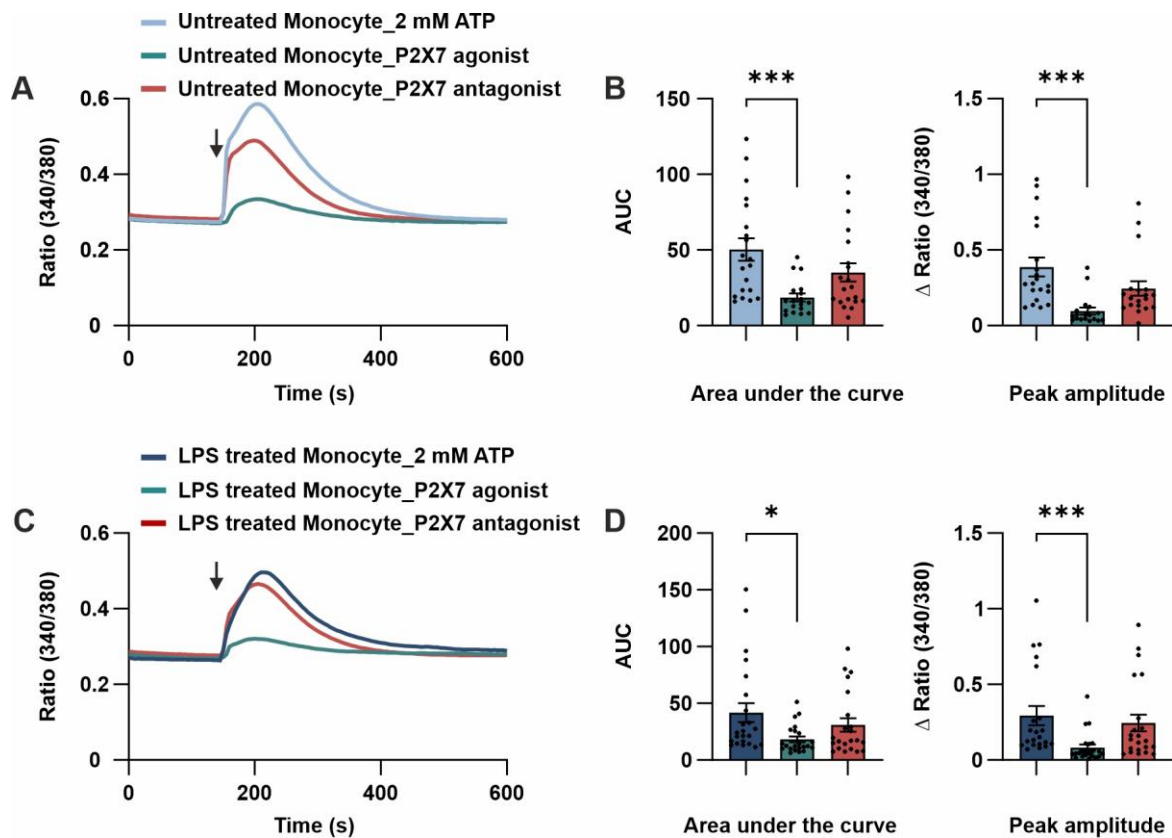


Figure 21 Effects of P2X7 agonist and antagonist on $[\text{Ca}^{2+}]_i$ in untreated and LPS treated primary monocytes.

Average traces representing changes in $[\text{Ca}^{2+}]_i$ of primary monocytes upon the application of either 2 mM ATP (blue) or 100 μM BzATP (green) to untreated cells (A) or LPS treated cells (B). The effect of the P2X7 antagonist was also measured by applying 2 mM ATP in presence of either 100 μM P2X7 antagonist (red) or the same v/v DMSO (blue). All measurements were performed in presence of 2 mM Ca^{2+} in extracellular buffer. (B, D) Analysis of the area under the curve and peak amplitude of corresponding Ca^{2+} signals traces. Data are shown as mean +SEM and significances were tested by one-way ANOVA followed by Dunnett's test (9 donors, total of 3149/ 1825/ 3110 untreated and 2146/ 2216/ 3369 LPS treated cells were subjected to ATP/ P2X7 agonist/ P2X7 antagonist application containing more than 600 cells in each condition) (* $P < 0.05$, ** $P < 0.01$, *** $P < 0.001$, **** $P < 0.0001$).

In contrast to the minor effects observed upon inhibition of P2Y2 and P2X7, a significant reduction in ATP induced Ca^{2+} peak and $[\text{Ca}^{2+}]_i$ was observed upon P2X4 inhibition in LPS treated cells, but not in untreated monocytes. Furthermore, the P2X4 agonist did not induce Ca^{2+} signals in either LPS treated or untreated monocytes (Fig. 22).

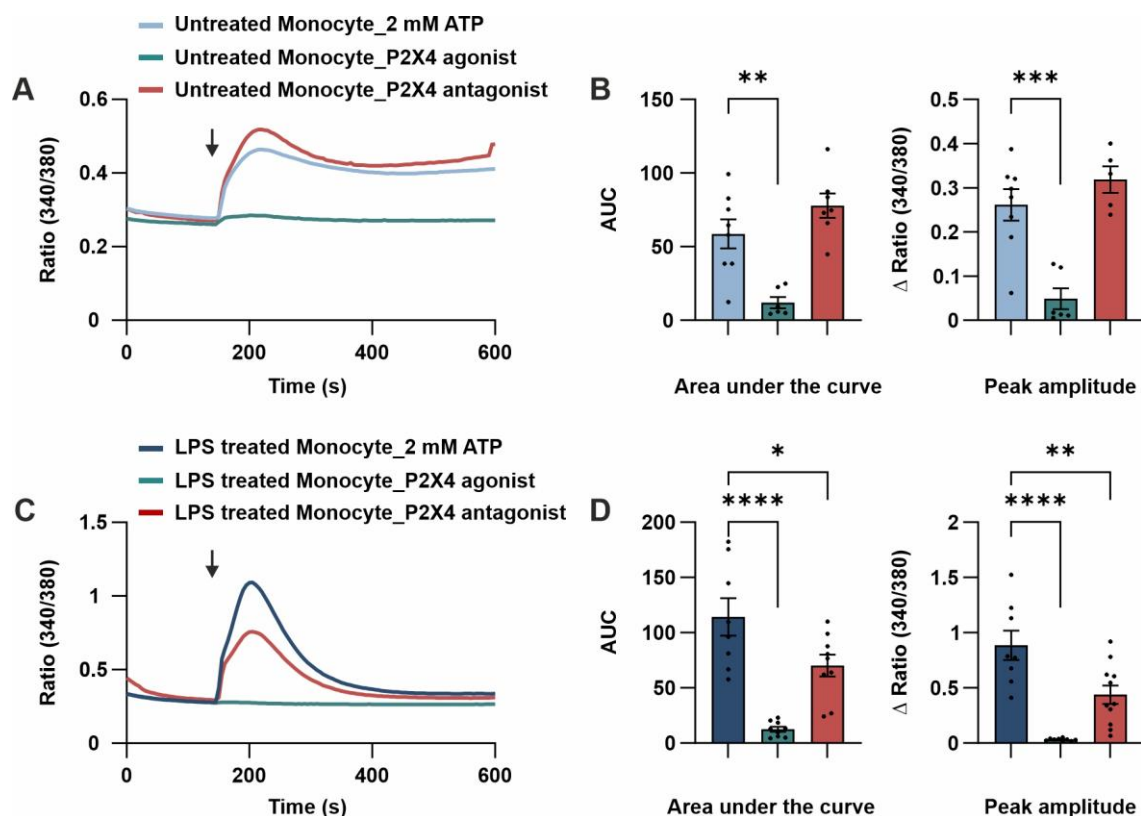


Figure 22 Effects of P2X4 agonist and antagonist on $[Ca^{2+}]_i$ in untreated and LPS treated primary monocytes.

Average traces representing changes in $[Ca^{2+}]_i$ in primary monocytes upon application of either 2 mM ATP (blue) or 3 μ M P2X4 agonist (green) to untreated cells (A) or LPS treated cells (C). The effect of P2X4 antagonist was also measured by applying 2 mM ATP in presence of either 10 μ M P2X4 antagonist (red) or same v/v DMSO (blue). All measurements were performed in an extracellular buffer containing 2 mM Ca^{2+} . (B, D) Analysis of the area under the curve and peak amplitude of corresponding Ca^{2+} signal traces. Data are shown as mean \pm SEM and significances were tested by one-way ANOVA followed by Dunnett's test (3-5 donors, total of 169/ 380/ 225 untreated and 910/ 1259/ 1079 LPS treated cells were subjected to ATP/ P2X7 agonist/ P2X7 antagonist+ ATP application containing more than 600 cells in each condition) (* $P < 0.05$, ** $P < 0.01$, *** $P < 0.001$, **** $P < 0.0001$).

Table 30 Effects of pharmacological modulation of purinergic receptors on $[Ca^{2+}]_i$.

Treatment		Area under the curve compared to control in Untreated cells (% \pm SEM)	Area under the curve compared to control in LPS treated cells (% \pm SEM)
P2X4	agonist	36.88 \pm 5	43.56 \pm 6
	antagonist	69.87 \pm 12	73.8 \pm 14
P2X7	agonist	23.57 \pm 7	10.98 \pm 2
	antagonist	153.16 \pm 16	61.36 \pm 8
P2Y2	agonist	97.76 \pm 12	44.81 \pm 11

antagonist	118.03 ± 29	252.52 ± 54
------------	-------------	-------------

Next, the effect of P2Ys and P2Xs inhibition on IL-1 α release was examined by ELISA. For this purpose, cells were treated with the antagonist of interest for 30 min before ATP application. The reagents used are listed in Table 18. No IL-1 α release was detected in monocytes cultures without LPS priming. IL-1 α secretion upon P2X4 and P2X7 inhibition was reduced by $\sim 59 \pm 9.7\%$ and $92 \pm 0.65\%$, respectively (Fig. 23A). Moreover, replacing ATP with agonists of a specific P2 receptor, as the second trigger for IL-1 α release, failed to induce IL-1 α secretion (Fig. 23-B).

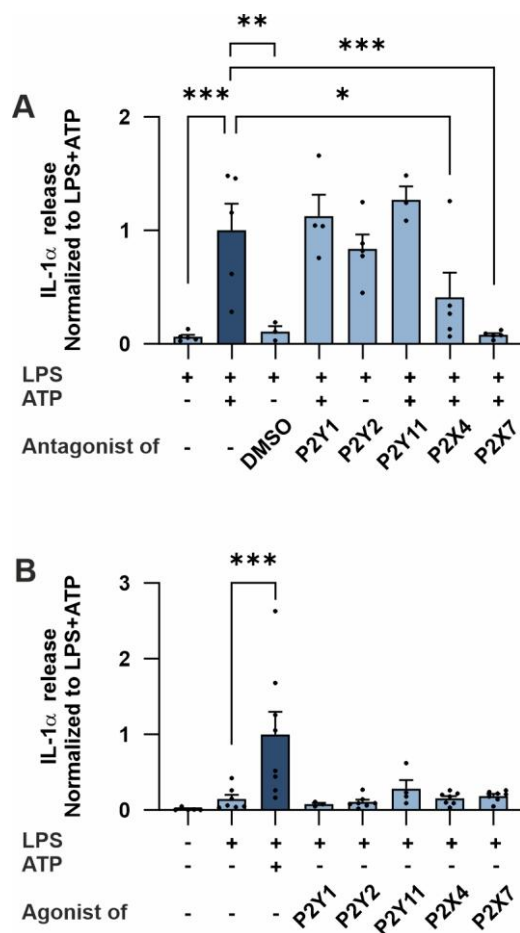


Figure 23 P2X4 and P2X7 play an essential role in IL-1 α release.

Graph representing the normalized concentrations of (A) IL-1 α released from LPS treated monocytes preincubated with either DMSO or different P2R's antagonists, in response to application of 2 mM ATP and (B) IL-1 α released from LPS treated primary monocytes in response to P2R's specific agonists with no further ATP application. Data are shown as mean +SEM and significances were tested by one-way ANOVA followed by Dunnett's test (n=3-8) (* P<0.05, ** P<0.01, *** P<0.001, **** P<0.0001).

The effect of P2Y2, P2X4 and P2X7 antagonists on IL-1 β was also examined (Fig. 24A). As seen for IL-1 α , inhibition of P2X4 and P2X7 antagonist significantly reduced IL-1 β release from LPS treated monocytes (Fig. 24A). Application of P2X7 and P2Y2 agonists failed to induce IL-1 β release (Fig. 24B). In conclusion, these results highlight the crucial role of P2X4 and P2X7 channels in IL-1 α and IL-1 β secretion.

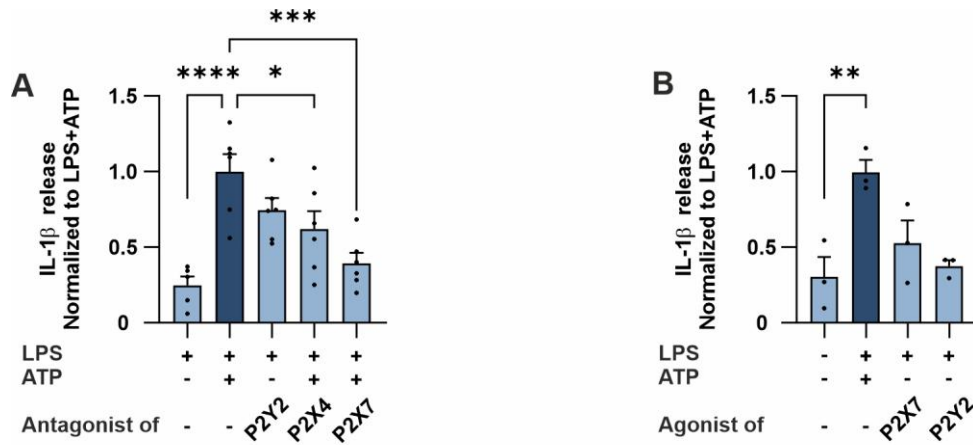


Figure 24 Inhibition of P2X7 and P2X4 result in reduced IL-1 β release from primary monocytes.

Graphs representing normalized concentrations of (A) IL-1 β released from LPS treated primary monocytes with or without preincubation with P2Y2, P2X4 or P2X7 antagonist, followed by application of 2 mM ATP and (B) IL-1 β released from LPS treated primary monocytes in response to application of either the P2X7 or P2Y2 agonist. Data are shown as mean +SEM and significances were tested by one-way ANOVA followed by a Dunnett's test (n=3-5) (* P<0.05, ** P<0.01, *** P<0.001, **** P<0.0001).

Western blot analysis showed a significant reduction in the mature, but not the pro-form of IL-1 α following P2X4, P2X7 and P2Y2 inhibition (Fig. 25B). We also analyzed the effects of P2X4, P2X7 and P2Y2 agonists on LPS treated cells without ATP application, which did not induce any significant release of IL-1 α compared to LPS treated cells (Fig. 25C).

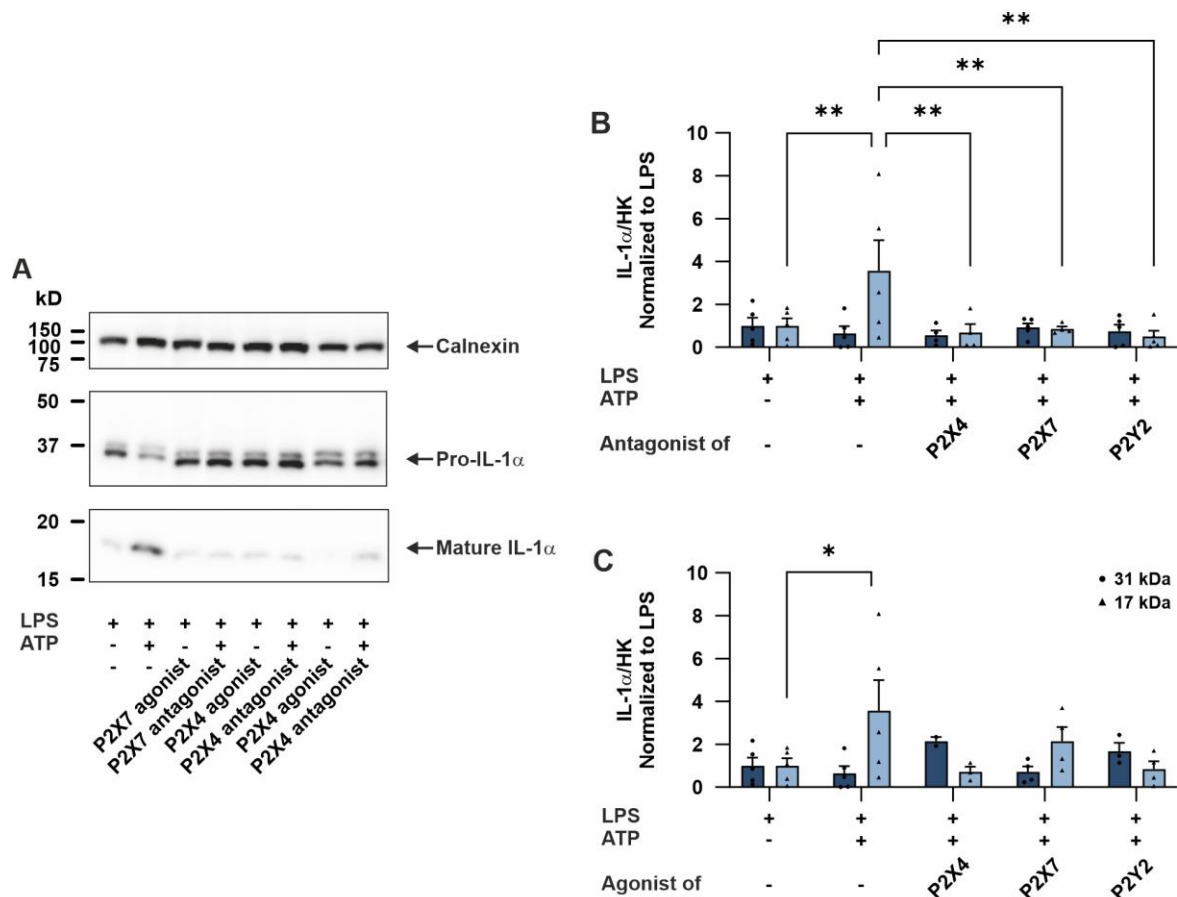


Figure 25 Inhibition of P2X4, P2X7 or P2Y2 reduces intracellular mature IL-1 α

(A) Representative image of Western blot of cell lysates from LPS primed primary monocytes treated with P2 agonists and antagonists. (B) Graphs representing Western blot analysis of the normalized intracellular concentrations of pro-IL-1 α (Dark blue) and mature IL-1 α (light blue) obtained from total cell lysates of LPS treated primary monocytes incubated with P2X4, P2X7 or P2Y2 antagonist, followed by 2 mM ATP application or (C) with P2X4, P2X7 or P2Y2 agonist or 2 mM ATP. Protein signal intensities were normalized to the housekeeping protein. To compare across treatments, all signal intensities were then normalized to the protein concentration of LPS-treated cells from the corresponding donor. Data are shown as mean \pm SEM and significances were tested by two-way ANOVA followed by a Bonferroni's test (* $P < 0.05$, ** $P < 0.01$, *** $P < 0.001$, **** $P < 0.0001$).

8 Signaling through P2X7 and P2X4 is altered in CKD derived monocytes.

Results in Figure 23 and Figure 25 showed an essential role for P2 receptors in IL-1 α release in healthy primary monocytes. The next aim was to identify which of the P2 receptors are involved in the altered purinergic signaling and subsequent changes in IL-1 α release in CKD patients. To answer this question, ATP-induced Ca^{2+} influx was measured in the presence of P2X7 or P2X4 inhibitor in untreated or LPS treated monocytes isolated from healthy and CKD donors. P2X7 inhibition did not alter ATP induced Ca^{2+} influx in healthy (Fig. 26A, B, C, D) or CKD monocytes (Fig. 26E, F, G, H) in either LPS treated or untreated cells. Due to donor-

to-donor variability observed in both ELISA experiments and Ca^{2+} measurements, we also analyzed the Ca^{2+} signals of antagonist-treated cells normalized to DMSO-treated controls of the same donor. Comparison of the normalized data showed a significant reduction of $[\text{Ca}^{2+}]_i$ only in LPS treated CKD monocytes (Fig. 29B).

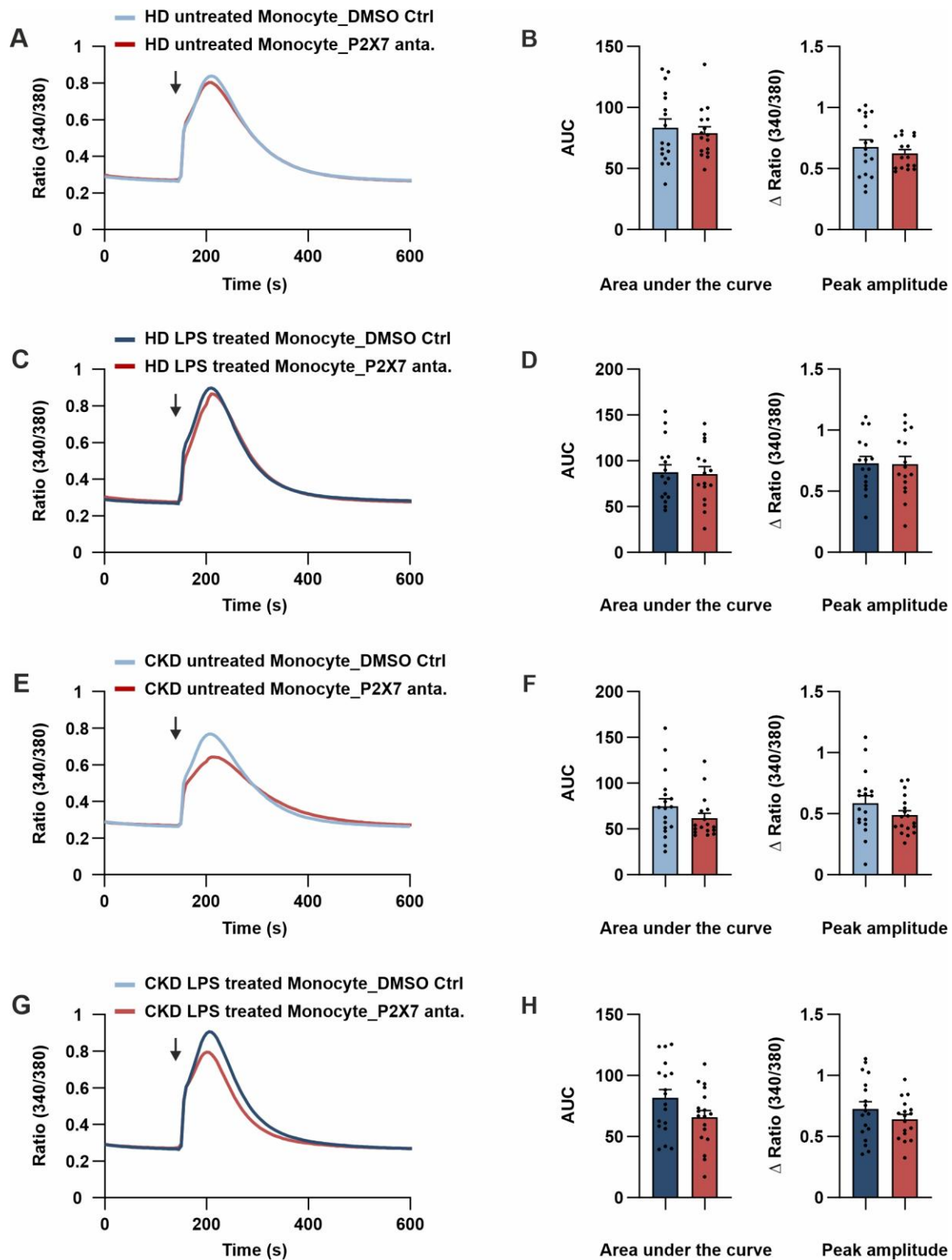


Figure 26 Effects of P2X7 antagonist on $[Ca^{2+}]_i$ in untreated and LPS treated primary monocytes from healthy or CKD donors.

Average traces representing changes in $[Ca^{2+}]_i$ in untreated (A) or LPS treated (C) primary monocytes from healthy subjects, pre-incubated with 100 μ M P2X7 antagonist followed by application of 2 mM ATP. Similar conditions were applied to untreated (E) or LPS treated (G) monocyte from CKD patients. (B, D, F, H) Analysis of the area under the curve and peak amplitude of corresponding traces. Data are shown as mean \pm SEM and significances were tested by unpaired t-test followed by Welch's correction test (6 healthy and 8 CKD donors, number of cells treated with DMSO+ATP/ P2X7 Inh + ATP was as follows: untreated 1879/ 1668, LPS treated 2392/ 2345 cells from healthy and untreated 2147/ 2012, LPS treated 2854/ 2702 cells from CKD) (* $P < 0.05$, ** $P < 0.01$, *** $P < 0.001$, **** $P < 0.0001$).

The effects of P2X7 inhibition on IL-1 α secretion were also measured. As shown in Figure 27, P2X7 inhibition led to a reduction in ATP-induced IL-1 α release in both groups. The P2X7 antagonist also abolishes IL-1 β secretion in both healthy and CKD monocytes.

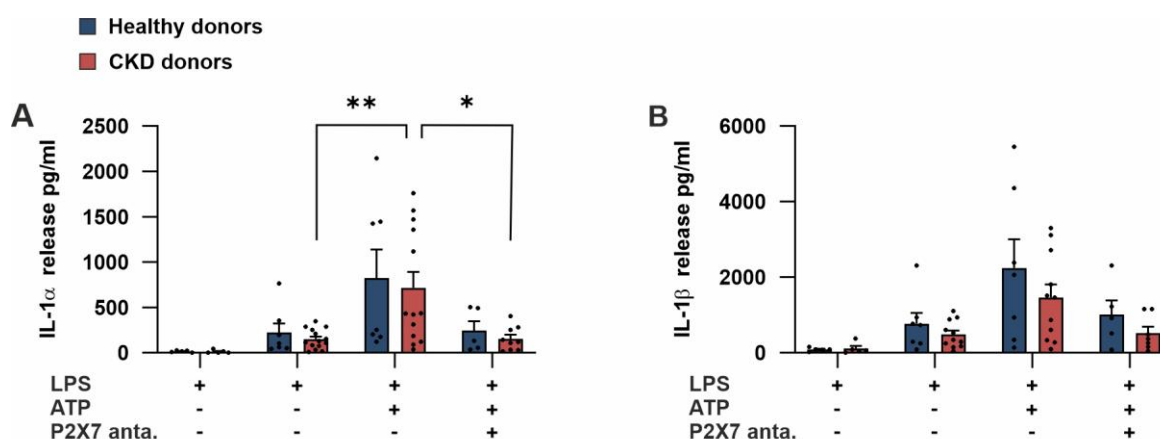


Figure 27 Effects of P2X7 inhibition on IL-1 α release from LPS treated monocytes are comparable between CKD and healthy individuals.

Graphs representing IL-1 α release from primary monocytes isolated from CKD (red) or healthy donors (blue). LPS treated cells were either incubated with P2X7 antagonist or same v/v DMSO before ATP application. Data are shown as mean \pm SEM and significances were tested by two-way ANOVA followed by Bonferroni's test ($n=4-11$) (* $P < 0.05$, ** $P < 0.01$, *** $P < 0.001$, **** $P < 0.0001$).

We also investigated the effect of P2X4 inhibition on CKD monocytes. As shown in Figure 28, P2X4 inhibition led to a reduction in Ca^{2+} response to ATP application in untreated and LPS treated healthy monocytes. This effect was also observed in LPS treated CKD cells, but surprisingly untreated CKD monocytes showed increased levels of $[Ca^{2+}]_i$ when P2X4 was inhibited. P2X4 has been shown to be significantly up-regulated upon LPS stimulation, and LPS treated cells exhibited lower Ca^{2+} entry compared to untreated cells (Fig. 13). Altogether,

these results and higher expression of P2X4 in CKD monocytes (Fig. 12C), suggest a regulatory role for P2X4 in untreated CKD monocytes.

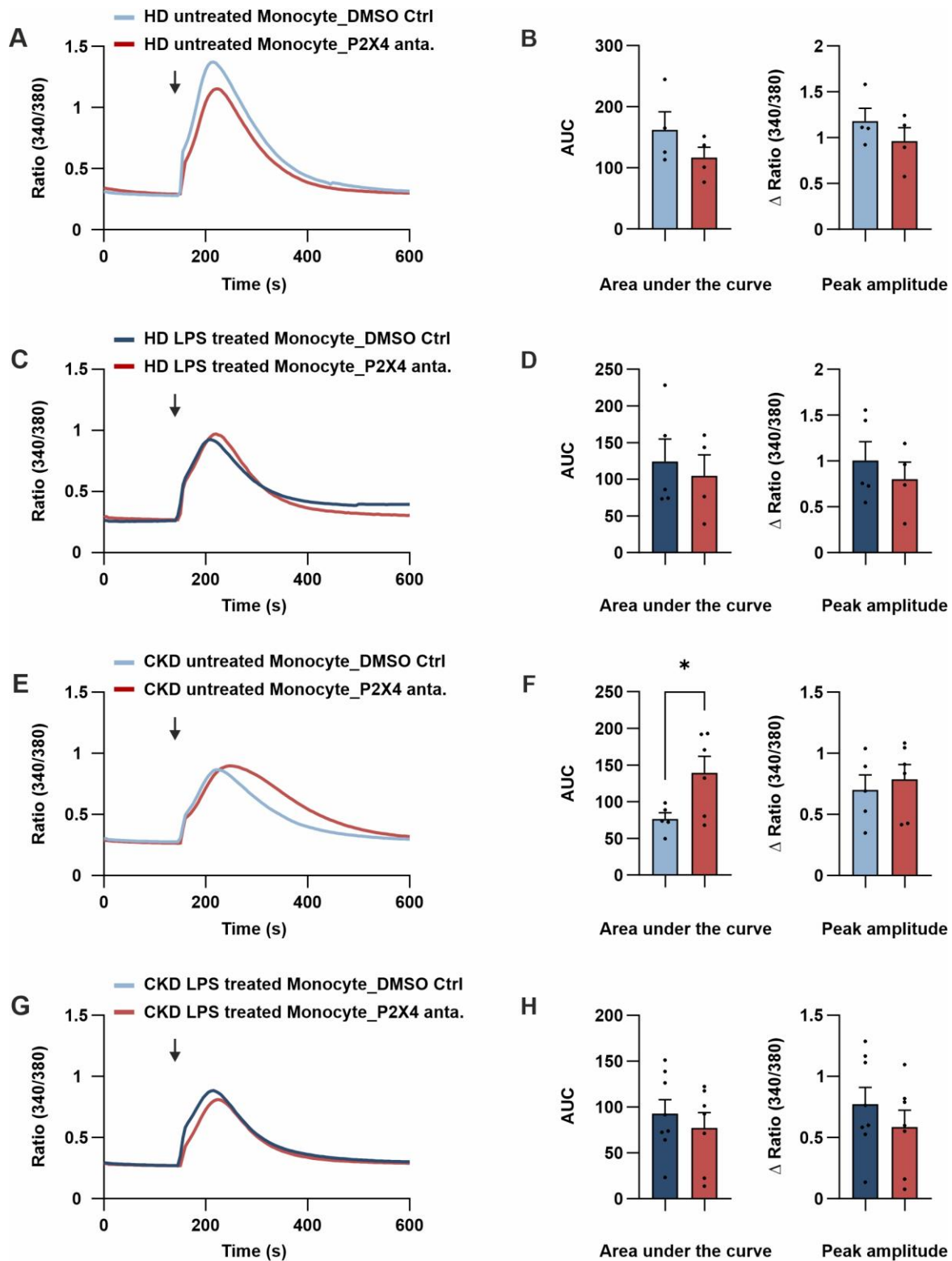


Figure 28 Effects of P2X4 antagonist on $[Ca^{2+}]_i$ in untreated and LPS treated primary monocytes from healthy or CKD donors.

Average traces representing changes in $[Ca^{2+}]_i$ in untreated (A) or LPS treated (C) primary monocytes from healthy subjects, preincubated with 100 μ M P2X4 antagonist followed by application of 2 mM ATP. Similar conditions were applied to untreated (E) or LPS treated (G) monocytes of CKD patients. (B, D, F, H) Analysis of the area under the curve and peak amplitude of corresponding traces. Data are shown as mean \pm SEM and significances were tested by unpaired t-test followed by Welch's correction test (2 healthy and 4 CKD donors, number of cells treated with DMSO+ATP/ P2X4 Inh.+ATP were as follows: untreated 378/ 244, LPS treated 296/ 345 cells from healthy and untreated 296/ 450, LPS treated 715/ 869 cells from CKD) (* $P<0.05$, ** $P<0.01$, *** $P<0.001$, **** $P<0.0001$).

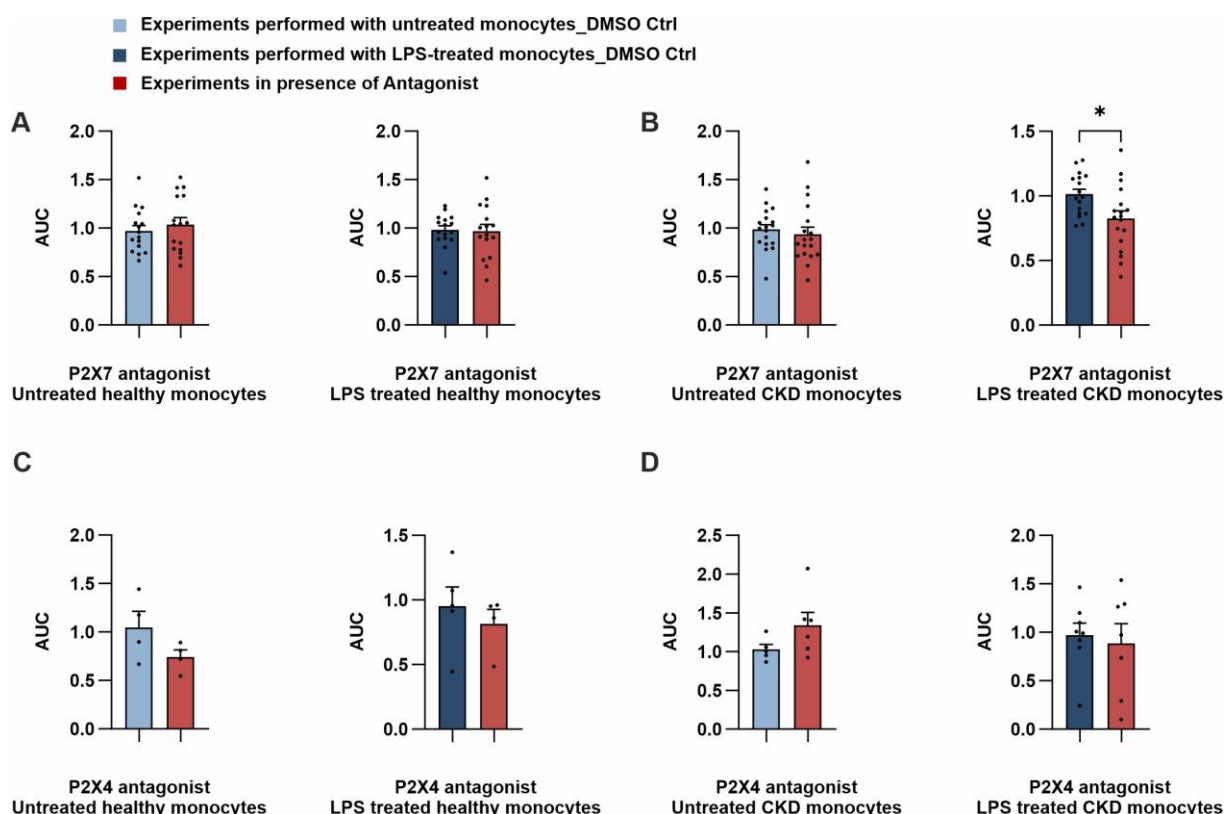


Figure 29 P2X7 has higher impact on ATP responses in CKD monocytes.

Graphs representing the area under the curve of Ca^{2+} imaging experiments, where the response to the agonist or antagonist is normalized to the average of the control condition. Untreated or LPS treated healthy monocytes were treated with P2X7 antagonist (A) or P2X4 antagonist (C). Untreated or LPS treated CKD monocytes were treated with P2X7 antagonist (B) or P2X4 antagonist (D). Data are shown as mean \pm SEM and significances were tested by unpaired t-test followed by Welch's correction test (* $P<0.05$, ** $P<0.01$, *** $P<0.001$, **** $P<0.0001$).

9 ATP stimulation affects surface expression of monocytes markers, which can be restored by P2X7 inhibition

PBMCs isolated from CKD or healthy donors were directly analyzed using immunophenotyping and gated as represented in Figure 30. The percentages of T-lymphocytes (CD3+), B-lymphocytes (CD19+) and Natural killer cells (CD56+) in each group are summarized in Table 31.

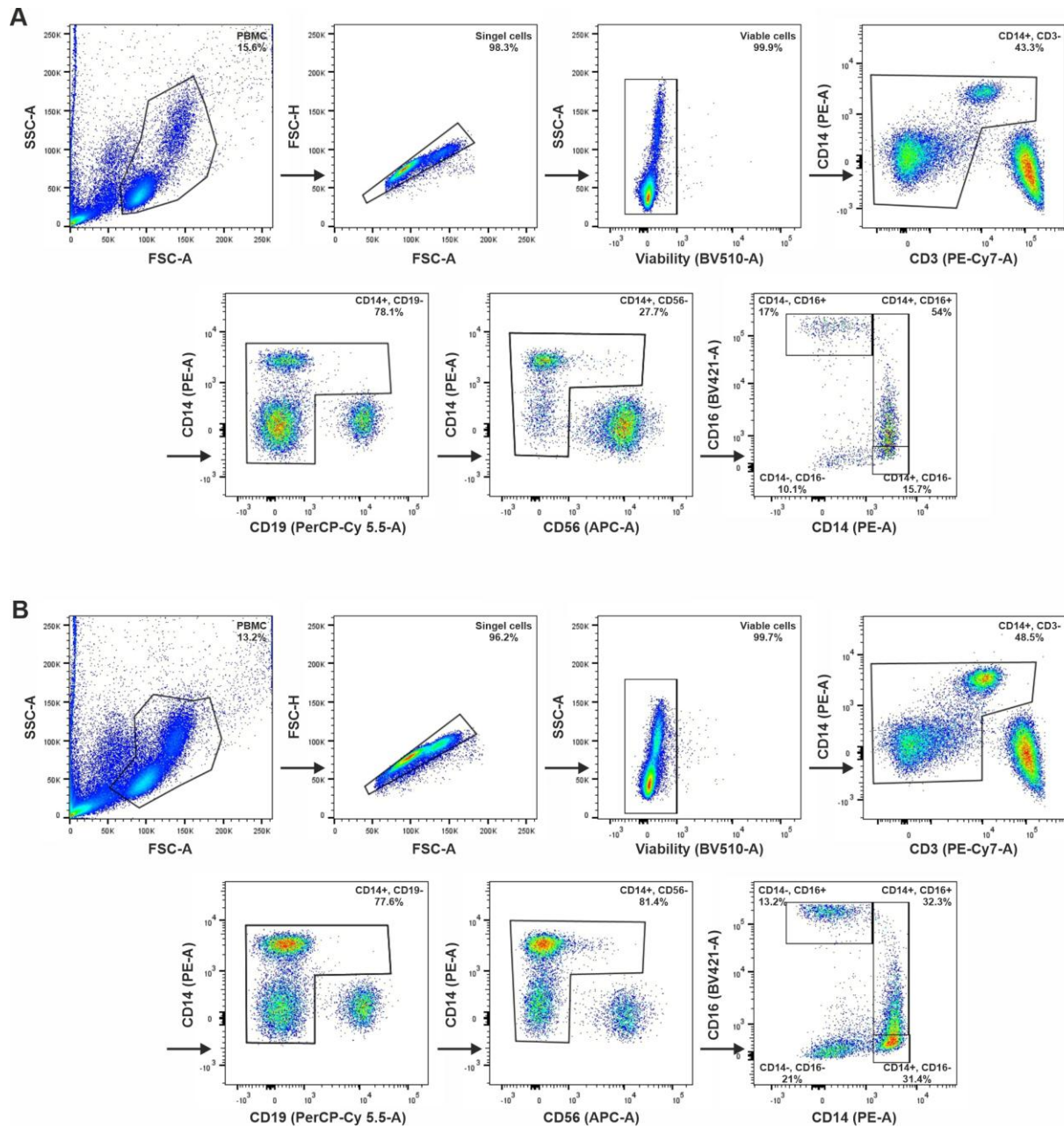


Figure 30 Immunophenotyping of PBMCs isolated from the whole blood of healthy and CKD donors.

Representative immunophenotyping graphs of PBMCs isolated from the whole blood of one healthy (A) and one CKD (B) donor. (A) Monocytes were first identified according to their size and granularity. After excluding doublets and dead cells, cells positive for CD3, CD19 and CD56 were sequentially excluded. Monocytes were then gated using CD16 and CD14 markers.

Table 31 Percentage of CD3+, CD19+ and CD56+ cells in CKD (n=6) and healthy (n=4) PBMC population.

	CD3+	CD19+	CD56+
Healthy monocytes	47.10 ± 2.60	11.20 ± 2.40	37.06 ± 4.51
CKD monocytes	51.06 ± 1.10	14.07 ± 2.78	25.06 ± 1.81

As explained in the introduction, different monocyte subpopulations have been shown to have specific functions and associations in different diseases, (reviewed by Cormican & Griffin, 2020; Ożańska et al., 2020; Takeuchi & Akira, 2010). Therefore, understanding changes in surface marker expression and monocyte subpopulations in CKD is crucial for the development of future clinical approaches. We aimed to investigate the percentage of each monocyte subpopulation in CKD and healthy isolated cells. To achieve this goal, CD14 and CD16 surface markers were analyzed in untreated cells, cells treated with LPS, LPS+ATP and LPS+ATP in the presence of the P2X7 antagonist. The percentage of total monocytes expressing CD14 was not altered by any of the treatments and was comparable between CKD and healthy cells (Fig. 31A, C, E, F). In healthy cells, the fraction of CD16⁺ or CD16⁻ cells was not significantly affected in response to ATP stimulation or P2X7 inhibition. However, CKD monocytes showed a significant reduction in CD16⁺ cells upon ATP application and a significant increase in CD16⁻ cells, which suggests shedding of the CD16 receptor upon ATP application (Fig. 31B, D, G, H). In cells incubated with P2X7 antagonist, application of ATP did not change the fraction of CD16 expressing cells. Additionally, comparing CD16 surface expression among CKD and healthy monocytes under different treatments showed significantly higher CD16 expression in CKD donors than in healthy cells. After ATP application, the expression of CD16 is comparable between the groups, suggesting greater CD16 shedding upon ATP stimulation in CKD cells (Fig. 31G). To summarize, comparing LPS treated monocytes from CKD donors to those from healthy donors shows a higher percentage of cells expressing CD16 on the cell membrane, which is significantly reduced upon ATP application, and this reduction is abolished by P2X7 inhibition. This suggests an important role for CD16 and P2X7 in mediating the ATP signal and the release of membrane bound pro-IL-1 α to the extracellular space.

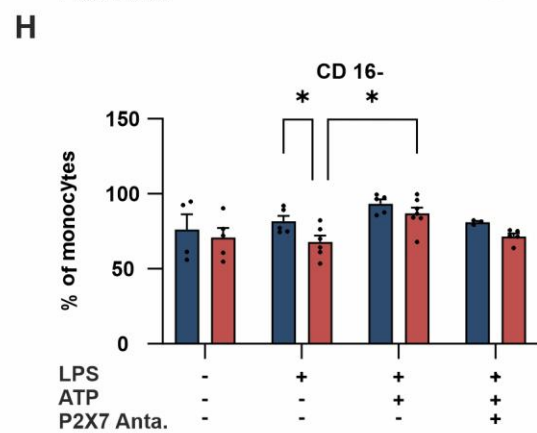
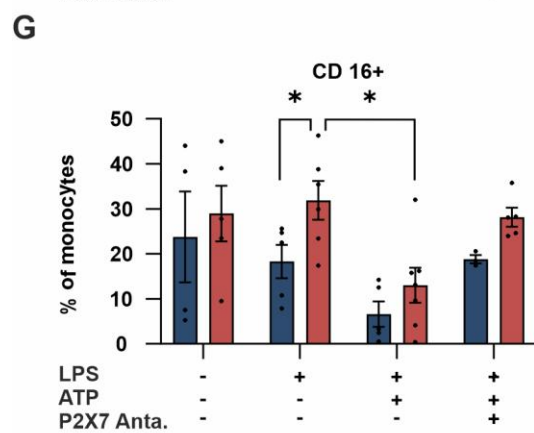
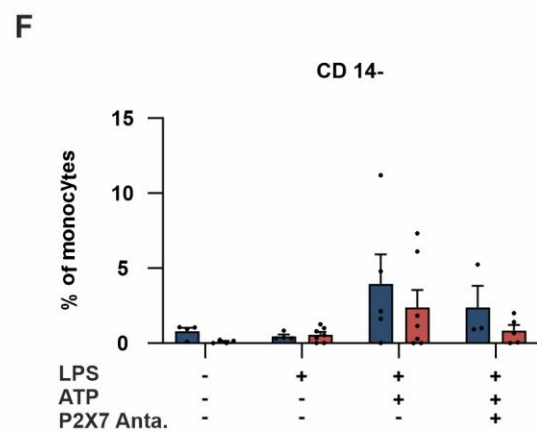
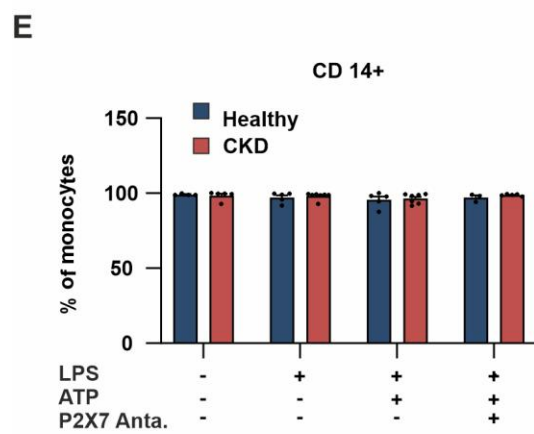
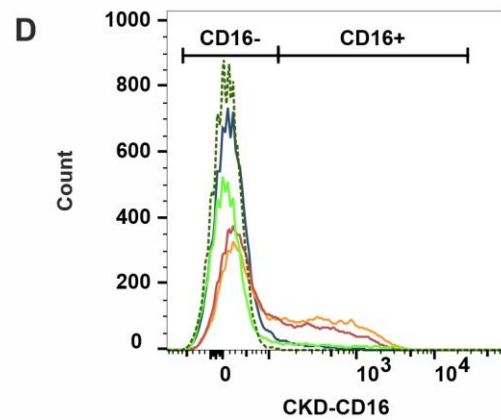
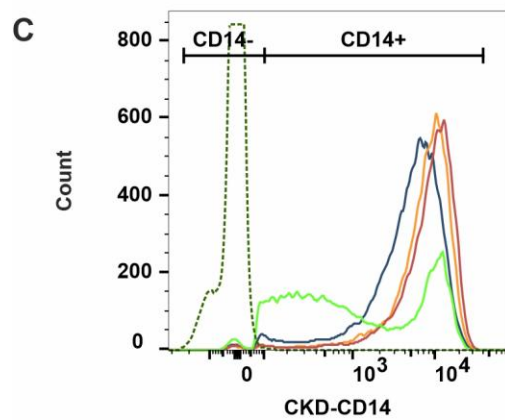
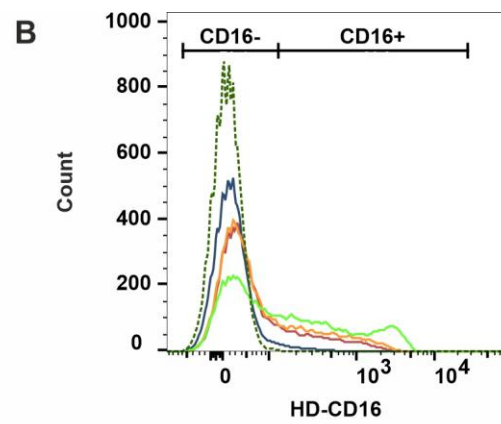
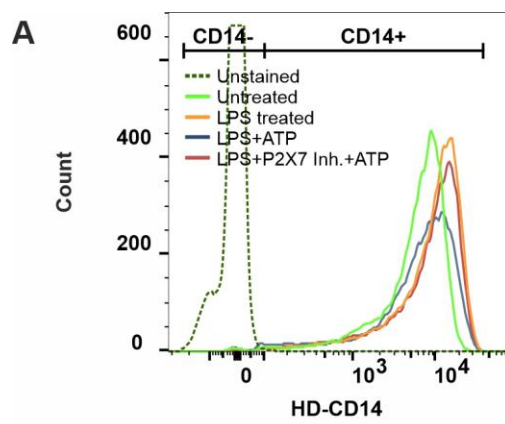


Figure 31 ATP application and P2X7 inhibition affect CD16 surface expression on CKD monocytes.

Representative histograms showing CD14 expression on monocytes isolated from healthy (A) or CKD (C) and CD16 surface expression on healthy (B) and CKD (D) monocytes. Graphs representing analysis of surface markers on healthy (blue) or CKD (red) primary monocytes without any treatment or upon treatment with LPS or LPS+ATP, with or without P2X7 inhibition. The percentage of CD14+ (E), CD14- (F), CD16+ (G) and CD16- (H) monocytes is compared among treatments and study groups. Data are shown as mean \pm SEM and significances were tested by two-way ANOVA followed by Bonferroni's test (n=3-7) (* P<0.05, ** P<0.01, *** P<0.001, **** P<0.0001).

We also investigated the effects of LPS, LPS+ATP and P2X7 inhibition during ATP stimulation on monocyte subtypes (Fig. 32). The fraction of monocytes in PBMCs was measured directly after isolation, showing no significant difference between CKD and healthy cells (Fig. 32D and Table 32). Treating the cells with LPS did not alter the percentage of monocytes subtypes compared to untreated cells within each group. However, the percentage of intermediate monocytes was significantly higher in LPS treated CKD cells than in healthy cells. Additionally, a significant reduction in the intermediate monocyte subpopulation was observed in CKD cells upon ATP stimulation, which was not observed in the presence of the P2X7 inhibitor (Fig. 32B). ATP application also induced a similar trend in healthy monocytes, although this was not significant. No significant changes were observed in classical and non-classical subtypes following different treatments or between CKD and healthy cells (Fig. 32A, C).

Table 32 Analysis of monocytes subpopulations in PBMC directly after isolation from CKD and healthy donors (Data are shown as mean \pm SEM)

	Classical	Non-classical	Intermediate
Healthy monocytes	39.37 \pm 4.21	19.57 \pm 1.82	40.87 \pm 4.01
CKD monocytes	25.36 \pm 2.09	17.54 \pm 2.15	56.66 \pm 1.82

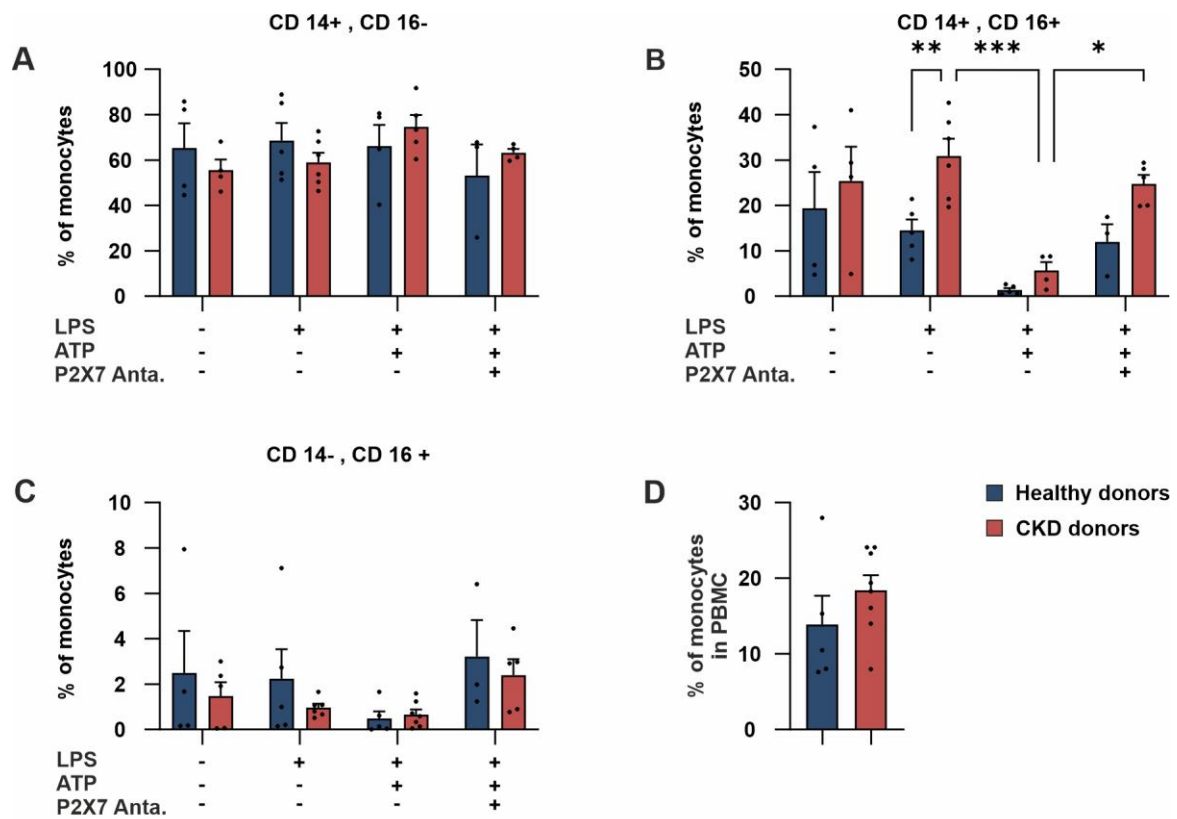


Figure 32 Intermediate monocytes population upon LPS treatment is significantly higher in CKD patients.

Analysis of healthy (blue) or CKD (red) monocyte subpopulations without any treatment or upon treatment with LPS or LPS and ATP, with or without P2X7 inhibition. Changes in classical (A), intermediate (B), and non-classical (C) monocytes populations among treatments and study groups. (D) Percentage of monocytes, after excluding dead cells, in total PBMC directly after isolation from CKD (red) and healthy (blue) donors' whole blood. Data are shown as mean +SEM and significances were tested by two-way ANOVA followed by Bonferroni's test (n=3-6) (* P<0.05, ** P<0.01, *** P<0.001, **** P<0.0001).

Further experiments were performed to investigate the correlation between IL-1 α surface expression and monocyte surface markers (Fig. 33 and Fig. 34). As shown in Figure 34, upon LPS treatment, an increase was observed in the percentage of cells expressing both CD14 and IL-1 α (Fig. 34B) in healthy monocytes (blue column), which correlates with a decrease in CD14+/IL-1 α - cells (Fig. 34A). This suggests that LPS treatment leads to surface expression of IL-1 α on CD14+ cells in healthy subjects. Non-significant trends of increased CD14+/IL-1 α + cells were also observed in CKD cells upon LPS treatment (Fig. 34B, red column). Moreover, LPS treatment led to a significant increase in CD16-/IL-1 α + monocytes from healthy donors (Fig. 34F), which was significantly higher than CKD cells. These findings suggest that in

healthy donors, LPS stimulation leads to significantly higher IL-1 α expression on the surface of CD14⁺ and CD16⁻ monocytes than in CKD cells.

ATP application significantly reduced the percentage of CD16⁺/IL-1 α ⁺ and CD16⁺/IL-1 α ⁻ monocytes in the CKD group and CD16⁻/IL-1 α ⁺ in healthy cells (Fig. 34C, D, F). Additionally, CD16⁻/IL-1 α ⁻ cells were also significantly increased upon ATP application in CKD cells (Fig. 34E), while no alterations in CD16⁻/IL-1 α ⁺ was observed (Fig. 34F). Considering that CD16⁺/IL-1 α ⁺ cells are reduced (Fig. 34D), but the percentage of CD16⁻/IL-1 α ⁺ cells does not increase (Fig. 34F), suggests a simultaneous detachment of CD16 and IL-1 α from CKD monocytes surface. Furthermore, P2X7 inhibition abolished all the mentioned effects observed upon ATP application in both CKD and healthy donors. This suggests that in CKD donors, ATP application leads to the detachment of IL-1 α from the surface of CD16⁺ cells, while IL-1 α expression on CD16⁻ cells remains unchanged. In contrast, in healthy donors, IL-1 α is primarily detached from CD16⁻ cells. The percentage of IL-1 α expressing monocytes upon each treatment condition is summarized in Table 33.

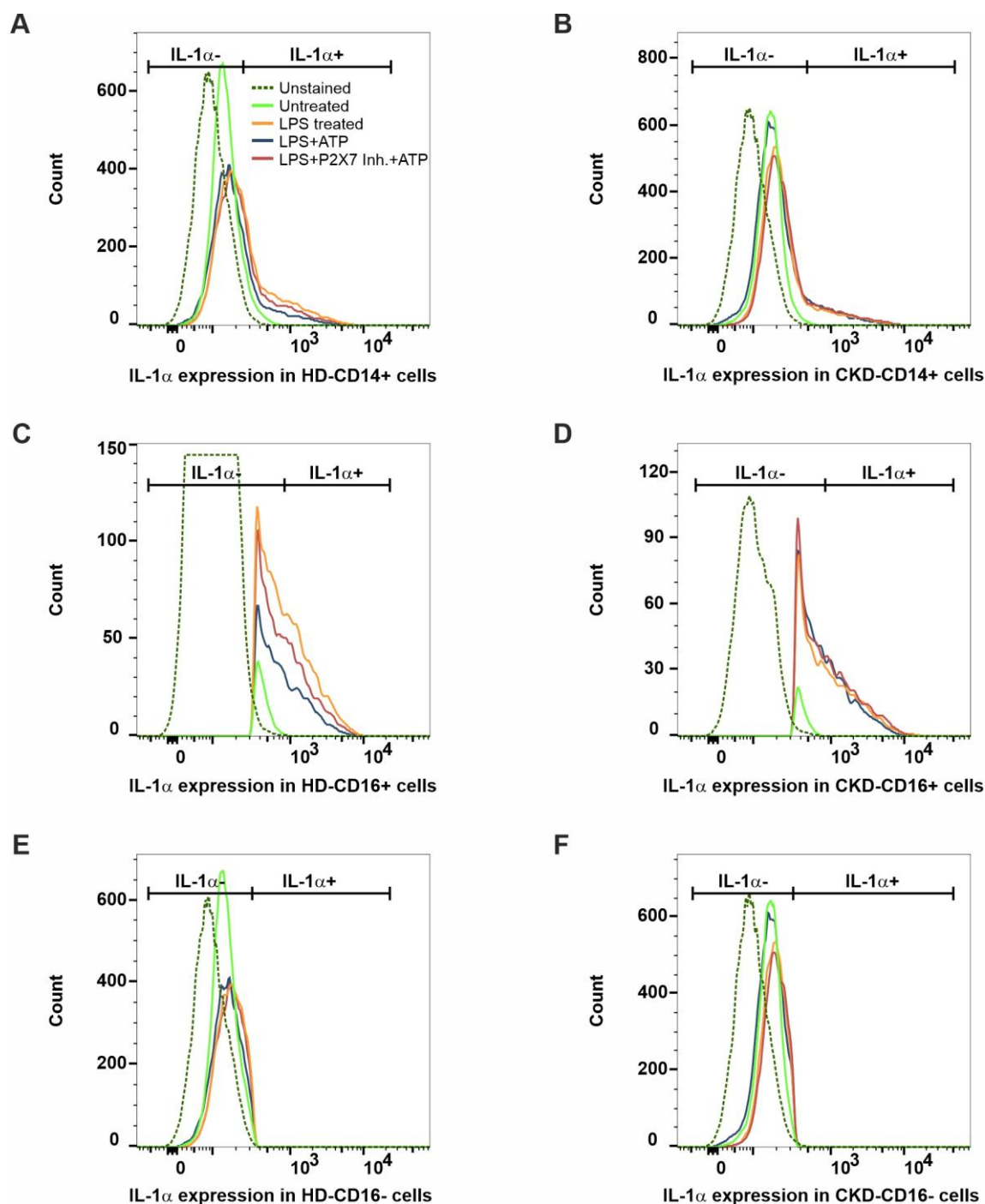


Figure 33 Representative histograms of IL-1 α surface expression on CKD and healthy monocytes in correlation with CD14 or CD16 markers.

Histograms representing IL-1 α expression on CD14+ (A and B), CD16+ (C and D) or CD16- (E and F) monocytes isolated from healthy (left panel) or CKD (right panel) donors. Flow cytometry was used to analyze the surface expression of IL-1 α on different monocytes subpopulations in untreated cells (green) or upon treatment with LPS (orange), LPS+ATP (blue) or LPS+ATP in presence of 100 μ M P2X7 Inh. (red).

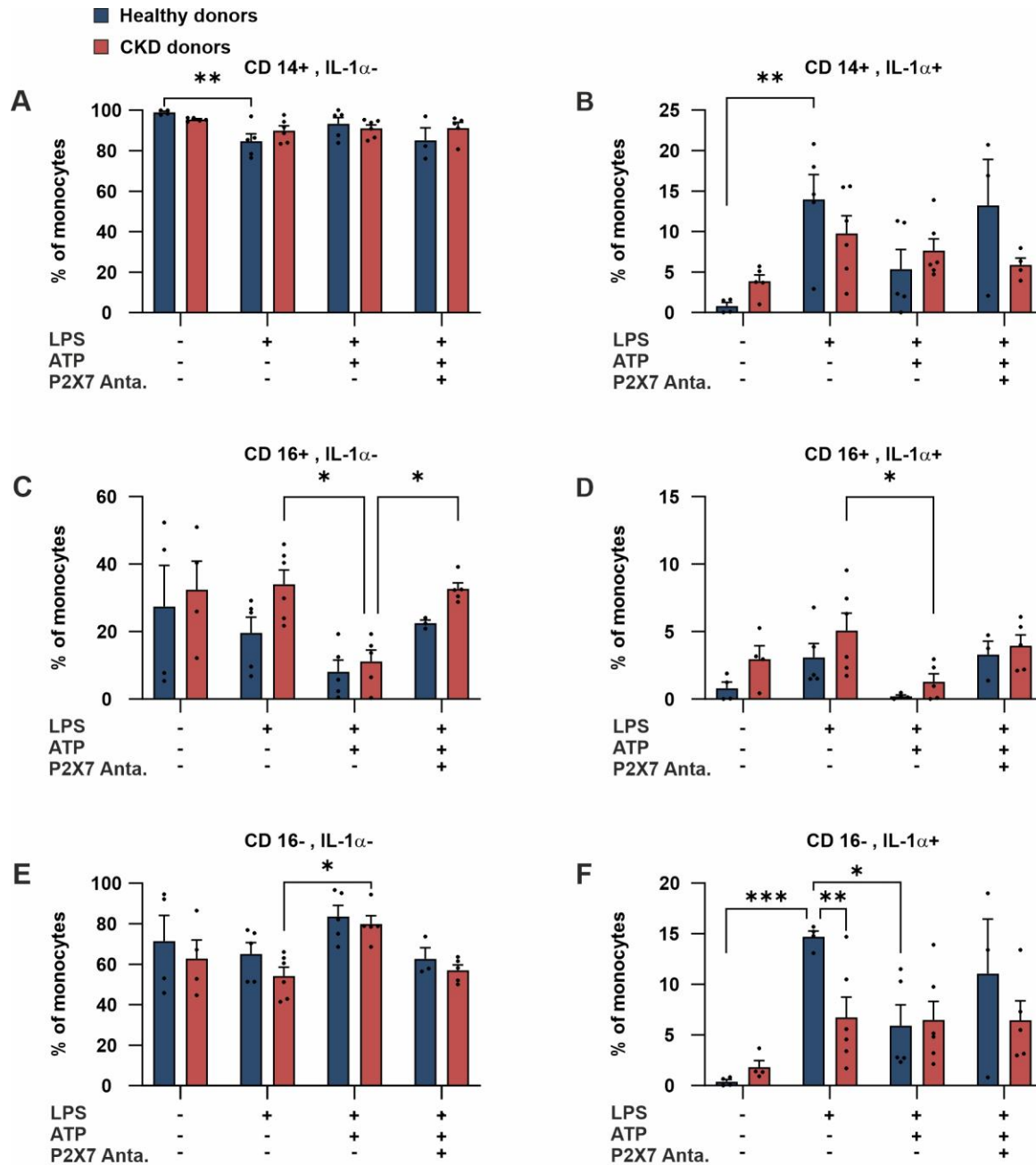


Figure 34 Analysis of IL-1α surface expression on CKD and healthy monocytes in correlation with CD14 or CD16 markers.

Graphs representing percent of CKD (red) and healthy (blue) monocytes which were classified as CD14+ IL-1α- (A), CD14+ IL-1α+ (B), CD16+ IL-1α- (C), CD16+ IL-1α+ (D) and CD16- IL-1α+ (E) in untreated cells or upon incubation with LPS, LPS+ATP or LPS+ATP in presence of P2X7 inhibitor. Data are shown as mean +SEM and significances were tested by two-way ANOVA followed by Bonferroni's test (n=3-6) (* P<0.05, ** P<0.01, *** P<0.001, **** P<0.0001).

Table 33 Percentage of IL-1 α expressing monocytes upon each treatment. (Data are shown as mean \pm SEM).

% of monocytes expressing IL-1α	Healthy	CKD
Untreated	0.79 \pm 0.3	2.11 \pm 0.13
LPS treated	11.46 \pm 1.54	12.99 \pm 2
LPS+ATP	4.47 \pm 1.07	10.33 \pm 1.89
LPS+ATP+P2X7 Inh.	12.42 \pm 3.46	7.56 \pm 1.48
% cells in LPS - % cells in LPS+ATP (p= 0.04)	7.00 \pm 0.76	1.86 \pm 0.55

10 Purinergic signaling regulates IL-1 α biogenesis by activating kinases

Several signaling cascades are activated downstream of Purinergic family activation, which involve many kinases, as shown in Figure 5. This leads to the hypothesis that modulating the activity of one or more kinases might influence the secretion or surface expression of IL-1 α . Inhibition of MEK1 and JNK has been shown to reduced IL-1 β secretion and PI3K inhibition did not cause any significant alterations in IL-1 β release (Tapia-Abellán et al., 2014). However, the effects of kinase inhibition on IL-1 α secretion or surface expression have not been studied yet. Therefore, we used specific inhibitors targeting several kinases activated in these cascades and monitored their effects on IL-1 α biogenesis. For this purpose, LPS treated primary monocytes were incubated with the inhibitors of interest at the concentrations and durations mentioned in Table 18, before ATP application. Analysis of IL-1 α release showed no significant effect upon inhibition of PI3 kinase, MEK, mTor, AKT, JNK, MAPK P38, NF κ B and ERK. Only PAN PKC β inhibition by Ro-31-8220 significantly reduced IL-1 α release by monocytes (Fig. 35A). Go 6983 has a half maximal inhibitory concentration (IC₅₀) of 6-60 nM for most of PKC isoforms but not for PKC β 2, while Ro-31-8220 has an IC₅₀ of 14 nM for this isoform (Gschwendt et al., 1996; Toullec et al., 1991; Wilkinson et al., 1993). To further investigate the role of PKC β 2 in IL-1 α release, a specific PKC β 2 inhibitor was used at 10 μ M and 100 μ M concentrations. Both concentrations significantly reduced IL-1 α release from primary monocytes (Fig. 35B). As shown in Figure 35-B, incubating the cells with inhibitors without ATP application resulted in IL-1 α levels comparable to those in the LPS condition. IL-1 β release was not significantly altered by inhibition of any of the mentioned proteins (Fig. 35C, D).

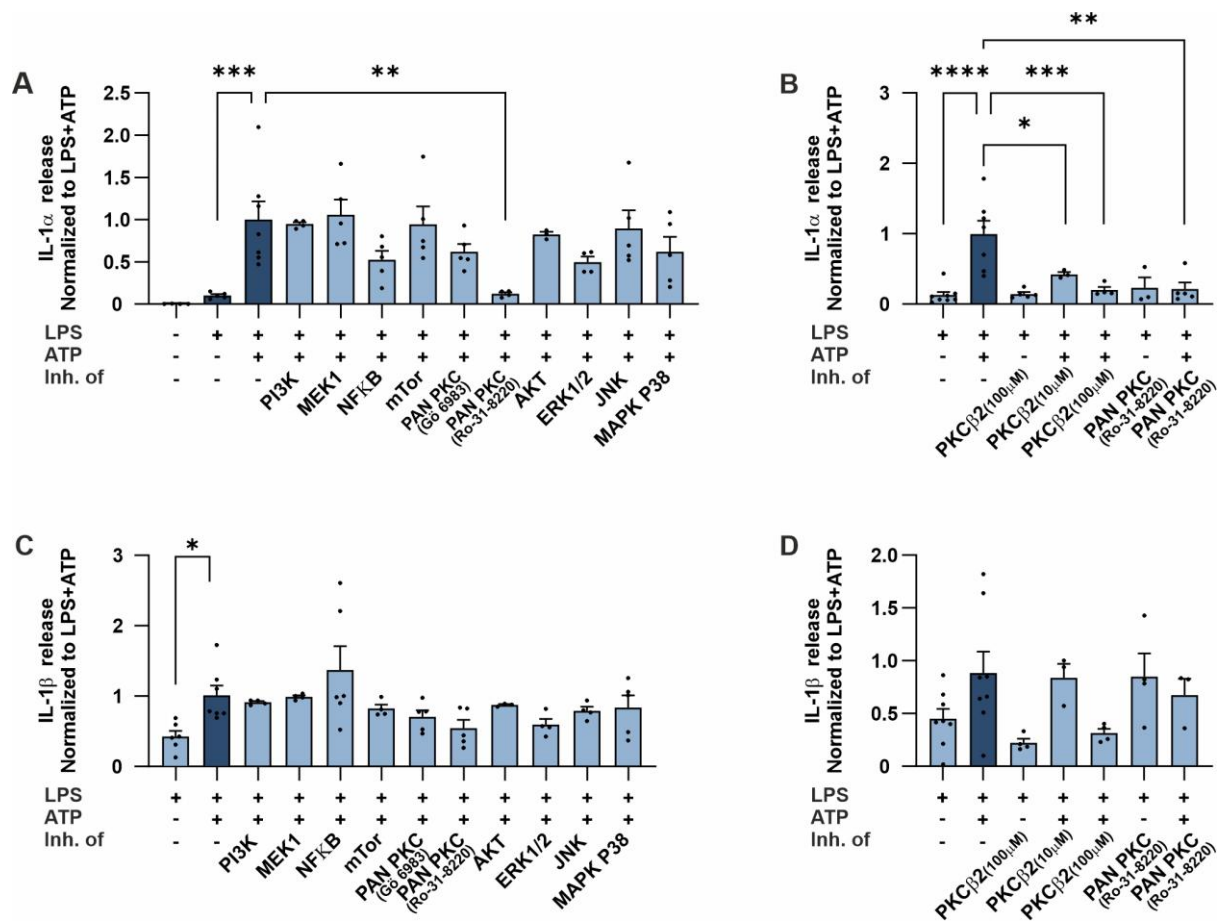


Figure 35 PKCβ2 activity is critical for IL-1α release.

Bar graphs representing normalized release of IL-1α into the medium upon inhibition of kinases activated downstream of P2 family. (A and B) IL-1α release from LPS treated monocytes in response to 2 mM ATP application upon incubation with the mentioned inhibitor. (C and D) IL-1β release from LPS treated monocytes in response to 2 mM ATP application upon incubation with the mentioned inhibitor. Cytokine concentrations were normalized to the Ctrl condition (LPS treated cells with ATP application) of the corresponding donor. Data are shown as mean +SEM and significances were tested by one-way ANOVA followed by Bonferroni correction test (n=3-7) (* P<0.05, ** P<0.01, *** P<0.001, **** P<0.0001).

Western blots analysis of IL-1α protein precipitated from the culture medium was comparable with ELISA results. Inhibition of PKCs using Ro-31-8220 reduced the 31 kDa IL-1α protein in the medium in two analyzed donors. However, due to the low number of replicates, statistical significance could not be tested. We were not able to detect the mature form of the protein (Fig. 36A, B). Using PKCβ2 specific inhibitor led to a significant reduction in both forms of IL-1α released from cells (Fig. 36C, D).

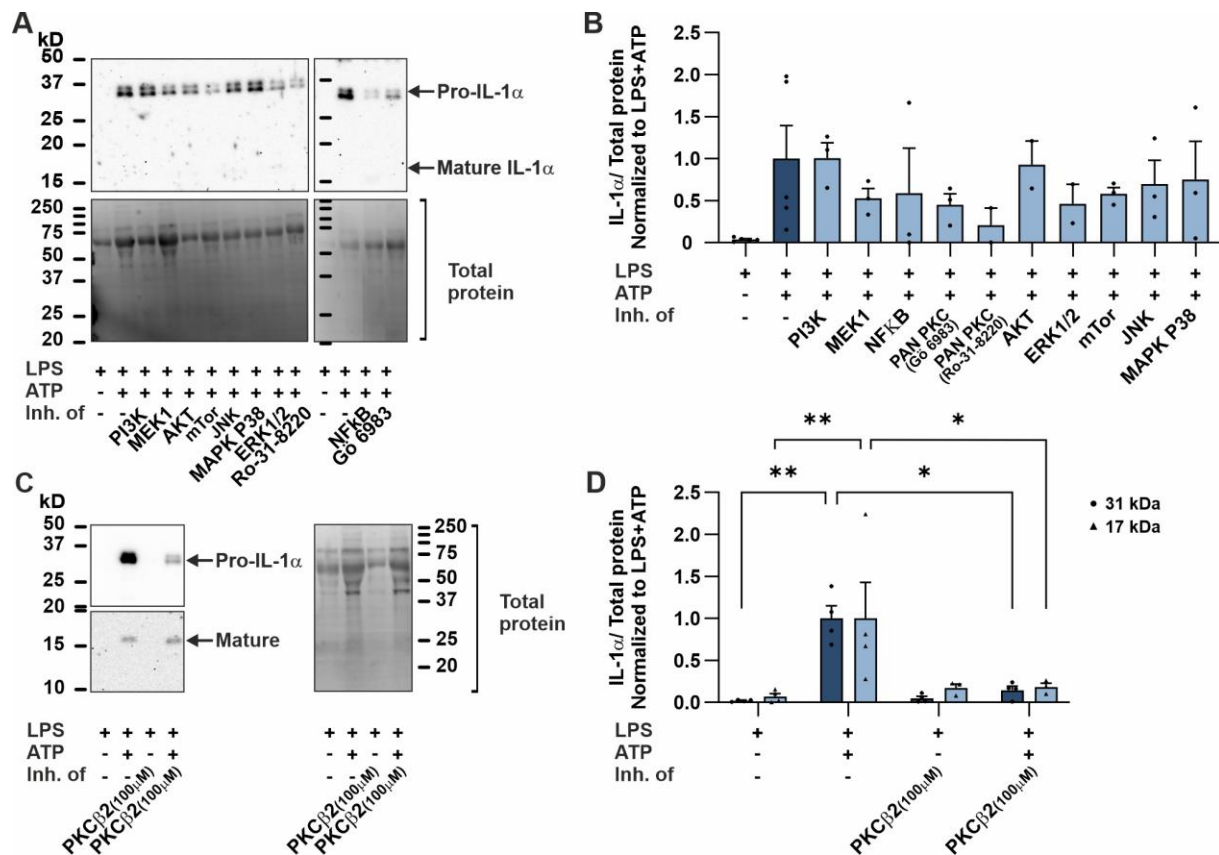


Figure 36 Both Pro and mature IL-1 α are reduced upon PKC β 2 inhibition.

Representative Western blot images of IL-1 α protein released in the medium by LPS treated primary monocytes in response to 2 mM ATP alone or after incubation with kinase inhibitor of interest (A and C). Graphs representing analysis of IL-1 α protein signal intensities in Western blots obtained from total proteins in the medium, which were concentrated by TCA acid protocol (B and D). For an accurate comparison, the amount of total protein loaded onto the gel was stained using No stain reagent and the signal intensities were used to normalize the IL-1 α protein signals. To compare between treatments, all signal intensities have been normalized to the protein concentration of the LPS+ATP treatment of corresponding donor. Data are shown as mean +SEM and significances were either tested by one-way ANOVA (A) or two-way ANOVA (B) followed by a Bonferroni's correction test. (n=2-5) (* P<0.05, ** P<0.01, *** P<0.001, **** P<0.0001)

In parallel, changes in intracellular levels of IL-1 α were investigated by western blot analysis of the cell lysate. NF κ B inhibition was analyzed in four donors, where mature IL-1 α protein expression increased, varying from 0.4- to 11-fold across the donors. Additionally, ERK1/2 inhibition led to a significantly higher concentration of mature IL-1 α in monocytes lysate. PKC Inhibition by RO-31-8220 showed a trend towards higher levels of both pro- and mature IL-1 α . Using a PKC β 2 specific inhibitor also resulted in increased intracellular IL-1 α protein levels, but due to the limited number of experiments, statistical significance could not be determined (Fig. 37).

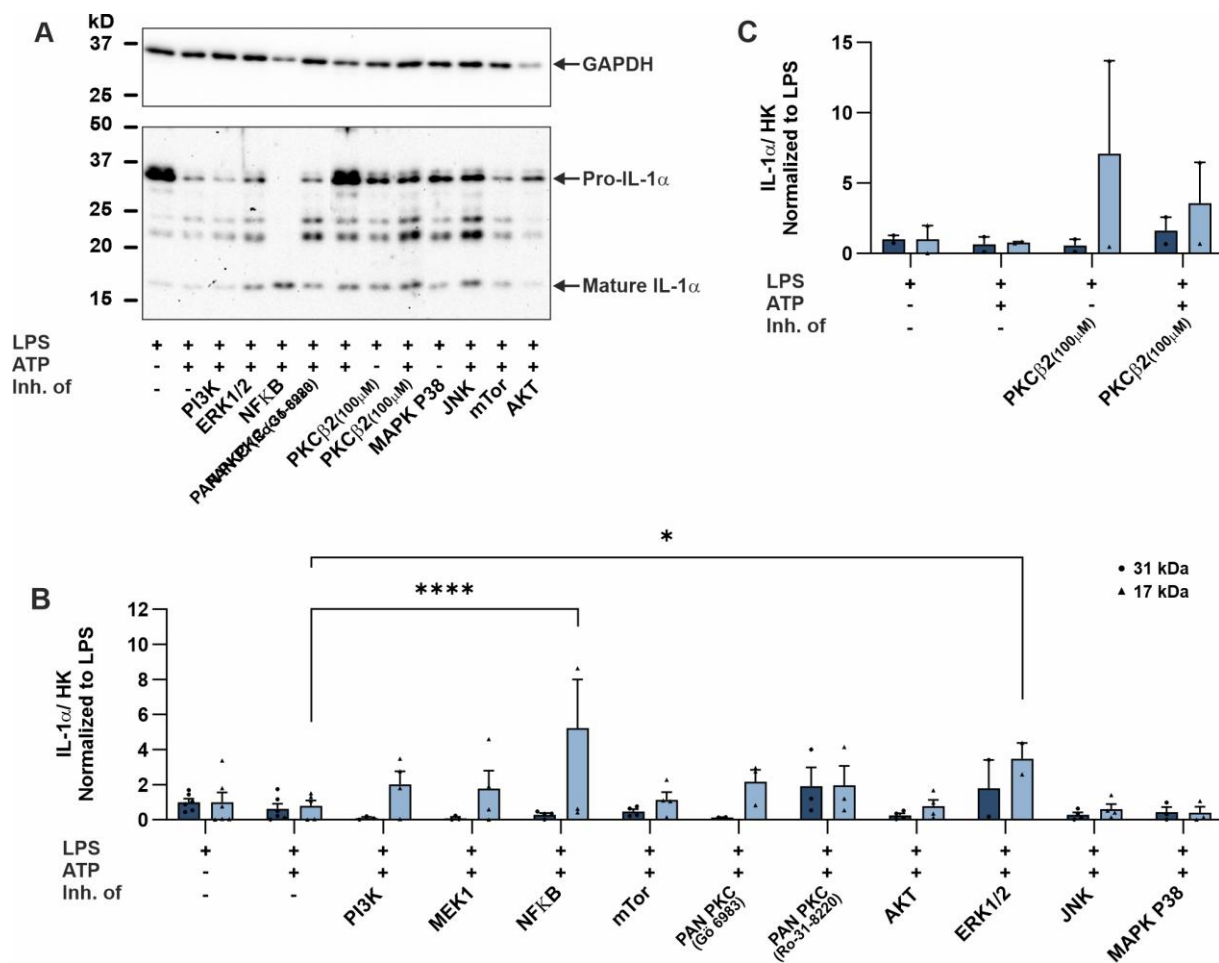


Figure 37 Effects of kinase inhibitions on intracellular IL-1α concentrations.

Representative Western blot images of intracellular IL-1α protein in LPS treated primary monocytes in response to 2 mM ATP alone or after incubation with kinase inhibitor of interest (A). Graphs representing analysis of IL-1α protein signal intensities in Western blots obtained from total proteins in the cell lysate (B and C). Protein signal intensities were normalized to housekeeping protein. To compare between treatments, all signal intensities have been normalized to the protein concentration of the LPS treatment of corresponding donor. Data are shown as mean +SEM and significances were tested by two-way ANOVA followed by Bonferroni's correction test. (n=2-6) (* P<0.05, ** P<0.01, *** P<0.001, **** P<0.0001)

To examine the effect of these kinases on IL-1α surface expression, we used flow cytometry to analyze the percentage of cells expressing surface IL-1α (Fig. 38). Among the inhibitors used, only inhibition of NFκB significantly increased the monocyte population with IL-1α surface expression (Fig. 39A). The data obtained from cells treated with Ro-31-8220 or the specific inhibitor of PKCβ2 were removed due to an autofluorescence, which interfered with the signal from IL-1α antibody.

CD16 and CD14 surface expressions upon treatment with kinase inhibitors were also analyzed. Interestingly, NFκB inhibition resulted in a significant increase in the number of cells

expressing CD16, even before ATP application (Fig. 39B) while the fraction of cells expressing CD14 was unaffected. (Fig. 39C). Altogether, this data suggests a direct effect of NF κ B on IL-1 α and CD16 surface expression in monocytes. This also highlights the role of CD16 in IL-1 α detachment from the monocytes surface.

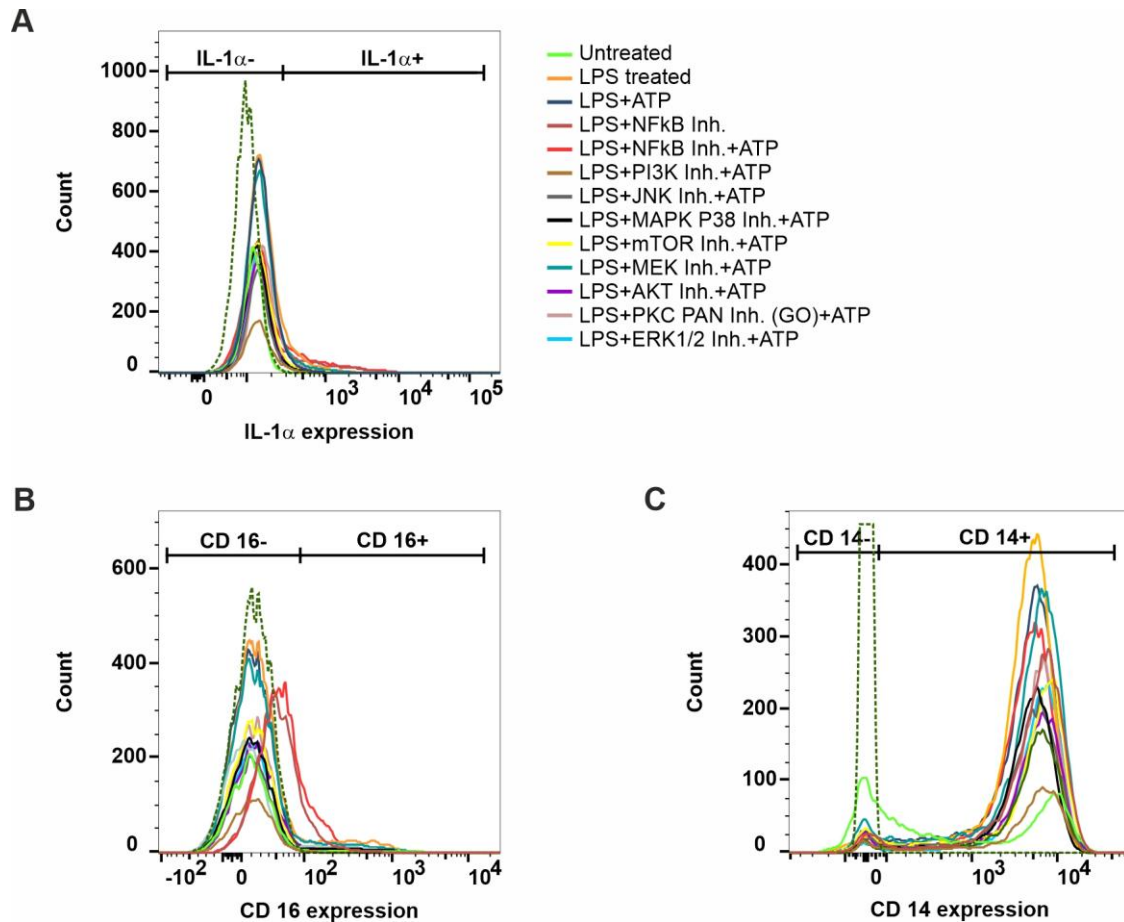


Figure 38 IL-1 α , CD16 and CD14 surface expression in human primary monocytes in presence of inhibitors.

Example histograms showing flowcytometry analysis of IL-1 α , CD14 and CD16 expression on the surface of human primary monocytes.

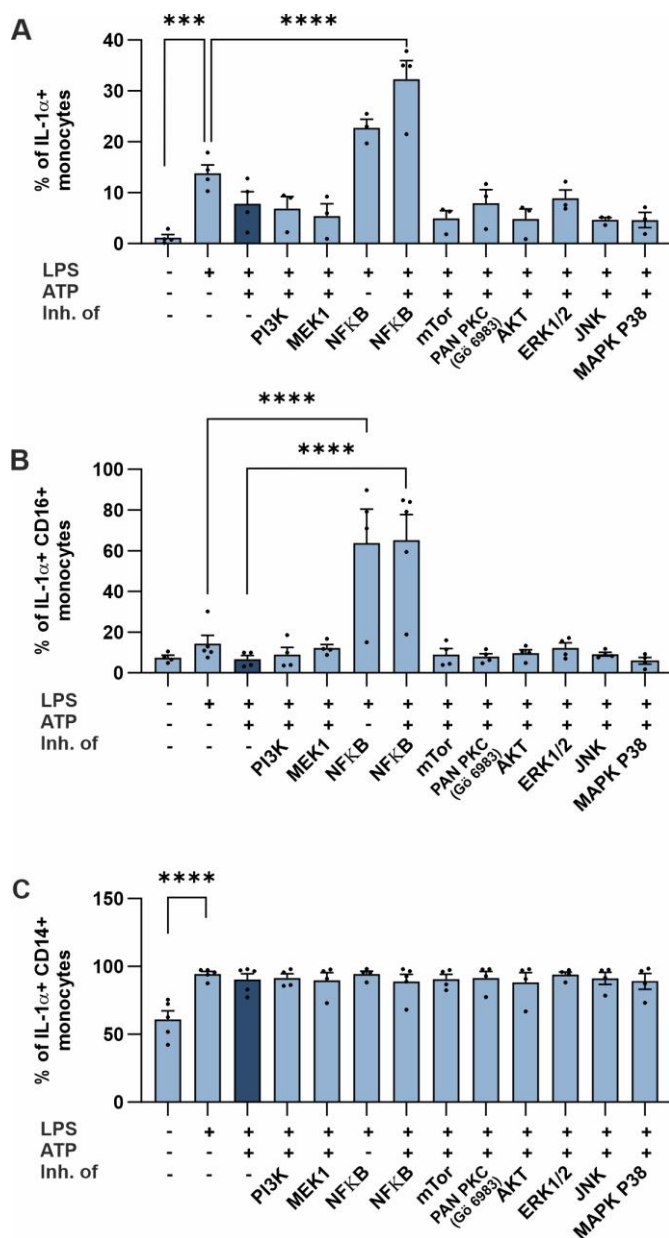


Figure 39 NFκB modulates the surface expression of IL-1α and CD16 on monocytes.

Bar graphs representing the effects of different kinase inhibitors on the percentage of cells exhibiting surface expression of IL-1α (A), CD16 (B) and CD14 (C). Expression of surface proteins was analyzed in untreated primary monocytes with no further treatment, or upon treatment with LPS, LPS+ATP and LPS+ATP in the presence of indicated inhibitors. Data are shown as mean +SEM and significances were tested by one-way ANOVA followed by Dunnett's correction test (n=3-5) (* P<0.05, ** P<0.01, *** P<0.001, **** P<0.0001).

11 IL-1α localization in overexpression systems

In monocytes, IL-1α can be present in three forms: the pro-form, the C-terminal (mature IL-1α) and N-terminal domains resulting from protease-mediated cleavage. The factors influencing the localization of these forms are not yet fully understood. To visualize IL-1α localization, we cloned a recombinant IL-1α construct containing two fluorescent tags forming a FRET reporter. In this technique, the fluorescence emitted by a donor fluorescent protein can excite an acceptor fluorescent protein, but only when both are in adequate vicinity. In our experiments we used GFP and mCherry as the FRET pair. Thus, pro-IL-1α would have the FRET signal, and after cleavage, the C-terminal and N-terminal fragments would be observed as either green or red, depending on their fluorescent tags.

We cloned two plasmids, the first plasmid encodes GFP at the N-terminal and mCherry at the C-terminal of IL-1 α , named as GIM (GFP-IL-1 α -mCherry). The second plasmid encodes mCherry upstream (at the 5' end) and GFP downstream (at the 3' end) of the calpain cleavage site, named as MCG (mCherry-calpain cleavage site-GFP). First, HEK293 cells were transfected with GIM construct as a transfection model. 4',6-diamidino-2-phenylindole (DAPI) was used to label the nucleus. As shown in Figure 40, the signal from GFP, mCherry and the FRET signal showed a nuclear localization in HEK293 cells. The exclusive nuclear localization in these cells could be due to the lack of essential proteins required for IL-1 α cleavage or due to mis-localization of the protein cleavage site caused by the addition of two large fluorescent tags.

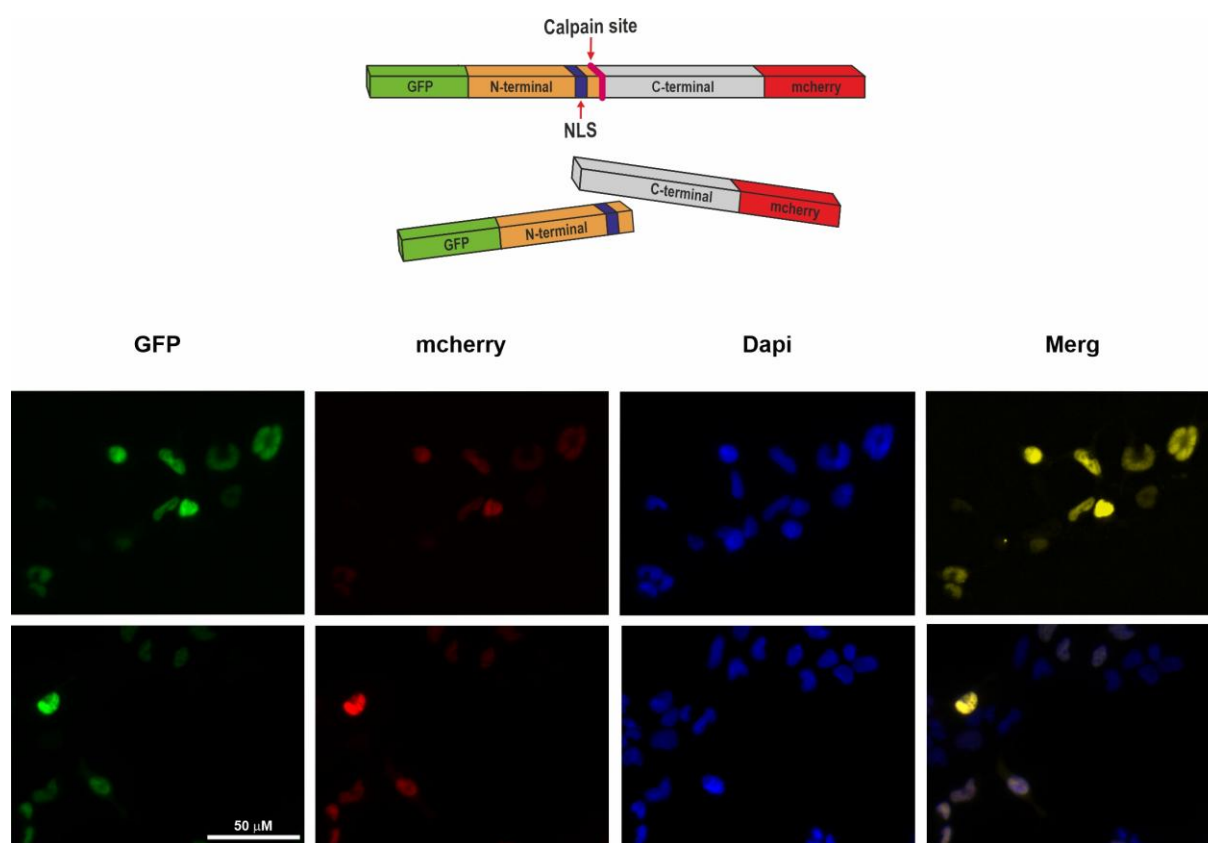


Figure 40 IL-1 α shows exclusive nuclear localization in HEK cells.

Fluorescent images representing HEK cells transfected with IL-1 α protein tagged with GFP at the N-terminal and mCherry at C-terminal. DAPI was used to label the nucleus.

In the next step, both GIM construct was transfected into primary monocytes using nucleofection, and the signal was detected using a TIRF system, which enables us to observe the signals on the plasma membrane as well. IL-1 α showed both nuclear and cytoplasmic localization in monocytes. Monocytes with a bean-shaped nucleus, known as mature

monocytes, showed a nuclear localization of IL-1 α , while cytoplasmic localization was observed in monocytes with a circular-shaped nucleus, characteristic of immature monocytes (Fig. 41). These findings were repeated using an Axio observer system. To reduce alterations in protein size, IL-1 α tagged with only GFP before the NLS signal was also cloned and transfected into the cells, which exhibited the same localization as the GIM construct in monocytes (Fig. 42).

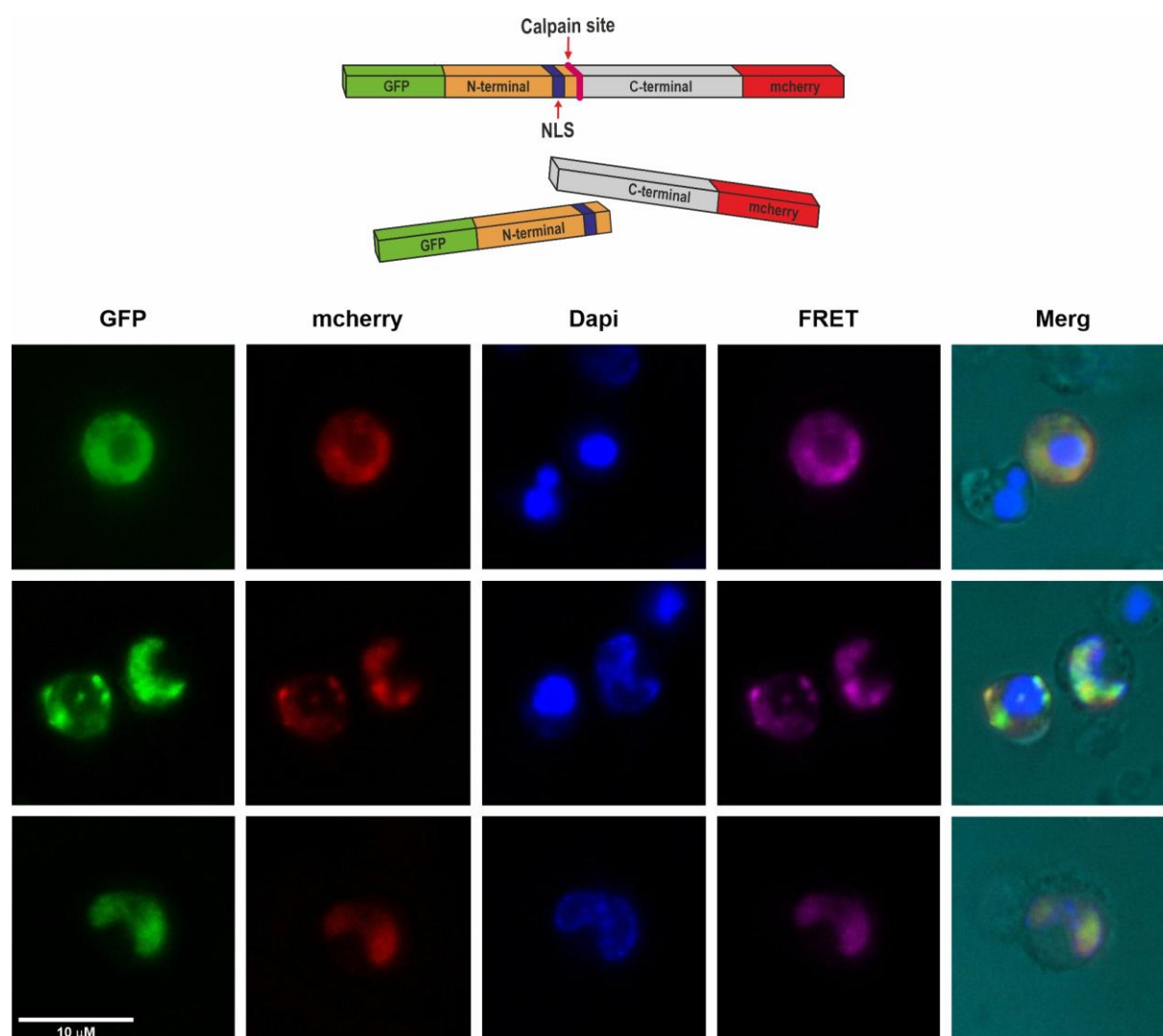


Figure 41 Exogenously expressed IL-1 α localization in primary monocytes.

Fluorescent images showing primary monocytes transfected with IL-1 α protein tagged with GFP at the N-terminal and mCherry at C-terminal. DAPI was used to label the nucleus.

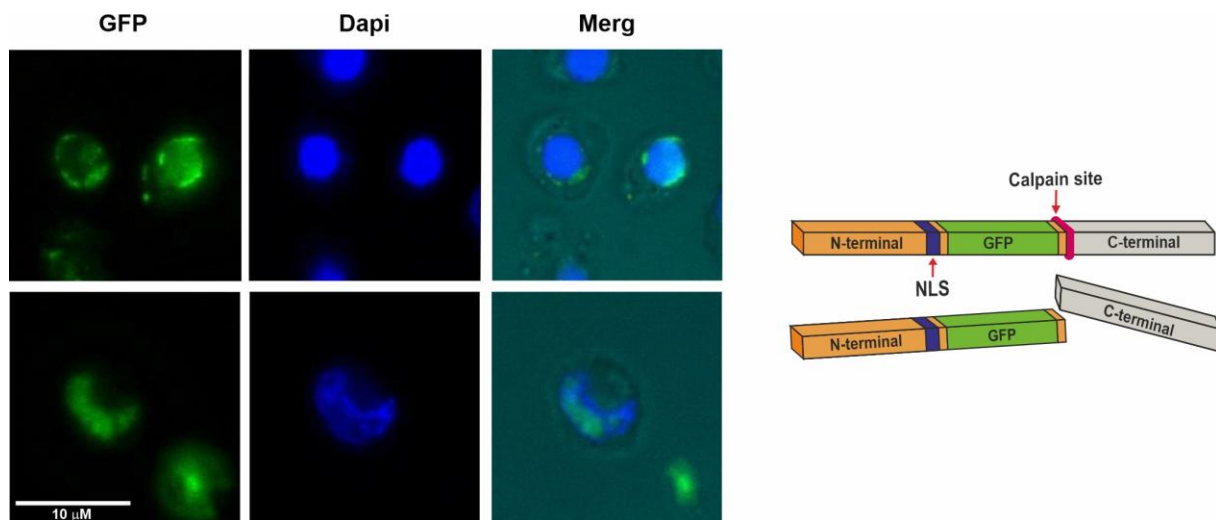


Figure 42 IL-1 α has both cytoplasmic and nuclear localization in primary monocytes.

Fluorescent images representing primary monocytes transfected with IL-1 α protein tagged with only GFP after NLS signal and before calpain cleavage site. DAPI was used to label the nucleus.

12 RNA sequencing showed altered CKD monocytes gene expression

RNA samples prepared from monocytes isolated from four healthy and four CKD donors were sent to Novogene for RNA sequencing. For this purpose, the quality of RNA samples were examined, and after non-stranded library preparation, the sequences were analyzed. Gene expression levels were reported as Fragments Per Kilobase of transcript sequence per Millions base pairs sequenced (FPKM) and compared between CKD and healthy donors. The analysis showed that 222 genes were differentially expressed in monocytes obtained from CKD donors. As shown in Figure 43, the volcano plot and heatmap indicated that 143 genes were significantly up-regulated, while 79 genes were significantly downregulated in CKD-derived cells. These genes are also listed in Table 34 and Table 35.

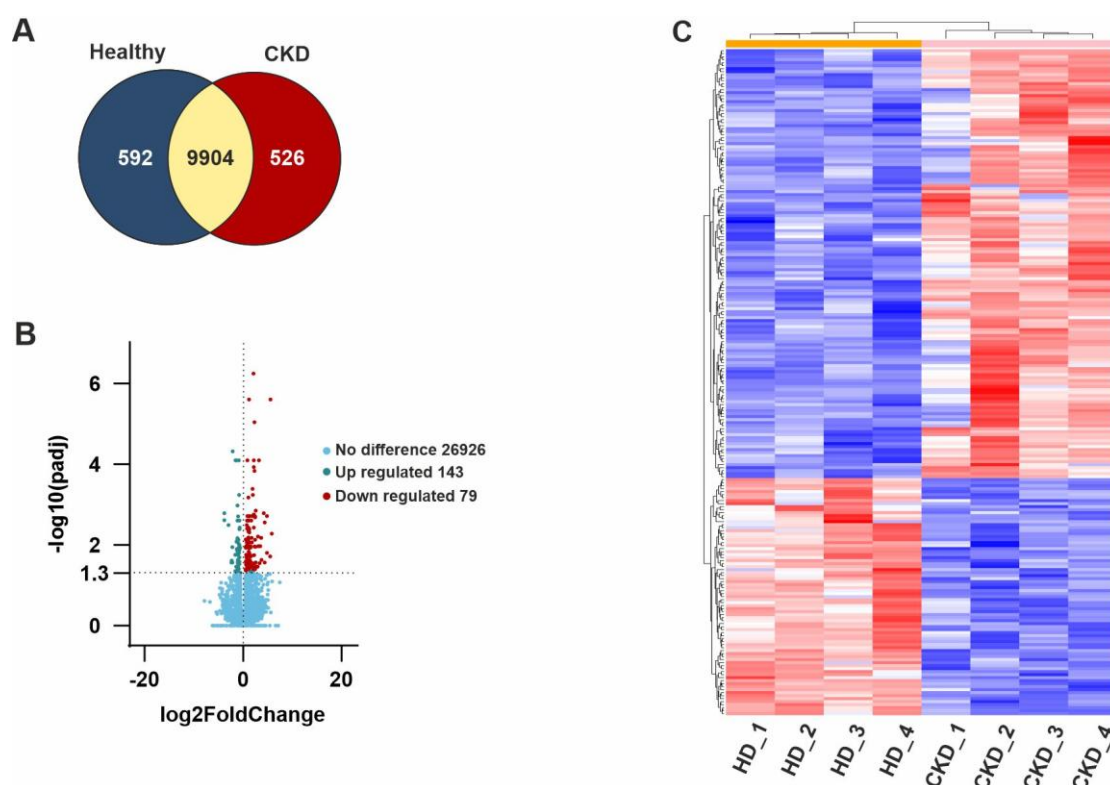


Figure 43 RNA sequencing comparison between healthy and CKD donors.

RNA sequencing analysis was performed on RNA isolated from four healthy and four CKD donors. (A) Venn diagram of the analyzed genes in CKD and healthy donors, (B) Volcano plot and (C) Heat map representing genes with different expression levels between CKD and healthy donor monocytes.

Table 34 Genes significantly up-regulated in CKD (Fold changes are calculated based on Read counts)

Gene Name	Gene description	Fold change	Adj. P value
<i>RNF150</i>	ring finger protein 150	40.20	9.15E-06
<i>DDIT4L</i>	DNA damage inducible transcript 4 like	23.14	0.001961
<i>AL139156.2</i>	pseudogene similar to part of alcohol dehydrogenase 5 (class III), chi polypeptidem (ADH5)	21.67	0.016041
<i>VGF</i>	VGF nerve growth factor inducible	16.40	0.027452
<i>IRX5</i>	iroquois homeobox 5	16.14	0.003208
<i>GPRC5A</i>	G protein-coupled receptor class C group 5 member A	14.63	0.001655
<i>PTGFR</i>	prostaglandin F receptor	10.11	0.006754
<i>MT1G</i>	metallothionein 1G	8.88	0.01087
<i>SPRY2</i>	sprouty RTK signaling antagonist 2	8.46	5.63E-07
<i>DNAJB5-DT</i>	DNAJB5 divergent transcript	8.22	0.028506
<i>IGHD</i>	immunoglobulin heavy constant delta	7.52	7.96E-05

<i>PHLDB1</i>	pleckstrin homology like domain family B member 1	6.94	0.01087
<i>FAM57A</i>	family with sequence similarity 57 member A	6.59	0.006574
<i>LAMB3</i>	laminin subunit beta 3	4.93	0.001655
<i>AC039056.2</i>	novel transcript, sense intronic to EHD4	4.65	0.027452
<i>NKX3-1</i>	NK3 homeobox 1	4.51	0.011301
<i>ABHD17C</i>	abhydrolase domain containing 17C	4.48	0.008333
<i>DUSP14</i>	dual specificity phosphatase 14	4.45	0.002456
<i>SLC7A5</i>	solute carrier family 7 member 5	4.26	0.002099
<i>ADRA2B</i>	adrenoceptor alpha 2B	4.15	0.040853
<i>TNFRSF21</i>	TNF receptor superfamily member 21	4.06	0.000405
<i>AC022778.1</i>	novel transcript	4.06	0.028474
<i>HIC1</i>	HIC ZBTB transcriptional repressor	4.05	4.80E-05
<i>AC093627.3</i>	novel transcript	4.00	0.011033
<i>CSF1</i>	colony stimulating factor 1	3.78	0.018202
<i>HSD3B7</i>	hydroxy-delta-5-steroid dehydrogenase, 3 beta- and steroid delta-isomerase 7	3.75	0.00195
<i>AC125437.1</i>	novel transcript, sense intronic to ATP9B	3.66	0.000118
<i>AREG</i>	amphiregulin	3.64	0.000147
<i>LRG1</i>	leucine rich alpha-2-glycoprotein 1	3.63	2.47E-06
<i>CXCL3</i>	C-X-C motif chemokine ligand 3	3.60	0.003728
<i>RNF152</i>	ring finger protein 152	3.59	0.035487
<i>ADGRG3</i>	adhesion G protein-coupled receptor G3	3.34	0.043739
<i>FAM20A</i>	FAM20A, golgi associated secretory pathway pseudokinase	3.29	0.032805
<i>RAPH1</i>	Ras association (RalGDS/AF-6) and pleckstrin homology domains 1	3.14	0.000578
<i>NIPAL4</i>	NIPA like domain containing 4	3.14	0.03622
<i>LINC00884</i>	long intergenic non-protein coding RNA 884	3.13	0.048679
<i>CCDC71L</i>	coiled-coil domain containing 71 like	3.09	0.000578
<i>AVP1I</i>	arginine vasopressin induced 1	3.07	0.007085
<i>AL359697.1</i>	novel transcript, sense intronic to DNAJC1	3.04	0.031222
<i>MUC1</i>	mucin 1, cell surface associated	2.96	0.030409

<i>NEDD4L</i>	neural precursor cell expressed, developmentally down-regulated 4-like, E3 ubiquitin protein ligase	2.92	0.007164
<i>UPB1</i>	beta-ureidopropionase 1	2.90	0.035407
<i>SERPINB2</i>	serpin family B member 2	2.89	0.00195
<i>CDCP1</i>	CUB domain containing protein 1	2.73	0.028336
<i>RGCC</i>	regulator of cell cycle	2.68	0.008743
<i>WEE1</i>	WEE1 G2 checkpoint kinase	2.65	0.019385
<i>RASGRP3</i>	RAS guanyl releasing protein 3	2.60	0.023527
<i>IDI1</i>	inhibitor of DNA binding 1, HLH protein	2.57	0.006793
<i>AC245128.3</i>	novel transcript	2.55	0.002478
<i>CXCL2</i>	C-X-C motif chemokine ligand 2	2.53	0.027452
<i>AC092849.1</i>	novel transcript	2.38	0.022066
<i>AC022706.1</i>	novel transcript	2.38	0.035109
<i>AC004825.2</i>	novel transcript	2.34	0.047031
<i>TSPOAP1</i>	TSPO associated protein 1	2.33	0.011881
<i>AL121899.1</i>	uncharacterized LOC388780	2.32	0.029992
<i>AC015912.3</i>	novel transcript	2.31	0.002763
<i>LINC-PINT</i>	long intergenic non-protein coding RNA, p53 induced transcript	2.30	0.011033
<i>CCNF</i>	cyclin F	2.23	0.048971
<i>AC069547.1</i>	TEC	2.21	0.035514
<i>ACSL3</i>	acyl-CoA synthetase long chain family member 3	2.19	0.035108
<i>DHCR24</i>	24-dehydrocholesterol reductase	2.17	0.021205
<i>MYO10</i>	myosin X	2.14	0.025732
<i>PDE4D</i>	phosphodiesterase 4D	2.07	0.020315
<i>ALOX5AP</i>	arachidonate 5-lipoxygenase activating protein	2.05	0.00195
<i>PIM1</i>	Pim-1 proto-oncogene, serine/threonine kinase	2.02	0.012535
<i>PTTG1</i>	pituitary tumor-transforming 1	2.01	0.040979
<i>HLX</i>	H2.0 like homeobox	1.97	0.00106
<i>MMP25</i>	matrix metalloproteinase 25	1.96	0.00911
<i>TSPYL2</i>	TSPY like 2	1.95	0.016041
<i>CXXC5</i>	CXXC finger protein 5	1.94	0.010368

<i>IL1RN</i>	interleukin 1 receptor antagonist	1.93	0.00411
<i>C20orf27</i>	chromosome 20 open reading frame 27	1.90	0.014644
<i>CD151</i>	CD151 molecule (Raph blood group)	1.89	0.005278
<i>ARRDC4</i>	arrestin domain containing 4	1.89	0.026617
<i>GNAI5</i>	G protein subunit alpha 15	1.88	0.001983
<i>ARPC5L</i>	actin related protein 2/3 complex subunit 5 like	1.85	2.47E-06
<i>TRAF3IP2</i>	TRAF3 interacting protein 2	1.84	0.015103
<i>HIST3H2A</i>	histone cluster 3 H2A	1.83	0.018694
<i>DUSP5</i>	dual specificity phosphatase 5	1.82	0.012321
<i>AC006449.6</i>	novel transcript	1.77	0.002478
<i>BCL2</i>	BCL2, apoptosis regulator	1.76	0.006648
<i>RCL1</i>	RNA terminal phosphate cyclase like 1	1.76	0.027452
<i>AC108673.2</i>	novel transcript, antisense to RAB43	1.74	0.00411
<i>PTGER2</i>	prostaglandin E receptor 2	1.73	0.007389
<i>INAFM1</i>	InaF motif containing 1	1.73	0.011213
<i>EAF1</i>	ELL associated factor 1	1.73	0.028383
<i>RFLNB</i>	refilin B	1.70	0.000736
<i>TLE3</i>	transducin like enhancer of split 3	1.68	0.003728
<i>CD63</i>	CD63 molecule	1.68	0.004932
<i>RELB</i>	RELB proto-oncogene, NF-kB subunit	1.67	0.034818
<i>GPR183</i>	G protein-coupled receptor 183	1.67	0.042526
<i>RETN</i>	resistin	1.66	0.014803
<i>AGFG1</i>	ArfGAP with FG repeats 1	1.65	0.031213
<i>AC245884.11</i>	novel transcript	1.64	0.041913
<i>AC006978.1</i>	proteasome (prosome, macropain) 26S subunit, ATPase, 5 (PSMC5) pseudogene	1.63	0.009806
<i>MAPKAPK2</i>	mitogen-activated protein kinase-activated protein kinase 2	1.60	0.017543
<i>FLVCR2</i>	feline leukemia virus subgroup C cellular receptor family member 2	1.60	0.035487
<i>SESN2</i>	sestrin 2	1.58	0.036583
<i>GLTPD2</i>	glycolipid transfer protein domain containing 2	1.56	0.035108
<i>CSNK1A1</i>	casein kinase 1 alpha 1	1.55	0.012693
<i>SLA</i>	Src like adaptor	1.55	0.023527

<i>AL445524.1</i>	novel transcript	1.55	0.034818
<i>SLC6A8</i>	solute carrier family 6 member 8	1.55	0.037241
<i>TIPARP</i>	TCDD inducible poly (ADP-ribose) polymerase	1.54	0.034818
<i>RPS9</i>	ribosomal protein S9	1.52	0.00195
<i>DTX4</i>	deltex E3 ubiquitin ligase 4	1.50	0.01087
<i>NINJ1</i>	ninjurin 1	1.50	0.040979
<i>BCL7B</i>	BCL tumor suppressor 7B	1.49	0.002478
<i>QSOX1</i>	quiescin sulfhydryl oxidase 1	1.48	7.96E-05
<i>PLAUR</i>	plasminogen activator, urokinase receptor	1.48	0.040979
<i>SNIP1</i>	Smad nuclear interacting protein 1	1.46	0.035042
<i>ZCCHC2</i>	zinc finger CCHC-type containing 2	1.45	0.030409
<i>ARID3B</i>	AT-rich interaction domain 3B	1.44	0.002478
<i>UBALD2</i>	UBA like domain containing 2	1.44	0.00411
<i>EHD4</i>	EH domain containing 4	1.42	0.035407
<i>CD99P1</i>	CD99 molecule pseudogene 1	1.41	0.024439
<i>NLRP3</i>	NLR family pyrin domain containing 3	1.40	0.012693
<i>REL</i>	REL proto-oncogene, NF-kB subunit	1.40	0.026324
<i>RUNX1</i>	runt related transcription factor 1	1.39	0.003728
<i>C1orf122</i>	chromosome 1 open reading frame 122	1.39	0.008743
<i>LRRC8A</i>	leucine rich repeat containing 8 VRAC subunit A	1.37	0.018161
<i>SH2B2</i>	SH2B adaptor protein 2	1.36	0.01087
<i>TRAPPC10</i>	trafficking protein particle complex 10	1.36	0.035108
<i>UBE2J1</i>	ubiquitin conjugating enzyme E2 J1	1.34	0.035407
<i>NAPRT</i>	nicotinate phosphoribosyltransferase	1.34	0.046237
<i>MRPL54</i>	mitochondrial ribosomal protein L54	1.33	0.038464
<i>DCTN5</i>	dynactin subunit 5	1.31	0.020315
<i>KDM5B</i>	lysine demethylase 5B	1.30	0.032784
<i>BCL6</i>	B cell CLL/lymphoma 6	1.29	0.00628
<i>UBA52</i>	ubiquitin A-52 residue ribosomal protein fusion product 1	1.29	0.01087
<i>GNE</i>	Glucosamine (UDP-N-acetyl)-2-epimerase/N-acetylmannosamine kinase	1.29	0.031459
<i>B4GALT1</i>	beta-1,4-galactosyltransferase 1	1.29	0.036583

<i>EPC1</i>	enhancer of polycomb homolog 1	1.27	0.017817
<i>NR1H2</i>	nuclear receptor subfamily 1 group H member 2	1.27	0.029228
<i>MMP24OS</i>	MMP24 opposite strand	1.25	0.012321
<i>NRBP1</i>	nuclear receptor binding protein 1	1.24	0.00751
<i>PUF60</i>	poly(U) binding splicing factor 60	1.22	0.025834
<i>HLA-B</i>	major histocompatibility complex, class I, B	1.22	0.03622
<i>SZRD1</i>	SUZ RNA binding domain containing 1	1.21	0.011885
<i>SLC15A3</i>	solute carrier family 15 member 3	1.21	0.036763
<i>ATP6V1F</i>	ATPase H ⁺ transporting V1 subunit F	1.21	0.044857
<i>MLF2</i>	myeloid leukemia factor 2	1.19	0.042439
<i>LAPTM5</i>	lysosomal protein transmembrane 5	1.17	0.040979

Table 35 Genes significantly down-regulated in CKD (Fold changes are calculated based on Read counts)

Gene Name	Gene description	Fold change	Adj. p value
<i>PSD4</i>	pleckstrin and Sec7 domain containing 4	0.556	0.049029
<i>NARS</i>	asparaginyl-tRNA synthetase	0.533	0.011885
<i>SNX1</i>	sorting nexin 1	0.519	0.03622
<i>CARD8</i>	caspase recruitment domain family member 8	0.515	0.043026
<i>GPR155</i>	G protein-coupled receptor 155	0.509	0.040979
<i>TRAPPC11</i>	trafficking protein particle complex 11	0.508	0.003965
<i>AKAP11</i>	A-kinase anchoring protein 11	0.501	0.017491
<i>ZFP36L2</i>	ZFP36 ring finger protein like 2	0.497	0.026324
<i>CREB1</i>	cAMP responsive element binding protein 1	0.496	0.01387
<i>TMEM87B</i>	transmembrane protein 87B	0.494	0.002484
<i>TMOD3</i>	tropomodulin 3	0.494	0.041913
<i>CRLF3</i>	cytokine receptor like factor 3	0.492	0.040979
<i>SLC30A7</i>	solute carrier family 30 member 7	0.489	0.01087
<i>LARS</i>	leucyl-tRNA synthetase	0.487	0.004639
<i>TMEM154</i>	transmembrane protein 154	0.487	0.015916
<i>SCIMP</i>	SLP adaptor and CSK interacting membrane protein	0.486	0.014644
<i>ECHDC1</i>	ethylmalonyl-CoA decarboxylase 1	0.486	0.021187

<i>ZBTB37</i>	zinc finger and BTB domain containing 37	0.482	0.030225
<i>TIA1</i>	TIA1 cytotoxic granule associated RNA binding protein	0.479	0.000666
<i>RPAP3</i>	RNA polymerase II associated protein 3	0.479	0.012358
<i>DCAF7</i>	DDB1 and CUL4 associated factor 7	0.476	0.010286
<i>OAS1</i>	2'-5'-oligoadenylate synthetase 1	0.470	0.037241
<i>EDEM3</i>	ER degradation enhancing alpha-mannosidase like protein 3	0.467	0.028231
<i>MPHOSPH8</i>	M-phase phosphoprotein 8	0.463	0.027187
<i>STX7</i>	syntaxin 7	0.462	7.96E-05
<i>IRF2</i>	interferon regulatory factor 2	0.458	0.011936
<i>SLC30A6</i>	solute carrier family 30 member 6	0.457	0.039275
<i>ATP10D</i>	ATPase phospholipid transporting 10D (putative)	0.448	0.03622
<i>CREBZF</i>	CREB/ATF bZIP transcription factor	0.447	0.040495
<i>NLN</i>	neurolysin	0.444	0.011885
<i>CHM</i>	CHM, Rab escort protein 1	0.438	0.014045
<i>CXorf38</i>	chromosome X open reading frame 38	0.432	0.030409
<i>TRIM27</i>	tripartite motif containing 27	0.431	0.011885
<i>APOBEC3G</i>	apolipoprotein B mRNA editing enzyme catalytic subunit 3G	0.431	0.016041
<i>SLC25A40</i>	solute carrier family 25 member 40	0.426	0.009806
<i>METTL17</i>	methyltransferase like 17	0.426	0.030409
<i>MFSD8</i>	major facilitator superfamily domain containing 8	0.424	0.00751
<i>NHSL2</i>	NHS like 2	0.420	7.96E-05
<i>SAMD9L</i>	sterile alpha motif domain containing 9 like	0.416	0.03622
<i>ACADM</i>	acyl-CoA dehydrogenase medium chain	0.414	0.03594
<i>ELF2</i>	ELL associated factor 2	0.413	0.018052
<i>AGPAT5</i>	1-acylglycerol-3-phosphate O-acyltransferase 5	0.412	0.035487
<i>ITGA4</i>	integrin subunit alpha 4	0.410	0.001961
<i>NUP43</i>	nucleoporin 43	0.409	0.023527
<i>CALHM2</i>	calcium homeostasis modulator family member 2	0.400	0.026324
<i>TNFAIP8L2</i>	TNF alpha induced protein 8 like 2	0.400	0.028336
<i>SLC26A1</i>	solute carrier family 26 member 1	0.399	0.048104
<i>ZNF767P</i>	zinc finger family member 767, pseudogene	0.391	0.027452

<i>KRCCI</i>	lysine rich coiled-coil 1	0.388	0.002478
<i>AARS</i>	alanyl-tRNA synthetase	0.388	0.007085
<i>PREPL</i>	prolyl endopeptidase like	0.387	0.040495
<i>SKP2</i>	S-phase kinase associated protein 2	0.386	0.006793
<i>AATBC</i>	apoptosis associated transcript in bladder cancer	0.381	0.007547
<i>MITD1</i>	microtubule interacting and trafficking domain containing 1	0.381	0.015916
<i>AFMID</i>	arylformamidase	0.378	0.001407
<i>TRIM5</i>	tripartite motif containing 5	0.373	0.014864
<i>RIC8B</i>	RIC8 guanine nucleotide exchange factor B	0.365	0.042042
<i>GIMAP6</i>	GTPase, IMAP family member 6	0.362	0.024469
<i>THOC3</i>	THO complex 3	0.355	0.020126
<i>AC004656.1</i>	novel transcript, overlapping to PDK3	0.349	7.96E-05
<i>GIMAP4</i>	GTPase, IMAP family member 4	0.346	0.012929
<i>XAF1</i>	XIAP associated factor 1	0.344	0.048532
<i>AP002761.4</i>	novel transcript, overlapping to P2RY2	0.341	0.013514
<i>ENOSF1</i>	enolase superfamily member 1	0.331	0.008743
<i>LINC01001</i>	long intergenic non-protein coding RNA 1001	0.318	0.034818
<i>MS4A14</i>	membrane spanning 4-domains A14	0.317	0.029041
<i>GIMAP8</i>	GTPase, IMAP family member 8	0.316	7.96E-05
<i>CCDC66</i>	coiled-coil domain containing 66	0.298	7.96E-05
<i>WDR17</i>	WD repeat domain 17	0.280	0.018052
<i>PUS7</i>	pseudouridylyl synthase 7	0.277	0.046108
<i>SLC46A2</i>	solute carrier family 46 member 2	0.190	7.96E-05
<i>AC123912.4</i>	novel transcript	0.184	0.027452
<i>AL627309.2</i>	novel transcript	0.178	0.011552
<i>ZNF780A</i>	zinc finger protein 780A	0.163	0.024469
<i>ATP7B</i>	ATPase copper transporting beta	0.159	0.027452
<i>CRYZ</i>	crystallin zeta	0.142	7.93E-09
<i>AC006033.2</i>	novel transcript	0.107	0.003208
<i>CCDC144A</i>	coiled-coil domain containing 144A	0.059	0.002478
<i>LITD1</i>	LINE1 type transposase domain containing 1	0.057	0.001761

We also specifically compared the expression of genes investigated in this study. As summarized in Figure 44, no significant differences were observed in IL-1 α and IL-1 β RNA expression between CKD and healthy donors. Among the IL-1 family receptors, the IL-1RN was significantly up-regulated in CKD patients. Additionally, analysis of the P2 family gene expression showed a significant downregulation of P2RX7, P2RY2, P2RY8, P2Y13, P2Y14 and a novel transcript of P2RY2 (gene ID ENSG00000260401) in CKD donors' monocytes (Fig. 44).

Previous studies have shown that matrix metalloproteinases (MMPs) regulate IL-1 β secretion and its degradation in extracellular space (Ito et al., 1996). By comparing the expression of MMPs, we observed a significant up-regulation of MMP9 and MMP25 in CKD donors (Fig. 44B).

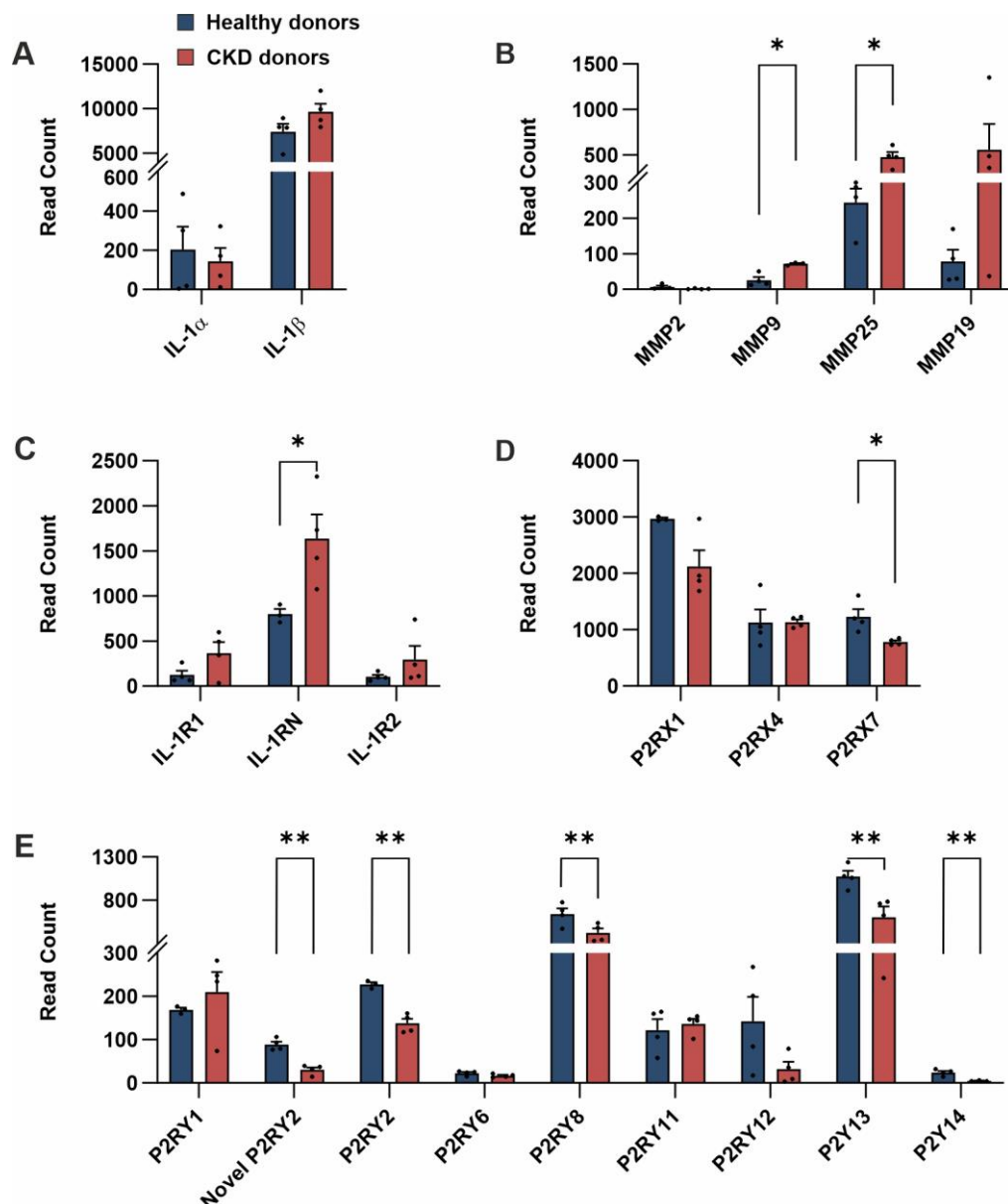


Figure 44 Expression analysis of some candidate genes measured by RNA sequencing.

Graphs representing the comparison of RNA sequencing results for several genes including, IL-1 α and IL-1 β (A) and their receptors (C), MMP2, MMP9, MMP25 and MMP19 (B), P2RXs (D) and P2RYs (E). Data were obtained from 4 healthy and 4 CKD donors and are shown as mean +SEM, and significances were tested by unpaired t-test followed by Welch's correction test (n=4) (* P<0.05, ** P<0.01, *** P<0.001, **** P<0.0001).

13 MMPs have multiple effects on IL-1 α biogenesis

Since RNA sequencing analysis showed altered MMP expression levels in CKD monocytes, we investigated the effects of MMPs on IL-1 α cleavage and secretion. For this purpose, LPS treated cells were first incubated with either an MMP PAN inhibitor or a specific MMP9 inhibitor, and after the incubation time 2 mM ATP was applied. As shown in Figure 45, ATP-induced IL-1 α release was significantly reduced upon incubation with the MMP PAN inhibitor,

while IL-1 β release remained unaffected. Moreover, the inhibition of MMP9 did not result in any significant changes in IL-1 α or IL-1 β release.

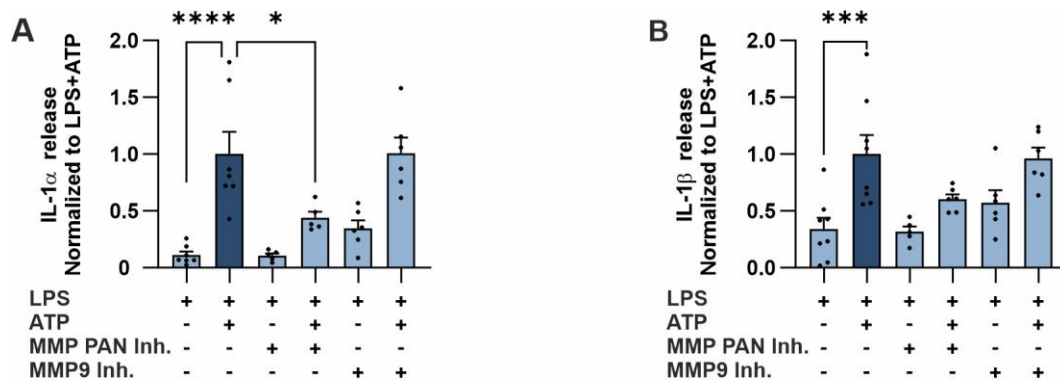


Figure 45 Inhibition of MMPs after LPS treatment leads to reduced secretion of IL-1 α in response to ATP.

Graphs representing normalized concentrations of IL-1 α (A) or IL-1 β (B) released from LPS treated primary monocytes measured by ELISA. LPS treated monocytes were incubated with either MMP9 or MMP PAN inhibitor followed by 2 mM ATP application. Data are shown as mean +SEM and significances were tested by one-way ANOVA followed by Bonferroni correction test (n=4-8) (* P<0.05, ** P<0.01, *** P<0.001, **** P<0.0001).

To test the effects of MMPs during the LPS priming phase, MMP PAN and MMP9 inhibitors were added to primary monocyte's cultures 60 min prior to LPS treatment and were kept in the medium until the end of the experiment. Cells treated with MMP9 specific inhibitor before LPS priming showed higher levels of released IL-1 α that were not further increased by ATP application. On the other hand, IL-1 β release was significantly increased by MMP9 inhibition before LPS treatment, both with and without ATP application. Inhibition of MMPS using the MMP PAN inhibitor before LPS treatment did not lead to a significant change in IL-1 α or IL-1 β release (Fig. 46A, B).

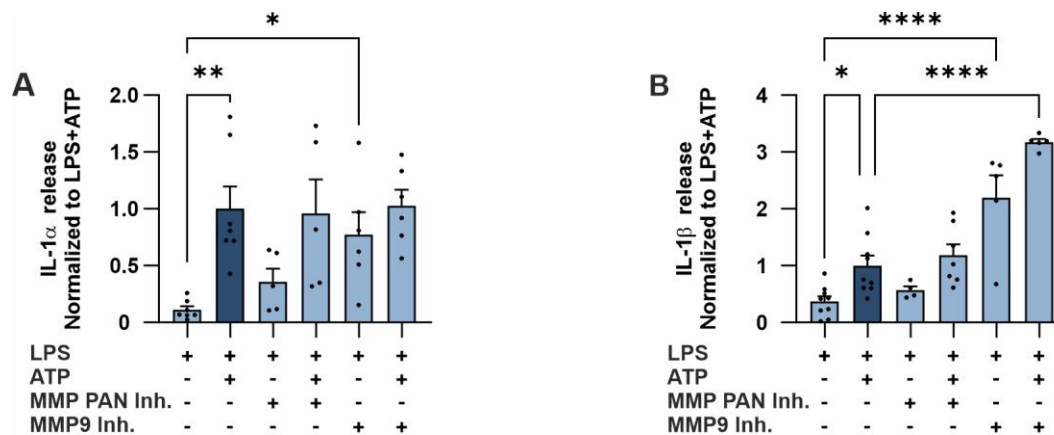


Figure 46 MMP9 inhibition before LPS treatment leads to higher IL-1 α and IL-1 β concentrations in medium.

Graphs representing normalized concentrations of IL-1 α (A) or IL-1 β (B) released from LPS treated primary monocytes measured by ELISA. Primary monocytes were first incubated with MMP9 or MMP PAN inhibitor and then LPS was added overnight to the medium in the presence of the inhibitor of interest. The next day, 2 mM ATP was applied for 30 minutes. Data are shown as mean +SEM and significances were tested by one-way ANOVA followed by Bonferroni correction test (n=4-9) (* P<0.05, ** P<0.01, *** P<0.001, **** P<0.0001).

Parallel TCA western blot analyses showed increased release of mature IL-1 α from cells treated with MMP9 specific inhibitor before LPS priming, regardless of ATP application. of ATP application to cells pretreated with the MMP9 inhibitor and then LPS did not induce further IL-1 α release, but a significant increase was observed compared to the control ATP condition (Fig. 47B). Incubation of cells with the MMP9 inhibitor after LPS priming also resulted in significantly increased levels of the 17 kDa protein in the medium upon ATP application (Fig. 47C). A trend toward increased levels of mature IL-1 α was observed in the medium collected from LPS treated cells incubated with MMP9 inhibitor (no ATP stimulation) compared to cells treated with only LPS. Treatment with the MMP PAN inhibitor did not show any significant effect either before or after LPS priming. Western blot analysis of intracellular proteins did not reveal any significant alterations upon these treatments (Fig. 48). Perhaps increasing the number of donors would provide a better understanding of the results.

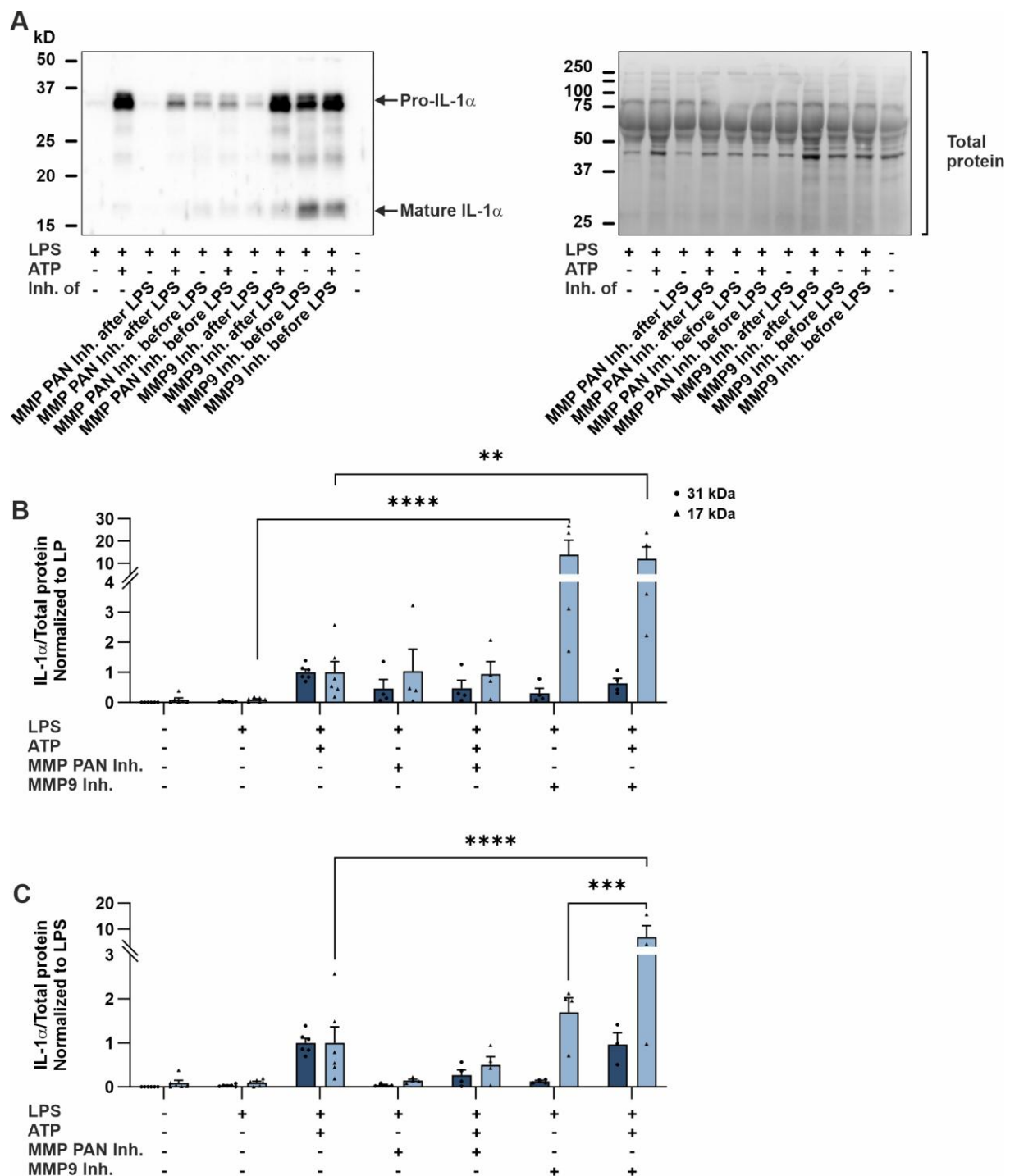


Figure 47 MMP9 inhibition before or after LPS treatment leads to a significant increase in mature IL-1 α concentration in the medium.

Representative Western blot images of IL-1 α protein released in the medium by LPS treated primary monocytes in response to 2 mM ATP alone or after incubation with MMP inhibitor of interest (A). Graphs representing analysis of IL-1 α protein signal intensities in western blots obtained from total proteins in the medium, which were concentrated using TCA acid protocol, from cells incubated with the inhibitor either before (B) or after (C) LPS treatment. For an accurate comparison, the amount of total protein loaded onto the gel was stained by No stain reagent and the signal intensities were used for normalizing the IL-1 α protein signals. To compare between treatments, all signal intensities were

normalized to the protein concentration of the LPS+ATP treatment of corresponding donor. Data are shown as mean +SEM and significances were tested by two-way ANOVA (B) followed by a Bonferroni's correction test (n=3-6) (* P<0.05, ** P<0.01, *** P<0.001, **** P<0.0001).

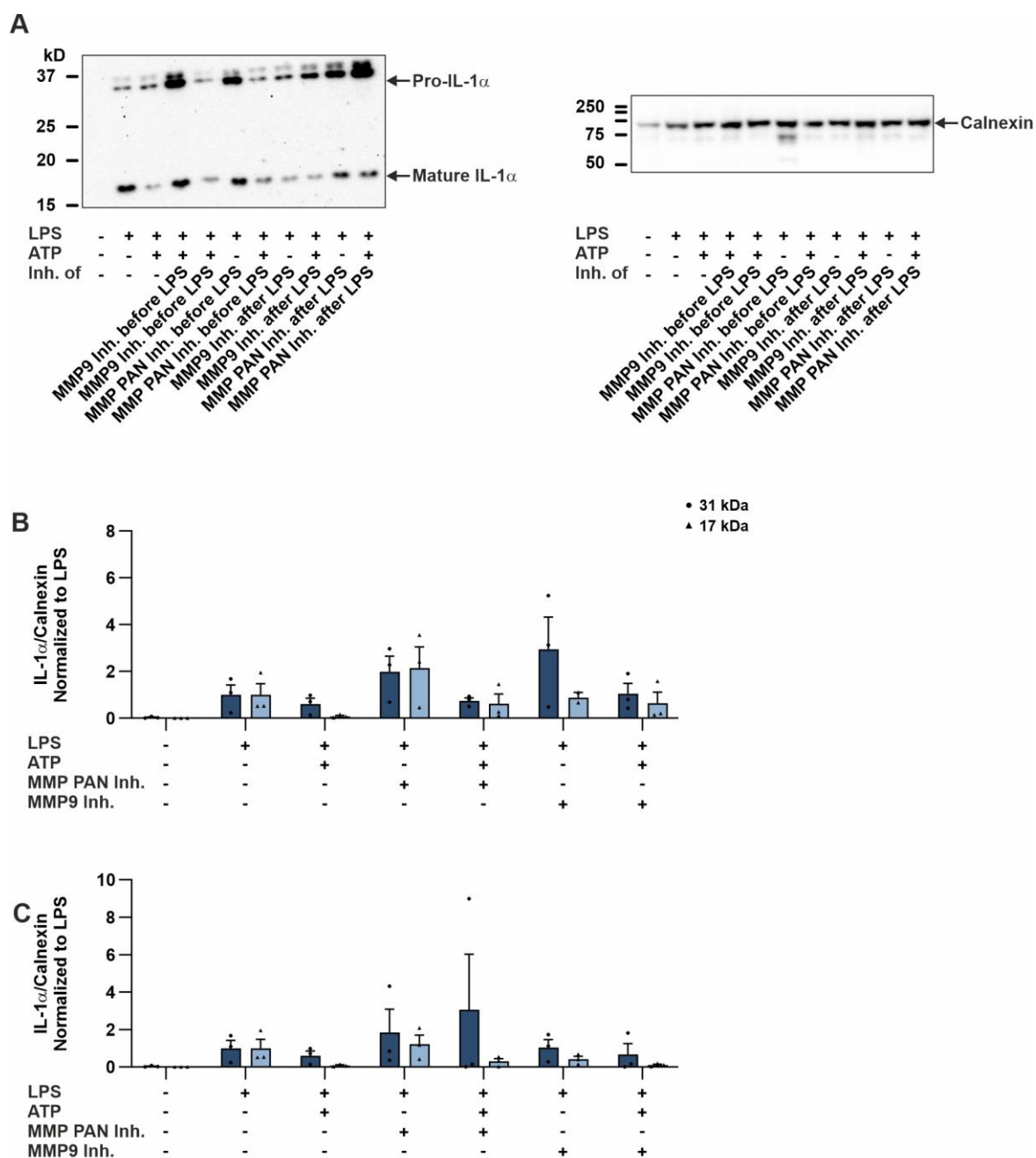


Figure 48 MMPs inhibition does not affect intracellular IL-1 α concentrations.

(A) Representative western blots images of intracellular IL-1 α protein in untreated or LPS treated primary monocytes in response to 2 mM ATP alone or after incubation with MMP inhibitor of interest. Graphs representing analysis of IL-1 α protein signal intensities in western blots obtained from total proteins in the cell lysate from cells incubated with the inhibitor either before (B) or after (C) LPS treatment. Protein signal intensities were normalized to the housekeeping protein and afterwards values of different treatments have been normalized to the protein concentration of the LPS treatment of corresponding donor. Data are shown as mean +SEM and significances were tested by two-way

ANOVA followed by a Bonferroni's correction test (n=2-3) (* P<0.05, ** P<0.01, *** P<0.001, **** P<0.0001).

The effects of MMP inhibition on the surface expression of IL-1 α were also measured by flow cytometry. We observed a significant increase in the percentage of monocytes expressing membrane bound IL-1 α in cells treated with the MMP PAN inhibitor before LPS priming. However, MMP inhibition after LPS priming did not have any significant effect on IL-1 α surface expression. Furthermore, MMP9 inhibition did not induce IL-1 α surface expression under any conditions (Fig. 49).

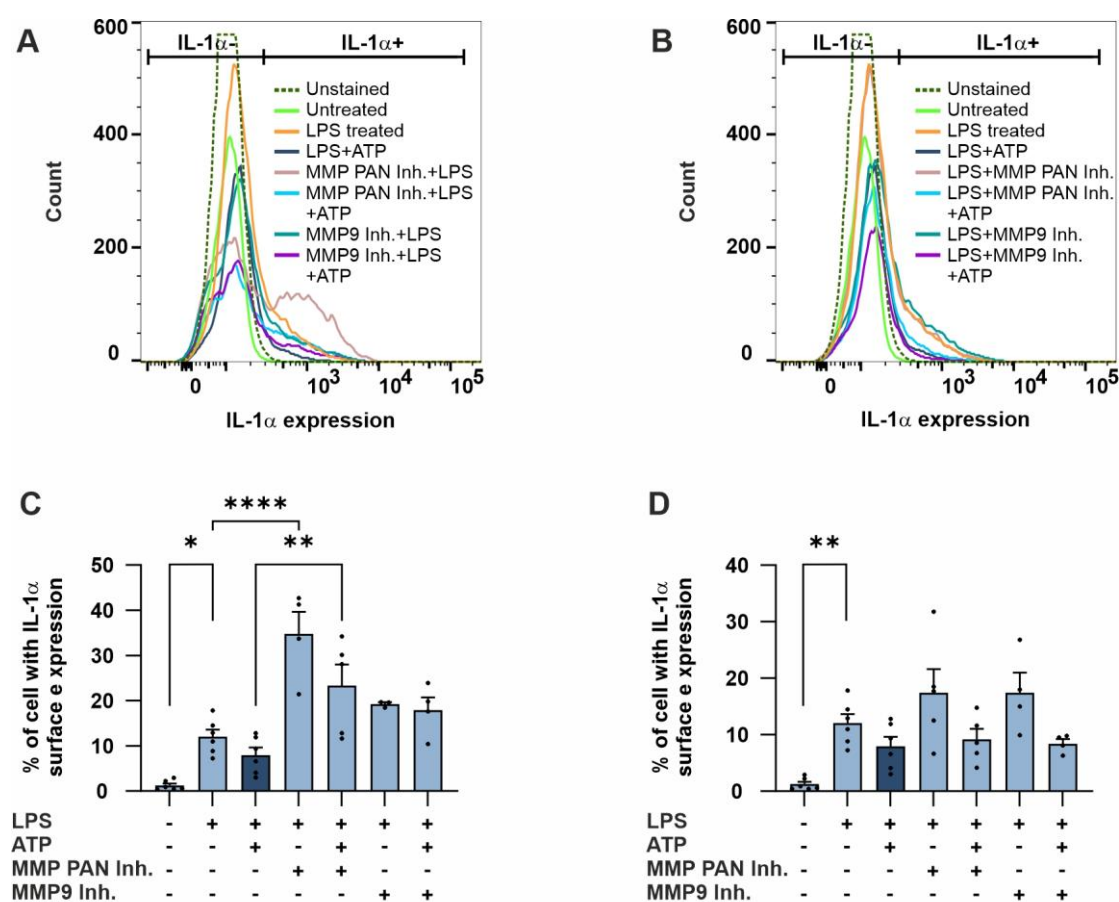


Figure 49 Membrane bound IL-1 α is cleaved by MMPs.

Graphs representing flow cytometry analysis of the percentage of human primary monocytes expressing IL-1 α on cell surface (A and B) and related histogram from an example donor, upon treatment with LPS and LPS+ATP, with or without inhibitor of interest. Primary monocytes were incubated with MMP9 or MMP PAN inhibitor either before (A and C) or after (B and D) LPS treatment followed by 2 mM ATP application. Data are shown as mean +SEM and significances were tested by one-way ANOVA followed by Bonferroni correction test (n=3-6) (* P<0.05, ** P<0.01, *** P<0.001, **** P<0.0001).

Discussion

1 Calcium is essential for IL-1 α secretion.

In the present study, we investigated the importance of Ca²⁺ signals, the underlying Ca²⁺ channels and the effects of altered Ca²⁺ signals on IL-1 α biogenesis. Inhibiting calpain, a calcium-dependent protease which cleaves pro-IL-1 α , resulted in a reduction in IL-1 α release, while IL-1 β release was not affected (Fig. 17). Similar to our findings, reduced release of IL-1 α has been reported upon calpain inhibition in Th17 cells in a dose dependent manner (Chao et al., 2023). Additionally, Kavita et. al. have shown that IL-1 β may be protected from calpain cleavage and that calpain is not involved in the IL-1 β maturation process (Kavita & Mizel, 1995). The importance of Ca²⁺ influx in IL-1 α release was also demonstrated in a study by Watanabe et. al., where treating carcinoma cells with the Ca²⁺ ionophore A23187, led to a higher Ca²⁺ influx and induced IL-1 α maturation and selective release of the mature form, without affecting the release of pro-IL-1 α (Watanabe & Kobayashi, 1994).

Chelating cytoplasmic Ca²⁺ by BAPTA-AM led to reduced secretion of both IL-1 α and IL-1 β (Fig. 16). A previous study has also shown that treating human macrophages with BAPTA-AM inhibits maturation and release of IL-1 β , in a dose dependent manner (Brough et al., 2003). Three more studies have also reported the inhibition of ATP induced IL-1 β release upon chelating Ca²⁺ by BAPTA-AM in RAW264.7 cells (Kawano et al., 2012), bone marrow derived macrophages (BMDMs) (G.-S. Lee et al., 2012) and J774A.1 cell (Yaron et al., 2015). On the other hand, chelating only extracellular Ca²⁺ by EGTA did not have any significant effect on primary monocytes IL-1 α release. In the study by Watanabe on carcinoma cells, chelating extracellular Ca²⁺ by EGTA resulted in blockage of the IL-1 α maturation process, with no effect on the release of the pro-form (Watanabe & Kobayashi, 1994). Based on our Western blot analysis of proteins released to the medium, the 31 kDa IL-1 α (pro-form) is the predominantly released form, therefore the minor effect of EGTA on IL-1 α release can be explained by the findings of Watanabe and colleagues. Additionally, reducing extracellular Ca²⁺ concentrations led to a reduction in ATP induced Ca²⁺ signals in LPS treated monocytes (Fig. 11 and Fig. 14). Reduced IL-1 β secretion was also reported upon incubating the macrophage cell line in Ca²⁺ free buffer (Kawano et al., 2012). Altogether, our data suggest that the inhibition of Ca²⁺ influx is not sufficient to inhibit IL-1 α release in response to ATP and the required Ca²⁺ signal for IL-1 α release is mediated by both Ca²⁺ release from internal stores and Ca²⁺ influx from

extracellular space. Signaling through P2X7 is essential for IL-1 α release, and the role of P2X4 requires further investigation.

Higher expression and secretion levels of IL-1 α in CKD patients' monocytes have been reported by Schunk et. al. (Schunk et al., 2021) and as discussed, an increase in cytosolic [Ca²⁺] is essential for IL-1 α release. To explore IL-1 α biogenesis and its role in CKD, we compared Ca²⁺ signaling pathways in monocytes from CKD patients and healthy controls. Our results show that the activation of TRPM2 Ca²⁺ channel and SOCE induces comparable Ca²⁺ signals in CKD and healthy monocytes. In agreement with Ca²⁺ imaging findings, analysis of mRNA expression levels of these channels and several other TRP channels revealed no significant alteration in CKD monocytes (Fig. 7 and Fig. 8). On the other hand, extracellular ATP application induced Ca²⁺ signals in monocytes, which were significantly altered in cells derived from CKD patients. Moreover, significantly higher mRNA expression levels of P2X4, P2X7 and P2Y11 in CKD monocytes were detected via qPCR analysis (Fig. 12). In contrast, RNA sequencing showed significantly lower expression levels of P2RX7, P2RY2, P2RY8, P2RY13 and P2RY14 in CKD monocytes. Although qPCR and RNA-seq both target RNA molecules, difference in the experimental techniques, methods for analyzing and normalizing the data, bioinformatic procedures, and the biases can lead to different outcomes. A proper comparison between the results obtained from these two methods has not yet been reported. Consistent with our qPCR results, Lajdova et. al. have reported increased expression of P2X7 in CKD patients' monocytes (Lajdova et al., 2017).

Furthermore, application of ATP to untreated primary monocytes induced higher intracellular Ca²⁺ responses compared to cells treated with LPS (Fig. 13). Additionally, removing extracellular Ca²⁺, drastically reduced ATP induced Ca²⁺ responses in untreated cells, whereas LPS treated cells were less affected (Fig. 14). Since the extracellular Ca²⁺ enters the cell via P2X receptors, these data suggest a higher impact of P2Xs on Ca²⁺ signals after LPS treatment. Gene expression analysis showed significantly reduced P2Y11 and increased P2X4 mRNA expression upon LPS priming in monocytes (Fig. 13). Furthermore, inhibiting P2X4 significantly reduced Ca²⁺ responses to ATP in LPS treated cells up to ~40%, but no significant effect was observed in untreated cells (Fig. 22, Table 30). This correlates with the reduced IL-1 α release from LPS treated cells upon P2X4 inhibition (Fig. 23). The structural and functional interactions between P2X4 and P2X7 has been studied in HEK293 and BMDMs by (Guo et al., 2007). Also, the regulatory effect of P2X4 on P2X7 was shown by the work of Sakaki and his colleagues. They demonstrated that expression of P2X4 is required for P2X7 dependent IL-1 β

and IL-18 release from mouse bone marrow derived dendritic cells (Sakaki et al., 2013). These studies and our results suggest a dual function of P2X4 in ATP mediated Ca^{2+} signaling, where it can function as an inhibitor or enhancer of ATP signals. Only recently have the effects of P2X4 on IL-1 β been investigated in P2X4 KO mice, where lower expression levels of IL-1 β were detected in kidney cells and plasma compared to control mice. However, the expression levels of IL-1 α in these KO mice have not been reported, either in monocytes or in kidney cells. Additionally, P2X4 KO mice were shown to be protected against ischemic acute kidney injury with significantly lower inflammation (S. J. Han et al., 2020). An increase in P2X4 currents and its mRNA expression was also observed upon LPS stimulation in BV-2 murine microglial cells, while P2X7 currents remained largely unaffected (Raouf et al., 2007). We were not able to find any study on the correlation between P2X4 and IL-1 α expression or release. In conclusion, these findings suggest that ATP induced Ca^{2+} signals are conducted by different P2 family members in cells treated with LPS or untreated cells, with a potential role of P2X4 in ATP induced Ca^{2+} signals in inflammatory conditions, as well as in CKD disease.

The structure of P2X7 channel consists of an LPS binding motif. It is suggested that this motif controls the channel surface trafficking and expression (Denlinger et al., 2003; reviewed by Kopp et al., 2019). Therefore, although no significant reduction has been observed in P2X7 expression upon LPS treatment, incubating cells with LPS can change the channel availability leading to lower Ca^{2+} influx into the cells. This LPS binding motif is also suggested to coordinate different signal transduction events in macrophages (Denlinger et al., 2001). Analysis of intracellular total protein from cells treated with P2X7 antagonist showed decreased levels of mature IL-1 α (Fig. 25). Additionally, inhibition of P2X7 blocked the effect of ATP application on cell surface expression of CD16 and IL-1 α (Fig. 31 and Fig. 34). In contrast to our findings, a study by Fettelschoss et. al. showed that in BMDMs from P2X7 knockout mice, IL-1 α and IL-1 β release was completely inhibited without alterations in IL-1 α surface expression (Fettelschoss et al., 2011). Moreover, P2X7 inhibition led to a significant reduction in ATP induced Ca^{2+} responses in LPS treated CKD monocytes, but not healthy individuals. A tendency toward reduction was also observed in untreated CKD monocytes (Fig. 29). This correlates with the higher expression of P2X7 observed in CKD cells (Fig. 12). This data agrees with Lajdova et. al. study, which has also shown that P2X7 antagonist can reduce Ca^{2+} signals in PBMCs of CKD donors, where no significant reduction was observed in healthy PBMCs (Lajdova et al., 2012). ATP induced IL-1 α release was completely abolished by P2X7 inhibition, which was comparable between CKD and healthy donors (Fig. 27). In a recent study,

inhibition of P2X7 by A804598 or oxATP significantly reduced IL-1 β release in THP-1 cells in response to ATP, while P2X4 inhibition did not alter IL-1 β secretion (Bockstiegel et al., 2023). The effects of P2X7 on IL-1 α have not yet been extensively studied.

We could not detect any increase in $[Ca^{2+}]_i$ upon P2Y2 agonist application on LPS treated monocytes and no IL-1 α release was also observed in either ELISA or Western blot analysis (Fig. 20, Fig. 23, Fig. 25). On the other hand, P2Y2 agonist led to Ca^{2+} signals comparable to those induced by ATP in untreated cells (inducing 97 % of ATP signals) (Table 30). Inhibition of P2Y2 increased the $[Ca^{2+}]_i$ in LPS treated cells upon ATP application, but it did not alter IL-1 α release. P2Y2 has been found to alter P2X7 kinetics in mouse osteoblasts (Mikolajewicz et al., 2021), therefore the increased levels of intracellular Ca^{2+} upon P2Y2 inhibition may be due to its effects on P2X7 signaling. Although signaling through P2Y2 has been shown to increase IL-1 β production in murine macrophages and its inhibition abolished this increase (de la Rosa et al., 2020), we did not detect any significant change in IL-1 β production either.

In another approach, we investigated IL-1 α release upon activating specific P2 family members by applying the ADP/UTP or by using different concentrations of ATP. Solo activation of purinergic family members or ATP concentrations below the P2X7 activation range did not induce IL-1 α release from cells, which highlights the role of P2X7 in IL-1 α release (Fig. 19). Considering that single agonist applications could not induce IL-1 α release, our data suggest that activation of more than one member of P2 family is needed to trigger IL-1 α release. As previously discussed, the interaction between P2Y2, P2X4 and P2X7 have been reported in several studies, demonstrating a close functional relationship between these channels (Antonio et al., 2011; Brock et al., 2022; Mikolajewicz et al., 2021; Schneider et al., 2017). Moreover, our Western blot analysis revealed a significant reduction in the mature form of IL-1 α upon inhibition of P2X4, P2X7 and P2Y2, suggesting a critical role for P2 family in IL-1 α cleavage (Fig. 25). The involvement of P2X7 and P2X4 in IL-1 α release or expression has not been reported previously. Thus, our findings suggest a novel role for P2X4 and P2X7 channels in IL-1 α release.

2 Signaling through P2X7 modulates monocyte subpopulations.

Analysis of surface expressions showed a higher percentage of LPS treated CKD monocytes expressing CD16 compared to healthy cells, which was significantly reduced by ATP application. Inhibition of P2X7 abolished the reduction in CD16 expressing cells upon ATP application. These changes were also observed in CD16⁻ cells in the opposite direction (Fig.

31). A cleavage region for ADAM17 has been identified on CD16, leading to CD16 shedding from the NK cells membrane (Jing et al., 2015). Additionally, P2X7 mediated ADAM 17 activation has been reported in the context of VCAM-1 shedding from AEC 1 cells (Mishra et al., 2016). Combining our results with the aforementioned studies, we suggest a regulatory role of P2X7 on CD16 shedding via ADAM17 from monocytes membrane.

Furthermore, upon LPS priming the intermediate subpopulation (CD14⁺ CD16⁺) was significantly increased in CKD monocyte population compared to healthy cells (Fig. 32A). ATP treatment led to a reduction in the intermediate subtype in a P2X7 dependent manner. A trend toward a reduction in the intermediate population upon ATP application is also observed in healthy cells, although it was not significant. This observation is consistent with a recent study by Cormican et. al., which showed an increased population of distinct proinflammatory intermediate monocytes in CKD patients (Cormican et al., 2023). Naicker and colleagues have also reported a higher fraction of intermediate monocytes in CKD patients, which negatively correlated with eGFR (Naicker et al., 2018). In another study monocyte subtypes of 119 non-dialysis CKD patients were followed for a period of 4.8-5 years and a positive correlation was found between the number of intermediate monocyte and cardiovascular events (Heine et al., 2008). Moreover, another study also showed that the proportion of intermediate monocytes, rather than total monocytes, correlates with the risk of cardiovascular events (Heine et al., 2008). Additionally, the role of intermediate monocytes in inflammatory diseases and high IL-1 β expression has been reported in several studies (Fingerle et al., 1993; Nockher & Scherberich, 1998), but the correlation between CD16 and IL-1 α release or their surface expression remains to be determined. Altogether, the observed increase in CD16 expressing cells and the intermediate monocyte population in the CKD-derived cells upon LPS treatment may be correlated with IL-1 α surface expression and release from the membrane, as well as monocyte adhesion and initiation of atherosclerosis. This could be the missing link in correlating the increased intermediate monocyte population with cardiovascular outcomes in CKD patients. Therefore, our data suggest P2X7 as a potential therapeutic target and a novel role of CD16 in CKD disease progression. Further experiments are required to identify the role of CD16 in IL-1 α release, either from the cytoplasm or membrane. Investigating the co-localization of IL-1 α and CD16 via fluorescent microscopy and immunoprecipitation assays or examining IL-1 α localization and release from CD16 Ko mouse monocytes could provide more information on the interaction between CD16 and IL-1 α .

3 Altered P2X7 Ca²⁺ signaling in CKD patients leads to altered IL-1 α surface expression.

We also analyzed the membrane bound IL-1 α in relation to CD14 or CD16 surface expression in CKD and healthy monocytes. In healthy monocytes, LPS treatment led to a significant increase in the percentage of CD14⁺/IL-1 α ⁺ (Fig. 34A), and CD16⁻/IL-1 α ⁺ cells (Fig. 34F) in healthy donors. The application of ATP to healthy cells significantly reduced the percentage of CD16⁻/IL-1 α ⁺ cells, but this population remained unchanged in CKD group (Fig. 34F). ATP application caused a significant reduction in both CD16⁺/IL-1 α ⁻ and CD16⁺/IL-1 α ⁺ populations (Fig. 34C, D) and a significant increase in CD16⁻/IL-1 α ⁻ cells in the CKD monocytes (Fig. 34E). Focusing on IL-1 α ⁺ cells, upon ATP application a significant reduction was only observed in CD16⁺ cells in CKD donors and CD16⁻ in healthy donors. This suggests that the IL-1 α release in CKD cells primarily originates from CD16⁺ cells. No significant alterations were observed in CD14⁺ cells upon ATP application, regardless of whether they expressed IL-1 α or not. On the other hand, upon LPS treatment ~12% of monocytes showed surface expression of IL-1 α in both groups. After ATP application ~7% of healthy cells release the membrane bound IL-1 α , while this was only around 1.86% in CKD cells. Interestingly, all changes in the surface expression of CD16, CD14 or IL-1 α upon ATP application were blocked by P2X7 inhibition. In a recent study by Schunk et. al. a significant increase of IL-1 α on the surface of classical, non-classical and intermediate monocytes was reported in association with cardiovascular events (Schunk et al., 2021). Higher IL-1 α release was also reported in CKD monocytes in the same study, which contrasts with our ELISA data. This discrepancy may be due to differences in monocytes isolation methods, as we used kit isolated monocytes, whereas Schunk et al. isolated monocytes via adherence to the plate. Another factor that may influence the results is our use of heparin-containing tubes for blood collection instead of EDTA, to prevent alterations in Ca²⁺ signaling. Furthermore, our RNA sequencing results did not show any significant change in IL-1 α expression. This could be due to the limited number of donors in ELISA and sequencing data in our experiments and the results may improve with a larger study group.

In conclusion, our results suggest a major role for P2X7 in modulating the surface expression of IL-1 α and CD16, thereby altering the distribution of monocyte subtypes. Additionally, we observed greater release of membrane bound IL-1 α from CD16⁺ monocytes in CKD and from CD14⁺ cells in healthy individuals, with a lower release rate from CKD cells. This may contribute to a higher risk of cardiovascular events.

4 PKC β 2 is modulating the expression and release of IL-1 α .

We also investigated the effects of some key signaling molecules activated downstream of P2R family, including several kinases and NF κ B on IL-1 α biogenesis. Inhibition of PI3K, MEK1, NF κ B, mTor, AKT, ERK1/2, JNK and MAPK P38 had no significant effect on IL-1 α release, as measured by ELISA and Western blot analysis of secreted proteins (Fig. 35 and Fig. 36). Similarly, IL-1 β release was not affected (Fig. 35). A significant reduction in IL-1 β release has previously been reported upon inhibition of MEK1 and JNK in peritoneal monocyte-derived macrophages, while MAPK P38 inhibition showed no significant effect. Additionally, in this study, inhibition of PI3K resulted in a significant increase in IL-1 β secretion (Tapia-Abellán et al., 2014). In another study by You et. al., IL-1 α mRNA expression in MDA231 TNBC (triple negative breast cancer cells) was reduced upon inhibition of MEK and PI3K, while JNK and STAT3 inhibition did not show a significant effect. This reduction was also observed in IL-1 α secretion as measured by ELISA, therefore a regulatory effect of MEK/ERK and PI3K/AKT pathways on IL-1 α release was proposed (You et al., 2021). Although we did not detect any significant alteration in released IL-1 α , analysis of intracellular IL-1 α showed a significant increase in mature IL-1 α upon NF κ B and ERK1/2 inhibition (Fig. 37). On the other hand, analysis of surface markers showed significantly higher IL-1 α and CD16 surface expression in monocytes upon NF κ B inhibition (Fig. 39). Notably, Inhibition of NF κ B and ERK1/2 has been reported to reduce ADAM17 mRNA and protein expression upon LPS stimulation in mouse brain endothelial cells (Wawro et al., 2019). We hypothesize that NF κ B inhibition leads to a reduction in ADAM17 protein levels on the cell membrane, thereby reducing CD16 shedding and impacting IL-1 α surface expression and cleavage, which remains to be investigated. The inhibitory effect of NF κ B on IL-1 β maturation has been reported by Greten et. al. in macrophages (Greten et al., 2007). Schunk et. al demonstrated that inhibition of NF κ B by Bay11-7082 leads to a significant reduction in IL-1 α release from LPS treated monocytes in response to Oxalate and Oleic acid. Bay11-7082 is an inhibitor of TNF- α which also inhibits NF κ B, therefore the observed results may be the consequence of TNF- α inhibition. Thus, more specific studies are needed to reveal the direct effects of NF κ B on IL-1 α expression. In our study, NF κ B inhibition increased intracellular concentrations of mature IL-1 α and the percentage of cells with IL-1 α surface expression (Fig. 37, Fig. 39).

Among the kinases investigated in this study, a significant reduction in IL-1 α release was observed upon PKC PAN inhibition by the compound Ro-31-8220, and more precisely by specific inhibition of PKC β 2 (Fig. 35B). Western blot analysis of secreted proteins showed a

significant reduction in both pro- and mature IL-1 α after PKC β 2 inhibition (Fig. 36D). Tendencies of higher 17 kDa IL-1 α was also observed in intracellular total protein analysis (Fig. 37C). PKC inhibition did not affect CD16 surface expression (Fig. 39). Interestingly, inhibiting PKCs by PKC PAN inhibitor or PKC β 2 inhibition had no significant effect on IL-1 β release (Fig. 35C, D). Reduced IL-1 β expression levels upon PKC inhibition was previously reported in mouse microglia cells, but the release was not investigated in this study (Fu et al., 2019). Another study showed that IL-1 β release triggered by Oxidized LDL from THP-1 monocytes with no pre-LPS priming is inhibited by both Go6976 and Ro-31-8220 (Tiwari et al., 2014). Since IL-1 β release in this study was induced by a different signaling pathway, these findings are not contradictory. Kishimoto et. al. have shown that PKCs, including PKC β 2, are substrates of calpains (Kishimoto et al., 1989). In a study on type 1 diabetic rats, PKC β was shown to upregulate calpain activation, leading to higher expression of intercellular adhesion molecule-1 and leukocyte endothelium interactions (Smolock et al., 2011). Additionally, activation of PKC β 2 requires both DAG and Ca²⁺ (reviewed by Lim et al., 2015). This emphasizes the role of P2Ys signaling through G α_q , like P2Y1, P2Y2, P2Y4, P2Y6 and P2Y11 in PKC β 2 activation. Among the mentioned P2Ys, P2Y2, P2Y4 and P2Y11 are activated upon ATP application (Lovász et al., 2021) and our expression analysis showed the expression of P2Y2 and P2Y11 in monocytes. Altogether, we hypothesize that signaling through P2Ys leads to increased intracellular Ca²⁺ and DAG formation, which in turn activates calpain. Activated calpain cleaves and activates PKC β 2, initiating a feedback loop that further activates calpain and modulates IL-1 α release from cells.

5 IL-1 α release and surface expression is regulated by MMPs

Our RNA sequencing results revealed increased expression of MMP9 and MMP25 in CKD patients' monocytes (Fig. 44). We examined the effects of MMPs on IL-1 α surface expression and release. Treating the cells with MMP PAN inhibitor prior to LPS had no significant effect on IL-1 α release. Similarly, the release of IL-1 β was not affected by MMP PAN inhibition (Fig. 45). However, specific inhibition of MMP9 prior to LPS treatment led to a significant increase in IL-1 α release from LPS treated cells. Western blot analysis of proteins released by MMP9 inhibitor treated cells showed significantly higher concentrations of mature IL-1 α in both LPS treated and LPS+ATP treated cells. There were no significant alteration in intracellular protein concentrations (Fig. 46, Fig. 47A, Fig. 48A). IL-1 β release was also significantly increased in cells pre-treated with the MMP9 inhibitor under LPS or LPS+ATP conditions. Additionally,

IL-1 α surface expression in both LPS treated and LPS+ATP treated conditions was elevated upon MMP PAN inhibition before LPS treatment (Fig. 49A). In a previous study, incubation of primary human monocytes with LPS for 3 hours was shown to induce the expression of MMPs (Ho et al., 2008). Another study on a murine macrophage cell line also showed a significant increase in MMP9 mRNA levels, protein expression and activity upon LPS stimulation (Yang et al., 2015). A study by Ito et. al. demonstrated that IL-1 β , but not IL-1 α , was degraded by MMPs such as MMP1, MMP2, MMP3 and MMP9, which resulted in the loss of its biological activity (Ito et al., 1996). In contrast, another study in 1998 suggested that cleavage of pro-IL-1 β by MMP2 and MMP9 produces biologically active IL-1 β (Schonbeck et al., 1998). Interestingly, in the aforementioned study, no effects of MMPs were observed on IL-1 α . In two other studies, IL-1 α in human skin cells (Y.-P. Han et al., 2005) and IL-1 β in human tracheal smooth muscle cells (Liang et al., 2007) were shown to induce pro-MMP9 expression.

The effects of MMPs inhibition differed when the inhibitors were used after LPS treatment and before ATP application. ELISA measurements showed that inhibiting MMP PAN after LPS priming significantly reduced IL-1 α released from LPS treated cells, while MMP9 inhibition showed no significant effect. Contrary to the ELISA results, Western blot analysis of secreted proteins showed higher concentrations of mature IL-1 α upon MMP9 inhibition after LPS treatment, but not upon MMP PAN inhibition. No significant changes were observed in the analysis of intracellular proteins or membrane bound IL-1 α . This suggests that a longer duration of MMP inhibition may be more effective in regulating IL-1 α concentrations.

According to previous findings, LPS stimulation induces IL-1 α , IL-1 β and MMP expression, where MMP2 and MMP9 are capable of cleaving IL-1 β (Gabellec et al., 1995; Ho et al., 2008). Since MMP9 inhibition before LPS treatment resulted in higher levels of IL-1 α in the medium, we hypothesize that upon LPS treatment, IL-1 α is partially released from cells without requiring a second signal, but is mostly degraded in the extracellular space by MMP9, a process that is prevented by MMP9 inhibition. Additionally, MMP PAN inhibition before LPS stimulation led to increased surface expression of IL-1 α , suggesting that MMPs mediated the cleavage of IL-1 α from the membrane.

6 IL-1 α localization differs in mature and immature monocytes

We also aimed to determine the cellular localization of IL-1 α . Transfection of GFP and mCherry tagged IL-1 α into HEK cells showed extensive nuclear localization (Fig. 40). Similarly, in mature monocytes with a bean shaped nucleus, a nuclear localization was observed, whereas in

monocytes with circular nucleus or immature monocytes, IL-1 α showed a cytoplasmic localization (Fig. 41). Our results align with the study by Carlsen et. al., where nuclear localization of IL-1 α was observed in Hela cells and human monocyte derived macrophages upon LPS treatment (Carlsen et al., 2015). Another study on microglia, the central nervous system macrophages, revealed a similar intracellular localization of IL-1 α (Luheshi et al., 2008). Werman et. al. reported nuclear localization after LPS priming in NIH/3T3, along with evidence of transcriptional activity (Werman et al., 2004). These findings suggest a potential role of IL-1 α in gene expression in both health and disease.

The findings presented here highlight novel and intricate mechanisms of IL-1 α regulation, involving calcium signaling, P2X receptor family members, PKC β 2, and MMPs, with significant implications for CKD-related inflammation and monocyte heterogeneity. However, several critical issues require further investigation. The limited donor sample size raises concerns about the statistical power and generalizability of the results. While evidence supports the necessity of activating multiple P2 members alongside P2X7 in modulating IL-1 α , the detailed interactions between these channels and their downstream signaling mechanisms remain poorly understood. Additionally, the relationship between CD16 shedding and IL-1 α surface expression requires deeper exploration. To improve the study of IL-1 α localization within cells before and after ATP application, smaller fluorescent marker proteins should be employed for greater accuracy. Future research should involve larger cohorts, advanced imaging techniques, and co-immunoprecipitation to elucidate the spatial and temporal dynamics between IL-1 α , purinergic channels, CD16, and MMPs. Sorting monocyte subtypes through FACS could also provide valuable insights into IL-1 α release and calcium homeostasis in specific subpopulations. These approaches will enhance our understanding of monocyte-driven inflammatory pathways in CKD and support the development of targeted therapeutic strategies involving P2X receptors, MMPs, and PKC β 2.

References

- Afonina, I. S., Tynan, G. A., Logue, S. E., Cullen, S. P., Bots, M., Lüthi, A. U., Reeves, E. P., McElvaney, N. G., Medema, J. P., Lavelle, E. C., & Martin, S. J. (2011). Granzyme B-dependent proteolysis acts as a switch to enhance the pro-inflammatory activity of IL-1 α . *Molecular Cell*, 44(2), 265–278. <https://doi.org/10.1016/j.molcel.2011.07.037>
- Aga, M., Watters, J. J., Pfeiffer, Z. A., Wiepz, G. J., Sommer, J. A., & Bertics, P. J. (2004). Evidence for nucleotide receptor modulation of cross talk between MAP kinase and NF-kappa B signaling pathways in murine RAW 264.7 macrophages. *American Journal of Physiology. Cell Physiology*, 286(4), C923–930. <https://doi.org/10.1152/ajpcell.00417.2003>
- Akira, S., & Takeda, K. (2004). Toll-like receptor signalling. *Nature Reviews Immunology*, 4(7), Article 7. <https://doi.org/10.1038/nri1391>
- Akira, S., Uematsu, S., & Takeuchi, O. (2006). Pathogen Recognition and Innate Immunity. *Cell*, 124(4), 783–801. <https://doi.org/10.1016/j.cell.2006.02.015>
- Amores-Iniesta, J., Barberà-Cremades, M., Martínez, C. M., Pons, J. A., Revilla-Nuin, B., Martínez-Alarcón, L., Di Virgilio, F., Parrilla, P., Baroja-Mazo, A., & Pelegrín, P. (2017). Extracellular ATP Activates the NLRP3 Inflammasome and Is an Early Danger Signal of Skin Allograft Rejection. *Cell Reports*, 21(12), 3414–3426. <https://doi.org/10.1016/j.celrep.2017.11.079>
- Amstrup, J., & Novak, I. (2003). P2X7 receptor activates extracellular signal-regulated kinases ERK1 and ERK2 independently of Ca²⁺ influx. *The Biochemical Journal*, 374(Pt 1), 51–61. <https://doi.org/10.1042/BJ20030585>
- Antonio, L., Stewart, A., Xu, X., Varanda, W., Murrell-Lagnado, R., & Edwardson, J. (2011). P2X4 receptors interact with both P2X2 and P2X7 receptors in the form of homotrimers. *British Journal of Pharmacology*, 163(5), 1069–1077. <https://doi.org/10.1111/j.1476-5381.2011.01303.x>
- Aranda, P. S., LaJoie, D. M., & Jorcyk, C. L. (2012). Bleach Gel: A Simple Agarose Gel for Analyzing RNA Quality. *Electrophoresis*, 33(2), 366–369. <https://doi.org/10.1002/elps.201100335>
- Bell, J. K., Mullen, G. E. D., Leifer, C. A., Mazzoni, A., Davies, D. R., & Segal, D. M. (2003). Leucine-rich repeats and pathogen recognition in Toll-like receptors. *Trends in Immunology*, 24(10), 528–533. [https://doi.org/10.1016/S1471-4906\(03\)00242-4](https://doi.org/10.1016/S1471-4906(03)00242-4)
- Berridge, M. J. (1993). Inositol trisphosphate and calcium signalling. *Nature*, 361(6410), 315–325. <https://doi.org/10.1038/361315a0>
- Bersudsky, M., Luski, L., Fishman, D., White, R. M., Ziv-Sokolovskaya, N., Dotan, S., Rider, P., Kaplanov, I., Aychek, T., Dinarello, C. A., Apte, R. N., & Voronov, E. (2014). Non-redundant properties of IL-1 α and IL-1 β during acute colon inflammation in mice. *Gut*, 63(4), 598–609. <https://doi.org/10.1136/gutjnl-2012-303329>

- Bikbov, B., Purcell, C. A., Levey, A. S., Smith, M., Abdoli, A., Abebe, M., Adebayo, O. M., Afarideh, M., Agarwal, S. K., Agudelo-Botero, M., Ahmadian, E., Al-Aly, Z., Alipour, V., Almasi-Hashiani, A., Al-Raddadi, R. M., Alvis-Guzman, N., Amini, S., Andrei, T., Andrei, C. L., ... Vos, T. (2020). Global, regional, and national burden of chronic kidney disease, 1990–2017: A systematic analysis for the Global Burden of Disease Study 2017. *The Lancet*, 395(10225), 709–733. [https://doi.org/10.1016/S0140-6736\(20\)30045-3](https://doi.org/10.1016/S0140-6736(20)30045-3)
- Bockstiegel, J., Engelhardt, J., & Weindl, G. (2023). P2X7 receptor activation leads to NLRP3-independent IL-1 β release by human macrophages. *Cell Communication and Signaling*, 21(1), 335. <https://doi.org/10.1186/s12964-023-01356-1>
- Bogeski, I., Kummerow, C., Al-Ansary, D., Schwarz, E. C., Koehler, R., Kozai, D., Takahashi, N., Peinelt, C., Griesemer, D., Bozem, M., Mori, Y., Hoth, M., & Niemeyer, B. A. (2010). Differential Redox Regulation of ORAI Ion Channels: A Mechanism to Tune Cellular Calcium Signaling. *Science Signaling*, 3(115), ra24–ra24. <https://doi.org/10.1126/scisignal.2000672>
- Bours, M. J. L., Dagnelie, P. C., Giuliani, A. L., Wesselius, A., & Di Virgilio, F. (2011). P2 receptors and extracellular ATP: A novel homeostatic pathway in inflammation. *Frontiers in Bioscience (Scholar Edition)*, 3(4), 1443–1456. <https://doi.org/10.2741/235>
- Braosi, A. P. R., de Souza, C. M., Luczyszyn, S. M., Dirschnabel, A. J., Claudino, M., Olandoski, M., Probst, C. M., Garlet, G. P., Pecoits-Filho, R., & Trevisatto, P. C. (2012). Analysis of IL1 gene polymorphisms and transcript levels in periodontal and chronic kidney disease. *Cytokine*, 60(1), 76–82. <https://doi.org/10.1016/j.cyto.2012.06.006>
- Brock, V. J., Wolf, I. M. A., Er-Lukowiak, M., Lory, N., Stähler, T., Woelk, L.-M., Mittrücker, H.-W., Müller, C. E., Koch-Nolte, F., Rissiek, B., Werner, R., Guse, A. H., & Diercks, B.-P. (2022). P2X4 and P2X7 are essential players in basal T cell activity and Ca²⁺ signaling milliseconds after T cell activation. *Science Advances*, 8(5), eabl9770. <https://doi.org/10.1126/sciadv.abl9770>
- Brody, D. T., & Durum, S. K. (1989). Membrane IL-1: IL-1 alpha precursor binds to the plasma membrane via a lectin-like interaction. *The Journal of Immunology*, 143(4), 1183–1187. <https://doi.org/10.4049/jimmunol.143.4.1183>
- Brough, D., Le Feuvre, R. A., Wheeler, R. D., Solovyova, N., Hilfiker, S., Rothwell, N. J., & Verkhatsky, A. (2003). Ca²⁺ stores and Ca²⁺ entry differentially contribute to the release of IL-1 beta and IL-1 alpha from murine macrophages. *Journal of Immunology (Baltimore, Md.: 1950)*, 170(6), 3029–3036. <https://doi.org/10.4049/jimmunol.170.6.3029>
- Budagian, V., Bulanova, E., Brovko, L., Orinska, Z., Fayad, R., Paus, R., & Bulfone-Paus, S. (2011). Signaling through P2X7 receptor in human T cells involves p56(lck), MAP kinases, and transcription factors AP-1 and NF- κ B. *The Journal of Biological Chemistry*, 286(11), 9894. <https://doi.org/10.1074/jbc.a110.206383>
- Buell, G., Chessell, I. P., Michel, A. D., Collo, G., Salazzo, M., Herren, S., Gretener, D., Grahames, C., Kaur, R., Kosco-Vilbois, M. H., & Humphrey, P. P. A. (1998). Blockade

- of Human P2X7 Receptor Function With a Monoclonal Antibody. *Blood*, 92(10), 3521–3528. <https://doi.org/10.1182/blood.V92.10.3521>
- Carlsen, T. G., Kjærsgaard, P., Jørgensen, T. L., Foldbjerg, R., Nielsen, M. L., Poulsen, T. B. G., Zabieglo, K., Christiansen, G., & Birkelund, S. (2015). Interleukin-1 α activation and localization in lipopolysaccharide-stimulated human monocytes and macrophages. *Journal of Immunological Methods*, 422, 59–71. <https://doi.org/10.1016/j.jim.2015.03.025>
- Chaintreuil, P., Kerrenneur, E., Bourgoin, M., Savy, C., Favreau, C., Robert, G., Jacquél, A., & Auberger, P. (2023). The generation, activation, and polarization of monocyte-derived macrophages in human malignancies. *Frontiers in Immunology*, 14. <https://doi.org/10.3389/fimmu.2023.1178337>
- Chambers, J. K., Macdonald, L. E., Sarau, H. M., Ames, R. S., Freeman, K., Foley, J. J., Zhu, Y., McLaughlin, M. M., Murdock, P., McMillan, L., Trill, J., Swift, A., Aiyar, N., Taylor, P., Vawter, L., Naheed, S., Szekeres, P., Hervieu, G., Scott, C., ... Livi, G. P. (2000). A G Protein-coupled Receptor for UDP-glucose*. *Journal of Biological Chemistry*, 275(15), 10767–10771. <https://doi.org/10.1074/jbc.275.15.10767>
- Chao, Y.-Y., Puhach, A., Frieser, D., Arunkumar, M., Lehner, L., Seeholzer, T., Garcia-Lopez, A., van der Wal, M., Fibi-Smetana, S., Dietschmann, A., Sommermann, T., Ćiković, T., Taher, L., Gresnigt, M. S., Vastert, S. J., van Wijk, F., Panagiotou, G., Krappmann, D., Groß, O., & Zielinski, C. E. (2023). Human TH17 cells engage gasdermin E pores to release IL-1 α on NLRP3 inflammasome activation. *Nature Immunology*, 24(2), 295–308. <https://doi.org/10.1038/s41590-022-01386-w>
- Chen, C.-J., Kono, H., Golenbock, D., Reed, G., Akira, S., & Rock, K. L. (2007). Identification of a key pathway required for the sterile inflammatory response triggered by dying cells. *Nature Medicine*, 13(7), 851–856. <https://doi.org/10.1038/nm1603>
- Chen, G. Y., & Nuñez, G. (2010). Sterile inflammation: Sensing and reacting to damage. *Nature Reviews Immunology*, 10(12), Article 12. <https://doi.org/10.1038/nri2873>
- Chen, K., Zhang, J., Zhang, W., Zhang, J., Yang, J., Li, K., & He, Y. (2013). ATP-P2X4 signaling mediates NLRP3 inflammasome activation: A novel pathway of diabetic nephropathy. *The International Journal of Biochemistry & Cell Biology*, 45(5), 932–943. <https://doi.org/10.1016/j.biocel.2013.02.009>
- Chen, L., Deng, H., Cui, H., Fang, J., Zuo, Z., Deng, J., Li, Y., Wang, X., & Zhao, L. (2017). Inflammatory responses and inflammation-associated diseases in organs. *Oncotarget*, 9(6), 7204–7218. <https://doi.org/10.18632/oncotarget.23208>
- Clemens, R. A., & Lowell, C. A. (2019). CRAC channel regulation of innate immune cells in health and disease. *Cell Calcium*, 78, 56–65. <https://doi.org/10.1016/j.ceca.2019.01.003>
- Communi, D., Govaerts, C., Parmentier, M., & Boeynaems, J.-M. (1997). Cloning of a Human Purinergic P2Y Receptor Coupled to Phospholipase C and Adenylyl Cyclase*. *Journal of Biological Chemistry*, 272(51), 31969–31973. <https://doi.org/10.1074/jbc.272.51.31969>

- Communi, D., Motte, S., Boeynaems, J. M., & Pirotton, S. (1996). Pharmacological characterization of the human P2Y₄ receptor. *European Journal of Pharmacology*, 317(2–3), 383–389. [https://doi.org/10.1016/s0014-2999\(96\)00740-6](https://doi.org/10.1016/s0014-2999(96)00740-6)
- Communi, D., Parmentier, M., & Boeynaems, J. M. (1996). Cloning, functional expression and tissue distribution of the human P2Y₆ receptor. *Biochemical and Biophysical Research Communications*, 222(2), 303–308. <https://doi.org/10.1006/bbrc.1996.0739>
- Cormican, S., & Griffin, M. D. (2020). Human Monocyte Subset Distinctions and Function: Insights From Gene Expression Analysis. *Frontiers in Immunology*, 11. <https://www.frontiersin.org/articles/10.3389/fimmu.2020.01070>
- Cormican, S., Negi, N., Naicker, S. D., Islam, M. N., Fazekas, B., Power, R., Griffin, T. P., Denny, M. C., MacNeill, B., Malone, A. F., & Griffin, M. D. (2023). Chronic Kidney Disease Is Characterized by Expansion of a Distinct Proinflammatory Intermediate Monocyte Subtype and by Increased Monocyte Adhesion to Endothelial Cells. *Journal of the American Society of Nephrology*, 34(5), 793. <https://doi.org/10.1681/ASN.0000000000000083>
- Cox, M. A., Gomes, B., Palmer, K., Du, K., Wiekowski, M., Wilburn, B., Petro, M., Chou, C.-C., Desquitado, C., Schwarz, M., Lunn, C., Lundell, D., Narula, S. K., Zavodny, P. J., & Jenh, C.-H. (2005). The pyrimidinergic P2Y₆ receptor mediates a novel release of proinflammatory cytokines and chemokines in monocytic cells stimulated with UDP. *Biochemical and Biophysical Research Communications*, 330(2), 467–473. <https://doi.org/10.1016/j.bbrc.2005.03.004>
- Cros, J., Cagnard, N., Woollard, K., Patey, N., Zhang, S.-Y., Senechal, B., Puel, A., Biswas, S. K., Moshous, D., Picard, C., Jais, J.-P., D'Cruz, D., Casanova, J.-L., Trouillet, C., & Geissmann, F. (2010). Human CD14^{dim} Monocytes Patrol and Sense Nucleic Acids and Viruses via TLR7 and TLR8 Receptors. *Immunity*, 33(3), 375–386. <https://doi.org/10.1016/j.immuni.2010.08.012>
- Czerkies, M., & Kwiatkowska, K. (2014). Toll-Like Receptors and their Contribution to Innate Immunity: Focus on TLR4 Activation by Lipopolysaccharide. *Advances in Cell Biology*, 4(1), 1–23. <https://doi.org/10.2478/acb-2014-0001>
- de la Rosa, G., Gómez, A. I., Baños, M. C., & Pelegrín, P. (2020). Signaling Through Purinergic Receptor P2Y₂ Enhances Macrophage IL-1 β Production. *International Journal of Molecular Sciences*, 21(13), 4686. <https://doi.org/10.3390/ijms21134686>
- Denlinger, L. C., Fisette, P. L., Sommer, J. A., Watters, J. J., Prabhu, U., Dubyak, G. R., Proctor, R. A., & Bertics, P. J. (2001). Cutting edge: The nucleotide receptor P2X₇ contains multiple protein- and lipid-interaction motifs including a potential binding site for bacterial lipopolysaccharide. *Journal of Immunology (Baltimore, Md.: 1950)*, 167(4), 1871–1876. <https://doi.org/10.4049/jimmunol.167.4.1871>
- Denlinger, L. C., Sommer, J. A., Parker, K., Gudipaty, L., Fisette, P. L., Watters, J. W., Proctor, R. A., Dubyak, G. R., & Bertics, P. J. (2003). Mutation of a dibasic amino acid motif within the C terminus of the P2X₇ nucleotide receptor results in trafficking defects and impaired function. *Journal of Immunology (Baltimore, Md.: 1950)*, 171(3), 1304–1311. <https://doi.org/10.4049/jimmunol.171.3.1304>

- Di Paolo, N. C., & Shayakhmetov, D. M. (2016). Interleukin 1 α and the inflammatory process. *Nature Immunology*, 17(8), 906–913. <https://doi.org/10.1038/ni.3503>
- Dinarello, C. A. (1996). Biologic basis for interleukin-1 in disease. *Blood*, 87(6), 2095–2147.
- Dinarello, C. A. (2018). Overview of the IL-1 family in innate inflammation and acquired immunity. *Immunological Reviews*, 281(1), 8–27. <https://doi.org/10.1111/imr.12621>
- Dong, S. X. M., Caballero, R., Ali, H., Roy, D. L. F., Cassol, E., & Kumar, A. (2020). Transfection of hard-to-transfect primary human macrophages with Bax siRNA to reverse Resveratrol-induced apoptosis. *RNA Biology*, 17(6), 755–764. <https://doi.org/10.1080/15476286.2020.1730081>
- Dsouza, C., & Komarova, S. V. (2021). Characterization of Potency of the P2Y13 Receptor Agonists: A Meta-Analysis. *International Journal of Molecular Sciences*, 22(7), 3468. <https://doi.org/10.3390/ijms22073468>
- El-Zayat, S. R., Sibaii, H., & Mannaa, F. A. (2019). Toll-like receptors activation, signaling, and targeting: An overview. *Bulletin of the National Research Centre*, 43(1), 187. <https://doi.org/10.1186/s42269-019-0227-2>
- Entsie, P., Kang, Y., Amofo, E. B., Schöneberg, T., & Liverani, E. (2023). The Signaling Pathway of the ADP Receptor P2Y12 in the Immune System: Recent Discoveries and New Challenges. *International Journal of Molecular Sciences*, 24(7), 6709. <https://doi.org/10.3390/ijms24076709>
- Erb, L., Liao, L., Seye, C., & Weisman, G. (2006). P2 receptors: Intracellular signaling. *Pflügers Archiv: European Journal of Physiology*, 452, 552–562. <https://doi.org/10.1007/s00424-006-0069-2>
- Espinoza, V. E., & Emmady, P. D. (2023). Histology, Monocytes. In *StatPearls*. StatPearls Publishing. <http://www.ncbi.nlm.nih.gov/books/NBK557618/>
- Farrell, R. E. (2023). Chapter 10 - RT-PCR: A science and an art form. In R. E. Farrell (Ed.), *RNA Methodologies (Sixth Edition)* (pp. 223–300). Academic Press. <https://doi.org/10.1016/B978-0-323-90221-2.00039-4>
- Feske, S., Wulff, H., & Skolnik, E. Y. (2015). Ion Channels in Innate and Adaptive Immunity. *Annual Review of Immunology*, 33(1), 291–353. <https://doi.org/10.1146/annurev-immunol-032414-112212>
- Fettelschoss, A., Kistowska, M., LeibundGut-Landmann, S., Beer, H.-D., Johansen, P., Senti, G., Contassot, E., Bachmann, M., French, L., Oxenius, A., & Kündig, T. (2011). Inflammasome activation and IL-1 target IL-1 for secretion as opposed to surface expression. *Proceedings of the National Academy of Sciences of the United States of America*, 108, 18055–18060. <https://doi.org/10.1073/pnas.1109176108>
- Fields, J. K., Günther, S., & Sundberg, E. J. (2019). Structural Basis of IL-1 Family Cytokine Signaling. *Frontiers in Immunology*, 10. <https://www.frontiersin.org/journals/immunology/articles/10.3389/fimmu.2019.01412>

- Fingerle, G., Pforte, A., Passlick, B., Blumenstein, M., Ströbel, M., & Ziegler-Heitbrock, H. W. (1993). The novel subset of CD14⁺/CD16⁺ blood monocytes is expanded in sepsis patients. *Blood*, 82(10), 3170–3176.
- Fu, S.-Y., Xiong, R.-P., Peng, Y., Zhang, Z.-H., Chen, X., Zhao, Y., Ning, Y.-L., Yang, N., Zhou, Y.-G., & Li, P. (2019). PKC Mediates LPS-Induced IL-1 β Expression and Participates in the Pro-inflammatory Effect of A2AR Under High Glutamate Concentrations in Mouse Microglia. *Neurochemical Research*, 44(12), 2755–2764. <https://doi.org/10.1007/s11064-019-02895-1>
- Gabay, C., Lamacchia, C., & Palmer, G. (2010). IL-1 pathways in inflammation and human diseases. *Nature Reviews Rheumatology*, 6(4), Article 4. <https://doi.org/10.1038/nrrheum.2010.4>
- Gabellec, M.-M., Griffais, R., Fillion, G., & Haour, F. (1995). Expression of interleukin 1 α , interleukin 1 β and interleukin 1 receptor antagonist mRNA in mouse brain: Regulation by bacterial lipopolysaccharide (LPS) treatment. *Molecular Brain Research*, 31(1), 122–130. [https://doi.org/10.1016/0169-328X\(95\)00042-Q](https://doi.org/10.1016/0169-328X(95)00042-Q)
- Goyal, A., Daneshpajouhnejad, P., Hashmi, M. F., & Bashir, K. (2024). Acute Kidney Injury. In *StatPearls*. StatPearls Publishing. <http://www.ncbi.nlm.nih.gov/books/NBK441896/>
- Grahames, C. B. A., Michel, A. D., Chessell, I. P., & Humphrey, P. P. A. (1999). Pharmacological characterization of ATP- and LPS-induced IL-1 β release in human monocytes. *British Journal of Pharmacology*, 127(8), 1915–1921. <https://doi.org/10.1038/sj.bjp.0702732>
- Greten, F. R., Arkan, M. C., Bollrath, J., Hsu, L.-C., Goode, J., Miething, C., Göktuna, S. I., Neuenhahn, M., Fierer, J., Paxian, S., Van Rooijen, N., Xu, Y., Cain, T. O., Jaffee, B. B., Busch, D. H., Duyster, J., Schmid, R. M., Eckmann, L., & Karin, M. (2007). NF- κ B is a negative regulator of IL-1 β secretion as revealed by genetic and pharmacological inhibition of IKK β . *Cell*, 130(5), 918–931. <https://doi.org/10.1016/j.cell.2007.07.009>
- Gschwendt, M., Dieterich, S., Rennecke, J., Kittstein, W., Mueller, H. J., & Johannes, F. J. (1996). Inhibition of protein kinase C μ by various inhibitors. Differentiation from protein kinase c isoenzymes. *FEBS Letters*, 392(2), 77–80. [https://doi.org/10.1016/0014-5793\(96\)00785-5](https://doi.org/10.1016/0014-5793(96)00785-5)
- Gudipaty, L., Munetz, J., Verhoef, P. A., & Dubyak, G. R. (2003). Essential role for Ca²⁺ in regulation of IL-1 β secretion by P2X7 nucleotide receptor in monocytes, macrophages, and HEK-293 cells. *American Journal of Physiology. Cell Physiology*, 285(2), C286–299. <https://doi.org/10.1152/ajpcell.00070.2003>
- Guo, C., Masin, M., Qureshi, O. S., & Murrell-Lagnado, R. D. (2007). Evidence for Functional P2X4/P2X7 Heteromeric Receptors. *Molecular Pharmacology*, 72(6), 1447–1456. <https://doi.org/10.1124/mol.107.035980>
- Han, S. J., Lovaszi, M., Kim, M., D’Agati, V., Haskó, G., & Lee, H. T. (2020). P2X4 receptor exacerbates ischemic AKI and induces renal proximal tubular NLRP3 inflammasome signaling. *FASEB Journal : Official Publication of the Federation of American Societies for Experimental Biology*, 34(4), 5465–5482. <https://doi.org/10.1096/fj.201903287R>

- Han, Y.-P., Downey, S., & Garner, W. L. (2005). Interleukin-1 α -induced proteolytic activation of metalloproteinase-9 by human skin. *Surgery*, 138(5), 932–939. <https://doi.org/10.1016/j.surg.2005.05.003>
- Harden, T. K., Sesma, J. I., Fricks, I. P., & Lazarowski, E. R. (2010). Signalling and pharmacological properties of the P2Y₁₄ receptor. *Acta Physiologica (Oxford, England)*, 199(2), 149–160. <https://doi.org/10.1111/j.1748-1716.2010.02116.x>
- Heine, G. H., Ulrich, C., Seibert, E., Seiler, S., Marell, J., Reichart, B., Krause, M., Schlitt, A., Köhler, H., & Girndt, M. (2008). CD14⁺⁺CD16⁺ monocytes but not total monocyte numbers predict cardiovascular events in dialysis patients. *Kidney International*, 73(5), 622–629. <https://doi.org/10.1038/sj.ki.5002744>
- Henderson, L. W., Koch, K. M., Dinarello, C. A., & Shaldon, S. (1983). Hemodialysis Hypotension: The Interleukin Hypothesis. *Blood Purification*, 1(1), 3–8. <https://doi.org/10.1159/000166438>
- Ho, H. H., Antoniv, T., Ji, J.-D., & Ivashkiv, L. B. (2008). LPS-induced Expression of MMPs in Human Monocytes is Suppressed by IFN- γ via Superinduction of ATF-3 and Suppression of AP-1 Proteins. *Journal of Immunology (Baltimore, Md. : 1950)*, 181(7), 5089–5097.
- Hoffman, E. A., Frey, B. L., Smith, L. M., & Auble, D. T. (2015). Formaldehyde Crosslinking: A Tool for the Study of Chromatin Complexes. *The Journal of Biological Chemistry*, 290(44), 26404–26411. <https://doi.org/10.1074/jbc.R115.651679>
- Huang, Z., Xie, N., Illes, P., Di Virgilio, F., Ulrich, H., Semyanov, A., Verkhatsky, A., Sperlagh, B., Yu, S.-G., Huang, C., & Tang, Y. (2021). From purines to purinergic signalling: Molecular functions and human diseases. *Signal Transduction and Targeted Therapy*, 6(1), Article 1. <https://doi.org/10.1038/s41392-021-00553-z>
- Ishani, A., Xue, J. L., Himmelfarb, J., Eggers, P. W., Kimmel, P. L., Molitoris, B. A., & Collins, A. J. (2009). Acute kidney injury increases risk of ESRD among elderly. *Journal of the American Society of Nephrology: JASN*, 20(1), 223–228. <https://doi.org/10.1681/ASN.2007080837>
- Ito, A., Mukaiyama, A., Itoh, Y., Nagase, H., Thøgersen, I. B., Enghild, J. J., Sasaguri, Y., & Mori, Y. (1996). Degradation of Interleukin 1 β by Matrix Metalloproteinases*. *Journal of Biological Chemistry*, 271(25), 14657–14660. <https://doi.org/10.1074/jbc.271.25.14657>
- Ivanov, A. A., Ko, H., Cosyn, L., Maddileti, S., Besada, P., Fricks, I., Costanzi, S., Harden, T. K., Van Calenbergh, S., & Jacobson, K. A. (2007). Molecular Modeling of the Human P2Y₂ Receptor and Design of a Selective Agonist, 2'-Amino-2'-deoxy-2-thio-UTP. *Journal of Medicinal Chemistry*, 50(6), 1166–1176. <https://doi.org/10.1021/jm060903o>
- Jacob, F., Novo, C. P., Bachert, C., & Van Crombruggen, K. (2013). Purinergic signaling in inflammatory cells: P2 receptor expression, functional effects, and modulation of inflammatory responses. *Purinergic Signalling*, 9(3), 285–306. <https://doi.org/10.1007/s11302-013-9357-4>

- James, M. T., Grams, M. E., Woodward, M., Elley, C. R., Green, J. A., Wheeler, D. C., de Jong, P., Gansevoort, R. T., Levey, A. S., Warnock, D. G., & Sarnak, M. J. (2015). A meta-analysis of the association of estimated GFR, albuminuria, diabetes mellitus, and hypertension with AKI. *American Journal of Kidney Diseases : The Official Journal of the National Kidney Foundation*, 66(4), 602–612. <https://doi.org/10.1053/j.ajkd.2015.02.338>
- Jing, Y., Ni, Z., Wu, J., Higgins, L., Markowski, T., Kaufman, D., & Walcheck, B. (2015). Identification of an ADAM17 Cleavage Region in Human CD16 (FcγRIII) and the Engineering of a Non-Cleavable Version of the Receptor in NK Cells. *PloS One*, 10, e0121788. <https://doi.org/10.1371/journal.pone.0121788>
- Kaneko, Y., & Szallasi, A. (2014). Transient receptor potential (TRP) channels: A clinical perspective. *British Journal of Pharmacology*, 171(10), 2474–2507. <https://doi.org/10.1111/bph.12414>
- Kanneganti, T.-D., Body-Malapel, M., Amer, A., Park, J.-H., Whitfield, J., Franchi, L., Taraporewala, Z. F., Miller, D., Patton, J. T., Inohara, N., & Núñez, G. (2006). Critical Role for Cryopyrin/Nalp3 in Activation of Caspase-1 in Response to Viral Infection and Double-stranded RNA *. *Journal of Biological Chemistry*, 281(48), 36560–36568. <https://doi.org/10.1074/jbc.M607594200>
- Kapellos, T. S., Bonaguro, L., Gemünd, I., Reusch, N., Saglam, A., Hinkley, E. R., & Schultze, J. L. (2019). Human Monocyte Subsets and Phenotypes in Major Chronic Inflammatory Diseases. *Frontiers in Immunology*, 10. <https://www.frontiersin.org/articles/10.3389/fimmu.2019.02035>
- Kavita, U., & Mizel, S. B. (1995). Differential Sensitivity of Interleukin-1α and -β Precursor Proteins to Cleavage by Calpain, a Calcium-dependent Protease (*). *Journal of Biological Chemistry*, 270(46), 27758–27765. <https://doi.org/10.1074/jbc.270.46.27758>
- Kawano, A., Tsukimoto, M., Mori, D., Noguchi, T., Harada, H., Takenouchi, T., Kitani, H., & Kojima, S. (2012). Regulation of P2X7-dependent inflammatory functions by P2X4 receptor in mouse macrophages. *Biochemical and Biophysical Research Communications*, 420(1), 102–107. <https://doi.org/10.1016/j.bbrc.2012.02.122>
- Khan, S., Yan-Do, R., Duong, E., Wu, X., Bautista, A., Cheley, S., MacDonald, P. E., & Braun, M. (2014). Autocrine activation of P2Y1 receptors couples Ca²⁺ influx to Ca²⁺ release in human pancreatic beta cells. *Diabetologia*, 57(12), 2535–2545. <https://doi.org/10.1007/s00125-014-3368-8>
- Kim, B., Lee, Y., Kim, E., Kwak, A., Ryoo, S., Bae, S. H., Azam, T., Kim, S., & Dinarello, C. A. (2013). The Interleukin-1α Precursor is Biologically Active and is Likely a Key Alarmin in the IL-1 Family of Cytokines. *Frontiers in Immunology*, 4, 391. <https://doi.org/10.3389/fimmu.2013.00391>
- Kim, H. W., Yang, H.-N., Kim, M. G., Choi, H. M., Jo, S.-K., Cho, W. Y., & Kim, H. K. (2011). Microinflammation in Hemodialysis Patients Is Associated with Increased CD14⁺CD16⁺ Pro-Inflammatory Monocytes: Possible Modification by On-Line

- Hemodiafiltration. *Blood Purification*, 31(4), 281–288. <https://doi.org/10.1159/000321889>
- Kishimoto, A., Mikawa, K., Hashimoto, K., Yasuda, I., Tanaka, S., Tominaga, M., Kuroda, T., & Nishizuka, Y. (1989). Limited Proteolysis of Protein Kinase C Subspecies by Calcium-dependent Neutral Protease (Calpain). *Journal of Biological Chemistry*, 264(7), 4088–4092. [https://doi.org/10.1016/S0021-9258\(19\)84966-9](https://doi.org/10.1016/S0021-9258(19)84966-9)
- Knörck, A., Marx, S., Friedmann, K. S., Zöphel, S., Lieblang, L., Hässig, C., Müller, I., Pilch, J., Sester, U., Hoth, M., Eichler, H., Sester, M., & Schwarz, E. C. (2018). Quantity, quality, and functionality of peripheral blood cells derived from residual blood of different apheresis kits. *Transfusion*, 58(6), 1516–1526. <https://doi.org/10.1111/trf.14616>
- Kobayashi, Y., Yamamoto, K., Saido, T., Kawasaki, H., Oppenheim, J. J., & Matsushima, K. (1990). Identification of calcium-activated neutral protease as a processing enzyme of human interleukin 1 alpha. *Proceedings of the National Academy of Sciences of the United States of America*, 87(14), 5548–5552. <https://doi.org/10.1073/pnas.87.14.5548>
- Kodakandla, G., Akimzhanov, A. M., & Boehning, D. (2023). Regulatory mechanisms controlling store-operated calcium entry. *Frontiers in Physiology*, 14. <https://doi.org/10.3389/fphys.2023.1330259>
- Kopp, R., Krautloher, A., Ramírez-Fernández, A., & Nicke, A. (2019). P2X7 Interactions and Signaling – Making Head or Tail of It. *Frontiers in Molecular Neuroscience*, 12. <https://doi.org/10.3389/fnmol.2019.00183>
- Koraishy, F. M., Bowe, B., Xie, Y., Xian, H., & Al-Aly, Z. (2018). Monocyte count modifies the association between chronic kidney disease and risk of death. *Clinical Nephrology*, 90(3), 194–208. <https://doi.org/10.5414/CN109434>
- Korcok, J., Raimundo, L. N., Ke, H. Z., Sims, S. M., & Dixon, S. J. (2004). Extracellular nucleotides act through P2X7 receptors to activate NF-kappaB in osteoclasts. *Journal of Bone and Mineral Research: The Official Journal of the American Society for Bone and Mineral Research*, 19(4), 642–651. <https://doi.org/10.1359/JBMR.040108>
- Kurt-Jones, E. A., Beller, D. I., Mizel, S. B., & Unanue, E. R. (1985). Identification of a membrane-associated interleukin 1 in macrophages. *Proceedings of the National Academy of Sciences of the United States of America*, 82(4), 1204–1208. <https://doi.org/10.1073/pnas.82.4.1204>
- Lajdova, I., Oksa, A., Chorvat, D., Topor, P., & Spustova, V. (2012). Purinergic P2X7 receptors participate in disturbed intracellular calcium homeostasis in peripheral blood mononuclear cells of patients with chronic kidney disease. *Kidney & Blood Pressure Research*, 35(1), 48–57. <https://doi.org/10.1159/000330349>
- Lajdova, I., Oksa, A., Horvathova, M., & Spustova, V. (2017). Expression of purinergic P2X7 receptors in subpopulations of peripheral blood mononuclear cells in early-stage of chronic kidney disease. *Journal of Physiology and Pharmacology: An Official Journal of the Polish Physiological Society*, 68(5), 779–785.

- Lamkanfi, M., & Dixit, V. M. (2014). Mechanisms and Functions of Inflammasomes. *Cell*, 157(5), 1013–1022. <https://doi.org/10.1016/j.cell.2014.04.007>
- Land, W. G. (2015). The Role of Damage-Associated Molecular Patterns (DAMPs) in Human Diseases. *Sultan Qaboos University Medical Journal*, 15(2), e157–e170.
- Lapointe, T. K., & Altier, C. (2011). The role of TRPA1 in visceral inflammation and pain. *Channels*, 5(6), 525–529. <https://doi.org/10.4161/chan.5.6.18016>
- Lee, G.-S., Subramanian, N., Kim, A. I., Aksentijevich, I., Goldbach-Mansky, R., Sacks, D. B., Germain, R. N., Kastner, D. L., & Chae, J. J. (2012). The calcium-sensing receptor regulates the NLRP3 inflammasome through Ca²⁺ and cAMP. *Nature*, 492(7427), 123–127. <https://doi.org/10.1038/nature11588>
- Lee, J.-W., Cho, E., Kim, M.-G., Jo, S.-K., Cho, W. Y., & Kim, H. K. (2013). Proinflammatory CD14⁺CD16⁺ monocytes are associated with vascular stiffness in predialysis patients with chronic kidney disease. *Kidney Research and Clinical Practice*, 32(4), 147–152. <https://doi.org/10.1016/j.krcp.2013.08.001>
- Levey, A. S., & Coresh, J. (2012). Chronic kidney disease. *The Lancet*, 379(9811), 165–180. [https://doi.org/10.1016/S0140-6736\(11\)60178-5](https://doi.org/10.1016/S0140-6736(11)60178-5)
- Liang, K.-C., Lee, C.-W., Lin, W.-N., Lin, C.-C., Wu, C.-B., Luo, S.-F., & Yang, C.-M. (2007). Interleukin-1 β induces MMP-9 expression via p42/p44 MAPK, p38 MAPK, JNK, and nuclear factor- κ B signaling pathways in human tracheal smooth muscle cells. *Journal of Cellular Physiology*, 211(3), 759–770. <https://doi.org/10.1002/jcp.20992>
- Lim, P. S., Sutton, C. R., & Rao, S. (2015). Protein kinase C in the immune system: From signalling to chromatin regulation. *Immunology*, 146(4), 508–522. <https://doi.org/10.1111/imm.12510>
- Linden, J. M. (1999). Purinergic Receptors. In *Basic Neurochemistry: Molecular, Cellular and Medical Aspects*. 6th edition. Lippincott-Raven. <https://www.ncbi.nlm.nih.gov/books/NBK27952/>
- Liu, J., Liu, S., Hu, S., Lu, J., Wu, C., Hu, D., & Zhang, W. (2023). ATP ion channel P2X purinergic receptors in inflammation response. *Biomedicine & Pharmacotherapy*, 158, 114205. <https://doi.org/10.1016/j.biopha.2022.114205>
- Liu, Y., Krueger, K., Hovsepian, A., Tepel, M., & Thilo, F. (2011). Calcium-dependent expression of transient receptor potential canonical type 3 channels in patients with chronic kidney disease. *Archives of Biochemistry and Biophysics*, 514(1–2), 44–49. <https://doi.org/10.1016/j.abb.2011.07.011>
- Lovász, M., Branco Haas, C., Antonioli, L., Pacher, P., & Haskó, G. (2021). The role of P2Y receptors in regulating immunity and metabolism. *Biochemical Pharmacology*, 187, 114419. <https://doi.org/10.1016/j.bcp.2021.114419>
- Luheshi, N. M., Rothwell, N. J., & Brough, D. (2008). The Dynamics and Mechanisms of Interleukin-1 α and β Nuclear Import. *Traffic (Copenhagen, Denmark)*, 10(1), 16–25. <https://doi.org/10.1111/j.1600-0854.2008.00840.x>

- Mariathasan, S., Weiss, D. S., Newton, K., McBride, J., O'Rourke, K., Roose-Girma, M., Lee, W. P., Weinrauch, Y., Monack, D. M., & Dixit, V. M. (2006). Cryopyrin activates the inflammasome in response to toxins and ATP. *Nature*, 440(7081), Article 7081. <https://doi.org/10.1038/nature04515>
- Medzhitov, R. (2008). Origin and physiological roles of inflammation. *Nature*, 454(7203), Article 7203. <https://doi.org/10.1038/nature07201>
- Mihai, S., Codrici, E., Popescu, I. D., Enciu, A.-M., Albuлесcu, L., Necula, L. G., Mambet, C., Anton, G., & Tanase, C. (2018). Inflammation-Related Mechanisms in Chronic Kidney Disease Prediction, Progression, and Outcome. *Journal of Immunology Research*, 2018, 2180373. <https://doi.org/10.1155/2018/2180373>
- Mikolajewicz, N., Smith, D., Komarova, S. V., & Khadra, A. (2021). High-affinity P2Y2 and low-affinity P2X7 receptor interaction modulates ATP-mediated calcium signaling in murine osteoblasts. *PLoS Computational Biology*, 17(6), e1008872. <https://doi.org/10.1371/journal.pcbi.1008872>
- Mishra, A., Guo, Y., Zhang, L., More, S., Weng, T., Chintagari, N. R., Huang, C., Liang, Y., Pushparaj, S., Gou, D., Breshears, M., & Liu, L. (2016). A Critical Role for P2X7 Receptor-Induced VCAM-1 Shedding and Neutrophil Infiltration during Acute Lung Injury. *The Journal of Immunology*, 197(7), 2828–2837. <https://doi.org/10.4049/jimmunol.1501041>
- Moradian, H., Roch, T., Lendlein, A., & Gossen, M. (2020). mRNA Transfection-Induced Activation of Primary Human Monocytes and Macrophages: Dependence on Carrier System and Nucleotide Modification. *Scientific Reports*, 10(1), 4181. <https://doi.org/10.1038/s41598-020-60506-4>
- Morrow, G. B., Nicholas, R. A., & Kennedy, C. (2014). UTP is not a biased agonist at human P2Y(11) receptors. *Purinergic Signalling*, 10(4), 581–585. <https://doi.org/10.1007/s11302-014-9418-3>
- Muruve, D. A., Pétrilli, V., Zaiss, A. K., White, L. R., Clark, S. A., Ross, P. J., Parks, R. J., & Tschopp, J. (2008). The inflammasome recognizes cytosolic microbial and host DNA and triggers an innate immune response. *Nature*, 452(7183), Article 7183. <https://doi.org/10.1038/nature06664>
- Naicker, S. D., Cormican, S., Griffin, T. P., Maretto, S., Martin, W. P., Ferguson, J. P., Cotter, D., Connaughton, E. P., Dennedy, M. C., & Griffin, M. D. (2018). Chronic Kidney Disease Severity Is Associated With Selective Expansion of a Distinctive Intermediate Monocyte Subpopulation. *Frontiers in Immunology*, 9. <https://www.frontiersin.org/article/10.3389/fimmu.2018.02845>
- Nicholas, R. A., Watt, W. C., Lazarowski, E. R., Li, Q., & Harden, K. (1996). Uridine nucleotide selectivity of three phospholipase C-activating P2 receptors: Identification of a UDP-selective, a UTP-selective, and an ATP- and UTP-specific receptor. *Molecular Pharmacology*, 50(2), 224–229.
- Nockher, W. A., & Scherberich, J. E. (1998). Expanded CD14⁺ CD16⁺ Monocyte Subpopulation in Patients with Acute and Chronic Infections Undergoing Hemodialysis. *Infection and Immunity*, 66(6), 2782–2790.

- Onohara, N., Nishida, M., Inoue, R., Kobayashi, H., Sumimoto, H., Sato, Y., Mori, Y., Nagao, T., & Kurose, H. (2006). TRPC3 and TRPC6 are essential for angiotensin II-induced cardiac hypertrophy. *The EMBO Journal*, 25(22), 5305–5316. <https://doi.org/10.1038/sj.emboj.7601417>
- Osman, M., Akkus, Z., Jevremovic, D., Nguyen, P. L., Roh, D., Al-Kali, A., Patnaik, M. M., Nanaa, A., Rizk, S., & Salama, M. E. (2021). Classification of Monocytes, Promonocytes and Monoblasts Using Deep Neural Network Models: An Area of Unmet Need in Diagnostic Hematopathology. *Journal of Clinical Medicine*, 10(11), 2264. <https://doi.org/10.3390/jcm10112264>
- Oury, C., Toth-Zsamboki, E., Vermylen, J., & Hoylaerts, M. F. (2002). P2X(1)-mediated activation of extracellular signal-regulated kinase 2 contributes to platelet secretion and aggregation induced by collagen. *Blood*, 100(7), 2499–2505. <https://doi.org/10.1182/blood-2002-03-0812>
- Ożańska, A., Szymczak, D., & Rybka, J. (2020). Pattern of human monocyte subpopulations in health and disease. *Scandinavian Journal of Immunology*, 92(1), e12883. <https://doi.org/10.1111/sji.12883>
- Panenka, W., Jijon, H., Herx, L. M., Armstrong, J. N., Feighan, D., Wei, T., Yong, V. W., Ransohoff, R. M., & MacVicar, B. A. (2001). P2X7-like receptor activation in astrocytes increases chemokine monocyte chemoattractant protein-1 expression via mitogen-activated protein kinase. *The Journal of Neuroscience: The Official Journal of the Society for Neuroscience*, 21(18), 7135–7142. <https://doi.org/10.1523/JNEUROSCI.21-18-07135.2001>
- Perlman, A. S., Chevalier, J. M., Wilkinson, P., Liu, H., Parker, T., Levine, D. M., Sloan, B. J., Gong, A., Sherman, R., & Farrell, F. X. (2015). Serum Inflammatory and Immune Mediators Are Elevated in Early Stage Diabetic Nephropathy. *Annals of Clinical and Laboratory Science*, 45(3), 256–263.
- Poznyak, A. V., Sadykhov, N. K., Kartuesov, A. G., Borisov, E. E., Sukhorukov, V. N., & Orekhov, A. N. (2022). Atherosclerosis Specific Features in Chronic Kidney Disease (CKD). *Biomedicines*, 10(9), 2094. <https://doi.org/10.3390/biomedicines10092094>
- Prinyakupt, J., & Pluempitiwiriyaew, C. (2015). Segmentation of white blood cells and comparison of cell morphology by linear and naïve Bayes classifiers. *BioMedical Engineering OnLine*, 14, 63. <https://doi.org/10.1186/s12938-015-0037-1>
- Rajagopal, M., Kathpalia, P. P., Thomas, S. V., & Pao, A. C. (2011). Activation of P2Y1 and P2Y2 receptors induces chloride secretion via calcium-activated chloride channels in kidney inner medullary collecting duct cells. *American Journal of Physiology - Renal Physiology*, 301(3), F544–F553. <https://doi.org/10.1152/ajprenal.00709.2010>
- Rajamäki, K., Lappalainen, J., Öörni, K., Välimäki, E., Matikainen, S., Kovanen, P. T., & Eklund, K. K. (2010). Cholesterol Crystals Activate the NLRP3 Inflammasome in Human Macrophages: A Novel Link between Cholesterol Metabolism and Inflammation. *PLOS ONE*, 5(7), e11765. <https://doi.org/10.1371/journal.pone.0011765>
- Raouf, R., Chabot-Doré, A.-J., Ase, A. R., Blais, D., & Séguéla, P. (2007). Differential regulation of microglial P2X4 and P2X7 ATP receptors following LPS-induced

- activation. *Neuropharmacology*, 53(4), 496–504.
<https://doi.org/10.1016/j.neuropharm.2007.06.010>
- Razak, M. R., Aris, A. Z., Yusoff, F. M., Yusof, Z. N. B., Kim, S. D., & Kim, K. W. (2022). Assessment of RNA extraction protocols from cladocerans. *PLOS ONE*, 17(4), e0264989. <https://doi.org/10.1371/journal.pone.0264989>
- Reiser, J., Polu, K. R., Möller, C. C., Kenlan, P., Altintas, M. M., Wei, C., Faul, C., Herbert, S., Villegas, I., Avila-Casado, C., McGee, M., Sugimoto, H., Brown, D., Kalluri, R., Mundel, P., Smith, P. L., Clapham, D. E., & Pollak, M. R. (2005). TRPC6 is a glomerular slit diaphragm-associated channel required for normal renal function. *Nature Genetics*, 37(7), 739–744. <https://doi.org/10.1038/ng1592>
- Rider, P., Carmi, Y., Guttman, O., Braiman, A., Cohen, I., Voronov, E., White, M. R., Dinarello, C. A., & Apte, R. N. (2011). IL-1 α and IL-1 β recruit different myeloid cells and promote different stages of sterile inflammation. *Journal of Immunology (Baltimore, Md.: 1950)*, 187(9), 4835–4843. <https://doi.org/10.4049/jimmunol.1102048>
- Roh, J. S., & Sohn, D. H. (2018). Damage-Associated Molecular Patterns in Inflammatory Diseases. *Immune Network*, 18(4), e27. <https://doi.org/10.4110/in.2018.18.e27>
- Sakaki, H., Fujiwaki, T., Tsukimoto, M., Kawano, A., Harada, H., & Kojima, S. (2013). P2X4 receptor regulates P2X7 receptor-dependent IL-1 β and IL-18 release in mouse bone marrow-derived dendritic cells. *Biochemical and Biophysical Research Communications*, 432(3), 406–411. <https://doi.org/10.1016/j.bbrc.2013.01.135>
- Salti, T., Khazim, K., Haddad, R., Campisi-Pinto, S., Bar-Sela, G., & Cohen, I. (2020). Glucose Induces IL-1 α -Dependent Inflammation and Extracellular Matrix Proteins Expression and Deposition in Renal Tubular Epithelial Cells in Diabetic Kidney Disease. *Frontiers in Immunology*, 11. <https://www.frontiersin.org/journals/immunology/articles/10.3389/fimmu.2020.01270>
- Santoni, G., Cardinali, C., Morelli, M. B., Santoni, M., Nabissi, M., & Amantini, C. (2015). Danger- and pathogen-associated molecular patterns recognition by pattern-recognition receptors and ion channels of the transient receptor potential family triggers the inflammasome activation in immune cells and sensory neurons. *Journal of Neuroinflammation*, 12(1), 21. <https://doi.org/10.1186/s12974-015-0239-2>
- Saul, S., Gibhardt, C. S., Schmidt, B., Lis, A., Pasioka, B., Conrad, D., Jung, P., Gaupp, R., Wonnemberg, B., Diler, E., Stanis, H., Vogt, T., Schwarz, E. C., Bischoff, M., Herrmann, M., Tschernig, T., Kappl, R., Rieger, H., Niemeyer, B. A., & Bogeski, I. (2016). A calcium-redox feedback loop controls human monocyte immune responses: The role of ORAI Ca²⁺ channels. *Science Signaling*, 9(418), ra26. <https://doi.org/10.1126/scisignal.aaf1639>
- Schneider, M., Prudic, K., Pippel, A., Klapperstück, M., Braam, U., Müller, C. E., Schmalzing, G., & Markwardt, F. (2017). Interaction of Purinergic P2X4 and P2X7 Receptor Subunits. *Frontiers in Pharmacology*, 8. <https://doi.org/10.3389/fphar.2017.00860>
- Schonbeck, U., Mach, F., & Libby, P. (1998). Generation of biologically active IL-1 beta by matrix metalloproteinases: A novel caspase-1-independent pathway of IL-1 beta processing. *J Immunol*, 161(7), 3340–3346.

- Schunk, S. J., Triem, S., Schmit, D., Zewinger, S., Sarakpi, T., Becker, E., Hütter, G., Wrublewsky, S., Küting, F., Hohl, M., Alansary, D., Prates Roma, L., Lipp, P., Möllmann, J., Lehrke, M., Laschke, M. W., Menger, M. D., Kramann, R., Boor, P., ... Speer, T. (2021). Interleukin-1 α Is a Central Regulator of Leukocyte-Endothelial Adhesion in Myocardial Infarction and in Chronic Kidney Disease. *Circulation*, 144(11), 893–908. <https://doi.org/10.1161/CIRCULATIONAHA.121.053547>
- Sherwood, E. R., & Toliver-Kinsky, T. (2004). Mechanisms of the inflammatory response. *Best Practice & Research Clinical Anaesthesiology*, 18(3), 385–405. <https://doi.org/10.1016/j.bpa.2003.12.002>
- Simon, J., Webb, T. E., King, B. F., Burnstock, G., & Barnard, E. A. (1995). Characterisation of a recombinant P2Y purinoceptor. *European Journal of Pharmacology: Molecular Pharmacology*, 291(3), 281–289. [https://doi.org/10.1016/0922-4106\(95\)90068-3](https://doi.org/10.1016/0922-4106(95)90068-3)
- Smolock, A. R., Mishra, G., Eguchi, K., Eguchi, S., & Scalia, R. (2011). Protein Kinase C Upregulates Intercellular Adhesion Molecule-1 and Leukocyte-Endothelium Interactions in Hyperglycemia via Activation of Endothelial Expressed Calpain. *Arteriosclerosis, Thrombosis, and Vascular Biology*, 31(2), 289–296. <https://doi.org/10.1161/ATVBAHA.110.217901>
- Swanson, K. V., Deng, M., & Ting, J. P.-Y. (2019). The NLRP3 inflammasome: Molecular activation and regulation to therapeutics. *Nature Reviews. Immunology*, 19(8), 477–489. <https://doi.org/10.1038/s41577-019-0165-0>
- Syed Mortadza, S. A., Wang, L., Li, D., & Jiang, L.-H. (2015). TRPM2 Channel-Mediated ROS-Sensitive Ca²⁺ Signaling Mechanisms in Immune Cells. *Frontiers in Immunology*, 6. <https://www.frontiersin.org/articles/10.3389/fimmu.2015.00407>
- Takahashi, N., Kozai, D., Kobayashi, R., Ebert, M., & Mori, Y. (2011). Roles of TRPM2 in oxidative stress. *Cell Calcium*, 50(3), 279–287. <https://doi.org/10.1016/j.ceca.2011.04.006>
- Takeuchi, O., & Akira, S. (2010). Pattern Recognition Receptors and Inflammation. *Cell*, 140(6), 805–820. <https://doi.org/10.1016/j.cell.2010.01.022>
- Tapia-Abellán, A., Ruiz-Alcaraz, A. J., Antón, G., Miras-López, M., Francés, R., Such, J., Martínez-Esparza, M., & García-Peñarrubia, P. (2014). Regulatory role of PI3K-protein kinase B on the release of interleukin-1 β in peritoneal macrophages from the ascites of cirrhotic patients. *Clinical and Experimental Immunology*, 178(3), 525–536. <https://doi.org/10.1111/cei.12428>
- Tissot, A. C., Spohn, G., Jennings, G. T., Shamshiev, A., Kurrer, M. O., Windak, R., Meier, M., Viesti, M., Hersberger, M., Kündig, T. M., Ricci, R., & Bachmann, M. F. (2013). A VLP-based vaccine against interleukin-1 α protects mice from atherosclerosis. *European Journal of Immunology*, 43(3), 716–722. <https://doi.org/10.1002/eji.201242687>
- Tiwari, R. L., Singh, V., Singh, A., Rana, M., Verma, A., Kothari, N., Kohli, M., Bogra, J., Dikshit, M., & Barthwal, M. K. (2014). PKC δ -IRAK1 axis regulates oxidized LDL-induced IL-1 β production in monocytes [S]. *Journal of Lipid Research*, 55(7), 1226–1244. <https://doi.org/10.1194/jlr.M045658>

- Toullec, D., Pianetti, P., Coste, H., Bellevergue, P., Grand-Perret, T., Ajakane, M., Baudet, V., Boissin, P., Boursier, E., & Loriolle, F. (1991). The bisindolylmaleimide GF 109203X is a potent and selective inhibitor of protein kinase C. *The Journal of Biological Chemistry*, 266(24), 15771–15781.
- Turner, M. D., Nedjai, B., Hurst, T., & Pennington, D. J. (2014). Cytokines and chemokines: At the crossroads of cell signalling and inflammatory disease. *Biochimica Et Biophysica Acta*, 1843(11), 2563–2582. <https://doi.org/10.1016/j.bbamcr.2014.05.014>
- Vonend, O., Turner, C. M., Chan, C. M., Loesch, A., Carmen Dell’Anna, G., Srai, K. S., Burnstock, G., & Unwin, R. J. (2004). Glomerular expression of the ATP-sensitive P2X7 receptor in diabetic and hypertensive rat models. *Kidney International*, 66(1), 157–166. <https://doi.org/10.1111/j.1523-1755.2004.00717.x>
- Wang, D., Li, X., Liu, J., Li, J., Li, L.-J., & Qiu, M.-X. (2014). Effects of TRPC6 on invasibility of low-differentiated prostate cancer cells. *Asian Pacific Journal of Tropical Medicine*, 7(1), 44–47. [https://doi.org/10.1016/S1995-7645\(13\)60190-X](https://doi.org/10.1016/S1995-7645(13)60190-X)
- Wang, L., Jacobsen, S. E. W., Bengtsson, A., & Erlinge, D. (2004). P2 receptor mRNA expression profiles in human lymphocytes, monocytes and CD34+ stem and progenitor cells. *BMC Immunology*, 5, 16. <https://doi.org/10.1186/1471-2172-5-16>
- Wang, P., Liu, D., Tepel, M., & Zhu, Z. (2013). Transient receptor potential canonical type 3 channels—Their evolving role in hypertension and its related complications. *Journal of Cardiovascular Pharmacology*, 61(6), 455–460. <https://doi.org/10.1097/FJC.0b013e31828748a1>
- Warny, M., Aboudola, S., Robson, S. C., Sévigny, J., Communi, D., Soltoff, S. P., & Kelly, C. P. (2001). P2Y6 Nucleotide Receptor Mediates Monocyte Interleukin-8 Production in Response to UDP or Lipopolysaccharide*. *Journal of Biological Chemistry*, 276(28), 26051–26056. <https://doi.org/10.1074/jbc.M102568200>
- Watanabe, N., & Kobayashi, Y. (1994). Selective release of a processed form of interleukin 1 α . *Cytokine*, 6(6), 597–601. [https://doi.org/10.1016/1043-4666\(94\)90046-9](https://doi.org/10.1016/1043-4666(94)90046-9)
- Wawro, K., Wawro, M., Strzelecka, M., Czarnek, M., & Bereta, J. (2019). The role of NF- κ B and Elk-1 in the regulation of mouse ADAM17 expression. *Biology Open*, 8, bio039420. <https://doi.org/10.1242/bio.039420>
- Weber, E. W., Han, F., Tauseef, M., Birnbaumer, L., Mehta, D., & Muller, W. A. (2015). TRPC6 is the endothelial calcium channel that regulates leukocyte transendothelial migration during the inflammatory response. *The Journal of Experimental Medicine*, 212(11), 1883–1899. <https://doi.org/10.1084/jem.20150353>
- Webster, A. C., Nagler, E. V., Morton, R. L., & Masson, P. (2017). Chronic Kidney Disease. *The Lancet*, 389(10075), 1238–1252. [https://doi.org/10.1016/S0140-6736\(16\)32064-5](https://doi.org/10.1016/S0140-6736(16)32064-5)
- Wehrhahn, J., Kraft, R., Harteneck, C., & Hauschildt, S. (2010). Transient Receptor Potential Melastatin 2 Is Required for Lipopolysaccharide-Induced Cytokine Production in Human Monocytes. *The Journal of Immunology*, 184(5), 2386–2393. <https://doi.org/10.4049/jimmunol.0902474>

- Werman, A., Werman-Venkert, R., White, R., Lee, J.-K., Werman, B., Krelin, Y., Voronov, E., Dinarello, C. A., & Apte, R. N. (2004). The precursor form of IL-1 α is an intracrine proinflammatory activator of transcription. *Proceedings of the National Academy of Sciences of the United States of America*, 101(8), 2434–2439. <https://doi.org/10.1073/pnas.0308705101>
- Wessendorf, J. H., Garfinkel, S., Zhan, X., Brown, S., & Maciag, T. (1993). Identification of a nuclear localization sequence within the structure of the human interleukin-1 alpha precursor. *The Journal of Biological Chemistry*, 268(29), 22100–22104.
- White, J. P. M., Urban, L., & Nagy, I. (2011). TRPV1 function in health and disease. *Current Pharmaceutical Biotechnology*, 12(1), 130–144. <https://doi.org/10.2174/138920111793937844>
- Wilkinson, S. E., Parker, P. J., & Nixon, J. S. (1993). Isoenzyme specificity of bisindolylmaleimides, selective inhibitors of protein kinase C. *The Biochemical Journal*, 294 (Pt 2)(Pt 2), 335–337. <https://doi.org/10.1042/bj2940335>
- Wong, K. L., Tai, J. J.-Y., Wong, W.-C., Han, H., Sem, X., Yeap, W.-H., Kourilsky, P., & Wong, S.-C. (2011). Gene expression profiling reveals the defining features of the classical, intermediate, and nonclassical human monocyte subsets. *Blood*, 118(5), e16–e31. <https://doi.org/10.1182/blood-2010-12-326355>
- Wu, H., Nie, Y., Xiong, H., Liu, S., Li, G., Huang, A., Guo, L., Wang, S., Xue, Y., Wu, B., Peng, L., Song, M., Li, G., & Liang, S. (2015). P2X7 Receptor Expression in Peripheral Blood Monocytes Is Correlated With Plasma C-Reactive Protein and Cytokine Levels in Patients With Type 2 Diabetes Mellitus: A Preliminary Report. *Inflammation*, 38(6), 2076–2081. <https://doi.org/10.1007/s10753-015-0189-y>
- Wuensch, T., Thilo, F., Krueger, K., Scholze, A., Ristow, M., & Tepel, M. (2010). High Glucose–Induced Oxidative Stress Increases Transient Receptor Potential Channel Expression in Human Monocytes. *Diabetes*, 59(4), 844–849. <https://doi.org/10.2337/db09-1100>
- Xing, S., Grol, M., Grutter, P., Dixon, S., & Komarova, S. (2016). Modeling Interactions among Individual P2 Receptors to Explain Complex Response Patterns over a Wide Range of ATP Concentrations. *Frontiers in Physiology*, 7. <https://doi.org/10.3389/fphys.2016.00294>
- Yamamoto, S., Shimizu, S., Kiyonaka, S., Takahashi, N., Wajima, T., Hara, Y., Negoro, T., Hiroi, T., Kiuchi, Y., Okada, T., Kaneko, S., Lange, I., Fleig, A., Penner, R., Nishi, M., Takeshima, H., & Mori, Y. (2008). TRPM2-mediated Ca²⁺ influx induces chemokine production in monocytes that aggravates inflammatory neutrophil infiltration. *Nature Medicine*, 14(7), 738–747. <https://doi.org/10.1038/nm1758>
- Yan, Y., Bai, J., Zhou, X., Tang, J., Jiang, C., Tolbert, E., Bayliss, G., Gong, R., Zhao, T. C., & Zhuang, S. (2015). P2X7 receptor inhibition protects against ischemic acute kidney injury in mice. *American Journal of Physiology-Cell Physiology*, 308(6), C463–C472. <https://doi.org/10.1152/ajpcell.00245.2014>
- Yan, Z., & Shao, T. (2023). Chronic Inflammation in Chronic Kidney Disease. *Nephron*, 1–9. <https://doi.org/10.1159/000534447>

- Yang, Y.-H., Li, D.-L., Bi, X.-Y., Sun, L., Yu, X.-J., Fang, H.-L., Miao, Y., Zhao, M., He, X., Liu, J.-J., & Zang, W.-J. (2015). Acetylcholine inhibits LPS-induced MMP-9 production and cell migration via the $\alpha 7$ nAChR-JAK2/STAT3 pathway in RAW264.7 cells. *Cellular Physiology and Biochemistry*, 36, 2025–2038. <https://doi.org/10.1159/000430170>
- Yaron, J. R., Gangaraju, S., Rao, M. Y., Kong, X., Zhang, L., Su, F., Tian, Y., Glenn, H. L., & Meldrum, D. R. (2015). K⁺ regulates Ca²⁺ to drive inflammasome signaling: Dynamic visualization of ion flux in live cells. *Cell Death & Disease*, 6(10), e1954–e1954. <https://doi.org/10.1038/cddis.2015.277>
- You, D., Jeong, Y., Yoon, S., Kim, S., Lo, E., Kim, S., Lee, J. E., Nam, S., & Kim, S. (2021). Entelon® (Vitis vinifera Seed Extract) Prevents Cancer Metastasis via the Downregulation of Interleukin-1 Alpha in Triple-Negative Breast Cancer Cells. *Molecules*, 26, 3644. <https://doi.org/10.3390/molecules26123644>
- Zawada, A. M., Rogacev, K. S., Rotter, B., Winter, P., Marell, R.-R., Fliser, D., & Heine, G. H. (2011). SuperSAGE evidence for CD14⁺⁺CD16⁺ monocytes as a third monocyte subset. *Blood*, 118(12), e50–e61. <https://doi.org/10.1182/blood-2011-01-326827>
- Zhong, Z., Zhai, Y., Liang, S., Mori, Y., Han, R., Sutterwala, F. S., & Qiao, L. (2013). TRPM2 links oxidative stress to NLRP3 inflammasome activation. *Nature Communications*, 4(1), Article 1. <https://doi.org/10.1038/ncomms2608>
- Zong, P., Lin, Q., Feng, J., & Yue, L. (2022). A Systemic Review of the Integral Role of TRPM2 in Ischemic Stroke: From Upstream Risk Factors to Ultimate Neuronal Death. *Cells*, 11(3), 491. <https://doi.org/10.3390/cells11030491>

Declaration of Academic Integrity

Declaration in accordance with Section 7 Paragraph 1 No. 4

I hereby declare in lieu of oath that I have researched and written this thesis myself, no passages of text have been taken from third parties without having been identified as such and that all tools, personal notifications, and sources used by the applicant have been indicated in the thesis.

The assistance of a professional consultant has not been utilized and no third parties have either directly or indirectly received monetary benefits from the candidate for work related to the contents of the submitted thesis.

The persons who have supported this work are listed below:

1. Western blots of P2 agonists and antagonists (Fig. 25A) were performed by Priska Jost.
2. The blood samples from CKD donors were collected in collaboration with Univ.-Prof. Dr. Dr. Thimoteus Speer group.
3. The isolation of PBMCs from the LRS or Amicus chambers was performed by Carmen Hässig.
4. Culture of cell lines was supported by Cora Hoxha, Gertrud Schäfer, Sandra Janku and Kathrin Fröderer.

No other people were involved in the preparation of the content of this thesis. I do not have the paid help from placement or Consultation services (doctoral advisors or other people) taken. Except for those specified.

The thesis has not been submitted to another examination authority in the same or a similar form in another procedure to obtain the doctoral degree, either in Germany or abroad. I affirm in lieu of an oath that I have told the truth to the best of my knowledge and have not concealed anything.

.....

Ort, Datum

.....

Signature of the doctoral candidate

.....

Signature of the official accepting the declaration in lieu of oath

Acknowledgments

I would like to express my heartfelt gratitude to Dr. Alansary and Prof. Niemeyer for granting me the opportunity to work on such an inspiring project. Their exceptional support and guidance throughout this journey have been invaluable. I am deeply grateful for all the knowledge I have gained—technically, scientifically, and personally—under their mentorship.

I also extend my sincere thanks to Prof. Markus Hoth for his invaluable support, both scientifically and emotionally. His encouragement has been a great source of strength during challenging times.

My heartfelt appreciation goes to Kathrin Fröderer, Cora Hoxha, Gertrud Bracic, Carmen Hässig, Sandra Janku, and Andrea Armbrüster for their invaluable help and unwavering support in the lab.

I am fortunate to have had incredible colleagues who became close friends, including Maylin Merino, Mona Knapp, Vanessa Poth, Priska Jost, and Lukas Jarzembowski. Your camaraderie has made this journey even more memorable.

My gratitude also extends to all the wonderful and talented individuals in the Biophysics group. I will always cherish the warm smiles and uplifting conversations we shared.

Special thanks to my family, who have supported me unconditionally with all their hearts. To my parents, Rouhangiz Khoram and Alinaghi Amini, who have shaped me into the person I am today. To my sister, Mahnaz Amini, whose inspiration encouraged me to pursue my PhD. To my brothers, Reza Amini and Morteza Amini, whose unwavering love and encouragement have always uplifted me. And to my partner, Moein Alinaghian, whose constant support and comforting embrace on my most exhausting and hopeless nights provided the relief I needed. You have stood by me every step of the way, and I couldn't have done this without you.

Lastly, I want to thank my incredible friends. The laughs, fun, talks and unforgettable moments we shared gave me the energy and motivation to keep moving forward.

Tag der Promotion: 17.10.2025

Dekan: Univ.-Prof. Dr. med. dent. Matthias Hannig

Berichterstatter: Prof. Dr. Barbara Niemeyer-Hoth

Prof. Dr. Martin van der Laan